HYDROFOIL RESEARCH PROJECT

FOR OFFICE OF NAVAL RESEARCH

NAVY DEPARTMENT, WASHINGTON, D.C.

CONTRACT NO. NONR-507(00)

HYDROFOIL HANDBOOK

VOLUME II

HYDRODYNAMIC CHARACTERISTICS OF COMPONENTS

BATH IRON WORKS CORP.

BY GIBBS AND COX, INC.

NEW YORK 6, N.Y.

1954

FOREWORD

THIS HYDROFOIL HANDBOOK HAS BEEN PREPARED BY GIBBS & COX, INC. ACTING AS THE DESIGN AGENT OF THE BATH IRON WORKS CORPORATION UNDER OFFICE OF NAVAL RESEARCH CONTRACT NONR-507(00). THE FOLLOWING WERE DIRECTLY RESPONSIBLE FOR THE PREPARATION OF THE TEXT OF VOLUME II:

Mr. W. H. Michel - Editor and Contributor
Mr. S. F. Hoerner - Contributor
Mr. L. W. Ward - Contributor
Mr. T. M. Buermann - Project Coordinator

ACKNOWLEDGEMENT

IN THE PREPARATION OF THIS HANDBOOK, USE HAS BEEN MADE OF WORK PUBLISHED BY OTHERS. EVERY ATTEMPT HAS BEEN MADE TO ACKNOWLEDGE: THIS FACT BY SUITABLE NOTATIONS AND LIST OF REFERENCES, THUS ANY OMISSIONS ARE INADVERTENT.

HYDROFOIL HANDBOOK

VOLUME II

HYDRODYNAMIC CHARACTERISTICS OF COMPONENTS

HYDROFOIL HANDBOOK

VOLUME II

HYDRODYNAMIC CHARACTERISTICS OF COMPONENTS

INTRODUCTION

The hydrodynamic characteristics of the various components that make up a hydrofoil craft must be known in order to prepare a design or to analyze a given design or craft. It is intended in this volume to present such information in the form of concise engineering formulations and methods, with some background material to give an understanding of the underlying hydrodynamic relationships, the scope and adequacy of available theory and data, and the general state of knowledge.

Material was extracted from exfsting reports on hydrofoil theory, analyses and experimental data and from pertinent established aerodynamic and marine information. Where sufficient reference material was lacking, it was necessary to derive certain properties during the preparation of this text, In other instances, where general relationships could not reasonably be established, available data and suggested

means of analyses and derivation are given. In order to maintain this work as a readily usable handbook for direct engineering use, hydrodynamic fundamentals and derivations are kept to a minimum, consistent with clear exposition of the various relationships. For those interested in reviewing the basic fundamentals or exploring further into the various subjects, comprehensive references are given on each subject.

In all cases, a conscientious effort was made to provide pertinent engineering information on all components of hydrofoil configurations, even though some of the proposed formulas may be tentative and even conjectural; so that there would be a definite basis on which to prepare a design and on which to make comparison when additional information is forthcoming.

It was felt that the hydrodynamic characteristics should be presented without qualifications as to what combination of components provide the best hydrofoil configuration. There is a wide variety of configurations, each of which may have some particular advantage under particular requirements; and to attempt to introduce such operational factors would complicate any presentation of basic information,

For similar reasons, only the "steady-state" characteristics of the components are considered, Investigations of dynamic stability, behavior in waves, turning characteristics, etc. should be undertaken

only after a complete configuration has been chosen tentatively on the basis of specified functional requirements,

Although treatment of the "best" foil size, öptimum" number of struts, "most effective" configurations, etc, has therefore not been included in this volume, some practical limitations as to size, speed, geometry, etc. were considered so that effort could be concentrated on deriving more exact properties in the range of applications considered to be most frequently employed. These limitations are based on evaluations of existing craft and analyses of general design studies, such as are indicated in Volume I, In most instances, it is stated in this text where such limitations are used and the procedure for obtaining information for cases beyond such limits is: shown or inferred,

The material contained herein is presented under chapter headings, as indicated in the table of contents, with the chapters so sequenced as to fall into three main groupings, Chapters 1-6 contain the basic hydrodynamic characteristics of the foils, including the effects of the various other influences on the foils. Chapters 7-11 deal with the characteristics of struts, hulls and the various other appurtenances in a configuration, Finally, Chapter 12 indicates the influence of cavitation on the characteristics of the various components. Cavitation is separately treated to stress its importance,, to show the ranges of craft speed and size in which it is a factor and those in which it can

be neglected, and possibly of greatest importance at the present time, to indicate the dearth of necessary information for predicting the hydrodynamic effects of cavitation on a foil configuration with sufficient accuracy,

Design examples have been distributed throughout the text to give ready indication of how to apply some of the important formulas and methods,, An appendix showing the detail calculations of the lift and drag of a chosen design is also included to serve as a summary of the progosed material and its application,

Since the basic principles (and geometry) of hydrofoils are the same as those of airfoils, most hydrofoil properties have been derived from airfoil theory and data, with airfoil nomenclature being generally adopted. Chapter 1, an introduction to airfoil principles, has therefore been included to familiarize the reader with this subject, which is necessary to the proper understanding of hydrofoil hydrodynamics.

On the other hand, the hydrodynamics of hulls have not been comprehensively presented in the text. Information on hull drag is readily available from many published sources, most of which are known to the naval architect, and the detailed coverage of such information in this work would be needless duplication, In this particular case, a short discussion herein with references to the more basic works has been considered sufficient.

The criterion for presenting information in this volume has been, therefore, to elaborate on subjects that are new to the naval architect, but to abridge the treatment of more familiar subjects which are amply treated in general marine texts.

CHAPTER I. AIRFOIL PRINCIPLES

'The essential principles of foil sections and wings are presented as the basic material used in developing hydrofoil characteristics. Fundamental airfoil theory is outlined, including those factors that are most applicable to hydrofoils. Viscous drag considerations are given, and the availability of airfoil data .for design use is pointed out .

1. Introduction

Basically, a hydrofoil is an airfoil operating in water. Aerodynamic foil principles can therefore be utilized in developing the hydrodynamic characteristics of a hydrofoil.

In some instances, such as where the foil operates at large distances below the water surface, established airfoil theory (in incompressible flow) and pertinent airfoil data can be used directly for determining the hydrodynamic characteristics of the foil. In more practical cases, the airfoil methods must be corrected by suitable factors to take account of the surface effects, supporting struts, high speeds (cavitation) and other factors associated with practical hydrofoil configurations.

In any case, aerodynamic foil principles form the basis for the development of hydrodynamic characteristics of hydrofoils. Therefore, this chapter is presented to familiarize the reader with the airfoil notation employed, the underlying airfoil theory that is most applicable to hydrofoils, and the availability of pertinent airfoil data for use in deriving hydrofoil characteristics,

2. Airfoil Notation

Foil Section Geometry

Figure 1.1 shows the typical airfoil section notation.. The chord C of the foil is the distance from the leading edge to'the trailing edge, and the angle of attack α is the angle between the chord line and the direction of advance, as indicated.

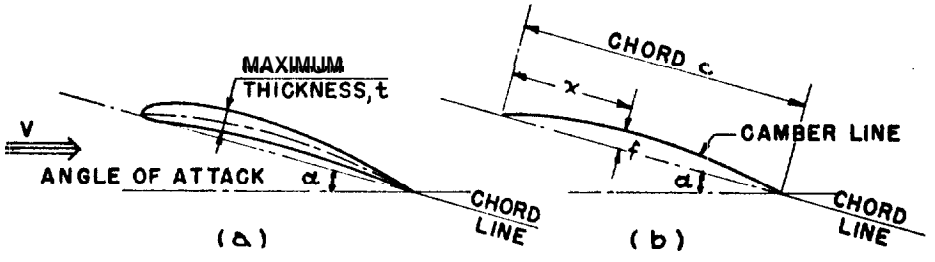

GEOMETRY OF AN AIRFOIL SECTION

a - SECTION WITH THICKNESS, t
b - THE SECTION'S "SKELETON". THE MEAN LINE (CAMBER LINE) HAS A MAXIMUM CAMBER, AT A DISTANCE x FROM THE LEADING EDGE

FIGURE 1.1

The mean line of the section is called the camber line, the camber being considered the maximum separation between this line and the chord line. For simple circular arc sections, the mean line has symmetrical camber with the maximum separation and maximum foil thickness at the mid-chord position, but for typical airfoil

sections the shape of the camber line and the chordwise location of maximum camber and maximum thickness vary, depending on the type of section employed. A description of modern airfoil section shapes employed by NACA is given by Abbott[1,2].

Wing Geometry

Figure 1.2 shows the typical wing geometry and notation. Dimensions are characteristically taken about the quarter-chord line (1/4 of the chord from the leading edge of the foil). Thus, the span is the projected distance between the tips of the quarter-chord line, and the sweep and dihedral angles are measured from the projected quarter-chord line in the horizontal and transverse planes respectively as indicated. Two important "parameters" in dealing with wings are2

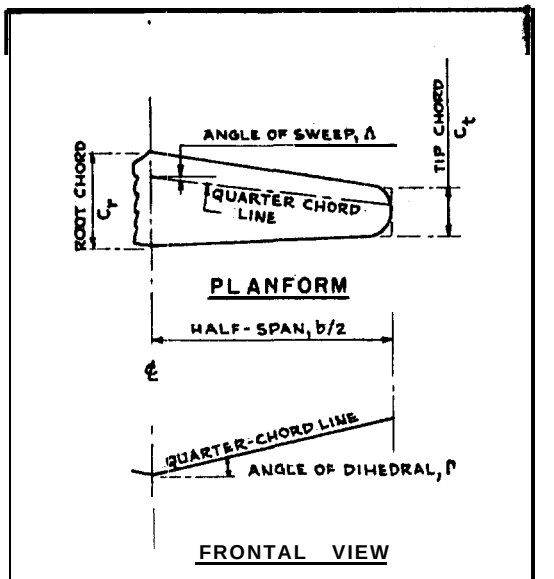

WING GEOMETRY

FIGURE 1.2

the plan form area, S - the projected area of the wing in a horizontal plane

the aspect ratio, A - the ratfo of span to mean chord, or b^2/S

The difference between "displacement bodies" and '"lifting surfaces " in the selection of reference areas should be noted here. For ships and similar bodies the total wetted area is usually chosen as the reference area, whereas for wings the projected area of one side of the wing is taken, '

Force Notation

The force system acting on a foil (or any body) may conveniently be referred to the components along and about the three co-ordinate axes of the body, These are identified, for the foil, as:

Lift - force in the vertical direction

Drag Force - force in the fore and aft direction

Side Force - force in the transverse direction

Pitching Moment - about the transverse axis

Rolling Moment - about the fore and aft axis

Yawing Moment - about the vertical axis

Considering the forces in the plane of symmetry for straight forward flight, the forces on the foil section are shown in Figure 1.3. (The transverse axis is taken to be at the "aerodynamic center", which is discussed below.)

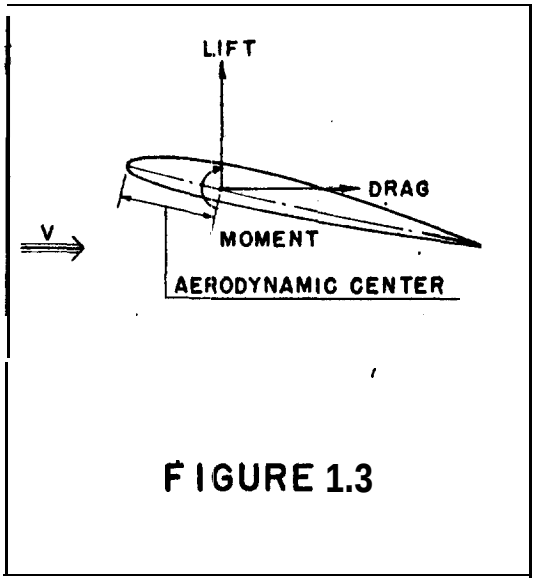

FIGURE 1.3

In many applications, pressures and forces in fluid flow are proportional to the "dynamic pressure"

$$q = \rho/2\ V^2 \qquad (lb/ft^2) \qquad (1.1)$$

where ρ = mass density of the fluid ($\#sec^2/ft^4$)

V = speed of advance (ft/sec)

The mass density of the fluid varies slightly with temperature. At the standard 59°F (15°C),

ρ = 1.94 ($\#sec^2/ft^4$) for fresh water

ρ = 1.99 ($\#sec^2/ft^4$) for salt water

Thus, using these units, $\rho/2$ may be considered equal to 1.0 and $q \approx V^2$ in water.

Example

What is the dynamic pressure in sea water at 30 knots?

$V = 1.69 \times 30 = 50.7$ ft/sec

$\rho = 1.99$ #sec^2/ft^4

$V^2 = 2570$ ft^2/sec^2

$q = 1.99/2 \times 2570 = 2558$ lb/ft^2

The forces on the foil may readily be represented in non-dimensional coefficient form, by referring them to the dynamic pressure and the foil area. Thus

$$\left.\begin{aligned} &\text{Lift Coefficient,} && C_L = L/qS \\ &\text{Drag Coefficient,} && C_D = D/qS \\ &\text{Pitching Moment Coefficient,} && C_m = M/qSc \end{aligned}\right\} \quad (1.2)$$

where L = lift of the foil

D = drag of the foil

M = pitching moment on the foil about some point on the foil chord - taken positive when tending to increase the foil angle of attack

S = planform area

C = foil chord

q = dynamic pressure

The pitching moment coefficient is essentially constant when moments are taken about the aerodynamic center., (Theoretically, this

point is nearly a quarter-chord distance behind the leading edge and is thus a good reference point for wing geometry, as shown in Figure 1.2.) For such moment center, the pitching moment coefficient is identified as $C_{m_{ac}}$.

Summary

The basic aerodynamic notation and the units usually employed are as follows:

A	aspect ratio	non-dimensional
b	projected foil span	ft.
c	foil chord	ft.
D	drag	lbs.
f	foil camber	ft.
L	lift	lbs.
M	pitching moment	ft.lbs.
q	dynamic pressure,	lbs/ft^2
S	projected foil area	$ft.^2$
t	foil thickness	ft.
V	speed of advance	ft/sec
α	angle of attack	radians
ρ	mass density of the fluid	$lbs.sec^2/ft^4$

A	angle of sweep	degrees
Γ	angle of dihedral	degrees
C_D	drag coefficient, D/qS	non-dimensional
C_L	lift coefficient, L/qS	non-dimensional
C_m	pitching moment coefficient, M/qSc	non-dimensional

3. Lifting-Line Airfoil Theory

General

Classical airfoil theory originally developed by scientists such as Prandtl, Lanchester, Glauert, Munk, et al, is available for study in many treatises on aerodynamics [3,4,5]. These works are based on the concept of a single lifting line,. which is sufficiently accurate for wings of large aspect ratio. Although in recent years advances have been made in the development of a lifting-surface theory (most applicable for foils of small aspect ratio), the lifting-line theory is still of foremost importance.

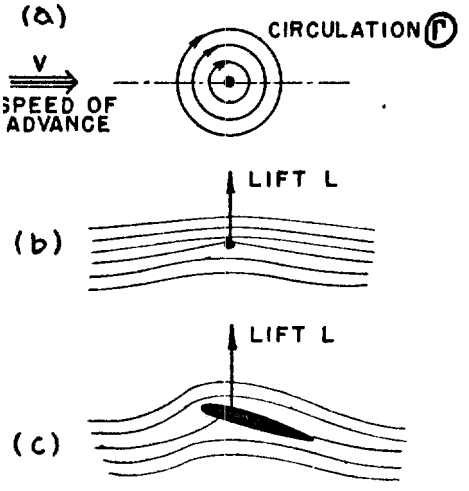

'ORIGIN OF LIFT

SUPERPOSITION OF CIRCULATION AND SPEED OF ADVANCE V IN (a) LEADS TO THE LIFTING VORTEX (b). A FOIL SECTION (C) PRODUCES THE SAME KIND OF FLOW PATTERN.

FIGURE 1.4

Two-Dimensional Theory

The basic theory of lift is derived from the concept of a rectilinear vortex advancing in a fluid in a direction normal to the vortex axis. The superposition of the circulatory motion of the vortex upon the free stream velocity, as shown in Figure 1.4, results in an

increase in velocity on one side of the vortex and a decrease on the other side. According to Bernoulli's theorem, therefore, the static pressure is decreased on the "suction" side and increased on the "pressure" side. The resultant lift force is perpendicular to the free-stream direction, and has the magnitude:

$$L = b\rho V \Gamma \quad \text{(lbs.)} \tag{1.3}$$

where ρ is the mass density of the fluid ($\#sec^2/ft^4$)

V is the fluid velocity (ft/sec)

Γ is the circulation of the vortex (the integral of the vortex velocity over a closed path encircling the vortex center) (ft^2/sec)

b is the foil span in ft. (assumed to be infinite in the considered two-dimensional flow pattern)

The relationship between circulation and the lift coefficient of a foil section can then be expressed as

$$\Gamma = C_L c V/2 \tag{1.4}$$

The value of the circulation around an airfoil of known geometry can be determined by fluid potential theory. Thus, for a "thin airfoil" section,

$$\left.\begin{aligned} \Gamma_\alpha &= \pi c V \alpha_0 && \text{(due to angle of attack, and applied at the quarter-chord position)} \\ \Gamma_f &= 2\pi V f && \text{(due to camber and applied at the half-chord position)} \end{aligned}\right\} \tag{1.5}$$

Then combining equations (1.4) and (1.5) we get

$$\left.\begin{aligned} C_L &= 2\pi\,(\alpha_o + 2f/c) \\ C_{m_{LE}} &= -\frac{\pi}{2}\,(\alpha_o + 4f/c) \end{aligned}\right\} \quad (1.6)$$

where C_L is the lift coefficient

$C_{m_{LE}}$ is the moment coefficient taken about the leading edge of the foil

α_o is the angle of attack in two-dimensional flow

f/c is the camber ratio of the foil.

From equation (1.6) it is seen that for a cambered foil, the lift is not zero at zero angle of attack (as measured in Figure 1.1). Rather, the angle of zero lift is seen to ber

$$\alpha_{L_o} = -2f/c \quad (1.7)$$

However, zero angle of attack does have a particular significance in cambered sections. In two-dimensional flow, it approximately indicates the flow pattern where locally there is no flow around the leading edge of the section from one side to the other. For this condition of "smooth entrance", the "symmetric" or "optimum" lift coefficient is approximately

$$C_{L_{opt}} = -4\pi f/c \quad (1.8)$$

Example

What is the lift coefficient of a "thin" foil section (in two-dimensional flow) having a camber ratio of $f/c = 3\%$ at an angle of attack of $\alpha = 5°$?

COMBINING EQUATIONS (1.6) AND (1.7),

$$C_l = 2\pi(\alpha_0 - \alpha_{L0})$$

NOW, $\alpha_0 = 5° = 0.09$ RADIANS

$\alpha_{L0} = -2 \times 0.03 = -0.06$ RADIANS (EQ. 1.7)

THEN, $C_l = 2\pi(0.09 + 0.06)$

$= 0.94$

The optimum lift coefficient of this section is theoretically (equation 1.8): $C_{L_{opt}} = 4\pi \times 0.03 = 0.38$

In practice, airfoil sections are not "thin", but have a finite thickness, as indicated in Figure 1.1 above. Properties 0% practical airfoil sections can also be determined by fluid potential methods. The calculations involved are arduous, however, and the results are not; really applicable due to viscous basses in the boundary-layer flow. Experimental data on the properties of airfoil sections, as discussed below should be employed in engineering applications. However, a review of the data for modern airfoil sections[1,2] indicates that the values given in equation (1.6) for the lift

and moment coefficients are reasonably accurate, and may be used for preliminary purposes,

Wing Theory

A wing, with chord c and span b, is the equivalent of a lifting line having finite (limited) length. As illustrated in Figure 1.5, around the ends or tips of this line, a flow is caused from the pressure side of the foil to the suction side. The circulation of the bound vortex, therefore, finds continuation in the form of a pafr of tip vortices, one originating from each wing tip, approximately as sketched in Figure 1.5. In other words, the single vortex (as visualized in Figure 1.4) is replaced by a vortex system, which is remotely similar in shape to a horseshoe, (thus, sometimes called a horseshoe vortex).

Within the space between the two tip vortices, their circulations combine, thus "inducing" a downwash velocity and causing as a consequence a downward deflection of the basic stream from its undisturbed direction. This deflection reaches a final angle at some distance behind the wing, as a component part of the vortex pair in Figure 1.5.

At the position of the foil or lifting line, the deflection of the fluid (one-half the final downwash angle) results in the "induced angle of attack". Because of this angle, the lift force is now

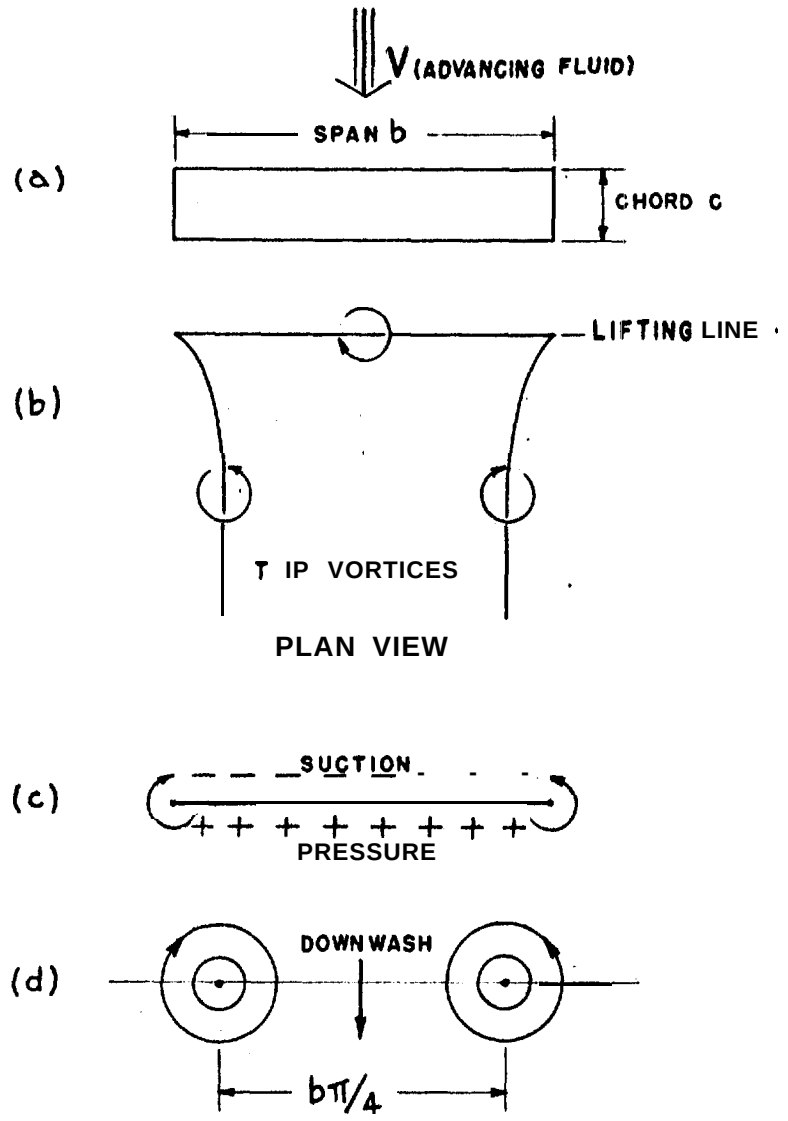

FLOW PATTERN PAST THREE-DIMENSIONAL WING

(a) WING PLANFORM

(b) EQUIVALENT VORTEX SYSTEM

(c) ORIGIN OF TIP VORTICES

(d) VORTEX PAIR FAR BEHIND WING

FIGURE 1.5

displaced from its direction normal to the free-stream flor and is tilted backward by the induced angle α_i, as illustrated in Figure 1.6. The lift (defined as the vertical component of , the foil force) is accordingly

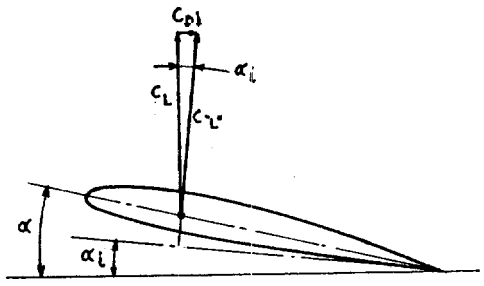

ORIGIN OF THE INDUCED RESISTANCE. $C_{Di} = C_L \tan \alpha_i$

FIGURE 1.6

$$C_L = C_{L''} \cos \alpha_i \approx C_{L''} \tag{1.9}$$

and there is now a component of drag or resistance (defined as the force component in direction of the motion) - the induced drag corresponding to

$$C_{D_i} = C_{L''} \sin \alpha_i = C_L \tan \alpha_i \approx C_L \alpha_i \tag{1.10}$$

Since within the scope of application of vortex-line theory, the induced angle is comparatively small, it is usual to assume

$$\cos \alpha_i \approx 1.0$$

$$\sin \alpha_i \approx \tan \alpha_i \approx \alpha_i$$

as indicated in equations (1.9) and 1.10).

For an actual foil, the loading (or circulation) is not constant along the span as was assumed for the simple horseshoe vortex but varies depending on the section geometry at each point along the span and on the downwash at that point due to the trailing vortices (for instance, the horseshoe vortex system leads to an infinite downwash at the tips, an untenable assumption).

The classical treatment of this consideration by Prandtl[3] indicates that an elliptic, distribution of lift along the span of the foil as shown in Figure 1.7, results in a constant value of downwash along the span (constant value of induced angle) and a minimum value of induced drag.

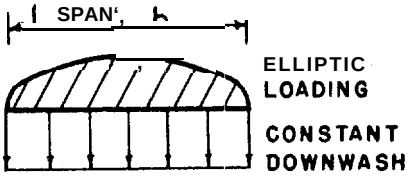

ELLIPTIC LOADING

FIGURE 1.7

For the case of elliptic lift distribution, the derived values of induced angle and induced drag are, in coefficient form:

$$\left.\begin{aligned} \alpha_i &= C_L/\pi A \\ C_{D_i} &= C_L\,\alpha_i = C_L^2/\pi A \end{aligned}\right\} \quad (1.11)$$

where A is the foil aspect ratio.

The expression for the lift coefficient based on the angle of attack in two-dimensional flow, equation (1.6), must be modified f'or the finite wing by taking the induced angle into account. Thus,

$$C_L = 2\pi (\alpha + \alpha_{L_o} - C_L/\pi A) \tag{1.12}$$

where α is the geometric angle of attack

α_{L_o} is the angle of zero lift, from equation (1.7).

The lift curve slope is an important concept in airfoil (and hydrofoil) analyses. Rearranging the terms of equation (1.12) and taking the derivative, the slope is

$$\frac{dC_L}{d\alpha} = \frac{1}{\frac{1}{2\pi} + \frac{1}{\pi A}} = \frac{2\pi}{1 + \frac{2}{A}} \tag{1.13}$$

It is frequently more convenient and useful, to invert equation (1.13) and determine the angle of attack necessary to produce a desired lift coefficient. Thus, the "inverse slope" or "lift angle" is

$$\left.\begin{aligned} \frac{d\alpha}{dC_L} &= \left(\frac{d\alpha}{dC_L}\right)_o + \left(\frac{d\alpha}{dC_L}\right)_i \\ &= \frac{1}{2\pi} + \frac{1}{\pi A} \end{aligned}\right\} \tag{1.14}$$

where $\left(\frac{d\alpha}{dC_L}\right)_o$ is the lift angle dye to the lifting-line vortex

$\left(\frac{d\alpha}{dC_L}\right)_i$ is the lift angle due to the trailing vortices

Example

What is the angle of attack of a wing with elliptical loading, having A = 5, needed to produce a lift coefficient of $C_L = 0.5$?

FROM EQUATION (1.14),

$$\frac{d\alpha}{dC_L} = \frac{1}{2\pi} + \frac{1}{5\pi} = 0.22$$

FOR A SYMMETRICAL FOIL (NO CAMBER)

$$\alpha = 0.22 \times 0.5 = 6.3^\circ$$

FOR THE 3% CAMBERED SECTION (PRECEDING EXAMPLE)

$$\alpha_{L=0} = -0.06 = -3.4^\circ$$

$$\alpha = 6.3 - 3.4 = 2.9^\circ$$

It should also be noted that, from equation (1.11):

$$\frac{d C_{D_i}}{d(C_L^2)} = \frac{d\alpha_i}{dC_L} = \frac{1}{\pi A} \qquad (1.15)$$

which is also a useful relationship in airfoil analysis,

4. Modifications to Lifting-Line Theory

Effect of Planform

The lifting line theory as outlined above is exact for wings of large aspect ratio, having elliptical lift distribution. Considering wings of simple geometry (i.e., straight, non-twisted, constant section shape), elliptical distribution is found only for wings of elliptical planform. It is therefore necessary to determine the effect of other planforms on the induced oharacterfstics.

The method proposed by Glauert[4] can be used to determine the corrections to be applied to the induced angle and induced drag terms for wings of various planforms, The induced terms of equation (1.15) now become

$$\left.\begin{aligned} \frac{d\alpha_i}{dC_L} &= \frac{1+\tau}{\pi A} \\ \frac{dC_{D_i}}{d(C_L^2)} &= \frac{1+\delta}{\pi A} \end{aligned}\right\} \qquad (1.16)$$

where τ, δ are the corrective terms for the induced angle and induced drag, respectively.

Figure 1.8 gives the τ and δ corrections for wings of rectangular planform in terms of the aspect ratio.

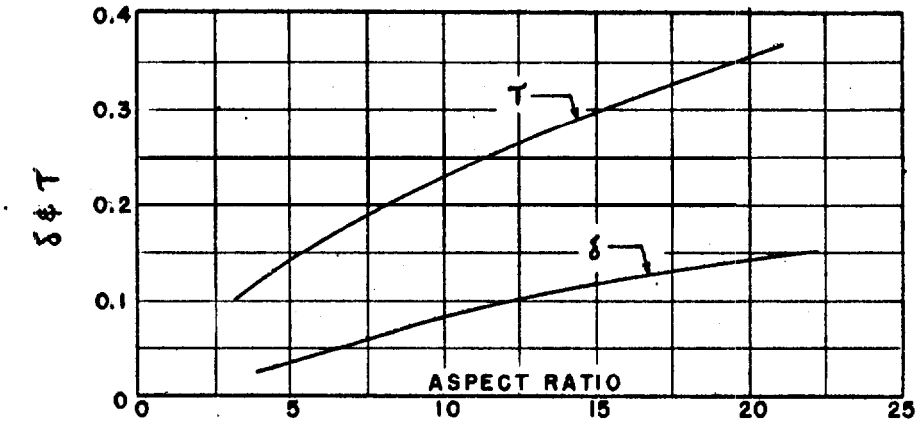

τ & δ FOR RECTANGULAR PLANFORMS

'FIGURE 1.8

Hueber[6] has calculated the correction terms for wings having straight taper from midspan to tip, for several aspect ratios as a function of taper ratio, as shown in Figure 1.9. The value of τ can be read off directly from Figure 1.9(a), interpolating as required for other aspect ratios. The value of δ for any aspect ratio can readily be determined from the function

$$\delta = \delta' A$$

where δ' is given in Figure 1.9(b) for any aspect ratio (as suggested by Hoerner[7]).

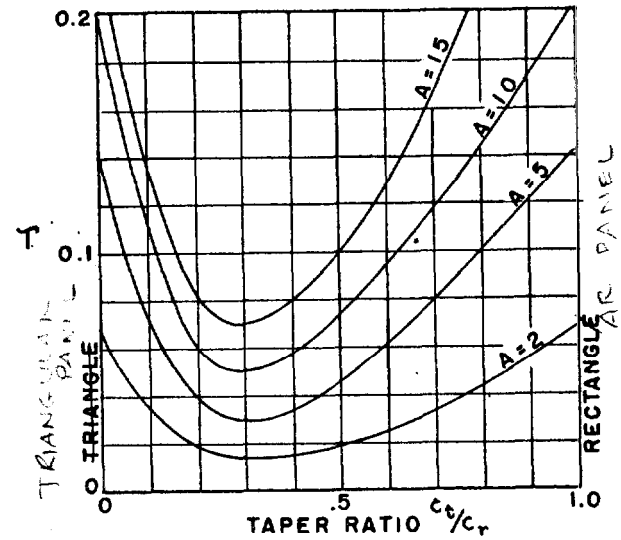

(a) τ FOR INDUCED ANGLE

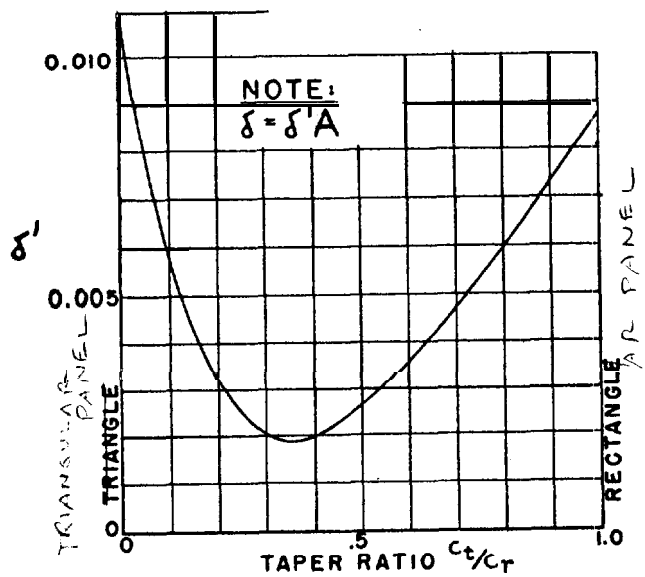

(b) δ FOR INDUCED DRAG

PLANFORM CORRECTIONS τ & δ

FIGURE 1.9

The above planform corrections are derived on the basis of the lifting line theory, without consideration of the finite chord. In the practical case, there is some advantage to be gained from hating square wing tips (both in planform and in lateral section) as they prevent the flow from "getting around" the wing tip, thus increasing the effective span and aspect ratio, It will be shown, in the discussion of lifting surface theory below, that for wings of low aspect ratio the rectangular planform is more effective (has less induced angle and drag) than those of rounded or tapered form.

Effects of Sweep

The effects of sweep on a foil have been investigated theoretically in several references[8,9]. A simplified method of approach is presented herein.,

For a swept wing (as illustrated in Figure 1.2), the reference angle of attack is that of the foil section at midspan. Thus, for the flow normal to the quarter-chord line, the nominal angle of attack is increased by $1/\cos\Lambda$ but the dynamic pressure is decreased by $\cos^2\Lambda$. The net effect is to decrease the section lift curve by the factor $\cos\Lambda$.

Equation (1.14) may then be written for the swept foil:

$$\left(\frac{d\alpha}{dC_L}\right)_\Lambda = \left(\frac{d\alpha}{dC_L}\right)_o \frac{1}{\cos\Lambda} + k\left(\frac{d\alpha}{dC_L}\right)_i \qquad (1.17)$$

$$= \frac{1}{2\pi\cos\Lambda} + \frac{k}{\pi A}$$

where $\left(\frac{d\alpha}{dC_L}\right)_0$ $\left(\frac{d\alpha}{dC_L}\right)_i$ are the section and induced lift angles for the unswept foil

Λ is the angle of sweep

k is a factor to be determined.

For elliptical lift distribution, the factor $k = 1$ and the induced term is the same as for a straight foil with elliptic distribution. However, the low taper ratios required for swept-back wings to make the lift distribution elliptical (as shown in Figure 1.14 below) are not practical, because of wing-tip stalling,

From an analysis of test data of swept wings, Hoerner[7] shows that k varies approximately as $1/\cos\Lambda$. Thus

$$\left(\frac{d\alpha}{dC_L}\right)_\Lambda = \left(\frac{d\alpha}{dC_L}\right)\frac{1}{\cos\Lambda} \qquad (1.18)$$

where $\left(\frac{d\alpha}{dC_L}\right)$ is the lift angle of the foil without sweep,

The induced drag term may also be expressed approximately as

$$\frac{dC_{D\Lambda}}{d(C_L^2)} = \frac{dC_D}{d(C_L^2)} \cdot \frac{1}{\cos\Lambda} \qquad (1.19)$$

Tests conducted by NACA[10,11] on various swept wings indicate that the lift curve and induced drag do not obey these simple formulations in all cases, particularly at large sweep angles. Wings with

sweep forward have different characteristics than those with sweep-back, and in some instances the induced drag increases with increase in aspect ratio. Therefore, the above relationships should only be used in the absence of specific test data,

Effects of Dihedral

According to a simple theory[12], each panel of a dihedraled or V-shaped wing has an induced angle (in the direction normal to the panel) equal to that of a complete wing with an aspect ratio which is twice that of the panel,

Referring the lift and drag forces to the projected area and span (see Figure 1.2 above), and noting that the reference angle of attack is that of the foil section at midspan (in a vertical plane), the lift angle may be simply expressed as

$$\left.\begin{aligned} \left(\frac{d\alpha}{dC_L}\right)_\Gamma &= \frac{1}{2\pi\cos\Gamma} + \frac{1}{\pi A} \\ \frac{dC_{D_\Gamma}}{d(C_L^2)} &= \frac{dC_D}{d(C_L^2)} = \frac{1}{\pi A} \end{aligned}\right\} \quad (1.20)$$

where Γ is the dihedral angle.

Example

What are the induced characteristics of a wing, having $\Lambda = 25°$ and $\Gamma = 25°$? According to equation (1.18)

$$\frac{d\alpha}{dC_L} \sim \frac{1}{\cos\Lambda} .$$

For $A = 25$" ($\cos 25° = 0.91$), the induced angle and induced drag are roughly increased by' 10%. The angle of dihedral does not affect the induced characteristics,

Lifting Surface Consfderations

The theory of lifting surfaces has been promoted in recent years to determine the aerodynamic characteristics of wings of small aspect ratio, Weinig[13] and Weissinger[14] have produced theories capable of being applied readily for engineering purposes. Lawrence[15] has more recently produced generalized functions that agree with Weissinger's results and further allow the determination of the chordwise load distribution.

The complete formula for the lift of an airfoil may be expressed as8

$$C_L = \frac{1}{\frac{E}{2\pi} + \frac{1}{\pi A}} \sin\alpha + 2\sin^2\alpha\cos\alpha \qquad (1.21)$$

where α includes the angle of zero lift, for cambered foils

E is the correction factor applied to the basic lifting line theory. Values of E are! given in Mgure 1.10.

$2\sin^2\alpha$ is a normal force coefficient, which can be derived rigorously for zero aspect ratio by any of several concepts. The simplest concept is that it represents the viscous drag coefficient normal to a two-dimensional flat plate ($C_D = 2,0$) with a fluid speed of $V\sin\alpha$.

Equation (1.21) is thus seen to represent the corrected lifting line theory (with $\sin\alpha$ substituted for α for greater accuracy at high angles) plus a non-linear term which is actually derived for zero aspect ratio but which appears to be valid throughout the range of low aspect ratios ($A < 2$).

The drag due to lift may be given approximately as:

$$C_{D_i} = \frac{C_{L_1}^2}{\pi A} + C_{L_2}\tan\alpha \qquad (1.22)$$

where C_{L_1} is the first term of equation (1.21)

C_{L_2} is the second term of equation (1.21).

Values of E can be derived from Figure 1.10, where $1/E$ is plotted against aspect ratio for rectangular foils. It is seen that Weinig and Weissinger show different values in the range of $A > 1$. An empirical factor $E = 1 + 2/A^2$ for $A > 2$ falls between the two theoretical values.

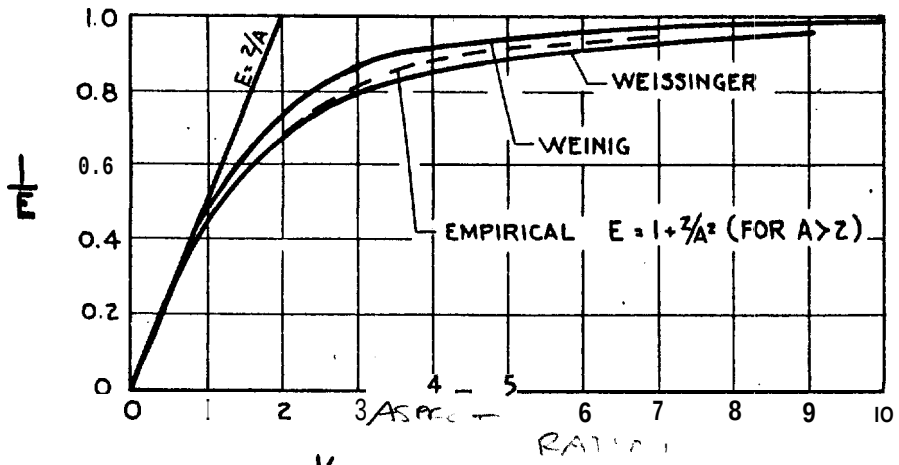

VALUES OF 1/E FOR RECTANGULAR FOILS AS A FUNCTION OF ASPECT RATIO

FIGURE 1.10

Lawrence (and Weissinger) also derived values for triangular wings. Figure 1.11 gives a comparison between the rectangular and triangular values of the complete factor $\frac{1}{\frac{E}{2\pi} + \frac{1}{\pi A}}$ and the lifting line theory (E = 1), for small aspect ratios.

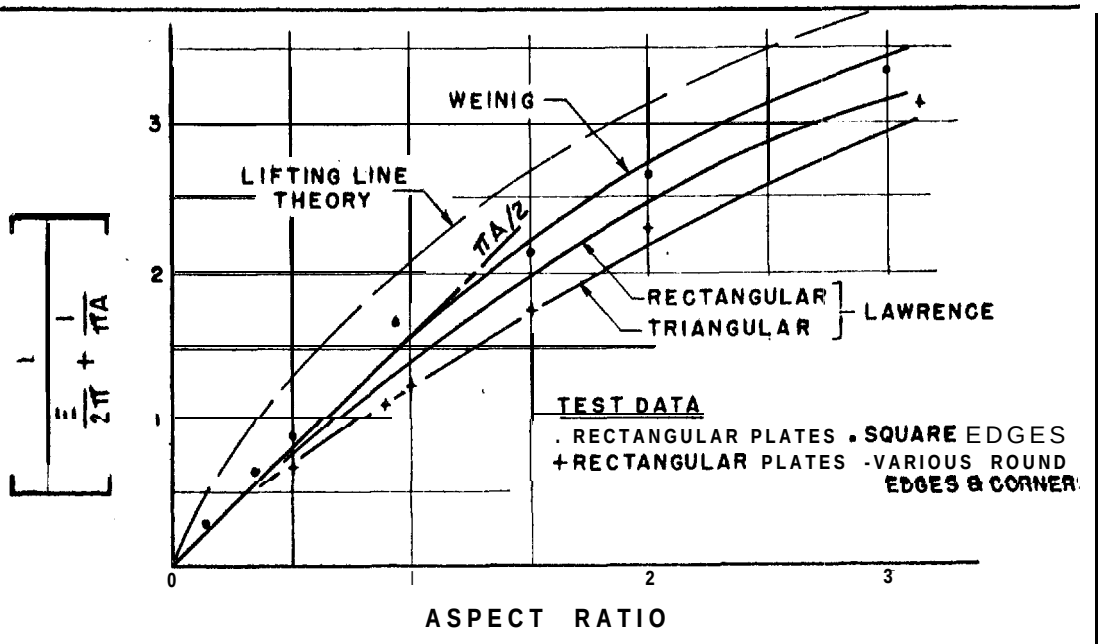

COMPARISON OF SMALL ASPECT RATIO THEORY & DATA

FIGURE 1.11

Various test data for rectangular foils have been analyzed by Hoerner*, and tke results are also shown in Figure 1.11. It is seen that the characteristics are dependent on the edge shape of the sections; those having square edges showing slightly greater lift than theory indicates while those having rounded edges and rounded corners are close to the theory for foils with triangular plan forms.

* in an unpublished memorandum

For foils of aspect ratio larger than 2.0, the angle of attack is usually small so that the second or non-linear term of equation (1.21) may be neglected, and the equation may then be rewritten:

$$\frac{d\alpha}{dC_L} = \frac{E}{2\pi} + \frac{1}{\pi A} \qquad (\text{FOR } A > 2) \qquad (1.23)$$

to which the planform, sweep and dihedral corrections can readily be applied, Thus, for the complete wing:

$$\left.\begin{aligned} \frac{d\alpha}{dC_L} &= \frac{1}{\cos\Lambda}\left[\frac{E}{2\pi\cos\Gamma} + \frac{1+\tau}{VA}\right] \\ \frac{dC_D}{d(C_L^2)} &= \frac{1+\delta}{\pi A\cos\Lambda} \end{aligned}\right\} \qquad (1.24)$$

where E is the lifting surface correction, $1\left[+\,2/A^2 \text{ FOR } A > 2\right]$

Λ is the angle of sweep

Γ is the angle of dihedral

τ, δ are the respective planform corrections.

5. The Influence of Fluid Boundaries

When the wing is operating close to a fluid boundary, its "free-flight" aerodynamic characteristics are modified, to an extent depending on the type of boundary and the distance of the wing from it.

There are two main types of boundary4 [illegible]

(a) the rigid boundary - the walls of a wind tunnel in which a wing is being tested, and the ground when an airplane is in the process of taking off or landing.

(b) the free boundary - the boundary of an "open-jet" tunnel, where a wing is being tested in a jet of air that is freely surrounded by the atmosphere. As will be shown below, this is also equivalent to the effect on one wing of an equal biplane.

The influence of fluid boundaries is treated in detail in many classical works[3,5] and will only be discussed briefly herein. For convenience, the term "ground effect" is used for the effect of a rigid boundary, and "biplane effect" for that of a free boundary. While the biplane effect need seldom be considered in modern

aerodynamics, it is basically involved in the influence of the water surface upon the characteristics of hydrofoils.

The presence of a rigid boundary at the distance h from the wing, as shown in Figure 1.12(a), affects the motion of the fluid about the tip vortices originating at the wing. By reasons of symmetry, this infuence is identical to that of a "mirror image" of the foil and vortex system at the same distance h beyond the boundary. (That is, the boundary can be replaced by the mirror image, in considering the effect on the wing.) It is easily seen that the downwash and the induced angle at the wing are reduced. As a consequence, the lift curve slope $dC_L/d\alpha$ is somewhat increased and the induced drag decreased in the presence of a rigid boundary.

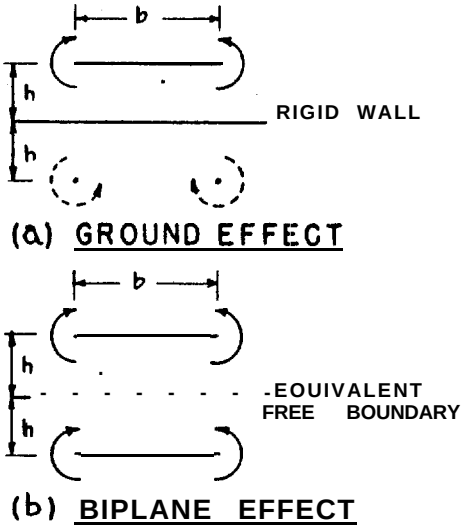

FIGURE 1.12

The biplane effect, on the other hand, produces the opposite results. Consider the biplane represented in Figure 1.12(b) with

the separation of 2h between the wings. Here, each wing provides the same lift and has identical vortex systems in the same direction, It is easily seen that the downwash and the induced angle at one wing are increased due to the vortex system of the other wing, in direct apposition to the ground effect discussed above. It can readily be shown that a free boundary a distance h from a wing can be replaced by a "biplane image" a distance $2h$ from the wing, and thus is equivalent to the "biplane" effect on one wing,

The influence of either the ground effect or biplane effect on the fnduced characteristics of the wing may be expressed as a factor, K, in the equation

$$\frac{d\alpha_i}{dC_L} = \frac{dC_{Di}}{d(C_L^2)} \qquad \frac{K}{\pi A} \tag{1.25}$$

The factor K is given in Figure 1.13*, as a function of h/b, K_b denoting biplane effect and K_g denoting ground effect, It is seen that at a given h/b the ground effect would decrease the fnduced terms by the same amount as the biplane effect would increase them, Whenh = o, the induced terms would vanish due to ground effect and

* See Figure 2.7, Chapter 2, for a more detailed graph.

would double due to biplane effect, when $K_b = Kg = 1.0$, the "free-flight" condition exists, i.e. no boundary effect.

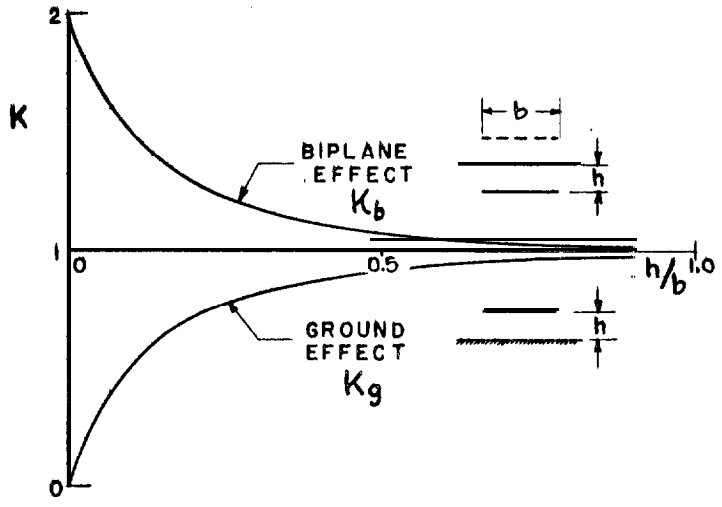

BIPLANE AND GROUND EFFECT FACTOR, K

FIGURE 1.13

For small values of h/b, corrections to K must be made for such things as the actual tip clearance of dihedraled or swept foils. Furthermore, there are the effects of the image of the lifting vortex which is also present (but which has *not* been shown) in the complete flow system near a boundary. Such image influences the foil section characteristics when the distance h is small as compared to the foil chord.

Usually, for aircraft the ratio h/b is sufficiently large so that these secondary influences are negligible, For hydrofoils, however, h/b is generally small and these effects must be considered, Therefore, the treatment of these secondary influences, as well as other boundary effects on the characteristics of hydrofoils, is given in Chapter 2,

6. Pitching Moment Characteristics

Foil Section Characteristics

As indicated in equations (1.5) and (1.6) above, the lift originating in a symmetrical foil section (due to angle of attack) can be represented as a single force applied approximately at the quarter-chord point, The lift due to camber, however, is centered at the half-chord point.

Taking the moments about the quarter-chord point, it is seen that the moment is only due to the lift developed by camber. Thus, from equation (1.6)

$$C_{m_{1/4}} = -\pi f/c \qquad (1.26)$$

and is a constant for any given foil section, f/c being the foil camber ratio, and is thus approximately independent of the magnitude of the lift.

Experimental data on airfoil sections[1,2] indicate that the value of the coefficient and the chordwise position are slightly different from the theoretical values given above. It is therefore usual to define the constant moment coefficient by

$$C_{m_{ac}}$$

which is taken about the aerodynamic center, or a.c.

Effect of Planform

The aerodynamic center and the corresponding moment coefficient for a complete wing depends on the geometry of the line of aerodynamic centers and the spanwise life distribution,

For wings employing the same section shape, $C_{m_{ac}}$ and the a.c. position are the same as for the foil section when the a.c. line is straight and normal to the direction of advance. (This applies to rectangular and tapered planforms without sweep, and is independent of lift distribution,)

For other cases, such as when sweep, twist and variations in section shape are employed, the effects must be determined as a function of geometry of the foil and the resultant lift distribution. Methods for determining the spanwise loading distribution for foils of arbitrary plan form are given by DeYoung and Harper[9].

In the particular case where the taper ratio bears a *certain* relation to the angle of sweep as indicated in Figure 1.14, the foil loading is elliptical and the aerodynamic center is given byx

$$a.c. = \frac{1}{4} + \frac{0.342 - 0.567\lambda - 0.908\lambda^2}{10(1+\lambda+\lambda^2)} A \tan \Lambda \qquad (1.27)$$

where λ = taper ratio (tip chord/root chord)

A = sweep angle

from which $C_{m_{ac}}$ can be determined.

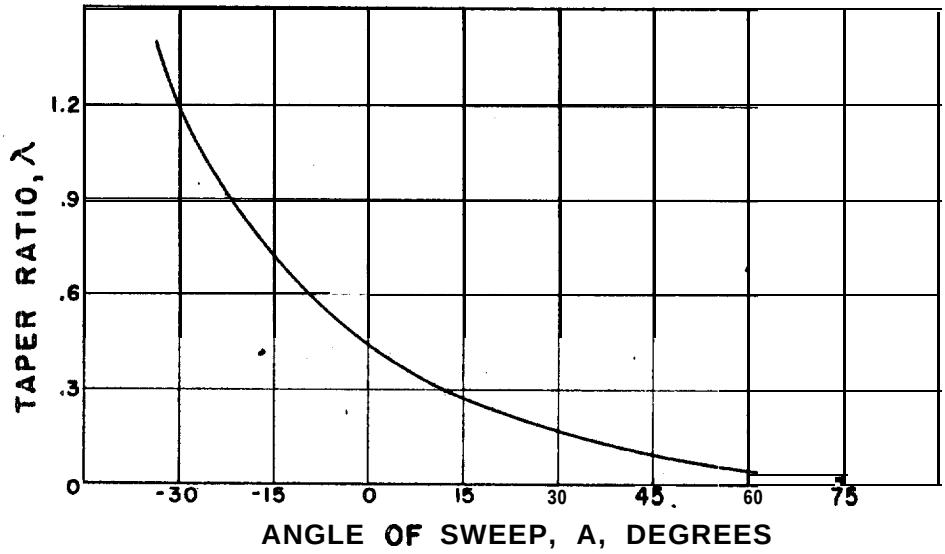

PLANFORM PARAMETERS FOR APPROXIMATE ELLIPTIC LOADING

FIGURE 1.14

Pitching moment characteristics of wings of various configurations are, however, most readily determined from wind tunnel tests. Thus, available test data on wings of various form (such as presented in references 10 and 11) can be utilized to determine the pitching moment of similar wings under consideration.

Small Aspect Ratio Wings

In his treatment of lifting surfaces, Lawrence15 also derives values of the aerodynamic center for rectangular and triangular wings of small aspect ratio. (Triangular wings were assumedto have the apex leading and the base trailing.) The values given in Figure 1.15 are for the linear portion of lift (the first term of equation 1.21), measured from the leading edge. The non-linear lift (second term of equation 1.21) is assumed to be uniformly applied over the planform, so that for the rectangular wing its center is at mid-chord, while for the triangular wing it is at the 2/3 chord position.

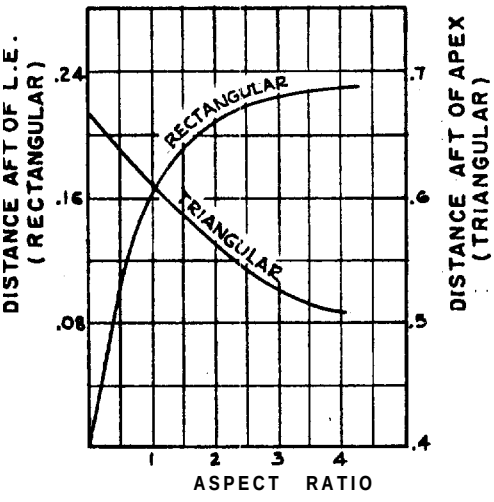

AERODYNAMIC CENTER FOR SMALL ASPECT RATIO FOILS

FIGURE 1.15

The effect of camber on the *moment* of small aspect ratio wings has not been investigated specifically. It is aasumed that the'lift due to camber is, applied at the mid-chord as for wings of larger aspect ratio.

7. Airfoil Drag

There are three basic types of drag (or resistance) that are experienced by an airfoil, which are

(a) the induced drag resulting from lift, as discussed above.

(b) the friction drag, resulting from the shear forces in the fluid at the body. As a function of the fluid velocity, these forces are set up tangential to the contour of the body, and the sum of the components in the direction of the free fluid flow represent the friction drag.

(c) the pressure drag, resulting from unequal pressures on the front and rear of the body. In a perfect fluid, the pressure (which acts normal to the contour of the body) would have components in the direction of free fluid flow which would sum up to zero, However, due to viscous effects, the pressures on the rear of the body are reduced, resulting in a net pressure drag. The magnitude of this drag depends primarily on the shape of the body, and is thus sometimes called "form drag".

The basic difference between friction drag and pressure drag can be best illustrated by considering the drag on a thin flat plate, as shown in Figure 1.16. When the plate lies parallel to the direction of flow, the 'drag is almost entirely frictional; when normal to the flow, entirely due to pressure. It is common procedure to couple friction and form drag together as "parasite drag", which is defined as that drag independent of, or not due to, lift.

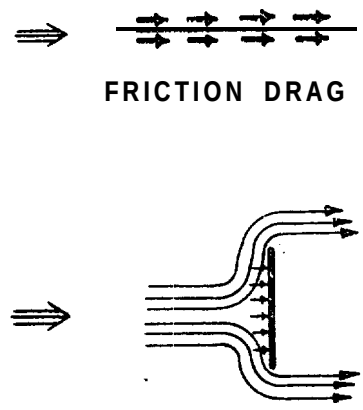

FRICTION AND PRESSURE DRAG ON A FLAT PLATE

FIGURE 1.16

Parasite drag is the most important component of the total drag on a foil in the high speed ranges of aircraft and hydrofoil craft, and is indeed an important consideration in all fields of fluid mechanics. A comprehensive treatment of the subject would be exhaustive and is not within the scope of this work,, Reference should be made to standard texts, Prandtl[3] for a presentation applicable to airfoils and to Hoerner[7] for a detailed treatment of the parasite drag of various aircraft components.

Since the standard naval architectural texts explain the concept of friction drag (frictional resistance of ships) and pressure drag (eddy making resistance), it is not considered necessary to dwell on the general aspects of this subject at this time. Particular application to hydrofoils is given in detail in following chapters.

It should be pointed out, however, that there are slight differences in the procedure of analyzing parasite drag as employed in aircraft and ship design. Airfoil drag coefficients are referred to the plan area of the wing, and other aircraft components (nacelles, fuselages, etc.) are referred to on the frontal or cross-sectional area; whereas the standard ship practice is to use the total wetted area of all submerged components. Furthermore, the marine industry has adopted the "Schoenherr line" for turbulent friction, whereas in aeronautics no standard has been adopted although the "Prandtl-Schlichting line" is in general favor.

The procedure employed herein is to use the reference areas employed in aerodynamics (except for hulls, where marine methods are retained) but basing the friction drag coefficients on Schoenherr's function,

8. Airfoil Data

The aircraft industry has published a wealth of information on airfoil characteristics.* The evolution of the characteristics of hydrofoils, as presented herein, has been accomplished by drawing heavily on this information, utilizing airfoil theory with such corrections as have been indicated by experimental data. This material has been applied directly or modified as required for surface effects, as can be seen in the chapters that follow.

Some of the data is of basic nature and is published in readily usable form so that it can be applied directly to the hydrofoil. Thus, NACA has published correlated section data on a wide variety of airfoil shapes[1,2,16], from which the basic section characteristics can be readily ascertained. Figure 1.17 shows a typical set of data available for one of the NACA series.

* See "Index of NACA Technical Publications" National Advisory Committee for Aeronautics, Washington, D. C.

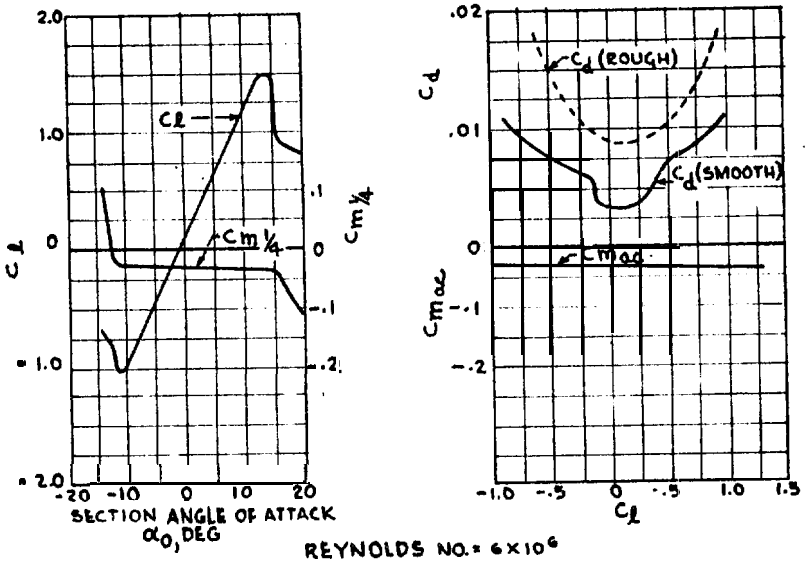

TYPICAL SECTION CHARACTERISTICS

FIGURE 1.17

From this particular data, the following two-dimensional characteristics can be found:

section lift coefficient

section lift curve slope

section drag coefficient (smooth and rough-various Reynolds numbers)

section moment coefficient (about the 1/4 chord and about the a.c.)

angle of zero lift

maximum lift coefficient

Data is also available on the characteristics of miscellaneous shapes and bodies, flaps, etc. as may be required for a detailed analysis of hydrofoils but which are too varied to allow individual treatment in the text that follows.

References

1. Abbott, von Doenhoff and Stivers — "Summary of Airfoil Data" NACA Report 824, 1945.

2. Abbott and von Doenhoff — "Theory of Wing Sections" McGraw-Hill, 1.949.

3. Prandtl and Tietjens — "Applied Hydro and Aero-mechanics" McGraw-Hill, 1.934.

4. Glauert — "Aerofoil and Airscrew Theory" MacMillan, 1944.

5. Durand — "Aerodynamic Theory" (6 Volumes) California Institute of Technology, 1943.

6. Hueber — "Properties of Tapered Wings" Zeitschr, Flugt, Motorluftsch, 1933.

7. Hoerner — "Aerodynamic Drag" Published by Author, 1951.

8. Toll and Queijo — "Approximate Relations and Charts for Low-Speed Stability Derivatives of Swept Wings", NACA Technical Note 1581, 1948.

9. DeYoung and Harper — "Theoretical Symmetrical Span Loading at Subsonic Speeds for Wings Having Arbitrary Plan Form" NACA Report 921, 1948.

10. Hieser and Whitcomb, — "Investigation of the Effects of a Nacelle on the Aerodynamic Characteristics of a Swept Wing and the Effects of Sweep on a Wing Alone" NACA Technical Note 1709, 1948.

11. Purser and Spearman — 'Wind-Tunnel Tests at Low Speeds of Swept and Yawed Wings Having Various Plan Forms" NACA Technical Note 2445, 1951.

12. Purser and Campbell — "Experimental Verification of a Simplified Vee-Tail Theory and Analysis of Available Data on Complete Models with Vee Tails" NACA Report 823, 1945.

13. Weinig — "Lift and Drag of Wings with Small Span" NACA Technical Memo 1151, 1947.

14. Weissinger — "The Lift Distribution of Swept-Back Wings" NACA Technical Memo 1120, 1947.

15. Lawrence — "The Lift Distribution on Low Aspect Ratio Wings at Subsonic Speeds" Journal of Aeronautical Sciences, October 1951.

16. Jacobs, Ward and Pinkerton — "Characteristics of 78 Related Airfoil Sections from Tests in the Variable-Density Wind Tunnel" NACA Report 460, 1935.

CHAPTER 2. SUBMERGED FOIL CHARACTERISTICS

Formulas are given for the lift produced by a fully submerged hydrofoil and for the effects due to lift, such as induced angle and induced drag, wave drag, and pitching moment. The effects of foil submergence and configuration are shown and examples given illustrating the use of the formulas. The principal formulas are summarized for convenient use and reference.

1. General Considerations

The hydrodynamic characteristics of hydrofoils operating in water are closely related to those of airfoil.3 operating in air. When the hydrofoil is so deeply submerged as to be considered operating in an infinite fluid, it is directly equivalent to the airfoil, taking into account the difference in density between water and air (and assuming that speeds are below those at which cavitation in water and compressibility in air would be influential).

In the practical case, the hydrofoil acts close to the water surface with a consequent effect on its hydrodynamic properties. This effect can be accounted for to some extent by classical airfoil treatment of the influence of fluid boundaries, but it also requires consideration of the gravity effect that is unique to a body operating near the water surface (the boundary between two fluids of great difference in density). This gravity effect produces an increase in drag on the foil and is represented physically by a wave system similar to that produced by a ship. (The wave system is treated in Chapter 6.)

The basic hydrofoil theory, therefore, takes into account all surface effects on a simple, fully submerged foil. From the relationships established from the theory, the "airfoil" effect3 and the "wave" effects can he separated and independently considered for general engineering application.

Corrections to the basic hydrofoil. characteristics for variations in foil geometry, the effects of struts and other appendages, and the influence of various operational factors can be readily and clearly indicated as functions of the "airfoil" and "wave" effects considered separately,

The hydrodynamic characteristics of the fully submerged foil are treated in this chapter along these lines; surface-piercing foils are treated in Chapter 3. The influence of cavitation has not been consfdered in the derivation of these foil characteristics. The conditions under which cavitation will occur, and the consequent effect on the foil properties are treated in Chapter 12,

2. Hydrofoil Theory

Two-Dimensional Theory

The concept of a rectilinear vortex advancing in a fluid has been used in the development of airfoil theory, as indicated in Chapter 1, It can be similarly used to develop hydrofoil theory, wfth the added condition that the vortex is located below a free water surface.

This case has been investigated by Kotchin[1], with the results that the lift is modified by the free surface and a drag on the vortex is produced (in association with a surface wave), The relationships are given as8

$$L = \rho V \Gamma b - b\rho\frac{\Gamma^2}{4\pi h}\Omega \tag{2.1}$$

$$D_w = \rho g \frac{\Gamma^2 b}{V^2} e^{-2gh/V^2} \tag{2.2}$$

where L is the lift

D_w is the "wave drag"

b is the span (considered to be infinite in the two-dimensfonab case)

h is the depth of submergence

V is the fluid velocity

Γ is the value of the circulation

ρ is the fluid density

g is the acceleration of gravity

and

$$\Omega = \left[1 - \frac{4gh}{V^2} e^{-2gh/V^2} \int_{-\infty}^{2gh/V^2} \frac{e^x dx}{x} \right]$$

Equation (2.1) indicates that the lift of the vortex in infinite fluid (the first term of the'equation, as shown in Chapter 1) is modified by an image system due to the proximity of the free surface. This image system changes the magnitude and direction of the fluid flow, resulting in a change in lift, indicated in equation (2.1) and a drag of the "induced" type, equation (2.2). It can be seen from the equations that both the drag and the change in lift reduce to zero as the submergence approaches infinity, thus reducing to the case for the foil in infinite fluid.

Values of the factor Ω are given in Figure 2.1 as a function

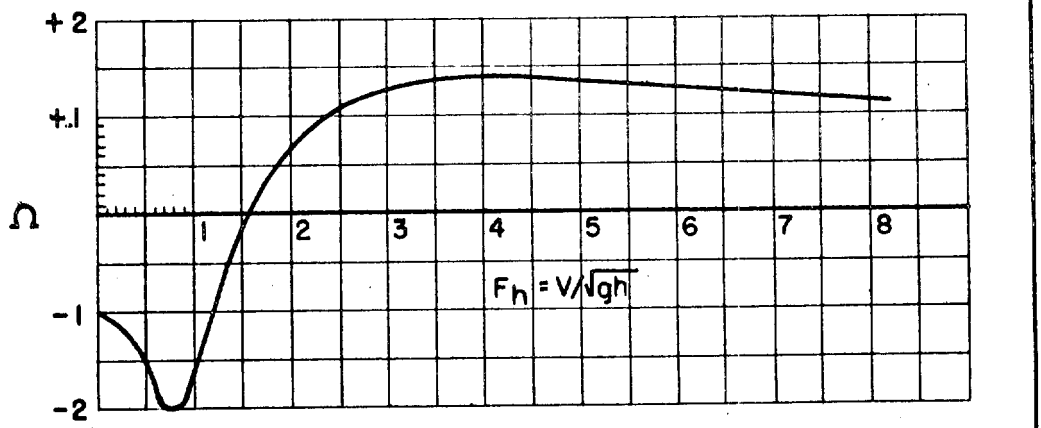

FIGURE 2.1

of the Froude number, $F_h = V/\sqrt{gh}$. It is seen that in the limiting cases

$$\Omega = -1.0 \quad \text{at} \quad F_h = 0$$

$$\Omega = 1.0 \quad \text{at} \quad F_h = \infty$$

and thus, from equation (2.1), the image system is- seen to be that of a"mirror" image at $F_h = 0$ and a "biplane" image at $F_h = \infty$, as indicated in Figure 2.2. In these cases, the image "produces" a change in fluid velocity past the vortex, but no change in fluid direction. Thus, the wave drag must be zero and is so indicated in evaluating equation (2.2) at these limiting Froude numbers. (At $F_h = \infty$, only when the submergence is not zero.)

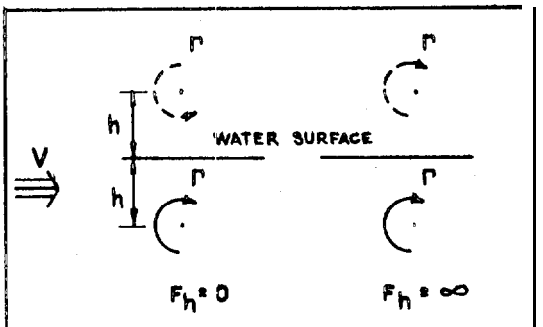

VORTEX SYSTEMS AT LIMITING FROUDE NUMBERS

FIGURE 2.2

For practical applications of hydrofoil craft, the speed is high and the foil submergence is relatively low so that the Froude number, $F_h = V/\sqrt{gh}$, is high, Insofar as the effect on fluid velocity is concerned, the value $\Omega = 1.0$ (from Figure 2.1) may be generally used without serious error.

Then, equation (2.1) may be written

$$L = \rho \Gamma (V-\mu) b \tag{2.3}$$

or $$\Gamma = \frac{C_L c}{2}\left(\frac{V}{V-\mu}\right)^2$$

where $\mu = \Gamma/4\pi h$, the decrease in fluid velocity at the vortex due to its biplane image.

$$C_L = L/\rho_2 V^2 S$$

Thus, the equation for the lift of the vortex near the free surface can be treated as that of a vortex in infinite flufd with the velocity $(V-\mu)$ instead of V. From Chapter 1, then, the circulation around the equivalent foil section can be written

$$\Gamma = \pi c \alpha_o (V-\mu) \tag{2.4}$$

where c is the foil chord

α_o is the angle of attack of the foil in two dimensions (measured from the angle of zero lift for cambered foils),

From equations (2.2), (2.3) and (2.4), the lift and drag can be derived for the foil, in coefficient forms

$$C_L = 2\pi\alpha_o \left(\frac{V-\mu}{V}\right)^2 \tag{2.5}$$

$$C_{D_W} = \left(\frac{V}{V-\mu}\right)^2 \frac{c}{h}\left(\frac{e^{-2/F_h^2}}{2F_h^2}\right) C_L^2 \tag{2.6}$$

where $C_{D_W} = D_W / \rho_{\frac{1}{2}} V^2 S$

$F_h = V/\sqrt{gh}$

$\left(\frac{e^{-2/F_h^2}}{2 F_h^2}\right)$ is given in Figure 2.6 as a function of F_h

Noting that $u = \Gamma/4\pi h$, the value of $\left(\frac{V-u}{V}\right)^2$ can be determined from equation (2.4),

$$\left(\frac{V-u}{V}\right)^2 = \left(\frac{1}{1 + c\alpha_0/4h}\right) \qquad (2.7)$$

At normally small angles of attack, the effect on the fluid velocity is negligible for submergences of over 1 chord, and

$$\left(\frac{V-u}{V}\right)^2 \approx 1.0 \qquad \text{when } h/c > 1.0$$

As the submergence decreases, however, the effect on lift becomes important. Furthermore, with a foil of finite chord, the Influence of the vortex image must be considered over the entire chord, instead of only at the lifting line as heretofore assumed,

Finite Chord Corrections

When the submergence is small, the curvature of the flufd flow due to the vortex image appreciably affects the lift characteristics of the foil. seetfon. Thfs can be treated by a simple approximate method familiar in aerodynamics[2], which is to consider the flow components at

a "control" point 1/2 chord behind the location of the lifting vortex, as indicated in Figure 2.3. The downward velocity component due to both vortices a% this point is then

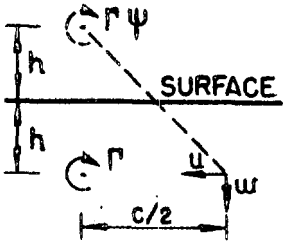

FIGURE 2.3

$$w = \frac{\Gamma}{2\pi}\left[\frac{1}{c/2} + \frac{c/2}{4h^2 + c^2/4}\right] \tag{2.8}$$

and the reduction in horfaontal velocity

$$u = \frac{\Gamma}{2\pi}\left[\frac{2h}{4h^2 + c^2/4}\right] \tag{2.9}$$

Now to satisfy the condition that there is no fluid flow through the foil, the angle of attack must be equal to the angle of fluid flow, or

$$\alpha_0 = \frac{w}{V-u}$$

which by combining equatfons (2.3) and (2.9) is

$$\alpha_0 = \left(\frac{V}{V-u}\right)^2\left[\frac{1}{2\pi} + \frac{1}{2\pi\left[(4h/c)^2+1\right]}\right] \tag{2.10}$$

to which must be added the "induced" wave angle. From equatfon (2.6)

$$\alpha_w = \frac{C_{D_w}}{C_L} = \left(\frac{V}{V-u}\right)^2 \frac{c}{h}\left(\frac{e^{-2/F_h^2}}{2F_h^2}\right) C_L \tag{2.11}$$

Combining equations (2.3) and (2.9), and noting that for small values of u/V, hfgher powers can be disregarded,

$$\frac{4\,h/c}{2\pi\left[(4h/c)^2+1\right]} C_L = \frac{u(V-u)}{V^2} \approx \frac{u}{V} \tag{2.12}$$

and

$$\left(\frac{V}{V-u}\right)^2 \simeq 1 + 2\frac{u}{V} = 1 + \mathcal{U} C_L \tag{2.13}$$

where $$\mathcal{U} = \frac{4\,h/c}{\pi\left[(4h/c)^2+1\right]}$$

The total foil angle (measured from the angle of zero lift) and the total wave drag coefficient can then be found by substitution of terms:

$$\alpha = (1+\mathcal{U}C_L) C_L \left[\frac{1}{2\pi} + \frac{\mathcal{U}}{8h/c} + \frac{c}{h}\left(\frac{e^{-2/F_h^2}}{2F_h^2}\right)\right] \tag{2.14}$$

$$C_{D_w} = (1+\mathcal{U}C_L) C_L^2 \frac{c}{h}\left(\frac{e^{-2/F_h^2}}{2F_h^2}\right) \tag{2.15}$$

The derivatives $d\alpha/dC_L$ and $dC_{D_w}/d(C_L^2)$ are similar in form, except that the respective factors for the effective fluid velocity are

$$(1 + 2uC_L)$$

$$(1 + 3/2\, uC_L)$$

instead of

$$(1 + uC_L)$$

Equations (2.14) and (2.15) are the basic equations for the hydrofoil in two dimensions* and indicate the following effects of the free surfaces

(a) The wave effects, as a function of submergence Froude number $V/\sqrt{gh}$ and submergence/chord ratio h/c. At infinite Froude number or infinite h/c, the wave effects disappear.

(b) The finite chord effect, as a function of h/c. At values of $h/c > 1.0$, the value of u becomes negligible,

* Complete- theories for the two-dimensional foil with finite chord have been advanced by Kotchin[3] and Keldysch-Lavrentiev[4] but the effects are not as clearly illustrated as in the treatment above, Krienes[5] evaluated the case for large Froude numbers (i.e. negligible wave effects) and the results agree closely with those given above.

The Foil of Finite Span

For the foil of finite span, there is the additional influence of the trailing vortex system. In Chapter 1, the induced effects on a finite wing in the presence of a fluid boundary were shown to be

$$\left(\frac{d\alpha}{dC_L}\right)_i = \frac{dC_{D_i}}{d(C_L^2)} = \frac{K}{\pi A}$$

which were added directly to the airfoil properties in two dimensions, to give the total wing characteristics,

However, this procedure cannot be used in the case of the hydrofoil, Both the finite chord and wave effects in two dimensions are modified by finite span considerations; and the airfoil induced effects are modified by the influence of gravity, Therefore, the hydrofoil of finite span must be investigated as an entity. The concept of separate, additive terms will be useful however in evaluating the characteristics of the foil, as till later be shown.

In the development of the theory of the hydrofoil of finite span, the vortex line concept is used. Finite chord effects are not considered herein, but will be re-introduced later.

The hydrodynamics of the vortex line of finite span in the vicinity of the free surface (and in infinitely deep water) have been investigated by several authors[6,7,8]. Reference should be made to the original works for the details and proeedure required to determine the theoretical

characteristics of the hydrofoil, since the expressions derived are rather complicated and do not lend themselves to simple formulation or evaluation.

Qualitatively, however, the characteristics can be shown to be composed of three major components, as follows:

(a) The aerodynamic induced effects of a foil in the presence of a rigid wall, This is identical to the ground effect discussed in Chapter 1, wherein the induced angle is modified by the factor, K_g .

(b) The lateral wave induced effect, due to the trailing vortex system (the trailing vortices from the foil tips and their images above the water surface), The induced factor varies with Froude number, from the limiting value $O_{(F=o)}$ to $(K_b - K_g)_{(F=\infty)}$, where K_b is the biplane factor,

The total effect of the above components added together results in a function similar to Ω , which is given in Ffgure 2.1 above.

(c) The transverse wave induced effect., due to the lifting vortex system (the lifting line vortex at the foil and its fmages above the free surface), This is similar to the two-dimensional wave effect discussed above, but decreases in magnitude as the submergence/span ratio increases.

Breslin[8] evaluated the drag of a foil of aspect ratio 10 at a submergence/span ratio of 0,084, The results for an assumed elliptical. lift distribution are shown in Figure 2.4, with the effect of each component befng indicated,

Practical Considerations

As indicated above and as shown in Figure 2.4, the combined aerodynamic and lateral wave effect is similar to the function given for the two-dimensional, case (compare Figure 2.1); and as in that case, it may be considered equivalent to the biplane effect at high Froude numbers. That is, the induced angle of the foil in infinite fluid is modified by the biplane factor, K_b .

However, Figure 2.4 indicates that the difference in transverse wave drag between the three-dimensional theory and the two-dimensional theory is significant. Evaluation of the three-dimensional formula is so arduous that it appears more reasonable for 'engineering purposes to use the two-dimensional formula, reduced by a suitable factor. Arbitrarily the factor $(K_b - 1)$ is used, which factor has a simple correlation to that used for the effect of the trailing vortices. Thus, the equation for the induced lift angle is in the presence of the free surface:

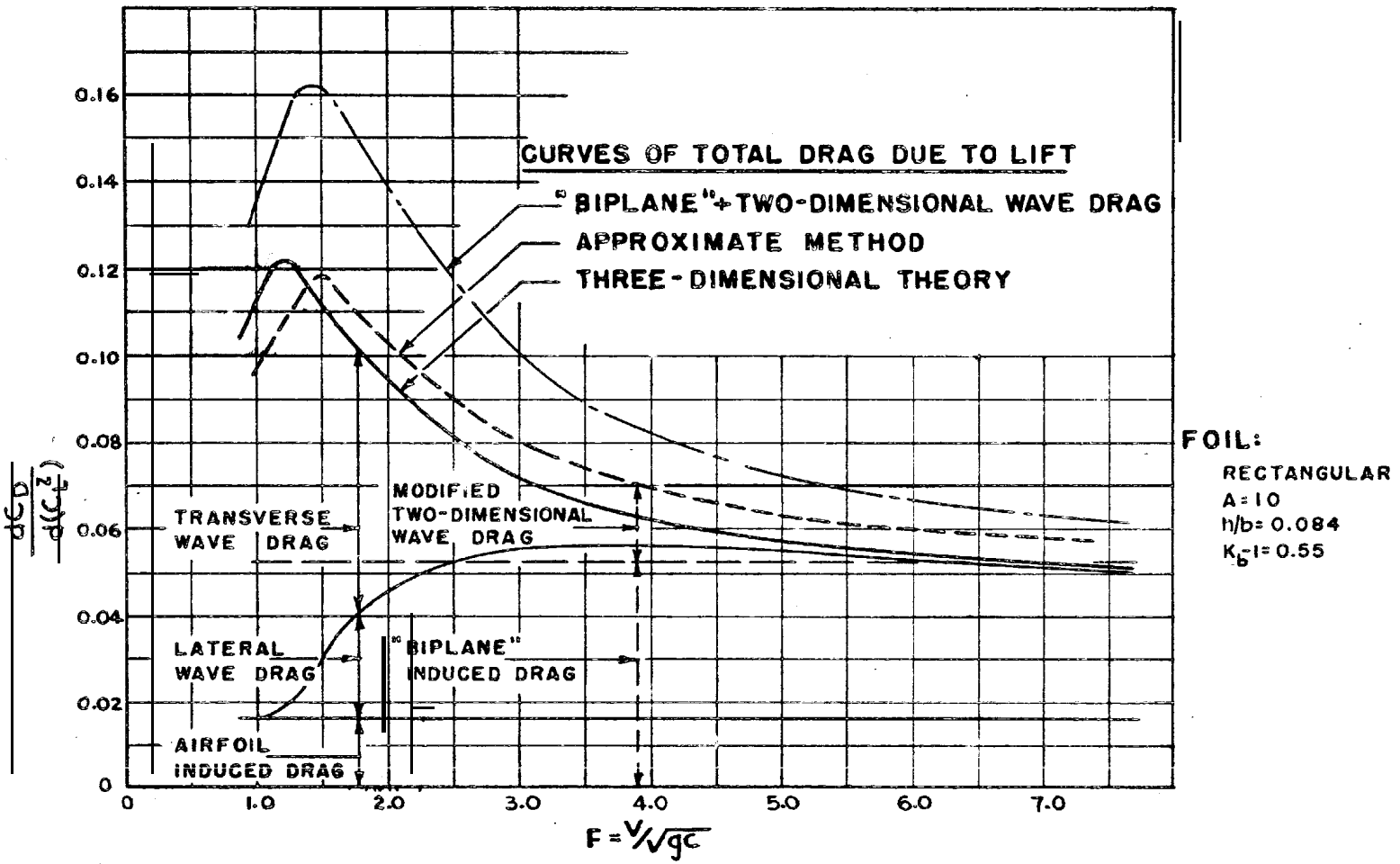

COMPARISON OF THEORETICAL VS SIMPLIFIED DRAG DUE TO LIFT

FIGURE 2.4

$$\frac{d\alpha_i}{dC_L} = \frac{K_b}{\pi A} = \frac{1}{\pi A} + \frac{K_b - 1}{\pi A}$$

$$= \left(\frac{d\alpha_i}{dC_L}\right)_\infty + \left(\frac{d\alpha_i}{dC_L}\right)_\infty (K_b - 1)$$

and the transverse wave lift angle is

$$\frac{d\alpha_w}{dC_L} = \left(\frac{d\alpha_w}{dC_L}\right)_0 (K_b - 1)$$

where $\left(\frac{d\alpha_i}{dC_L}\right)_\infty$ is the indueed lift angle in infinite fluid

$\left(\frac{d\alpha_w}{dC_L}\right)_0$ is the wave lift angle in two-dimensional flow.

From this, the following concept can be stated:

> The induced angle of a foil of finite span in infinite fluid is increased by two additive terms as the foil approaches the free water surface, One of these is due to the effect of the surface on the trailing vortices, the other on the lifting vortex, Each of these terms is modified in the same degree by a common factor that depends on the submergence-span ratio of the foil.

The use of thfs factor $(K_b - 1)$ for the transverse wave effects may have little theoretical justification, but is considered to be of the proper magnitude, Applying this factor to the ease shown in Figure 2.4, the total drag is seen to agree reasonably with that derived by the complete theory,

3. Basic Foil Characteristfes

As indicated in the preceding section, the hydrodynamic characteristics of the hydrofoil are approximately given as the sum of two distinct components:

(a) The aerodynamic characteristics of a foil operating near a free fluid boundary. These are identiffed as the basic airfoil effects, denoted by the subscript a in the equations.

(b) The additional transverse wave effects (occurring in the presence of the water surface. These are identified as the wave effects, denoted by the subscript w in the equations.

The basic airfoil effects are given in Chapter 1. For the hydrofoil, however, the finite chord and reduced fluid velocity corrections must be added to account for small foil submergence. The correction terms involving $\mathcal{U}$ (introduced in the preceding section for the two-simensional case) must then be added. For finite foils, the values of $\mathcal{U}$ have been calculated along the span, and the average value determined. Thus, the airfoil terms can be shown to be:

$$\left(\frac{d\alpha}{dC_L}\right)_a = (1+2\mathcal{U}C_L)\left[\frac{E}{2\pi} + \frac{\mathcal{U}}{8h/c} + \frac{1+T}{\pi A}K\right] \tag{2.16}$$

$$\frac{dC_{D_a}}{d(C_L^2)} = \left(1+\frac{3}{2}\mathcal{U}C_L\right)\frac{1+\delta}{\pi A}K \tag{2.17}$$

where u is the factor denoting change in fluid flow, and is given in Figure 2.5

E is the lifting surface correction, $1 + 2/A^2$

τ, σ are the respective planform correction terms, given in Chapter 1

U is the biplane factor, generalized to account for various foil configurations, as later indicated. For the basic foil, the factor is K_b given in Figure 2.7.

The wave effects are readily determined from the hydrofoil theory given in the preceding section:

$$\left(\frac{d\alpha}{dC_L}\right)_w = (1 + 2uC_L)\frac{c}{h}\left(\frac{e^{-2/F_h^2}}{2F_h^2}\right)(K_b - 1) \qquad (2.18)$$

$$\frac{dC_{Dw}}{d(C_L^2)} = (1 + \tfrac{3}{2}uC_L)\frac{c}{h}\left(\frac{e^{-2/F_h^2}}{2F_h^2}\right)(K_b - 1) \qquad (2.19)$$

Values of $\left(\frac{e^{-2/F_h^2}}{2F_h^2}\right)$ and $(K_b - 1)$ are given in Figure 2.6.

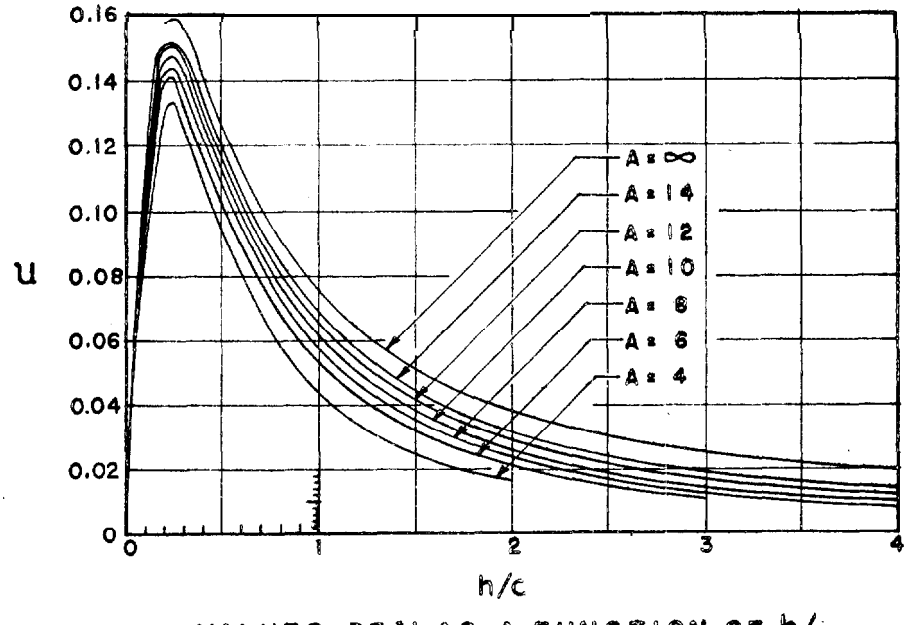

VALUES OF u AS A FUNCTION OF h/c

FIGURE 2.5

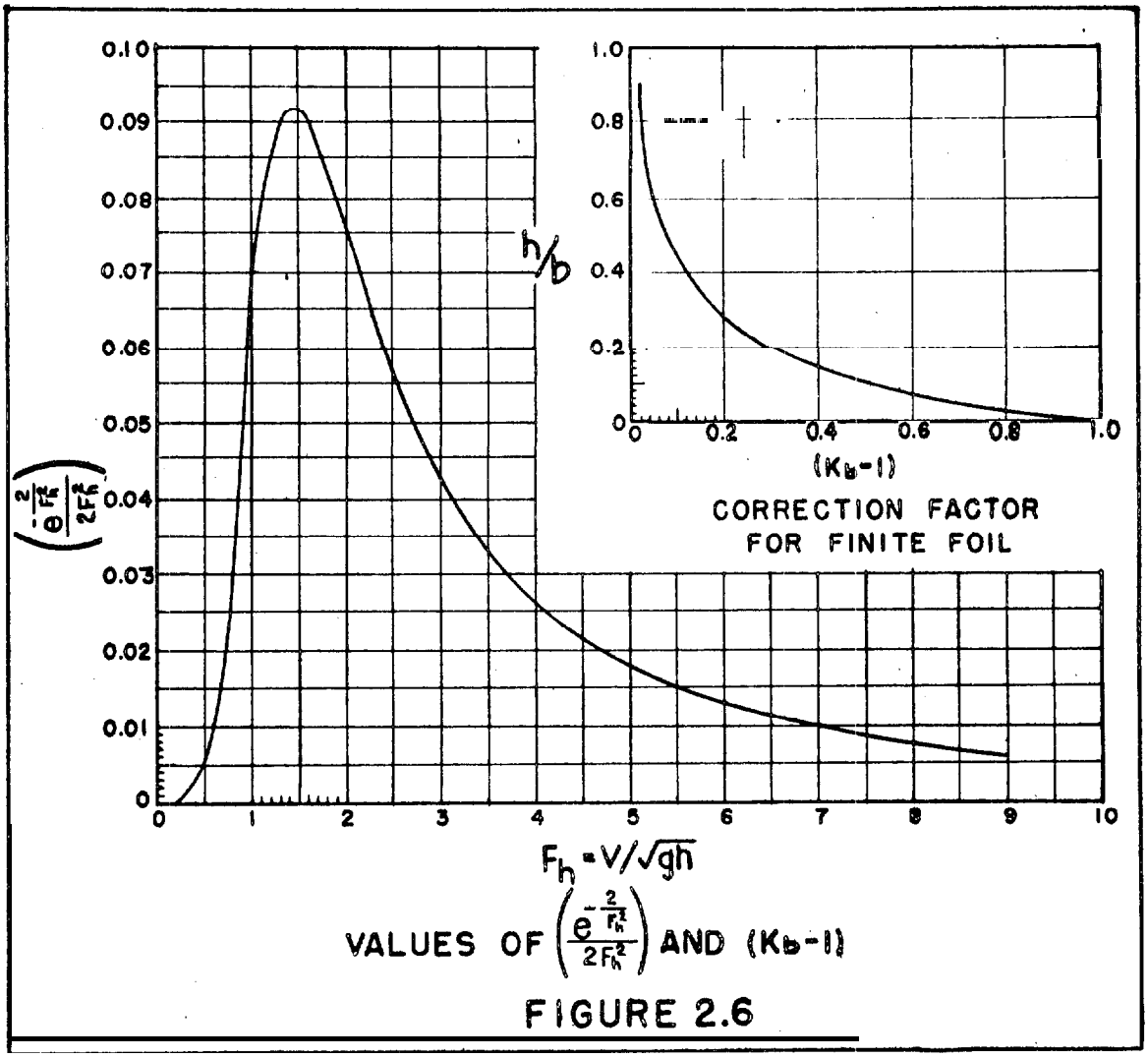
0.10
0.09
0.08
0.07
0.06
0.05
0.04
0.03
0.02
0.01
0
h/b
1.0
0.8
0.6
0.4
0.2
0
0.2
0.4
0.6
0.8
1.0
(Kb-1)
CORRECTION FACTOR
FOR FINITE FOIL
0
1
2
3
4
5
6
7
8
9
10
Fh = V/√gh
VALUES OF (e^(-2/Fh²) / 2Fh²) AND (Kb-1)

FIGURE 2.6

Shallow Water Corrections

Operations in shallow water affect both the airfoil and wave induced characteristics. For the airfoil components, the induced effects are reduced by the usual ground effect, but this involves such extremely shallow water (depth from foil to bottom of 1/2 foil span or less) that it is not a practical operating condition and can be ignored,

However, the wave induced components are influenced in moderately deep water by the presence of the bottom, depending on the speed at which the foil is travelling. Thus, when the depth of water is less than V^2/g (or the craft speed is above the critical value, $V_c = \sqrt{gd}$) the transverse wave effects vanish. In the subcritical range, the wave effects are modiffed to some extent which has not been determined.*

Tentatively, the following factor is proposed for correcting the wave drag in shallow water operations:

$$\left.\begin{aligned} \eta &= 1 - \left(\frac{V}{V_c}\right)^2 = 1 - V^2/gd \quad \text{for } V < \sqrt{gd} \\ \eta &= 0 \quad \text{for } V \geq \sqrt{gd} \end{aligned}\right\} \quad (2.20)$$

by which the wave induced effects, equations (2.18) and (2.19) should be multiplied.

---

* A two-dimensional theory of wave drag in shallow water has been advanced by Meyer[9], but shows little correlation with model tests of finite span foils. The test results[10,11] are also obscure in that, the actual shallow water effect cannot be determined, because there are no experimental results on the wave drag in deep water to afford comparison.

Summary of Basic Foil Characteristics

The total effects of the foil are then determined by adding the two components, thus:

$$\frac{d\alpha}{dC_L} = \left(\frac{d\alpha}{dC_L}\right)_a + \left(\frac{d\alpha}{dC_L}\right)_w \tag{2.21}$$

$$\frac{dC_D}{d(C_L^2)} = \frac{dC_{D_a}}{d(C_L^2)} + \frac{dC_{D_w}}{d(C_L^2)} \tag{2.22}$$

where for the simple, horizontal foil the airfoil effects are given in equations (2.16) and (2.17) and the wave effects in equations (2.18) and (2.19). In the following sections of this chapter, the effects of struts and other appurtenanoes, changes in foil geometry, etc. are considered as they affect the airfoil characteristics of the simple foil. The wave induced effects are not considered changed from that given above (except where specifically noted), The total characteristics would still be expressed as the sum of the airfoil and wave effects, but with modified values as required.

DESIGN EXAMPLE NO. 2.1

SH 1 OF 2

DETERMINE THE CHARACTERISTICS OF A FULLY SUBMERGED FOIL

THE FOIL IS RECTANGULAR, WITH A SPAN OF 20FT. AND A CHORD OF 2 FT., OPERATING' AT A SUBMERGENCE OF 3 FT.

DETERMINE THE EFFECTS AT SPEEDS OF 30,35 & 40KNOTS AT AN AVERAGE WATER DEPTH OF 200 FT.

PARTICULARS

$A = 10$

$h/c = 1.5$

$h/b = 0.15$

V =	50.7	59.2	67.6	(ft/sec)
$Fh = V/\sqrt{gh}$ =	5.16	6.02	6.89	
V^2/gd =	040	0.54	0.71	

AIRFOIL EFFECTS

$E = 1.02$

$U = 0.04$ (Figure 2.5)

$K = K_b = 1.37$ (Figure 2.7).

$\tau = 0.228$

$\delta = 0.078$ } (Figure 1.8 of chapter I)

From Equation (2.16):

$$\left(\frac{d\alpha}{dC_L}\right)_a = (1+0.08C_L)\left[\frac{1.02}{2\pi} + \frac{0.04}{12} + \frac{1.228\times1.37}{10\pi}\right]$$

$$= 0.219(1+0.08C_L, I$$

From Equation (2.17)

$$\frac{dC_{Da}}{d(C_L^2)} = (1+0.06C_L)\left(\frac{1.078\times1.37}{10\pi}\right.$$

$$= 0.047(1+0.06C_L)$$

DESIGN EXAMPLE NO. 2. t

WAVE EFFECTS

From Figure 2.6

$\frac{e^{-2/Fh^2}}{2\,Fh^2}$ -- **0.017**, 0.013, 0.0105

K_b-1 = 0.37

From Equations (2.18), (2.19), and (2.20)

$$\left(\frac{d\alpha}{dC_L}\right)_w = (1+0.08\,C_L)\frac{0.37}{1.5}\times$$

$0.017(1-0.40) = 0.0025(1+0.08\,C_L)$

$0.013(1-0.54) = 0.0015(1+0.08\,C_L)$

$0.0105(1-0.71) = 0.00075(1+0.08\,C_L)$

$$\frac{dC_{Dw}}{d(C_L^2)} = \begin{matrix} 0.6025\ (1+0.06\ CL) \\ 0.0015\ (1+0.06\ C_L) \\ 0.00075(1+0.06\ C_L) \end{matrix}$$

TOTAL EFFECTS

Assume a design C_L = **0.50 at 30 Knots**

V KNOTS	C_L	$\left(\frac{d\alpha}{dC_L}\right)_a$	$\left(\frac{d\alpha}{dC_L}\right)_w$	$\frac{dC_{Da}}{d(C_L^2)}$	$\frac{dC_{Dw}}{d(C_L^2)}$	TOTAL $\frac{d\alpha}{dC_L}$	TOTAL $\frac{dC_D}{d(C_L^2)}$
30	0.50	0.228	0.003	0.049	0.003	0.231	0.052
35	0.368	0.225	0.002	0.048	0.002	0.227	**0.050**
40	**0.288**	0.224	**0.001**	0.048	**0.001**	0.225	0.049'

4. Effects of Struts, End Plates and Nacelles

The changes in induced effects due to struts, end plates, nacelles and other similar attachments to the foil can be #considered due to two separate causes:

First, a favorable effect due to the retarding of spanwise flow. This is the commonly known "end plate effect" and may be considered as a redistribution of trailing vortices along the surface of the attached member rather than the foil, resulting in a reduction of induced angle and drag. Theoretical analyses have been made for airfoils and the results are readily adapted to hydrofoils,

Second, an adverse effect (generally) which is a function of the thickness (spanwise extent) of the attachment. This effect is generally identified as "interference" and is due to the interruption of spanwise lift distribution and/or due to the constriction in flow past the body,, Analysis of test data is the most suitable means for evaluatfng this effect.

End Struts and End Plates

Analysis of the biplane, boxplane and end plate effects on airfoils have been made by several authors, and are as given by Durand[12]. Hoerner[13] has shown these effects referred to a hydrofoil, and the

functions are reproduced in Figure 2.7 in terms of the factors, K, by which the basic airfoil induced effect must be modified, Thuso

K_b is the hydrofoil "biplane" effect, a function of

K_{bo} is the hydrofoil with end struts, "boxplane" effect, a function of

K_e is the end plate effect, a function of

The following relationships are seen to exist, approximately%

$$K_{bo} = K_b \frac{1}{1 + h/b} \tag{2.23}$$

$$K_e = \frac{1}{1 + 2h_e/b} \tag{2.24}$$

The end plate effect,&, is derived for a foil in infinite fluid with a pair of end plates of actual height, h_e. However, for the hydrofoil, the end plate effectiveness is modified by the presence of the free surface and an effective end plate wefght must be substitued for the actual height in equation (2.24).

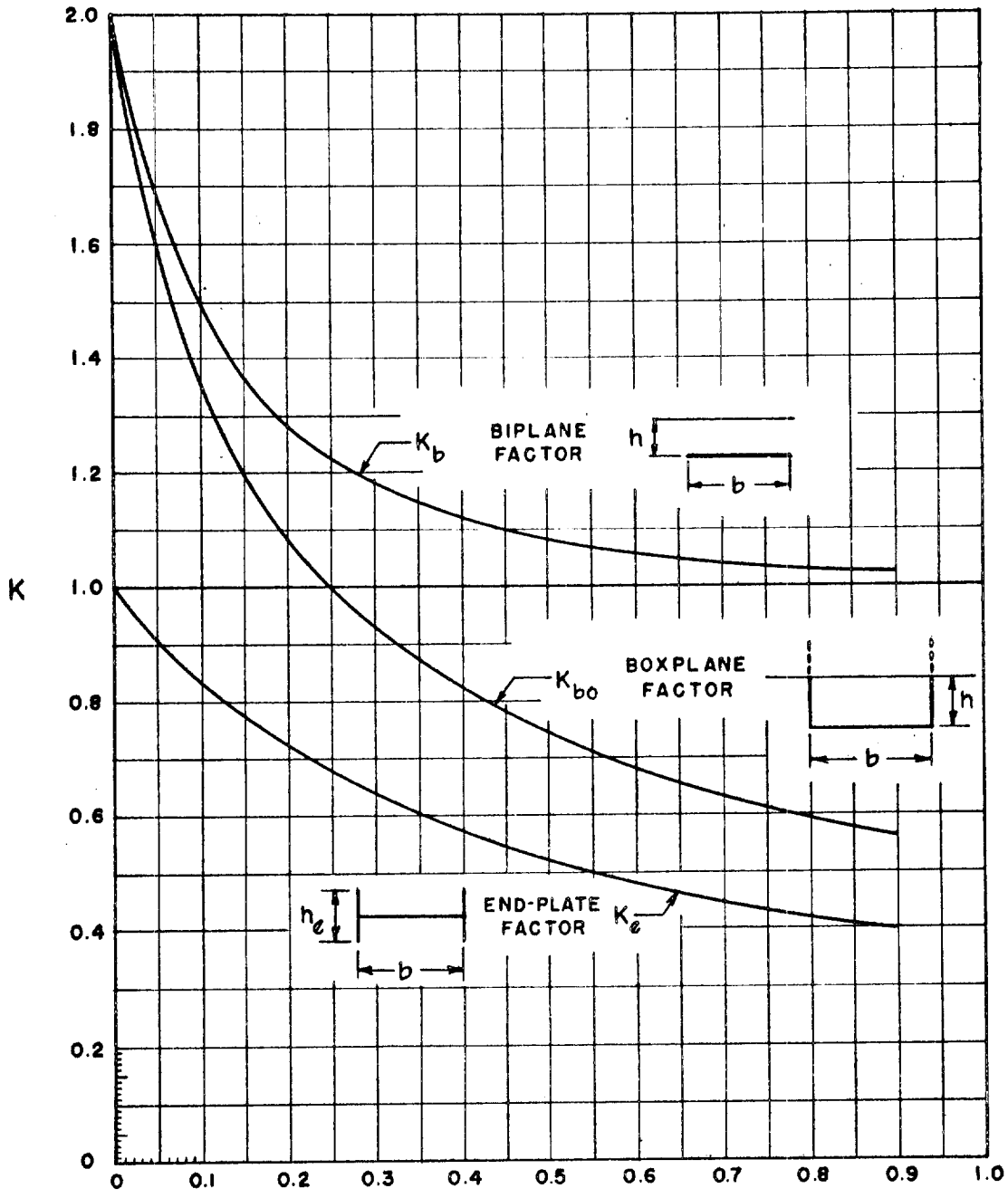

BIPLANE AND END PLATE FACTOR, K

FIGURE 2.7

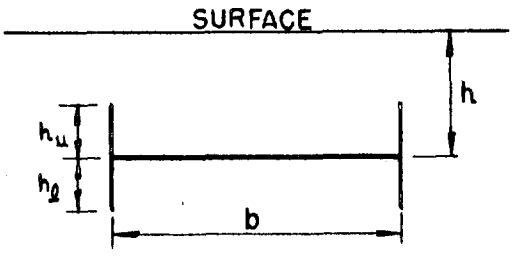

FIGURE 2.8

From Figure 2.8, considering the upper portion of the end plate only, the end plate effect approaches the boxplane condition when the ratio h_u/h approaches 1.0, and the effective end plate height is then 1/2 that of the actual height, from equations (2.23) and (2.24). For the lower portion of the end plate, the effectiveness is increased as h/h_ℓ approaches zero (due to the influence of its image), so that at $h/h_\ell = 0$, the effective end plate height is twice the actual height.*

Thus, depending on submergence, the effective height varies between 1/2 and 1.0 for the upper end plate and between 2.0 and 1.0 for the lower end plate. An empirical formula to determine

* This can be visualized as follows! the biplane image of the trailing vortex reduces the spanwise flow of fluid on the upper foil surface (inward) and increases the spanwise flow on the lower surface (outward), Therefore, the upper end plate is less effective, the lower end plate more effective than in infinite fluid.

the total end plate effectiveness at a submergence, h , is as follows

$$\left(\frac{h_e}{b}\right)_{eff} = \frac{h_u}{b}\left(\frac{2h-h_u}{2h}\right) + \frac{h_\ell}{b}\,\frac{2(h+h_\ell)}{2h+h_\ell} \qquad (2.25)$$

Effect of Struts and Plates Inboard of Foil Tips

The effectiveness of struts and end plates is reduced as the member is moved inward from the foil tips. Mangler[14] calculated the effectiveness of end plates in various spanwise positions on an airfoil and the results are shown by Hoerner[13] to be a function of the spanwise position, a/b , and the end plate height, h_e/b . It can be shown that a good approximation for any h_e/b is that the effective height is reduced in the ratio

$$\left(\frac{a}{b}\right)^3$$

where $a/2$ is the distance of the plate from the midspan of the foil. Assuming this correction to apply for both plates and struts for the hydrofoil, the total K factor can then be determined for the hydrofoil. Thus, for a foil of the configuration shown in Figure 2.9:

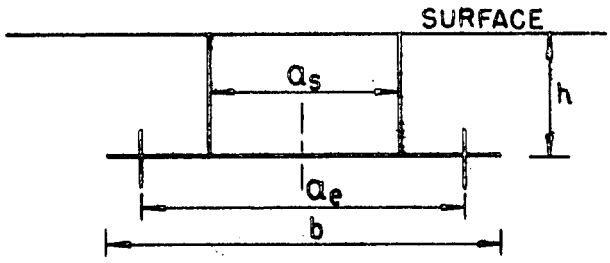

FIGURE 2.9

$$K = K_b \left[\frac{1}{1 + \left(\frac{a_s}{b}\right)^3 \frac{h}{b} + 2\left(\frac{a_e}{b}\right)^3 \left(\frac{h_e}{b}\right)_{eff}} \right] \qquad (2.26)$$

where $\left(\frac{h_e}{b}\right)_{eff}$ is determined from equation (2.25).

DESIGN EXAMPLE NO. 2.2

SH 1 OF 1

DETERMINE THE K FACTOR FOR THE FOLLOWING CONFIGURATION.

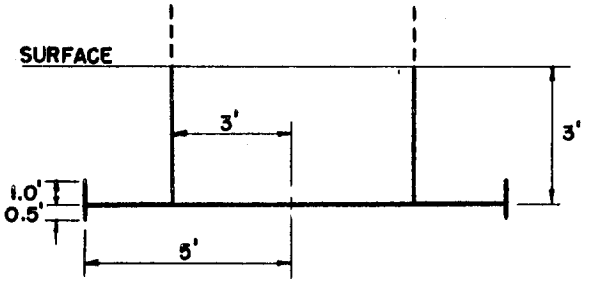

AVERAGE CHORD = 1.5 FOR FOIL, STRUTS & END PLATES

BIPLANE FACTOR

From Figure 2.7

$K_b = 1.183$ (at $h/b = 0.3$)

END-PLATE EFFECTIVENESS

From Equation (2.25)

$$\left(\frac{he}{b}\right)_{eff} = \frac{1}{10} \times \frac{5}{6} + \frac{1}{20} \times \frac{7}{6.5} = 0.136$$

TOTAL K FACTOR

From Equation (2.26)

$$K = 1.183 \left[\frac{}{1+(0.3)^3 0.3 + 2x0.136_3} \right] \frac{1.183}{1.280}$$

$$= 0.924$$

End Plate Effect of Nacelles

It has been shown by Hoerner[15] that a nacelle (wing tank) of cylindrical shape has an effective end plate height of 1/2 the diameter of the nacelle., When located at the wing tip, however, this effect is counteracted by the rolling up of the trailing vortices more readily due to the round tfp, with a consequent reduction in effective span equal to 1/2 the nacelle diameter, Thus, in this case, when considering the overall span to the outside of the nacelle, there is no end plate effect,

However, in order to formulate the end plate! effect for all spanwise locations of the nacelle, the nominal span may be considered to be between centers of the tfp nacelles. Then, adding the end plate effect, the same net relationshfp is derived. As indicated in Figure 2.10, the total end plate effect of nacelles can be estimated by considering:

(a) the height is equal to 1/2 the rounded part of the nacelle plus the full height of any flat sides

(b) the spanwise location is measured to the center of the nacelle,

With these dimensions, the effect can then be calculated on the basis of the end plate formulas derived above.

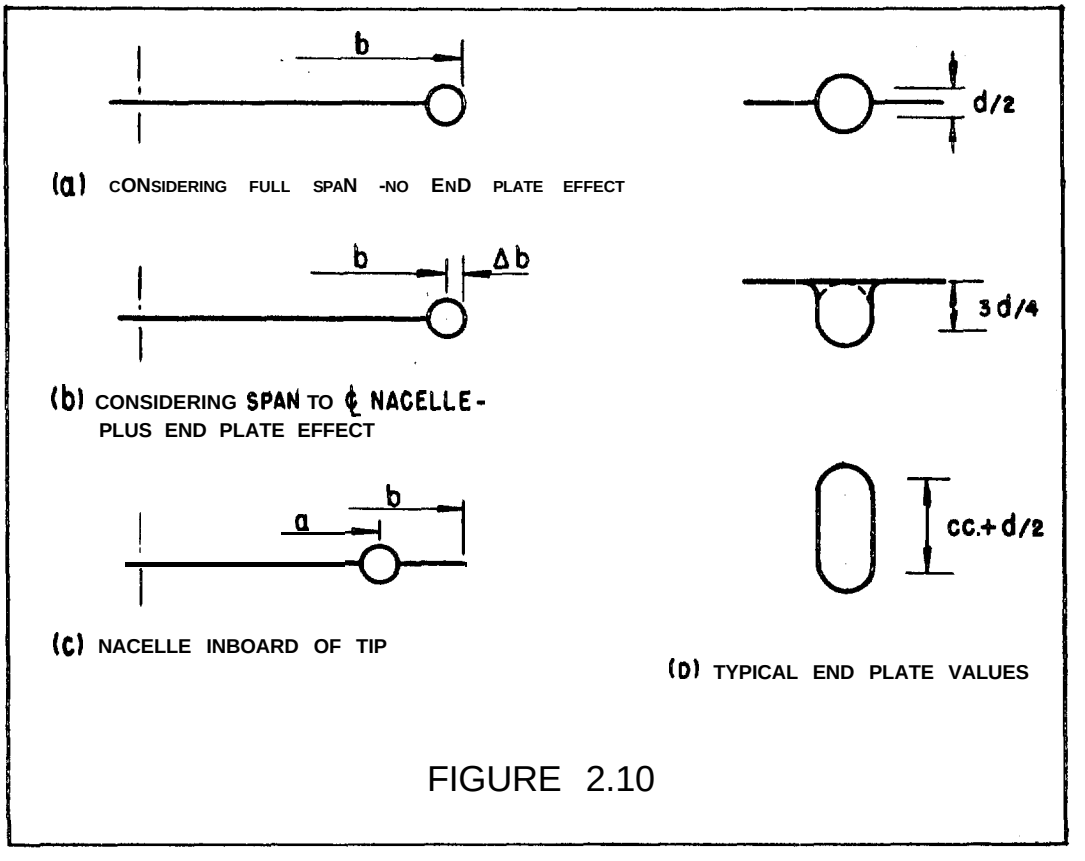

FIGURE 2.10

Effect of Lateral Area on End Plate Effect

The above formulations for struts, end plates and nacelles have been derived on the basis of these members having a chord (longitudinal extent) equal to that of the foil. However, depending on the total lateral area of the member, and the shape of that area, the effect may be greater or smaller than indicated above. There are no definite formulas available to account for this effect, but tendencies can be noted, as in Figure 2.11. Generally, where these

members are full at the foil and tapering towards the upper and/or lower ends they are more effective than those (such as struts) that are full at the ends and taper towards the foil. For rectangular or near rectangular members, the effective height may be considered to vary directly as the ratio of the mean chord of the lateral area to the chord of the fofl.

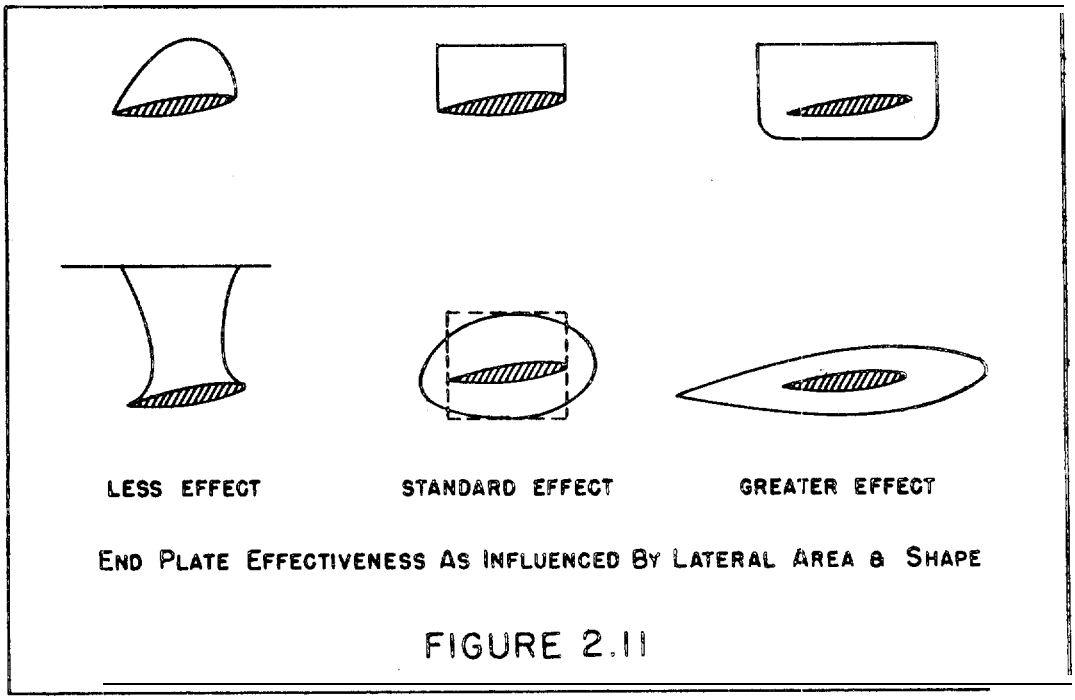

END PLATE EFFECTIVENESS AS INFLUENCED BY LATERAL AREA & SHAPE

FIGUKE 2.11

Interference

The "interference" effects arise due to the disruption of flow at the foil caused by the superposition of other bodies on the foil. Such interferences cause additional viscous effects (as treated in Chapter 4) and additional induced effects.

The lift induced effects are due to disruption of spanwise distribution of lift; i.e. the superimposed body removes a portion of lift-producing foil area, causing a reduction in lift and a redistribution of lift along the remaining span of the foil. Opposing this effect, the constriction of fluid flow at the sides of the body results in super-velocities of the fluid and thus a local increase of foil lift at the intersection.

Test data[13] indicates that the overall effect of a foil-strut intersection is to reduce the lift (or increase the induced angle and induced drag for a given lift). A simple analytical expression can be derived for this effect by assuming the lift to be lost over that portion of the foil span occupied by the struts, t_s, and neglecting the effect of super-velocities, By further assuming the upper foil surface develops 2/3 of the total lift, it can be shown that the interference effect on the lift angle slope and the induced drag may be approximately expressed as

$$\left.\begin{aligned} \frac{d\alpha}{dC_L} &= (1+\eta)\left[\frac{d\alpha}{dC_L}\right] \\ \frac{dC_D}{d(C_L^2)} &= (1+\eta)^2\left[\frac{dC_D}{d(C_L^2)}\right] \end{aligned}\right\} \quad (2.26a)$$

where $\left[\frac{d\alpha}{dC_L}\right]$, $\left[\frac{dC_D}{d(C_L^2)}\right]$ are the values derived without interference effects

η is a factor which depends on the strut thickness, foil span and spanwise location of the strut, This is given by

$$\eta = 0.8\, t_s/b \left[1 - (a/b)^3\right]$$

t_s/b is the maximum strut thickness to foil span ratio

a/b is the strut location ratio, as given above.

The above relationships are given for each strut on the upper surface of a foil, where the junction is well-filleted, and as such agrees well with experimental data. For other conditions, the value of η given above must be multiplied bys

(a) the number of struts

(b) 1/2 - for lower surface struts

(c) 2 - for unfilleted junction8

It should be noted that the above relationship represents the interference effect of a foil-strut junction as a function of lift (or angle of attack). It is not known exactly whether this effect is induced or parasitic in nature; for convenience it is represented herein as induced, The interference effect at zero lift is essentially parasitic and is given in Chapter 4.

The induced interference effect8 of nacelles are more difficult to evaluate, being sensitive to nacelle size and position. Theoretical investigation8[12, 16] indicate that the effect8 of superimposed nacelles of small extent on the induced characteristics of wings are small. Test data[17] on wing-fuselage intersections indicates that,

an increase in induced drag is accompanied by an increase in lift, both effects being minimized by appropriate fairings at the junctions. Therefore, in the absence of specific test data for considered foil-nacelle configurations, the interference effect of nacelles may be neglected.

DESIGN EXAMPLE NO. 2.3

DETERMINE THE K FACTOR FOR THE FOLLOWING FOIL- STRUT -NACELLE CONFIGURATION.

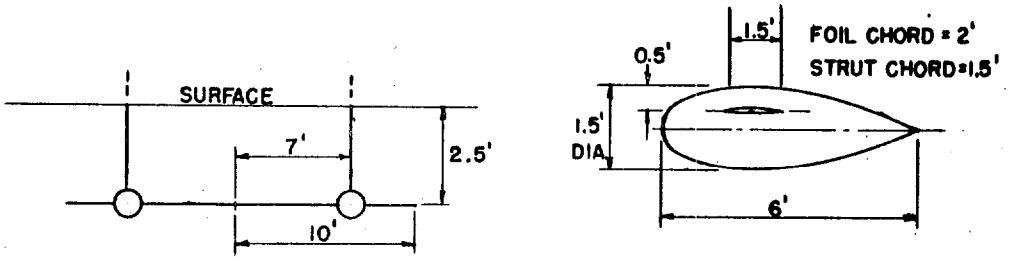

BIPLANE FACTOR

From Figure 2.7 ; $K_b = 1.42$ (at $h/b = 0.125$)

END · PLATE EFFECTIVENESS

struts - The strut effect ive height is $2.5 \times \frac{1.5}{2} = 1.875$

Nacelles

Assume an effective nacelle length of 3.5 f.t. Then the effective heights are

$h_u = 0.5\,(3.5 - 1.5)/2 = 0.50$ (deducting strut chord)

$h_l = 1.0 \times 3.5/2 = 1.75$

Then, from equation (2.25)

$$\left(\frac{h_e}{b}\right)_{eff} = \frac{0.50}{20} \times \frac{4.5}{5} + \frac{1.75}{20} \times \frac{8.5}{6.75} = 0.133$$

TOTAL K FACTOR

From Equation (2.26)

$$K = 1.42 \left[\frac{1}{1 + (0.7)^3 \frac{1.875}{2} + (0.7)^3 \times 0.133 \times 2}\right] = \frac{1.42}{1.234}$$

$$= 1.15$$

5. Effects of Planform. Sweep and Dihedral

Effects of Planform

Corrections to the induced angle and induced drag for a wing not having elliptical lift distribution have been indicated in Chapter 1. The corrective factors are $(1+\tau)$ and $(1+\delta)$ respectively, τ and δ being derived from the methods indicated,

In the presence of a free surface or in an equivalent biplane, the value of the planform corrections and their relationship to the biplane factor are not exactly known., Glauert[18] proposed that τ and δ derived for the monoplane be added directly to the biplane factor to give combined factors $(\tau + K)$ and $(\delta + K)$. It appears more convenient to apply each factor independently, so that the combined factors are

$$K(1+\tau) \quad \text{and} \quad K(1+\delta)$$

with little loss in accuracy. This latter method is used herein, as indicated in equations (2.16) and (2.17) above.

In regard to the wave induced effects, it has been shown by Breslin[8] that uniform lift distribution results in less wave effects than elliptical distribution. Dependfng therefore on the relative magnitude of airfoil effects and wave effects,, the optimum planform is probably somewhat between the elliptical and rectangular, However,

the difference is small at high Froude numbers, and in view of the empirical correction already applied to the wave effects of a finite foil, equations (2.18) and (2.19), the effect of planform may be disregarded in numerical computations of wave effects,

Effects of Sweep

As shown in Chapter 1, the effect of sweep may be expressed as

$$\left(\frac{d\alpha}{dC_L}\right)_\Lambda = \frac{1}{\cos\Lambda}\left(\frac{d\alpha}{dC_L}\right)_o + k\left(\frac{d\alpha}{dC_L}\right)_i \qquad (2.27)$$

where Λ is the angle of sweep

$\left(\frac{d\alpha}{dC_L}\right)_o$ is the section lift angle, a function of the lifting vortex

$\left(\frac{d\alpha}{dC_L}\right)_i$ is the induced lift angle, a function of the trailing vortices

k is a factor, determined from specific test data.

It was also shown that $k \approx 1/\cos\Lambda$ generally, and so in the absence of specific test data,

$$\left(\frac{d\alpha}{dC_L}\right)_\Lambda = \frac{1}{\cos\Lambda}\left(\frac{d\alpha}{dC_L}\right)$$

$$\frac{dC_{D_\Lambda}}{d(C_L^2)} = \frac{1}{\cos\Lambda}\,\frac{dC_D}{d(C_L^2)} \qquad (2.28)$$

where $\left(\frac{d\alpha}{dC_L}\right)$ and $\frac{dC_D}{d(C_L^2)}$ are the complete airfoil functions in the absence of sweep.

For deeply submerged hydrofoils, the above relationships can be used, substituting the appropriate values of $\left(\frac{d\alpha}{dC_L}\right)_a$ and $\frac{dC_{D_a}}{d(C_L^2)}$ given in equations (2.16) and (2.17) for the airfoil effects. The wave effects are unchanged, the average submergence of the swept foil being used in equations (2.18) and (2.19).

However, at small submergence, the above relationships are not expected to be accurate when large angle of sweep are employed. The biplane effect derived from the relatively simple lifting line theory is considered inadequate to show the influence of the swept geometry and the variation in submergence (between the midspan and tip of the foil at angles of attack).

The wave induced effects would also be modified 'by these factors, considering the interference in the waves generated along the span.

It is therefore necessary to obtain test data on hydrofoils of large sweep and low submergences before accurate characteristics can be determined.

Effects of Dihedral

The effects of dihedral on a fully submerged foil can be estimated from the two established conditions for which the foil properties are known. Thus, as indicated in Chapter 1, dihedral does not affect the induced characteristics for a foil in infinite fluid; while for a foil

with the tips touching the surface (surface-piercing foil), the induced effects are equivalent to those of a foil with end struts (boxplane condition) at the' submergence $h = b \tan \Gamma/4$, as is shown in Chapter 3 following.

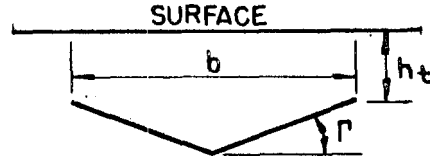

FIGURE 2.12

The effects of dihedral for any submergence can then be estimated from the following

$$K_\Gamma = K_b \frac{1 + h_t/b}{1 + h/b} \qquad (2.29)$$

where Γ is the dihedral angle

h_t/b is the tip submergence/foil span ratio

h/b is the average foil submergence ratio, $h_t/b + \tan \Gamma/4$

K_b is the biplane coefficient (as may be modified by other factors given previously) for the average submergence ratio,,

It is seen that at large values of h_t/b, K_b approaches 1.0. At $h_t/b = 0$ (surface-piercing foil), K_Γ Es equal to the boxplane effect given in equation (2.23) for a submergence of $\frac{b \tan \Gamma}{4}$.

As indicated in Chapter 1, the effect of dihedral modifies the foil section angle by the factor $1/\cos \Gamma$. The total effect of

dihedral on the airfoil lift angle can then be written

$$\left(\frac{d\alpha}{dC_L}\right)_\Gamma = \left(\frac{d\alpha}{dC_L}\right)_o \frac{1}{\cos\Gamma} + \left(\frac{d\alpha}{dC_L}\right)_i \frac{(1 + h_t/b)}{(1 + h_{t/b} + \frac{\tan\Gamma}{4})} \qquad (2.30)$$

where $\left(\frac{d\alpha}{dC_L}\right)_o$ and: $\left(\frac{d\alpha}{dC_{iL}}\right)_i$ are the lift angles for the foil without dihedral (at the mean submergence $h = h_t + \frac{b \tan\Gamma}{4}$)

α is the foil angle measured at the foil midspan in the vertical plane.

The wave effects can be estimated by using the submergence $h = h_t + \frac{b \tan\Gamma}{4}$ in equations (2.18) and (2.19).

DESIGN EXAMPLE NO. 2.4

SH 1 OF 1

DETERMINE THE K FACTOR FOR A SUBMERGED FOIL HAVING SWEEP AND DIHEDRAL

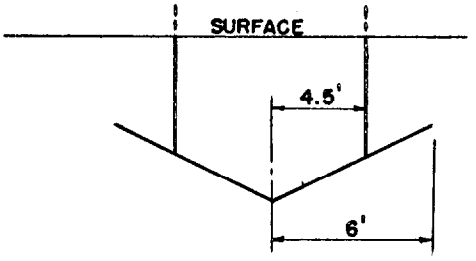

DIHEDRAL, Γ = 15°
SWEEP, Λ = 30°
FOIL CHORD = 2 FT.
STRUT CHORD = 2 FT.
TIP SUBMERGENCE = 2.5 FT.

DIHEDRAL EFFECT

From Equation (2.29)

$$h/b = h_t/b + (\tan\Gamma)/4 = 2.5/12 + 0.268/4 = 0.275$$

From Figure 2.7

$$K_b = 1.20$$

Then,

$$K_\Gamma = 1.20\ \frac{1+2.5/12}{1+0.275} = 1.137$$

SWEEP EFFECT

From Equation (2.28), taking K_Γ as the necessary K_b

$$K_{\Lambda,\Gamma} = K_\Gamma/\cos 30° = 1.313$$

STRUT EFFECT

Since some "end-plate" effect is achieved by dihedral, as above, the actual strut length is used (instead of average submergence)

Then, $h_s/b = \dfrac{2.5 + 1.5\tan 15°}{12} = 0.24$

TOTAL K FACTOR

$$K_{s,\Lambda,\Gamma} = 1.313\left[\frac{1}{1+\left(\frac{4.5}{6}\right)^3 \cdot 0.24}\right] = \frac{1.313}{1.101}$$

$$= 1.193$$

6. Foils of Small Aspect Ratio

For hydrofoils of small aspect ratio operating at a greater submergence than 1 chord or 1 span (whichever foil dimension is larger), the airfoil formulas for lift and drag given in Chapter 1 should apply.

At smaller submergences, the biplane images will have an effect as heretofore shown, with several important distinctions. As indicated in Figure 2.13, the bound vortex fmage acts on the foil at a point $c/2E$ behind the lifting vortex (as suggested by DeYoung and Harper[19]). Also, since angles of attack tend to be large for small aspect ratio foils, thfs must be considered in determining u and w , as shown. Thus, the image effects are not linear and must be determined for each indfvidual case,

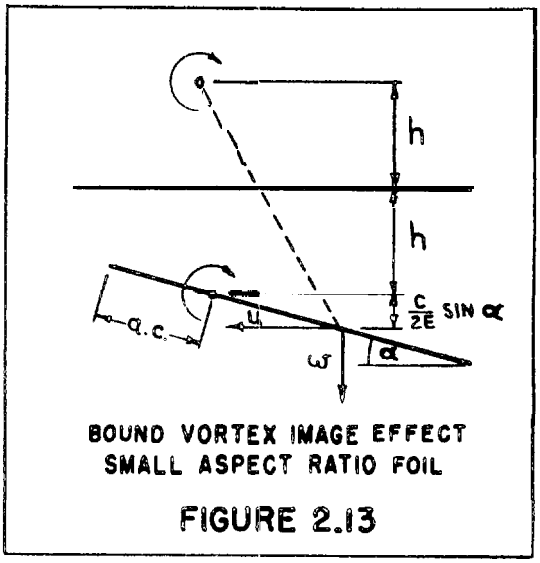

BOUND VORTEX IMAGE EFFECT
SMALL ASPECT RATIO FOIL

FIGURE 2.13

Generally, the expression for the lift would have the following form:

$$C_L = f(u)\left[\frac{1}{\frac{E}{2\pi} + f(w) + \frac{K}{\pi A}} \sin\alpha + 2\sin^2\alpha\cos\alpha\right] \qquad (2.31)$$

where $f(u)$ and $f(w)$ must be determined,

Since foils of small aspect ratio are not considered of general or important application in hydrofoil craft, the above factors have not been evaluated. Tests[20] have been conducted on foils of A = 1/4 and A = 1.0 at various small submergencea and the data can be utilized directly in estimating the lift, drag and pitching moment characteristics of similar foils.

7. Pitching Moment Characteristics

For deeply submerged foils, the pitching moment characteristics given in Chapter 1 for airfoils may be used without serious error. Thus, the pitching moment and the aerodynamic center can be determined from airfoil section characteristics (either theoretical or experimental) and applied over the foil when the "equivalent wing" lift distribution is ascertained,

For foils of shallow submergence (one chord or less), the pitching moment characteristics are expected to be affected by the influence of the vortex images, particularly when the foil employs large angles of sweep and dihedral. It is considered necessary to run tank tests on the configuration when accurate pitching moment characteristics are required (particularly in cases where controllable foils are employed, pivoting around some given axis).

For preliminary purposes and where simple planforms are employed, the pitching moment characteristics can be estimated from the following considerations,,

The biplane image of the lifting vortex has been shown to cause an increase in section lift angle; or, inversely, it causes a decrease in section lift at a given angle of attack. This is due to the curvature of the fluid flow at the foil, which may be considered

equivalent to a reduction in effective foil camber. Thus, there is an increment of lift acting downward at the mid-chord position. This increment of lift can be shown to be

$$\left.\begin{aligned} \Delta C_L &= - \frac{dC_l}{d\alpha_o} \cdot \Delta\alpha_o \\ &= - \frac{2\pi}{E} \cdot \frac{u}{8h/c} \cdot C_L \end{aligned}\right\} \quad (2.32)$$

where $\frac{dC_l}{d\alpha_o}$ is the lift slope of the foil in infinite fluid

$\Delta\alpha_o$ is the increase in section lift angle due to the vortex image

u is given in Figure 2.5.

For foils of large aspect ratio $A \simeq 10$, the two-dimensional value of u can be used without serious error (see equation 2.13), and equation (2.32) reduces to

$$\Delta C_L = \frac{C_L}{\left[(4h/c)^2 + 1\right]} \quad (2.33)$$

The forces on the foil can then be represented as shown in Figure 2.14. $C_{m_{ac}}$ and the a.c. position in infinite fluid, and can be found as indicated in Chapter 1. The total foil pitching moment characteristics can then readily be determined.

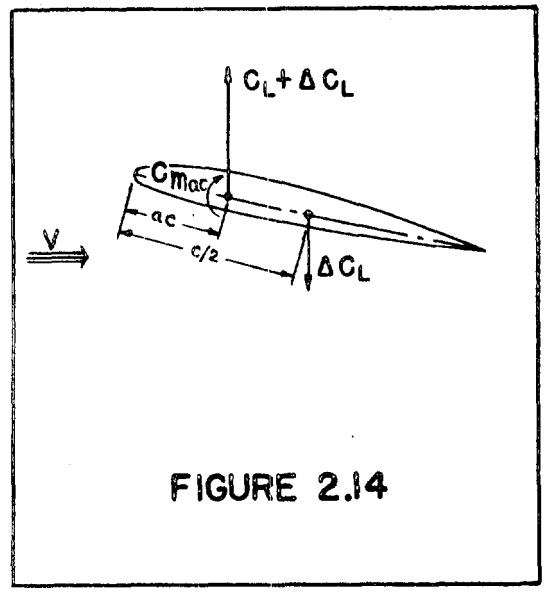

FIGURE 2.14

It is seen that the value of ΔC_L increases with decrease of submergence, and the center of pressure correspondingly moves forward towards the leading edge. Available test data[20] on the center of pressure of hydrofoils shows qualitative agreement with the relationships given above,

8. Summary of Submerged Foil Characteristics

Angle of Attack

The basic equation for the "lift angle" (inverse lift curve slope) is

$$\frac{d\alpha}{dC_L} = \left(\frac{d\alpha}{dC_L}\right)_o + \left(\frac{d\alpha}{dC_L}\right)_i + \left(\frac{d\alpha}{dC_L}\right)_w \qquad (2.34)$$

$$= (1+2\tau C_L)\left[\left(\frac{E}{2\pi}+\frac{\tau'}{\partial h/c}\right)\frac{1}{\cos\Lambda\cos\Gamma}+\frac{(1+\tau)}{\pi A}K+\frac{h}{c}\left(\frac{e^{-2/F_h^2}}{2F_h^2}\right)(K_b-1)\right]$$

from which

$$\alpha - \alpha_{L_0} = (1+\tau C_L)C_L\ [\ \text{same}\ ] \qquad (2.35)$$

where $\left(\frac{d\alpha}{dC_L}\right)_o$ is the foil sectfon lift angle, a function of the lifting vortex and its biplane image

$\left(\frac{d\alpha}{dC_L}\right)_i$ is the airfoil induced lift angle, a function of the trailing vortices and their biplane images

$\left(\frac{d\alpha}{dC_L}\right)_w$ is the wave induced lift angle, a function of the gravity image system

α_{L_0} is the angle of zero lift, measured in the same plane as A . The section angle of zero lift must be corrected: $\alpha_{L_0} = (\alpha_{L_0})_o \frac{\cos\Lambda}{\cos\Gamma}$

Drag Due to Lift

The "induced" drag is given by

$$\frac{dC_D}{d(C_L^2)} = \frac{dC_{Di}}{d(C_L^2)} + \frac{dC_{Dw}}{d(C_L^2)} \qquad (2.36)$$

$$= (1+\tfrac{3}{2}UC_L)\left[\frac{1+\delta}{\pi A}K + \frac{h}{c}\left(\frac{e^{-2/F_h^2}}{2F_h^2}\right)(K_b-1)\right]$$

and

$$C_{D(\text{due to lift})} = (1+UC_L)C_L^2\,[\text{ same}] \qquad (2.37)$$

where $\frac{dC_{Di}}{d(C_L^2)}$ is the airfoil induced drag (as a function of lift)

$\frac{dC_{Dw}}{d(C_L^2)}$ is the wave induced drag (as a function of lift)

Factors

The various factors in equations (2.34) to (2.37) which have to be evaluated on the basis of given foil parameters are as follows:

U the term denoting a reduction in fluid velocity, given in Figure 2.5 as a function of h/c

E the lifting surface correction, $1 + 2/A^2$

K_b the biplane induced correction factor, given in Figure 2.7 as a function of h/b

U the generalized biplane induced factor, which is derived from the biplane factor corrected for various configuration effects. Thus

$$K = K_b \cdot f_1 \cdot f_2 \cdot f_3 \cdots$$

where f_1 is the strut or end plate factor such as in equation (2.26)

f_2 is the sweep factor $1/\cos\Lambda$, equatioq (2.28) or as derived experimentally

f_3 is the dihedral factor given in equation (2.29)

other factors as may be required.

F_h submergence Froude number, $V/\sqrt{gh}$

$\left(\frac{e^{-2/F_h^2}}{2F_h^2}\right)$ the wave factor given in Figure 2.6 as a function of

τ, δ the planform correction factors, from Chapter 1.

Foils of Small Aspect Ratfo ($A < 2.0$)

The following must be used for foils of aspect ratio less than 2.0:

$$C_L = \frac{1}{\frac{E}{2\pi} + \frac{1}{\pi A}} \sin\alpha + 2\sin^2\alpha\cos\alpha \qquad (2.38)$$

$$C_{D_L} = \frac{1}{\pi A}\left[\frac{1}{\frac{E}{2\pi} + \frac{1}{\pi A}}\sin\alpha\right]^2 + 2\sin^3\alpha \qquad (2.39)$$

where E is given in Figure 1.10 of Chapter 1.

Equations (2.37) and (2.38) are taken from Chapter 1, and are applicable for $h/b > 1.0 < h/c$. For smaller submergences, surface effects must be included as indicated previously in this chapter.

Pitching Moment Characteristics

For foils of $h/c > 1.0$, the pitching moment, may be determined as in Chapter 1 for airfoils. At smaller submergences, a correction must be applied as indicated in this chapter,

References

1. Kotchin, Kible & Rose — "Theoretical Hydromechanics", Chapter VIII, Article 19 (Translated from Russian by Prof. Korvin-Kroukovsky, Stevens Institute of Technology, Hoboken, N. J.).

2. Wieghardt — "Chordwise Load Distribution of a Simple Rectangular Wing", NACA TM963, 1940.

3. Kotchin — "On the Wave-Making Resistance and Lift of Bodies Submerged in Water", SNAME Technical and Research Bulletin Nos. 1-8, 1951.

4. Keldysch & Lavrentiev — "On the Motion of an Airfoil Under the Surface of a Heavy Fluid, i.e. A Liquid" (Translation No, 306, by F. X. Prior,, Science Translation Service, Cambridge, Mass.).

5. Krienes — As reported in Critical Review of "KBR-SF Hydrodynamisches Archiv" by S. F. Hoerner, Jan. 1953. Enclosure (B) to Gibbs & Cox, Inc. Letter (Confidential), 13531/A9(1-1180) dated 23 January 1953 to ONR (R1-23-53 - 4006).

6. Meyer — "Three-Dimensional Vortex-Line Theory of a Hydrofoil Operating in Water of Large Depth", Hydrofoil Corp. Confidential Technical Rpt, No, HR-4, February 1951.

7. Wu — "A Theory for Hydrofoils of Finite Span", Hydromechanfcs Lab,, Calif. Institute of Tech., May 1953, Rpt. 26-8.

8. Brealin — "A Linearized Theory for the Hydrofoil of Finite Span in a Fluid of Infinite Depth", Bath Iron Works Corp. by Gibbs & Cox, Inc. Confidential Technical Rpt. No. 16, January 1954.

9. Meyer — "Two-Dimensional Vortex Line Theory of a Hydrofoil Operating in Water of Finite Depth", Hydrofoil Corp. Confidential Rpt. HR-1, Nov. 1950.

10. 'Wadlin, Shuford & McGehee — "A Theoretical and Experimental Investigation of the Lift and Drag Characteristics of a Hydrofoil at Subcritical and Supercritical Speeds", NACA RML52D23a, July 1952.

11. Bath Iron Works Corp. by Gibbs & Cox, Inc. Confidential Technical Rpt. No. 2, "Detailed Analysis of Hydrofoil Model Data", Contract No. Nonr-507(00), October 1951.

12. Durand — "Aerodynamic Theory", Vol. II, California Institute of Technology, 1943.

13. Hoerner — "The Influence of End Plates, Struts and Nacelles Upon the Characteristics of Hydrofoils"', Bath Iron Works Corp. by Gibbs & Cox, Inc. Confidential Technical Rpt. No, 14, Contract No. Nonr-507(00), August 1953.

14. Mangler — "Lift Distribution of Wings with End Plates", Lufo 1939.

15. Hoerner — "Aerodynamic Drag", (Published by the Author), 1951.

16. Vladea — "Effect of Fuselage and Engine Nacelles on Some Aerodynamic Properties of an Airplane Wing", NACA Technical Memo No. 736.

17. Jacobs & Ward — "Interference of Wing and Fuselage from Tests of 209 Combinations in the N.A.C.A. Variable-Density Tunnel", NACA Rpt. No. 540, 1935.

18. Glauert — "Aerofoil and Airecrew Theory", MacMillan', 1944.

19s DeYoung & Harper — "Theoretical Symmetrical Span Loading at Subsonic Speeds for Wings Having Arbitrary Plan Form", NACA Rpt. No; 921, 1948.

20. Wadlin, Ramaen & Vaughan — "The Hydrodynamic Characteristics of Modified Rectangular Flat Plates Having Aspect Ratios of 1.00 and 0.25 and Operating Near a Free Water Surface", NACA Technical Note 3079, 1954.

CHAPTER 3. SURFACE-PIERCING FOIL CHARACTERISTICS

1. General Considerations
2. Characteristics Prior to Ventilation
3. Ventilated Characteristics
4. Design Considerations

Formulas are given for the lfft and drag characteristics of surface-piercing foils in non-ventilated and ventilated condftfons. These formulas are based on a limited series of tests and are considered primarily applicable only to foils hating similar geometry and operating under similar conditions as those tested.

1. General Considerations

Foil Geometry and Notation

The characteristics of a surface-piercing foil are referred to the projected dimensions of the submerged foil area as indicated in Figure 3.1, and all lift and drag formulas can be referred to these dimensions, after appropriate corrections.

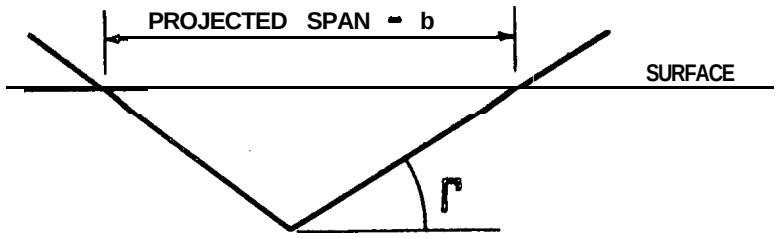

FIGURE 3.1

The specific notation for surface-piercing foils is as follows:

- b the projected span of the submerged foil (the horizontal distance between foil tips)
- c the foil chord
- Γ the dihedral angle
- α angle of attack, measured in the vertical plane
- f/c camber ratio, measured on the actual foil section (in the plane normal to the quarter-chord line)
- A the projected aspect ratio (b/c for a rectangular foil)

S_p the projected foil area (bc for a rectangular foil)

S/S_p the ratio of actual foil area to projected foil area.

Status of Existing Information

Available information on the hydrodynamic characteristics of surface-piercing foils is limited to preliminary theoretical investigations[1] and several sets of tests on specific configurations[2,3,4]. Neither the theory nor the test data is sufficient to allow accurate prediction of the hydrodynamic characteristics covering the wide range of configurations that employ surface-piercing foil elements. There are many varieties of shape as shown in Figure 3.2 and variation in planform, camber, twist, etc. that are considered to have noticeable effect on the overall foil characteristics.

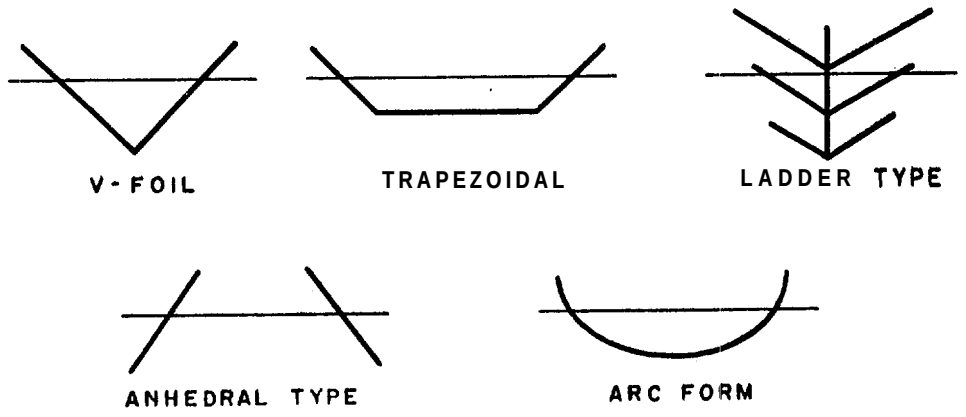

TYPICAL SURFACE - PIERCING FOILS

FIGURE 3.2

Sottorf's Experiments

Sottorf[2] ran a series of tests on various surface-piercfng V-foils and trapezoidal foils of 26.5° and 45° dihedral angle, with a varfety of sectional shapes (constant along the span) and submergence over a range of angle of attack. Reference should be made to the original report for the complete results of these tests; however, certain representative data are reproduced herein in Figures 3.3 and 3.4 to illustrate the adequacy of the formulas proposed below.

Application of Data

The data and formulas proposed are considered strictly to apply to those types of foils tested, although they may be applied generally in the absence of more specific information for other types,

> At this stage, it is recommended that tank tests be run on particular surface-piercing foils considered for use, in order to determine more accurate characteristics over the range of speeds and angles of attack described.

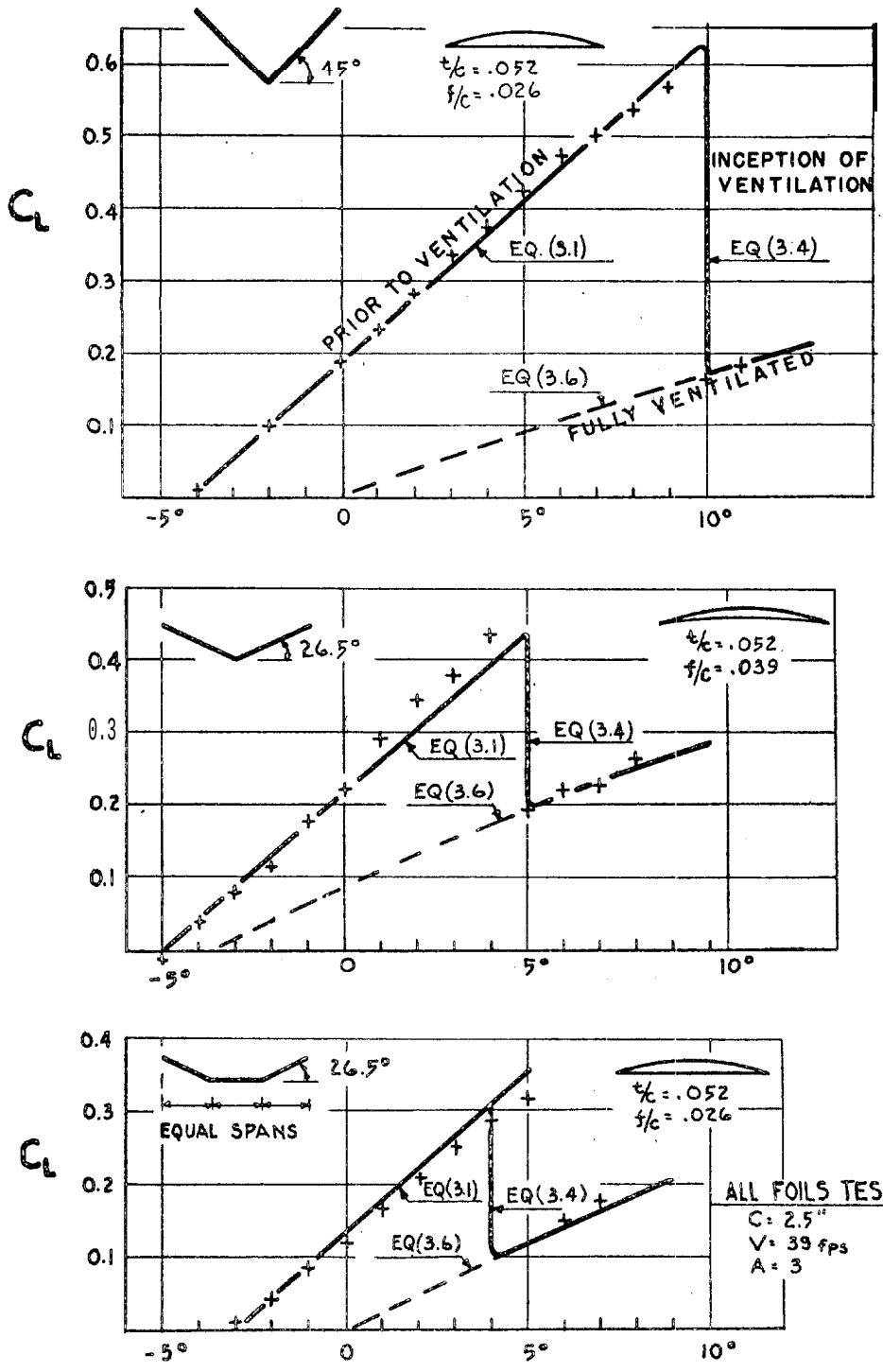

SURFACE-PIERCING FOIL LIFT DATA

FIGURE 3.3

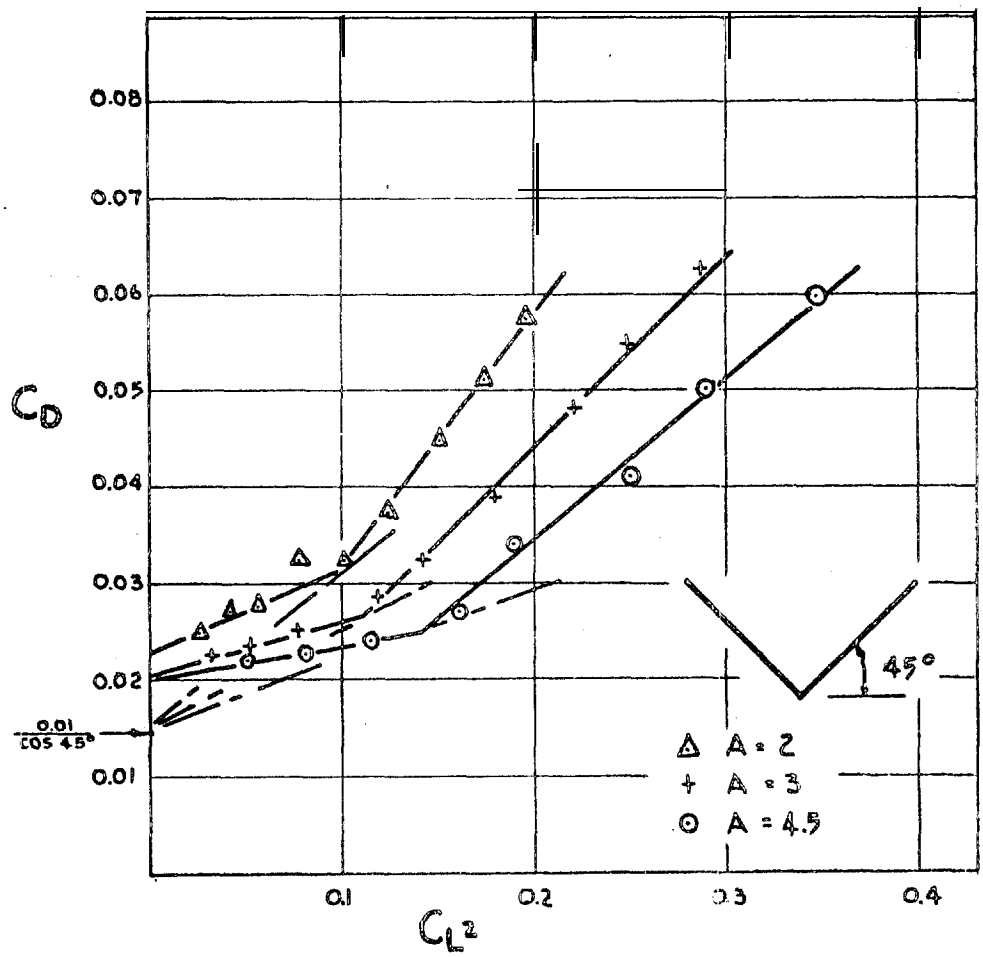

FOR ALL TESTS

C = 2.5"

V = 39 fps

t/c = 0.052 CIRCULAR ARC SECTIONS

SURFACE-PIERCING FOIL DRAG DATA

FIGURE 3.4

2. Characteristics Prior to Ventilation

Airfoil Effects

The airfoil induced characteristics of a surface-piercing foil may be given approximately as those of an equivalent submerged foil with end struts (boxplane condition), as indicated in Figure 3.5. The equivalent "boxplane" has the same projected span and encloses the same water area within its perimeter as the foil it replaces, Thus, the boxplane submergence is the average submergence of the surface-piercing foil; for example, it is 1/2 the maximum submergence of a V-foil and 2/3 that of a parabolic foil,

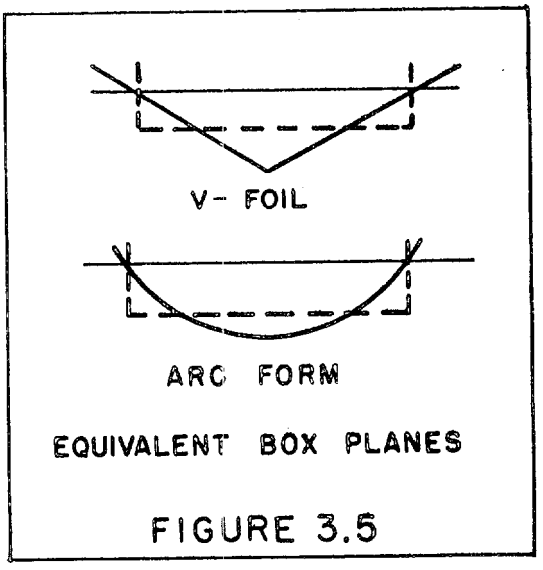

FIGURE 3.5

The airfoil effects of the surface-piercing foil may then be given, from the equations in Chapter 2 for the submerged foil:

$$\left(\frac{d\alpha}{dC_L}\right)_a = (1+2UC_L)\left[\left(\frac{E}{2\pi}+\frac{U}{8k}\right)\frac{S}{S_p}+\frac{1+\tau}{\pi A}K_{bo}\right] \qquad (3.1)$$

$$\frac{dC_{Da}}{d(C_L^2)} = \left(1+\frac{3}{2}UC_L\right)\frac{1+\delta}{\pi A}K_{bo} \qquad (3.2)$$

where h Is the average submergence of the foil

K_{bo} is the boxplane factor, based on the average submergence, Values are given in Figure 2.7

S/S_p is the foil area ratio (equivalent to $1/\cos\Gamma$ for a V-foil, where Γ is the dihedral angle)

other notation as given above and in Chapter 2.

Wave Effects

The wave effects for a surface-pieraing foil may be estimated to be the same as that for the submerged foil at the equivalent average submergence.

$$\left(\frac{d\alpha}{dC_L}\right)_w = (1+2UC_L)\frac{c}{h}\left(\frac{e^{-2/F_h^2}}{2F_h^2}\right)(K_b-1)$$

$$\frac{dC_{Dw}}{d(C_L^2)} = (1+\tfrac{3}{2}UC_L)\frac{c}{h}\left(\frac{e^{-2/F_h^2}}{2F_h^2}\right)(K_b-1) \qquad 3 \qquad (3.3)$$

where, h is the average submergence of the foil
other notation as given above and in Chapter 2.

Effeate of Sweep

The effects of sweep on the airfoil or wave effects of a surface-piercing foil are not definitely known. There are no known reports in the literature dealing with the theory or test results of surface-piercing foils employing sweep. Specific tests would have to be made, at the present time, to determine such effects.

Comparison with Test Data

Comparison is made between the test data on V-foils, given in Figures 3.3 and 3.4, and the formulas as derived above. It is noted that the test speeds are very high ($V/\sqrt{gc} \approx 9.0$), and therefore the wave effects, equation (3.2), may be neglected.

For the cambered foil tested, the angle of zero lift may be simply derived:

$$\alpha_{L_0} = -2\, f/c \cdot \frac{1}{\cos\Gamma}$$

The lift curve was calculated from equation (3.1) for the foil tested, and the results are shown in Figure 3.3. Agreement with the test data is seen to be reasonably good.

However, analysis of the drag data given in Figure 3.4 indicates that equation (3.2) holds only at an "optimum" lift coefficient, Above and below this value, the drag is noticeably higher.

The theoretical curves shown in the figure are derived by considering the section drag coefficient in the order of 0.01 (at the test Reynolds number of 6×10^5) which leads to the total expression

$$C_D = \frac{0.01}{\cos 45^\circ} + \frac{(1+\delta) K_{b_0} (1+4C_L) C_L^2}{\pi A}$$

It is seen that this is valid only at an optimum lift coefficient,

From the data shown in the figure, it is seen that above the optimum point, the slope of the drag curve is approximately twice the theoretical value, while below the optimum the slope is roughly one-half the theoretical value. What signffciance this relationship has, and over what range of configurations it can be applied is not presently known, Qualitatively, however, this increase in drag appears to be due to two considerations:

(1) The interference effect at the surface which causes spray and replaces circulatory flow at the tips by less efficient "planing" flow.

(2) The section pressure drag (see Chapters 1 and 4). For airfoil shapes, this drag increases according to the factor $(1 + \Delta C_L^2)$, where ΔC_L is measured from the optimum point. However, for the sharp nosed, circular arc sections at the low Reynolds number of 6×10^5 employed in the tests it is considered that the pressure drag is much higher than this value.

The relative magnitude of these factors could be determfned by further test data.

DESIGN EXAMPLE NO. 3.1

SH 1 OF 1

DETERMINE THE LIFT CURVE FOR THE FOLLOWING SURFACE - PIERCING FOIL (PRIOR TO VENTILATION)

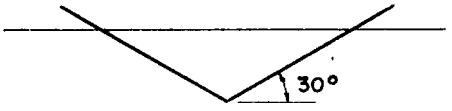

CHARACTERISTICS : $\Gamma = 30°$
$A = 5$
RECTANGULAR PLANFORM
SECTION : 10 % THICK, ARCFORM WITH FLAT PRESSURE SIDE

The equivalent "box-plane" ratios are:

$$h/b = \frac{1}{4} \tan 30° = 0.144$$

$$h/c = 5 \times 0.144 = 0.72$$

LIFT ANGLE

From Chapters 1 and 2:

$U = 0.07$ (Figure 2.4)
$K_{bo} = 1.22$ (Figure 2.7)
$\tau = 0.14$ (Figure 1.8)
$E = 1 + 2/5^2 = 1.08$

Then, using equation (3.1)

$$\frac{d\alpha}{dC_L} = \left[\left(\frac{1.08}{2\pi} + \frac{0.07}{8 \cdot 0.72} \right) \frac{1}{\cos 30°} + \frac{1.14 \times 1.22}{5\pi} \right] (1 + 0.14 C_L)$$

$$= 0.301 (1 + 0.14 C_L)$$

ANGLE OF ZERO LIFT

$$\alpha_{Lo} = -2 f/c \times \frac{1}{\cos 30°} = -0.10/0.866 = -0.115 \text{ radians } (-6.6°)$$

TOTAL CURVE

$$\alpha = -0.115 + 0.301 C_L + 0.021 C_L^2$$

3. Ventilated Characteristics

Inception of Ventilation

The phenomenon of ventflatfon occurs when air from the atmosphere displaces the low pressure water on the upper surface of the foil. Some accumulation of boundary layer fluid at the water surface is necessary to "trigger" such air entrance, which condition is most readily met at large angles of attack,

From a study of the existing test data for surface-piercing foils (and for vertical struts as shown in Chapter 7) the fnoeptfon of ventilation appears to be a local condition, depending on the foil geometry at the water surface, An empirical expression has been found that agrees well wfth the data of Ffgure 3.2. In terms of the foil. angle of attack, α , the fneeptfon pofnt is

$$\alpha_v = \beta \tan \Gamma \sqrt{\sin \Gamma} \qquad (3.4)$$

where β is the angle between the chord line and the upper surface of the foil section at the leading edge

Γ is the dihedral angle at the water surface,

Equation (3.4) can only be applied when the speed of advance is large enough for the foil to normally develop sub-atmospheric pressure on the suction side over the entire span,

The angle, β, is easily determined for a foil with sharp leading edge, but has no exact definition for an airfoil section. It appears reasonable to use the angle formed by a circular arc tangent to the section at the point of maximum thickness and passing through the leading edge, as indicated in. Figure 3.6.

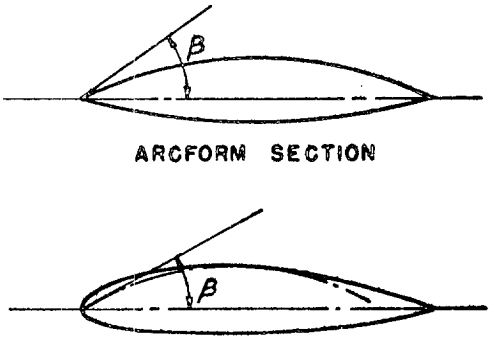

MEASUREMENT OF ANGLE β

FIGURE 3.6

When the foil angle exceeds that given in equation (3.4) above, the lift of the foil falls off more or less rapidly until the fully ventilated condition is reached, as indicated in Figure 3.3 (and as further indicated in references 4 and 5).

It is not apparent why, in some instances, the lift falls off immediately after.& is exceeded, whereas in others the lift falls off gradually with angle of attack. In the fatter cases, there is some evidence of instability with the lift alternatively assuming non-ventilated and ventilated values for different test runs under seemingly identical conditions. Further tests and analyses are required to resolve this phenomenon,

Lift and Drag Characteristics - Fully Ventilated

The lift and drag of a fully ventilated foil (with flat pressure side) can be readily determined by the use of Rayleigh's formula[6] for the lift of a flat plate in discontinuous flow. This formula is expressed for the normal force on the plate as

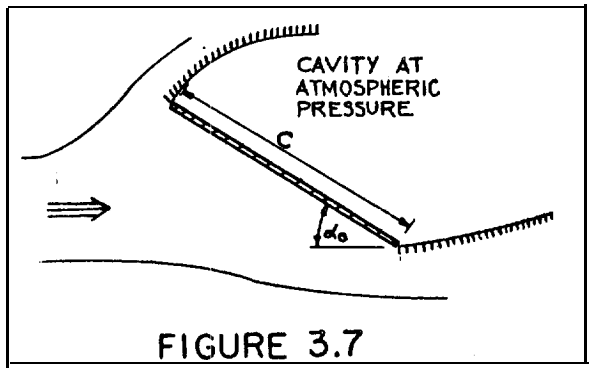

FIGURE 3.7

$$C_N = \frac{2\pi \sin\alpha_o}{4 + \pi \sin\alpha_o} \qquad (3.5)$$

which strictly applies only to a two-dimensional flat plate,,

However, since for a foil with both ends piercing the surface the actual flow across the tips is limited (in a spanwise direction), it is expected that this formula should approximately hold,

Therefore, referring this force to the case of the surface-piercing V-foil, we get for small angles

$$C_{L_v} = \frac{2\pi\alpha \cos\Gamma}{4 + \pi\alpha \cos\Gamma} \qquad (3.6)$$

which is in excellent agreement with the data shown in Figure 3.3. The angle of zero lift is dependent only on the shape of the lower

surface of the foil. In particular, it is apparently that angle at which the trailfng edge of the pressure side is in line wfth the flow.

The drag of a fully ventflated foil having a flat pressure side is evidently a simple function of the angle of attack. Including one-half of the conventional friction profile drag (since only the lower surface of the foil is wetted) the total drag coefficient for a V-foil is then

$$C_{D_v} = \frac{1}{2}\frac{C_{D_0}}{\cos\Gamma} + C_{L_v}\alpha\cos\Gamma \qquad (3.7)$$

where C_{D_0} is the basic section drag coefficient (see Chapter 4)

C_{L_v} is the lift coefficient of equation (3.6).

Note: Wave drag considerations have not been included in the fully ventflated condition. In practical applications, such ventilation is expected to occur only at high speeds where the wave drag is negligible. Where consfdered to be a factor, the wave effects may be calculated in accordance with equation (3.3) given for the non-ventilated condition.,

DESIGN EXAMPLE NO. 3.2

ESTIMATE THE VENTILATING CHARACTERISTICS OF THE FOLLOWING SURFACE-PIERCING FOIL

$\Gamma = 30°$
A = 5
10 % THICK, ARCFORM SECTION WITH FLAT PRESSURE SIDE

AS IN EXAMPLE 3.1

Inception of Ventilation

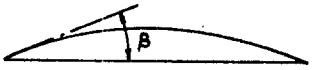

For the section employed, β . 0.385 radians (22½° approx)

From Equation (3.4)

$$\alpha_v = 0.385 \times 0.577\sqrt{0.500} = 0.157 \text{ radians}$$

$$= \underline{9.0°}$$

Lift

From Equation (3.6)

$$C_{L_v} = \frac{2\pi\alpha \cos 30°}{4 + \pi\alpha \cos 30°} = \frac{3.62\alpha}{4 + 1.81\alpha}$$

4. Design Considerations

The various correction factors for struts,: planform, etc. can be applied to the airfoil effects of a surface-piercing foil in a manner similar to that for a fully submerged foil, the principles of which are given in Chapter 2.

However, it is necessary to re-emphasize that the formulas given herein for the surface-piercing foil are tentative, being based on a minimum of test data and theoretical investigation, and should be checked by tank tests where the configuration is different from those on which the formulas are based.

References

1. Weinig — "On the Theory of Hydrofoils and Planing Surfaces" NACA - T.M. #845, 1938.

2. Sottorf — "Experimental Investigation of Hydrofoils" German ZWB Document FB 1319 (1940) by Inst. Seeflug-*wesen* Hamburg

3. Hoerner — Critical Review of "KBR-SF Hydrodynamisches Archiv", Jan, 1953. Enclosure (B) to Gibbs & Cox, Inc. Letter (Confidential), 13531/A9 (l-1180) dated 23 January 1953 to ONR (Rl-23-54-4006)

4. Benson and Land — "An Investigation of Hydrofoils in the NACA Tank" NACA Wartime Report L-758,, 1942.

5. Hoerner — "Some Characteristfes of Spray and Ventilation" B.I.W. Corp. by Gibbs & Cox, Inc. Technical Report No. 15, Contract No. Nonr-507(00), 1953.

6. Milne-Thomson — "Theoretical Hydrodynamics" Macmillan, 1950

3. Drag of Small Projections

General Considerations

On the foil surface there is likely to be small irregularities or projections in the form of plate joints, rivet or screw heads, control surface gaps, e-tc. that have unique drag characteristics due to their presence within the fluid boundary layer. (For large protuberances that extend beyond the boundary layer, see Chapter 9.) The drag of these projections can be determined as a function of their shape, height and chordwise location on the foil.

> The material which follows is taken almost entirely from Hoerner's "Aerodynamic Drag"[4]. For a more detailed, complete coverage, reference should be made to that work.

Spanwise Plate Joints and Other Spanwise Projections

The drag coefficient of continuous spanwise projections can be represented in the form

$$C_{D_\bullet} = \boxed{C_D} \cdot 3\sqrt[3]{h/x} \qquad (4.14)$$

where $C_{D_\bullet}$ is the drag coefficient based on the frontal area of the projection (or depression)

C_R is an "independent" coefficient, which is a function of the type of projection.

h/x is the ratio of projection height to distance of the projection from the leading edge of the foil.

This relationship is valid for h/x less than 0.02.

Values of C_D are shown in Figure 4.6 for various plate joints and projections.

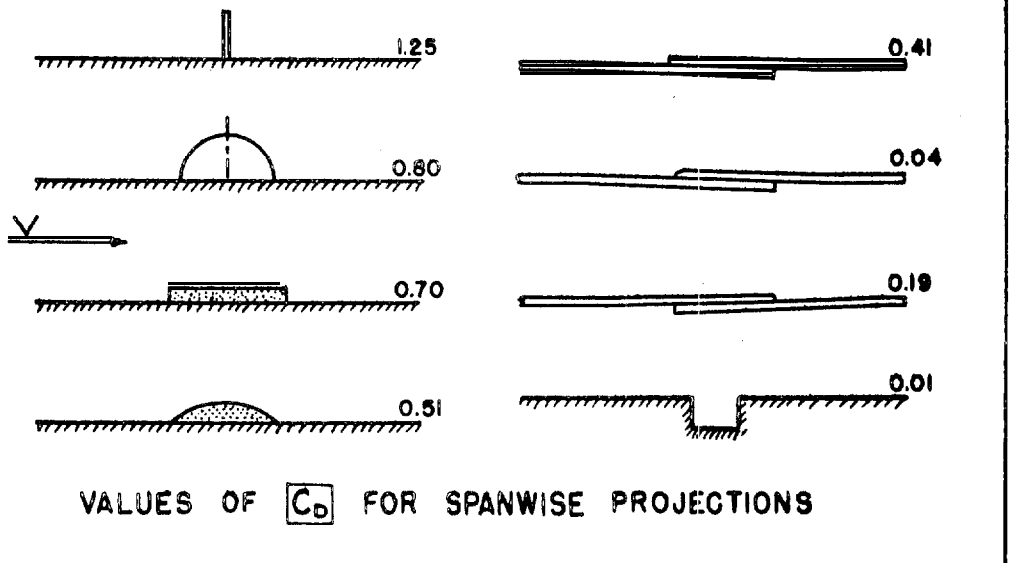

VALUES OF C_D FOR SPANWISE PROJECTIONS

FIGURE 4.6

Rivet Heads and Other Local Projections

The drag coefficient of rivet and bolt heads and similar "spot-like" projections takes the same form as equation (4.14) above for plate joints, except that the coefficient is referred to the plan area of the projection. Thus

$$C_{D_f} = C_D \cdot 3\sqrt[3]{h/x} \qquad (4.15)$$

where C_{D_f} is based on plan area of the projection,.

Again, the relationship is valid for h/x less than 0.02,

Values of C_D for various rivet and bolt heads are shown in Figure 4.7.

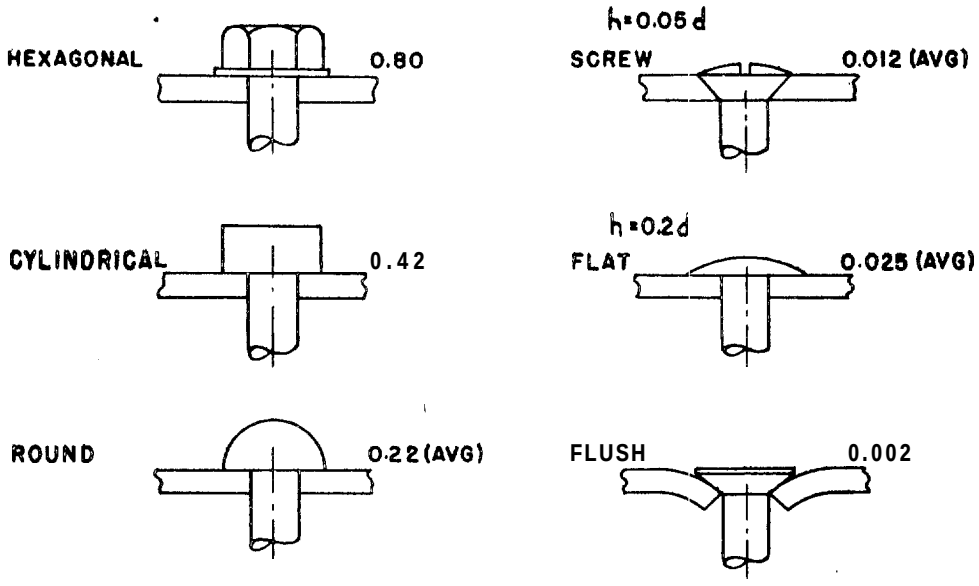

VALUES OF C_D FOR LOCAL PROJECTIONS

FIGURE 4.7

Control Gaps

The drag due to the gap between a foil and a control flap can be estimated on the basis of the gap (measured as indicated in Figure 4.8). Thus, based on the plan area of the gap,

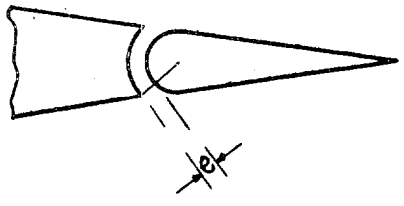

CONTROL GAP MEASUREMENT

FIGURE 4.8

C_{D_+} = 0.02 for the pressure side

C_{D_+} = 0.03 for the suction side

or for the simple arrangement shown in the figure

$$\Delta C_{D_o} = 0.05\ e/c \cdot a_f/b \qquad (4.16)$$

where e/c is the gap/chord ratio

a_f is the spanwise extent; of the control flap

b is the foil span.

ΔC_{D_o} is then added directly as a component of foil parasite drag.

DESIGN EXAMPLE NO. 4.2

SH 1 OF 1

DETERMINE THE EFFECT OF A BUTT STRAP ON THE PARASITE DRAG OF A FOIL

FOR THE 24" CHORD FOIL GIVEN IN EXAMPLE 4.1 THERE IS A 2" X 3/16" BUTTSTRAP ON THE EXPOSED UPPER & LOWER FOIL SURFACES, LOCATED AT MID-CHORD, EACH SECURED BY A DOUBLE ROW OF 1/4" DIA. COUNTERSUNK, OVAL HEAD MACHINE SCREWS SPACED 5 DIAMETERS.

For the Strap

From equation (4.14) and Figure 4.6

$h/x = \frac{3/16}{12} = 0.015$ (less than 0.02, so is applicable)

$\boxed{C_D} = 0.7$

Therefore,

$C_{D_0} = 0.7 \times 3(0.015)^{\frac{1}{3}} = 0.52$

and $\Delta C_{D_0} = \frac{3/16}{24} \times 0.52 = \underline{0.0041}$

For the Screws

1/4" dia. countersunk, oval head screws have a diameter $\approx$ 0.5" and height $\approx$ 0.025"

From equation (4.15) and Figure 4.7

$h/x = 0.025/12 = 0.0021$ (again, less than 0.02)

$\boxed{C_0} = 0.012$

Therefore

$C_{D_+} = 0.012 \times 3(0.0021)^{1/3} = 0.0046$

The screw plan area, per unit of span is

$2 \times \frac{\pi}{4}(\frac{1}{2})^2 \times \frac{4}{5} = 0.314$ in²/in

and $\Delta C_{D_0} = \frac{0.314}{24} \times 0.0046 = \underline{0.0001}$

Total

From Example 4.1, $C_{D_0}(std) = 0.0086$

Therefore, the total is $C_{D_0} = 0.0086 + 0.0041 + 0.0001 = \underline{0.0128}$

4. Interference Effects

Foil-Strut Junctions

At the junction of a foil and strut, there is an additiorial drag due to reaction between the fluid boundary layers of the two bodies. Analysis of test results[7] indicates that this drag can be approximately expressed as a function of the thicknesses of the strut and foil. Figure 4.9 shows the drag coefficient of various tested configurations in terms of the "thickness":

$$C_{D_t} = \frac{D}{q t'^2} \qquad (4.17)$$

where $t' = \sqrt{t_1 t_2}$

for junctions with and without fillets.

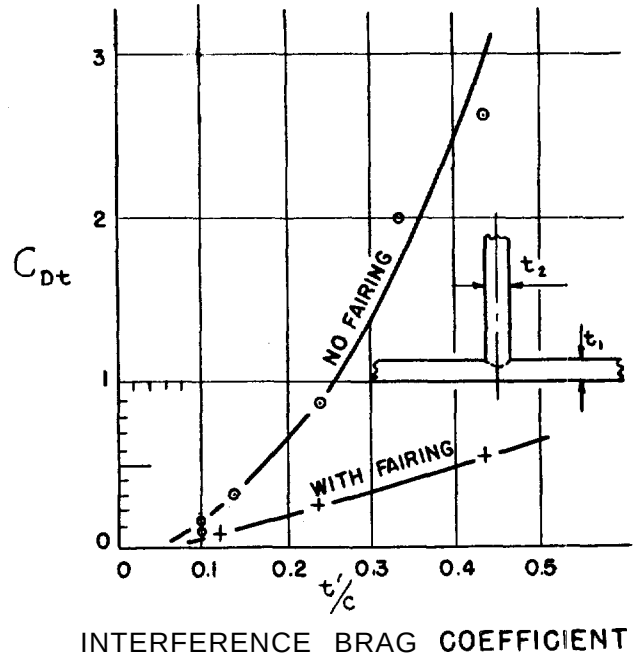

INTERFERENCE BRAG COEFFICIENT

FIGURE 4.9

These test results are for fofls and struts of the same chord and are probably not exaet when the respective chords are different. However, it is felt that the differences would be small and it is suggested that the data shown can be used for all cases, basing the co-ordinate t/c on the chord of the foil.

It is also considered that the fillet should have a radius in the order of $\sqrt{t_1 t_2}$ for the corresponding location along the chord.

There is an additional interference effect when the foil has an angle of attack, as indicated by teat data[7]. However, ft is not known how much can be attributed to viscous influences and how much to induced drag (due to loss in lift), For convenience, it has been considered an induced effect and an empirical relationship is given in Chapter 2 (equation 2.26a).

Foil Nacelle Junctions

There is a similar parasitic drag increment that arises at the junctions of foils and nacelles. However, since the nacelle replaces a certain portfon of foil area, the reduction in foil drag (calculated on the basis of a plain wing, as is usually done) offsets the interference drag to a large extent.

That is, adding the parasite drag of a nacelle (see Chapter 9) to the parasite drag of a foil results in a drag value that reasonably represents the total parasite drag of the combined configuration, since the mutual interference drag is offset by the reduction in surface area.

The actual total effect of the nacelle-foil configuration is dependent on many geometric factors., The shape of the nacelle, the relative spanwise, fare and aft;, and vertical location of the nacelle with respect to the foil, and the type of fairing employed at the junction are all important considerations and no general relationship can be found to cover all conditions,

Rather, it is necessary to refer to test data for configurations similar to that which is being considered. Reports such as that by Jacobs and Ward[8] on tests of wing-fuselage or wing-nacelle configurations can be utilized for this purpose,

DESIGN EXAMPLE NO. 4.3.

SH 1 OF 1

DETERMINE THE STRUT INTERFERENCE EFFECT ON THE PARASITE DRAG OF A FOIL

FOR THE FOIL GIVEN IN EXAMPLE 4.1 , A SPAN OF 12' IS TAKEN (WITH RECTANGULAR PLANFORM), SUPPORTED ON THE SUCTION SIDE BY TWO STRUTS OF 24" CHORD, 10% MAXIMUM THICKNESS.

From example 4.1, the foil has 24" chord, 12% thickness

Therefore, from equation (4.17)

$$t'/c = \sqrt{0.10 \times 0.12} \approx 0.11$$

And from figure 4.9

C_{D_t} = 0.22 (without fairing)
0.07 (with fillet fairing)

Converting C_{D_t} to the proper increase in foil drag coefficient,

$$\Delta C_{D_o} = 2 C_{D_t} (t'/c)^2/A = C_{D_t} \times 2(0.11)^2/6$$
$$= 0.004 C_{D_t}$$

Thus, ΔC_{D_o} = 0.0009 (without fairing)
= 0.0003 (with fillet fairing)

References

1. Rossell and Chapman — "Principles of Naval Architecture" Vol. II The Society of Naval Architects & Marine Engineers 1941.

2. Prandtl & Tietjens — "Applied Hydro- and Aero-Mechanics" McGraw-Hill 1934.

3. — "Uniform Procedure for the Calculation of Frictional Resistance and the Expansion of Model Test Data to Full Size" The Society of Naval Architects & Marine Engineers Bulletin No, l-2, 1948.

4. Hoerner — "Aerodynamic Drag" Published by the Author, 1951.

5. Abbott, von Doenhoff & Stivers — "Summary of Airfoil Data" N.A.C.A. Report No. 824, 1945.

6. Hoerner — "The Effect of Roughness Density Upon the Frictional Drag" to be published in the Journal of the American Society of Naval Engineers, 1954.

7. Hoerner — "The Influence of End Plates, Struts and Nacelles Upon the Characteristics of Hydrofoils", Bath Iron Works Corp, by Gibbs & Cox, Inc, Technical Report No. 14, Contract No, Nonr-507(00), August 1953.

8. Jacobs & Ward — "Interference of Wfng and Fuselage from Tests of 209 Combinations in the NACA Variable-Density Tunnel", N.A.C.A. Report No. 540, 1935.

CHAPTER 5. FLAP CHARACTERISTICS

Relationships for plain flaps and ailerons are given for hydrofoils, derived from airfoil theory and data, Methods to determine characteristics of flapped foils with full or partial-span flaps are indicated. It is indicated that airfoil relationships may not be sufficient for flaps piercing or within one chord of the surface, and specific test data is required for such cases.

1. General Considerations

Flaps and ailerons are applicable to hydrofoil configurations for several purposes. Ailerons may be used on controllable foil craft and for assisting turns, while flaps may be used on fixed foil configurations for changing trim and 'submergence as desired for changes in craft speed or load.

Some of the flaps developed for airfoils are illustrated in Figure 5.1. On a practical basis, the plain flap or aileron appears to be the most attractive for hydrofoil use due to its mechanic and hydrodynamic simplicity and its ability to serve as an aileron or a trim flap, as desired. Theoretical relationships and test data are more readily correlated for plain flaps, and formulations more readily applied to design. Therefore, the characteristics shown below are primarily applicable to plain flaps or ailerons,

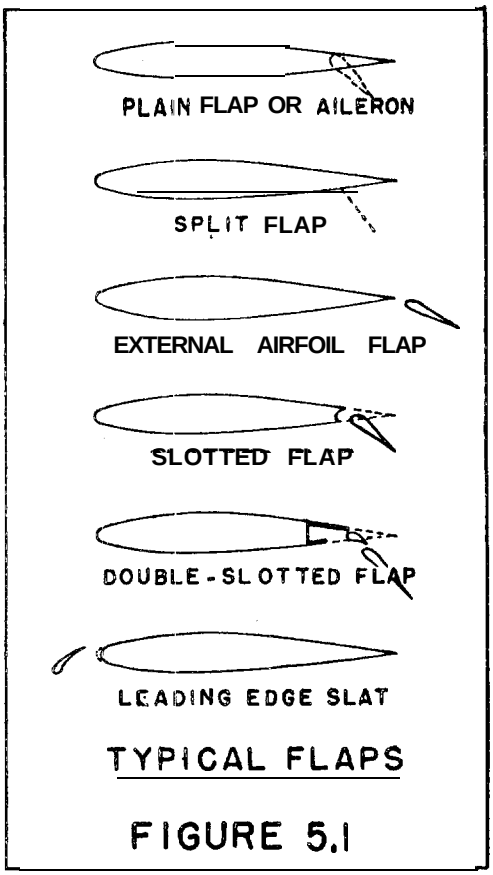

TYPICAL FLAPS

FIGURE 5.1

For details of flap theory and additional data on flaps of all types, reference should be made to pertinent airfoil treatises [1-5].

There is no available data on the characteristics of flaps on a foil in the vicinity of the water surface. Generally, it is considered that the effects, of a flap on an airfoil will apply also to a hydrofoil, taking into account the properties of the unflapped hydrofoil. This concept should apply where the submergence is greater than 1 chord, but for smaller submergences (including surface-piercing foils) the flap characteristics may well be different due to the local flow conditions set up by the biplane image system. In this latter case, model tests should be employed to determine flap effects more accurately.

The notation employed for plain flaps is indicated in Figure 5.2. The flap chord, C_f, is measured from the pivot point and the flap deflection is measured from the chord line, as shown. Flap hinge moments are taken about the pivot point.

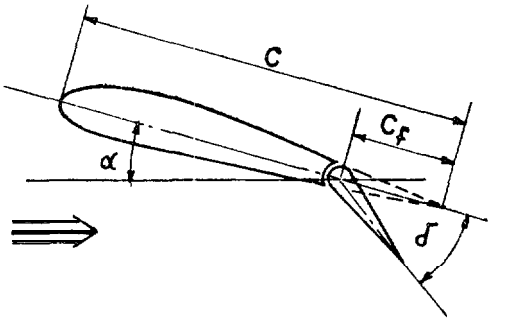

FLAP NOTATION

FIGURE 5.2

2. Lift Characteristics

Section Characteristics

The deflection of a flap has an effect on the foil. similar to that of a change in camber of the section, expressed as an increment of effective angle of attack:

$$\Delta \alpha_o = k_f \delta \tag{5.1}$$

where k_f is a function of the flap chord ratio. The theoretical value of k_f, shown in Figure 5.3, gives results that are somewhat higher than those derived from experiment. For flap deflections of not over 10" to 15°, the experimental data is well fitted by the empirical formula

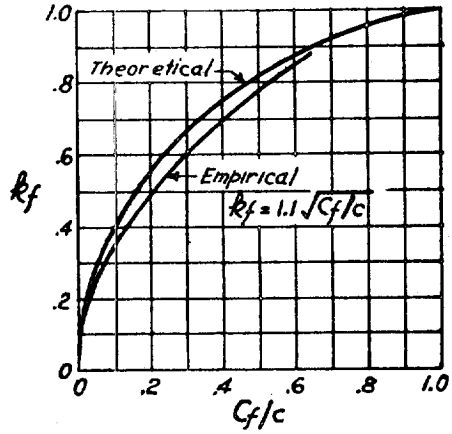

FLAP-EFFECTIVENESS
FIGURE 5.3

$$k_f = 1.1\sqrt{c_f/c} \tag{5.2}$$

below the value $c_f/c = 0.7$.

The section lift equation for a flapped foil in infinite fluid is then

$$C_\ell = 2\pi(\alpha_o - \alpha_{Lo} + k_f \delta) \tag{5.3}$$

where α_o is the foil section angle

α_{Lo} is the unflapped angle of zero lift

δ is positive downward,

Foil With Full Span Flaps

The lift of a hydrofoil with flaps extending the full span can readily be determined from

$$C_L = \left(\frac{dC_l}{d\alpha}\right)(\alpha - \alpha_{Lo} + k_f \delta) \tag{5.4}$$

where $\left(\frac{dC_l}{d\alpha}\right)$ is the lift curve slope of the unflapped foil, as determined In Chapters 2 and 3.

Foils With Partial Span Flaps

When flaps extend only over a portion of the foil span, the flap effectiveness must be suitably modified by an additional factor k_f' so that the total factor is $k_f k_f'$. This additional factor is shown[3,5] to be a function of the basic spanwise lift distribution of the unflapped foil, and thus for any but an elliptically loaded foil a function of aspect ratio, An approximate value for the factor k_f' can be readily determined once the basic spanwise distribution is known, by the ratio of the basic lift over the span

of the flapped foil to the lift of the entire foil, as illustrated in Figure 5.4(a). For an elliptically loaded foil (of any aspect ratio) the factor k_f' can be determined from Figure 5.4(b) in terms of the ratio a/b, where $a/2$ is the span of the flap that extends to midspan. For partial flaps at the tips or within the span, the factor can be determined from:

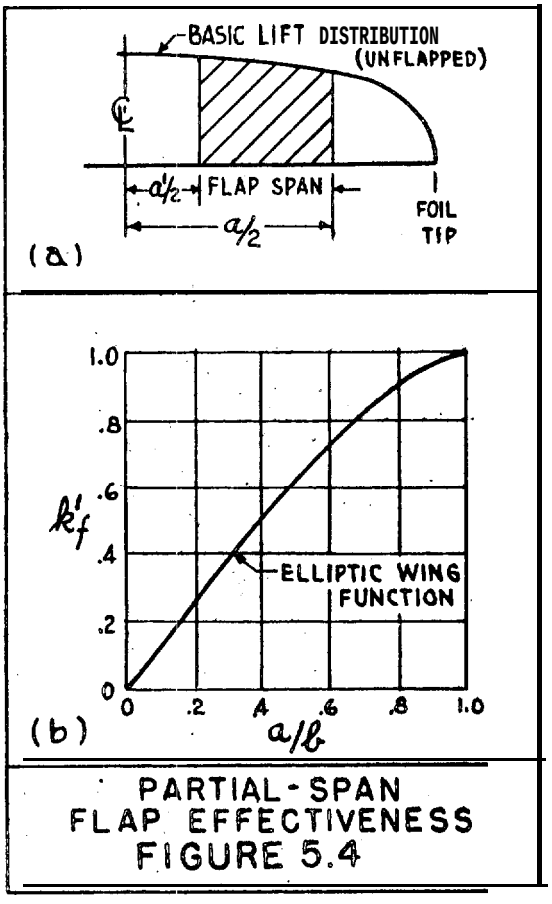

PARTIAL-SPAN FLAP EFFECTIVENESS
FIGURE 5.4

$$k_f' = k_f'(\text{at } a) - k_f'(\text{at } b)$$

The elliptically loaded case may be used for all foils without serious error.

A further correction is required for the hydrofoil where greater accuracy is required, due to the biplane image of the incremental lift over the flapped span. This may be determined from the relationships derived for a biplane with unequal spans

(see Dursnd[6]). However, for preliminary purposes, such corrections may be neglected.

Lift of Flaps

The normal force on the flaps is given approximately by the equation

$$C_{n_f} = n_1 C_l + n_2 \delta \tag{5.5}$$

where C_l is the section lift of the wrapped foil determined for each point along the span of the flap from the basic lift distribution.

n_1, n_2 are coefficients given in Figure 5.5.

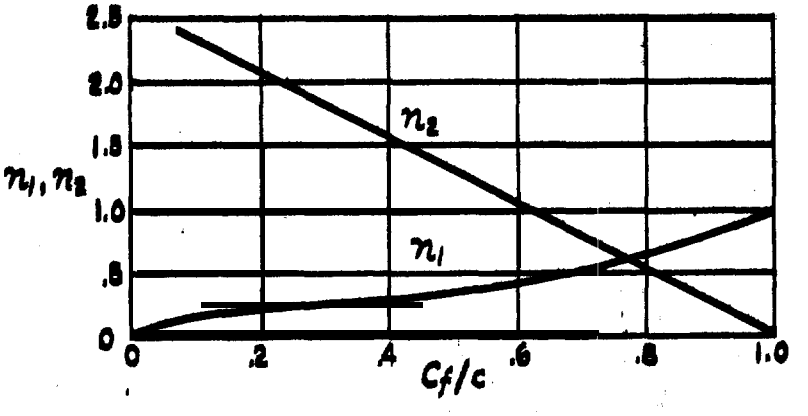

FIGURE 5.5

DESIGN EXAMPLE NO. 5.1

SH 1 OF 1

ESTIMATE THE FLAP EFFECTIVENESS FACTOR FOR A PARTIAL-SPAN FLAP

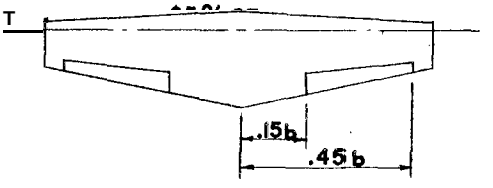

A PAIR OF FLAPS HAVING 4 CHORD EQUAL FOIL, CLOSED, AND AN OVERALL SPAN OF 60% OF THE FOIL SPAN ARE INSTALLED ON A 2:1 TAPERED FOIL, AS SHOWN ON THE SKETCH

From **equation** (5.2), **the effectiveness** of the flap section is

$$k_f = 1.1\sqrt{0.25} = 0.55$$

The foil has approximately an elliptic lift distribution, (as indicated in Chapter 1);

Therefore, from Figure 5.4, and pages 5.5 and 5.6

$$k_f' = k_f' \text{ (at } a/b = .9) - k_f' \text{ (at } a/b = .3)$$

$$= 0.97 - 0.38 = 0.59$$

Then, the total flap effectiveness factor is

$$k_f k_f' = \underline{0.325}$$

3. Moment Characteristics

Pitching Moment

The section pitching moment about the quarter-chord line of the foil, due to flap deflection is given by the equation

$$\Delta C_{m_{1/4}} = \left(\frac{d C_{m_{1/4}}}{d\delta}\right)\delta \qquad (5.6)$$

where $\frac{dC_{m_{1/4}}}{d\delta}$ is given in Figure 5.6, and is seen to be a function only of flap chord ratio.

For full span flaps, the total pitching moment about the quarter-chord can then be determined readily by the methods indicated in Chapter 2.

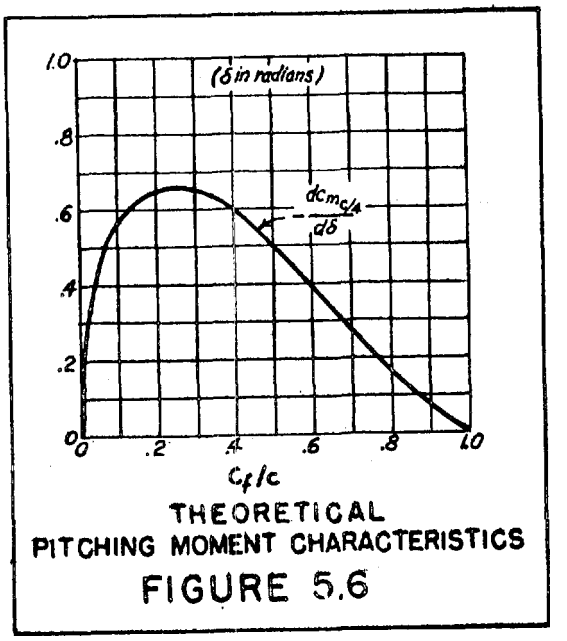

THEORETICAL PITCHING MOMENT CHARACTERISTICS

FIGURE 5.6

For partial span flaps, the total pitching moment due to flaps must be determined from the basic lift distribution (spanwise) of the foil, as indicated above for the lift due' to flaps.

Flap Hinge Moments

The section hinge moments on a flap are given by the equation

$$C_h = \left(\frac{dC_h}{dC_l}\right) C_l + \left(\frac{dC_h}{d\delta}\right) \delta \qquad (5.7)$$

where C_h is the coefficient of the moment about the flap hinge in terms of the flap chord

C_l is the flapped foil lift coefficient

$\left(\frac{dC_h}{dC_l}\right)$, $\left(\frac{dC_h}{d\delta}\right)$ are factors given in Figure 5.7 and are seen to be functions of the flap chord ratio.

The total hinge moment for a full span flap is readily determined from equation (5.7) for the section, by the procedure given in Chapter 2 for foil pitching moments, For the simple case where the flap chord ratio is constant across the span, the total hinge moment is found merely by substituting C_L (for the foil) in place of C_l (for the foil section).

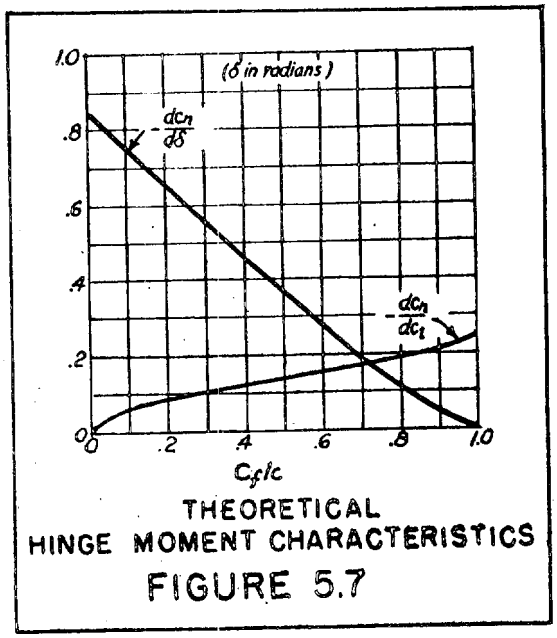

THEORETICAL HINGE MOMENT CHARACTERISTICS

FIGURE 5.7

For partial span flaps, the hinge moment at each section must be determined from the basic lift distribution of the unflapped foil, as previously indicated,

DESIGN EXAMPLE NO. 5.2

SH 1 OF 1

ESTIMATE THE PITCHING MOMENT & HINGE MOMENT CHARACTERISTICS FOR A PARTIAL-SPAN FLAP ,

FOR THE FOIL-FLAP ARRANGEMENT GIVEN IN EXAMPLE 5.1

From Figure 5.6, the section pitching moment factor for $C_f/c = 0.25$ is

$$\left(\frac{d C_{m\,1/4}}{d\delta}\right) = 0.66$$

From Figure 5.7, the section hinge moment factors are

$$\left(\frac{d C_h}{d C_\ell}\right) = 0.10$$

$$\left(\frac{d C_h}{d\delta}\right) = 0.60$$

Since the foil quarter-chord line is straight (as shown in example 5.1), the section pitching moment factor can be modified by the factor k_f' (a function of lift distribution along the span), given in example 5.1

Thus $k_f' = 0.59$

and the total moment factors for the foil are

$$\left(\frac{d C_{m\,1/4}}{d\delta}\right) = 0.66 \times 0.59 = 0.389$$

$$\left(\frac{d C_H}{d C_L}\right) = 0.10 \times 0.59 = 0.059$$

$$\left(\frac{d C_H}{d\delta}\right) = 0.60 \times 0.59 = 0.354$$

4. Drag Characteristics

Parasite Drag

The parasite drag of a foil section increases with deflection of the flaps, as indicated by experiment[2,3]. However, such increase is small, being of the same order of mangftude as that experienced when the unflapped foil is given an equivalent angle of attack,

In other words, the simple relationship of the foil parasite drag varying as the factor $(1 + \Delta C_L^2)$ given in Chapter 4 appears valid whether the lift is due to angle of attack of the foil or deflection of the flap, and no additional parasite drag term need by considered.

Induced Drag

For full span flaps, the expression for the induced drag in terms of the lift as given in Chapters 2 and 3 is valid, without further correction.

For partial span flaps, however, the induced drag must be derived in terms of the redistributed spanwise loading due to the flaps. The airfoil case involves several additional parameters (see reference 3) and the hydrofoil presents the additional consideration of biplane images. Qualitatively, partial span flaps increase the induced drag due to departure of the lift distribution from an optimum whereas

the biplane factor is reduced (when considering the effect over the entire foil. See Durand[6] for biplanes of unequal spans).

It is presently considered that such additional factors need not be considered for preliminary estimating purposes. Test data on partially-flapped foils should be obtained for actual configurations under consideration.

References

1. Abbott & von Doenhoff — "Theory of Wing Sections" McGraw-Hill, 1949.

2. Cahill — "Summary of Section Data on Trailing-Edge High-Lift Devices" NACA Research Memorandum No. L8OD9, 1948.

3. Young — "The Aerodynamic Characteristics of Flaps", ARC Technical Report No, 2622, 1953.

4. Ames & Sears — "Determination of Control-Surface Characteristics from NACA Plan-Flap and Tab Data", NACA Report No, 721, 1941.

5. Pearson & Anderson — "Calculation of the Aerodynamic Characteristics of Tapered Wings with Partial Span Flaps", NACA Report No. 665, 1939.

6. Durand — "Aerodynamic Theory", Vol. II California Institute of Technology, 1943.

CHAPTER 6. HYDROFOIL WAKE

The pattern of the wave produced by a hydrofoil is discussed qualitatively and illustrated by specific test results. Methods to determine the sub-surface flow are given, the significance of the various flow factors for different types of hydrofoil craft are discussed, and data is presented on the waves and flow fields behind a foil.

1. General Considerations

The wake produced by a hydrofoil operating close to the water surface consists of two distinct flows. First,, the foil produces a gravity flow, expressed in a surface wave with its concomitant sub-surface flow field. Secondly, the foil also produces a flow similar to that of an airfoil operating in afr but which is restricted due to the proximity of the water surface. This "aerodynamic" flow is independent of the gravity flow and does not produce a surface disturbance.

All components of a hydrofoil configuration that are located in the wake are affected by the flow characteristics of the wake, Thus, it is necessary to investigate the effects of the flow field on such components located in the wake as: additional foils, struts and rudders, flaps, and propellers,

2. The Wave Pattern

The Wave Produced by a Point Disturbance

The pattern of the wave produced by a hydrofoil is essentially that produced by a series of point disturbances distributed along the lifting line of the foil, and the observed characteristics of the wave pattern can most readily be explained on this basis, Therefore, the characteristics of the wave produced by a single point disturbance will be illustrated briefly,

The pattern of the wave produced by a point disturbance was derived by Havelockl and later by Lunde[2] and is the well-known ship pattern consisting of lateral and transverse waves, as illustrated in Figure 6.1. The formulas for the wave amplitudes are only valid "far behind" the origin and do not represent the conditions close to the origin. Furthermore, the exact amplitudes are not readily ascertained and the relative amplitudes throughout the wave region are extremely difficult to evaluate. Generally, however, the amplitude of each crest is greatest near the "cusp" line, where the lateral and transverse waves combine to produce a high, short crested wave, called the cusp.

The amplitudes of successive crests and troughs decrease in proportion to the distance from the origin, with the transverse waves

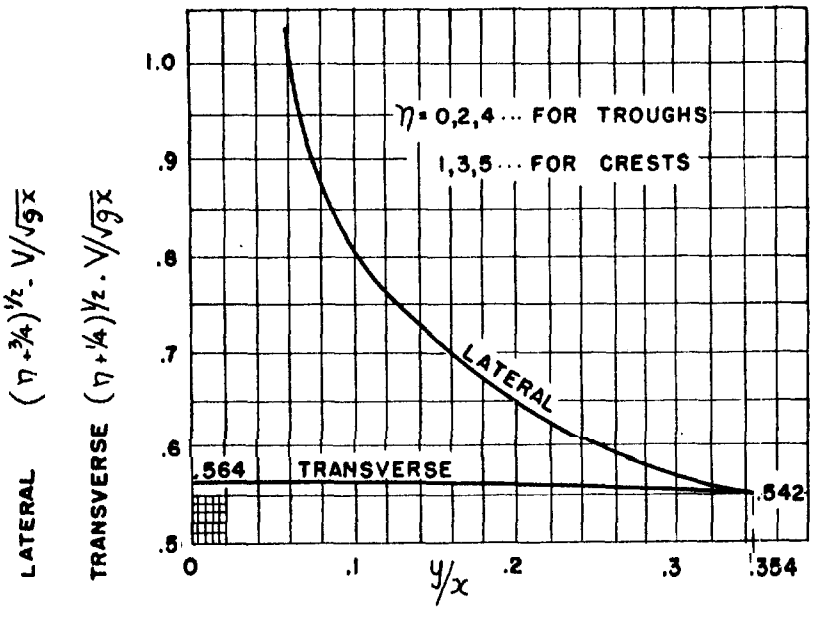

COORDINATES OF CRESTS & TROUGHS

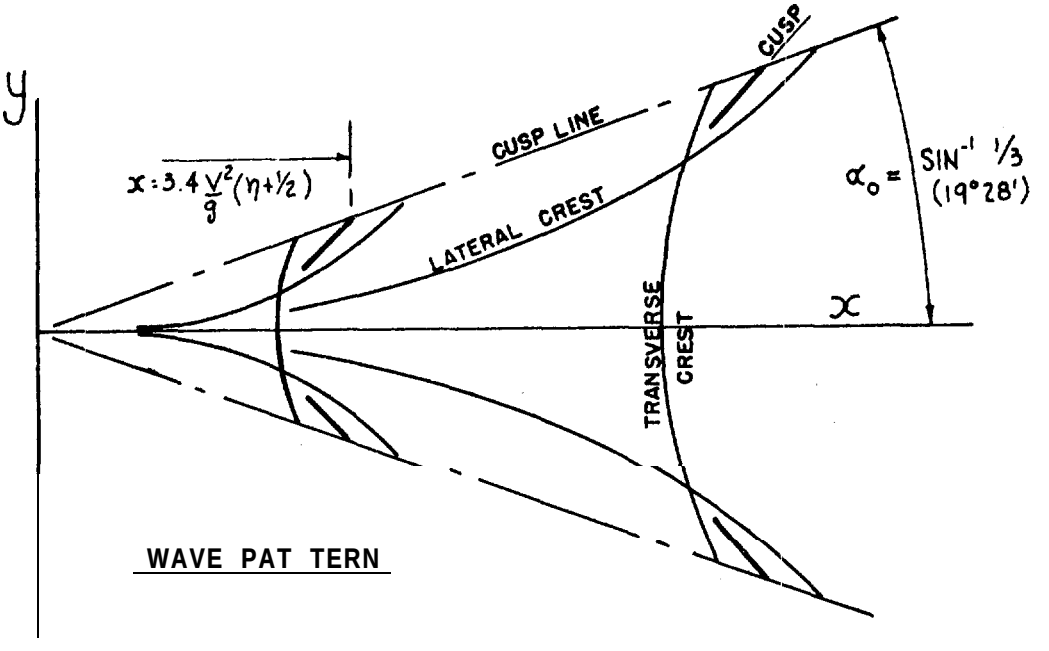

WAVE PAT TERN

CHARACTERISTICS OF WAVES PRODUCED BY A POINT DISTURBANCE

FIGURE 6.1

decreasing at a greater rate. Far aft of the origin, the lateral waves at the cusps are greatly predominant.

In shallow water of depth, d, the characteristics of the wave are markedly different from those in deep water given above. Above a speed $V \simeq a\sqrt{gd}$ the cusp line angle increases from its deep water value of 19°28', with consequent spreading of the lateral waves and decrease in transverse wave amplitude. Theoretically, at the critical speed $V_c = \sqrt{gd}$, the cusp line angle is 90° with a solitary wave proceeding along in line with the origin and no following disturbance. At' supercritical speeds, the pattern is as shown in Figure 6.2, where the transverse waves have disappeared, the lateral waves are concave to the centerline, and the "wave front" is defined by the angle $\alpha_o = \sin^{-1}\sqrt{gd}/V$.

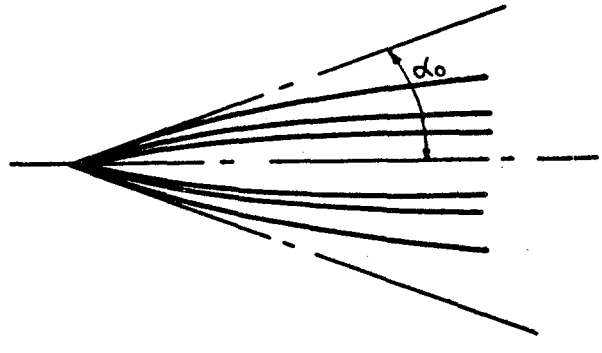

WAVE AT SUPERCRITICAL SPEED

FIGURE 6.2

The Two-Dimensional Wave

A continuous distribution of point disturbances along a line of infinite span would result in transverse waves only, with the crests parallel to the line of disturbance. The wave has been shown by Meyer[3] to be a simple sine wave extending aft with a superimposed local disturbance in the vicinity of the foil. Figure 6.3 shows the wave profile and indicate6 that the local disturbance disappears approximately 1/4 wave length downstream. The equation of the sine wave is given as

$$Z_o = - C_L c \, e^{-gh/V^2} \sin gx/V^2 \qquad (6.1)$$

and the slope of the wave

$$\frac{dz_o}{dx} = \varepsilon_o = - C_L \frac{gc}{V^2} e^{-gh/V^2} \cos gx/V^2 \qquad (6.1a)$$

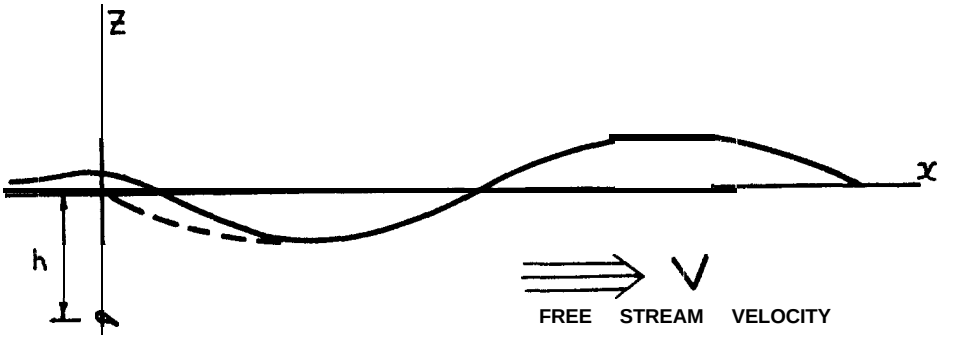

WAVE PROFILE IN TWO DIMENSIONS

FIGURE 6.3

The Three-Dimensional Wave

From the above considerations, the pattern of the wave produced by a hydrofoil of finite span can be shown. In the region between the converging cusp lines emanating from the foil tips, there is a cancellation of lateral waves and a strengthening and straightening of transverse waves, simulating the two-dimensional sinusoidal pattern. Outboard of these converging cusp lines, the pattern approaches that due to a single point disturbance, and is equivalent to it at the cusp lines diverging from the tips. Figure 6.4 shows the pattern, as described above.

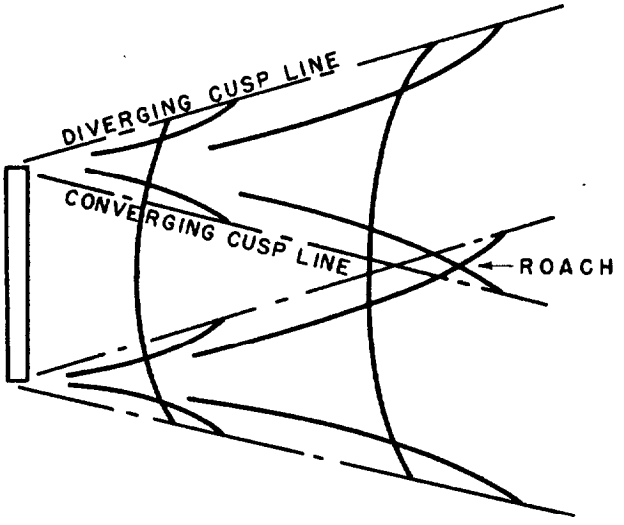

WAVE PATTERN FROM A HYDROFOIL

FIGURE 6.4

Wave contours measured from hydrofoil model tests are shown in Figure 6.5, showing the general pattern indicated above.

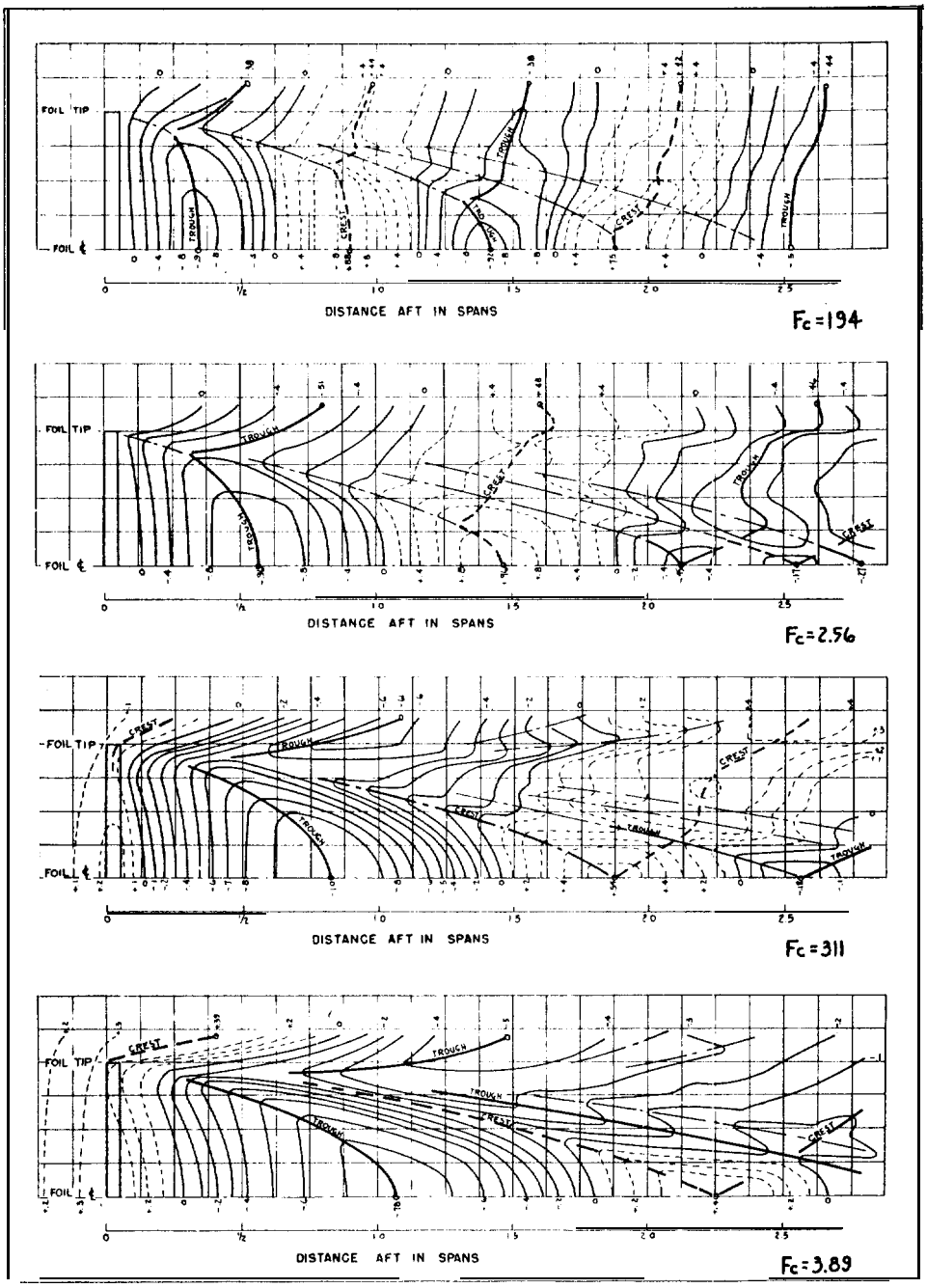

PARTICULARS

RECTANGULAR FOIL — A = 20
SUBMERGENCE — 1 CHORD
DEPTH OF WATER — 18 CHORDS
FROUDE NUMBER — $F_c = V/\sqrt{gc}$ - AS INDICATED

CONTOURS

SOLID CONTOURS DENOTE SURFACE DEPRESSION
BROKEN CONTOURS DENOTE SURFACE ELEVATION
CONTOURS ARE MEASURED IN UNITS OF $y/C_L \cdot c$
WHERE y IS SURFACE ELEVATION
C_L IS FOIL LIFT COEFFICIENT
C IS FOIL CHORD

SURFACE WAVES PRODUCED BY A HYDROFOIL OF LARGE ASPECT RATIO

FIGURE 6.5

3. Sub-Surface Flow

The sub-surface flow in the wake of a foil is due to two effects, namely:

1. that gravity flow associated with the surface wave
2. that due to the "aerodynamic" effects of the foil.

The relative importance of these effects is a function of Froude number, as will be discussed below,

Gravity Flow

The gravity flow at any depth, h, below the surface is easily determined from the surface wave by the classical "decay" formula:

$$\varepsilon_w = \varepsilon_o \cdot e^{-gh/V^2} \tag{6.2}$$

where ε_w is the flow angle at the submergence, h

ε_o is the flow angle at the surface.

Aerodynamic Flow

The basic airfoil wake will first be considered, after which the influence of the surface will be taken into account, The vortex sheet emanating from the foil wraps up into two distinct vortices approximately within one span behind the foil, as indicated in Figure 6.6. The separation between vortices, b', and the radius of the vortex: core, h', are functions of the foil load distribution, and can be determined by methods indicated by Durand[4].

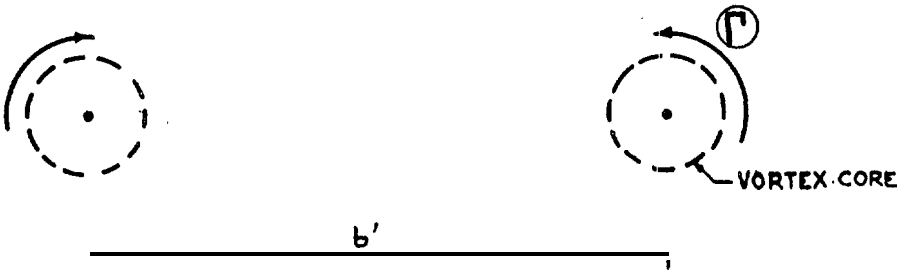

TRAILING VORTEX' SYSTEM FAR BEHIND FOIL

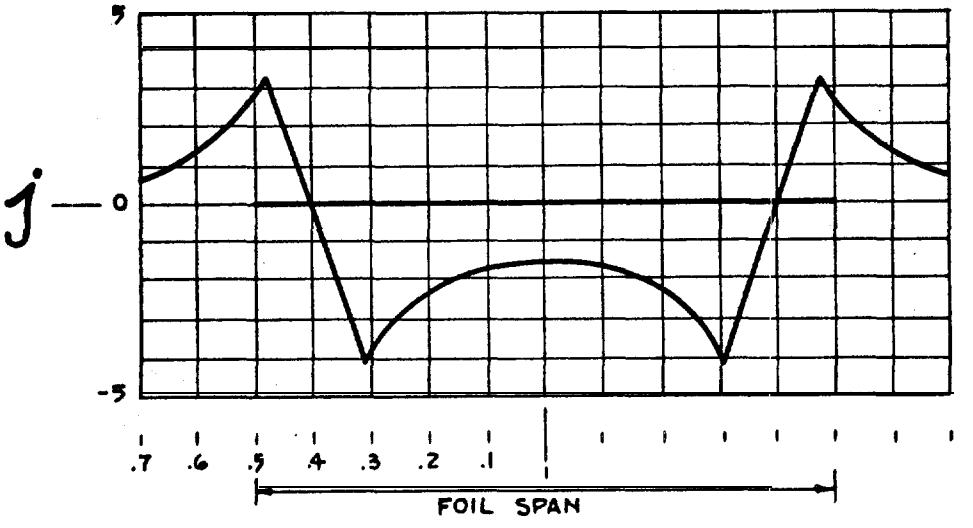

DOWNWASH FACTOR FOR ELLIPTICALLY LOADED FOIL

AERODYNAMIC WAKE

FIGURE 6.6

It is considered sufficiently accurate to assume elliptic loading for the foil when determining the flow in the wake far behind the foil. Then Durand[4] gives the following values

$$\left.\begin{aligned} b' &= \frac{\pi}{4} b \\ h' &= 0.0855\, b \\ \Gamma &= \frac{4}{\pi}\frac{L}{\rho V b} = \frac{2}{\pi}\frac{C_L V b}{A} \end{aligned}\right\} \quad (6.3)$$

The downwash angles in the plane of the vortex lines can be readily determined from the following expression

$$\varepsilon = \alpha_i\, j = \frac{C_L}{\pi A}\, j \quad (6.4)$$

where ε is considered positive for upwash

j is a factor depending upon spanwise location, and is given in Figure 6.6.

Low Froude Numbers

At very low Froude numbers, the "aerodynamic" effect is that of an airfoil near a rigid wall at the water surface, as indicated in Chapter 2, Then the aerodynamic flow angle would be determined by the trailing vortex system and its mirror image as indicated in Figure 6.7. In the plane of the vortices,

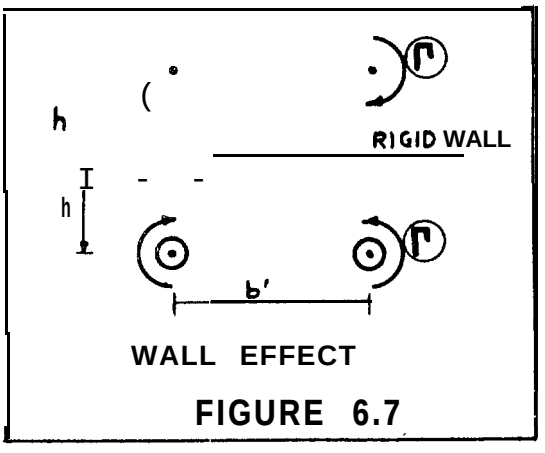

WALL EFFECT

FIGURE 6.7

the downwash angle given in equation (6.4) would be modified to the value

$$\varepsilon_a = \frac{C_L}{\pi A} j (2-K) \qquad (6.5)$$

where K is the generalized factor determined for the foil, as Indicated in Chapter '2.

Then the total sub-surface flow angle at low Eroude Number is

$$\varepsilon_h = \varepsilon_a + \varepsilon_w \qquad (6.6)$$

High Froude Numbers

At high Froude numbers, the wave effects become negligible and the total effect is that of the "biplane", as indicated in Chapter 2. Then the total flow angle is determined by the trailing vortex system and its biplane image as indicated in Figure 6.8. Thus, at high Froude numbers, ε_w may be neglected.

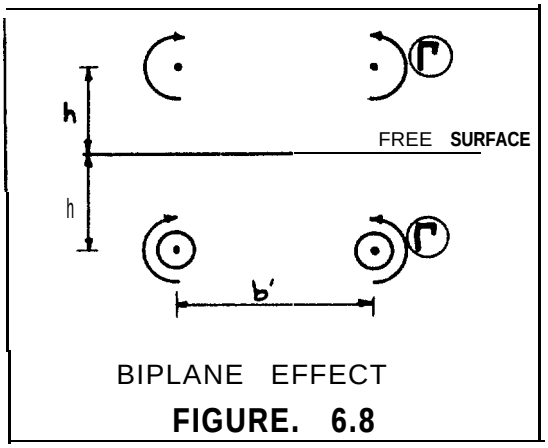

BIPLANE EFFECT

FIGURE. 6.8

In the plane of the vortices, the total sub-surface flow angle at high Froude numoers is

$$\varepsilon_h = \frac{C_L}{\pi A} j K \qquad (6.7)$$

4. Significance of the Wake

The significance of the flow conditions in the wake of a foil as they affect other components naturally depends on the type of hydrofoil configuration investigated. Thfs in turn depends on the type of craft to be designed. Generally, it is necessary to evaluate the influence of the wake although some aspect which may be important in one design is negligible in another, and vice-versa.

How the emphasis on different aspects of the wake changes with different designs can be illustrated by examples of two different types of craft.

(a) The large, slow-speed craft

For a hydrofoil craft of several hundred tons or more and a design speed of less than 40 knots, the hydrofoil configuration would be of the large span, tandem foil type, The wake from the forward foil would be essentially two-dimensional in nature, as in Figures 5.3 and 6.5. Assuming the two-dimensional case for the purpose of illustration, the upwash on the aft foil would be, from equations (6.1) and (6.2):

$$\varepsilon_2 = e^{-gh_1/V^2}\frac{dz}{dx} = C_{L_1}\frac{gc_1}{V^2}\, e^{-g(h_1+h_2)/V^2}\cos gx/V^2 \qquad (6.8)$$

where the subscripts 1 and 2 denote the forward and aft foils respectively,

Since the upwash changes the direction of the lift produced on the second foil by the angle ε_2 resulting in a drag component, the total drag due to lift would be

$$C_{D_W} = C_{D_{W_1}} + C_{D_{W_2}} - \varepsilon_2 C_{L_2}$$

which for foils of equal geometry, submergence and lift can be shown to be

$$C_{D_W} = 2 C_{D_{W_1}} (1 + \cos 9x/V^2) \qquad (6.9)$$

(since $C_{D_{W_1}} = C_L^2 \frac{9c}{2V^2} e^{-2gh/V^2}$ for the foil in two dimensions, as shown in Chapter 2).

Thus, depending on the separation between the foils, the total wave drag could have a value varying from zero to twice that of the configuration without upwash.

(b) *The* small, high speed craft

For a hydrofoil craft of under 100 tons and a speed of over 40 knots, the foils would be small and short in span. The wave produced would be of the type shown in Figure 6.5 (for high Froude numbers), and the wake would have the following features:

a. neglfgible transverse wave pattern

b. strong "aerodynamic" downwash

c. important lateral wave crests and roaches

For this type of wake, the transverse location of the components of the configuration is important as compared to example (a) where the fore-and-aft location is important.

Foils and control surfaces should be positioned so as not to be in the strong flow of the aerodynamic wash; and furthermore, vertical struts and rudders should be positioned to avoid roaches (particularly when located at or near the centerline) and strong lateral cusps, On the other hand, it may prove beneficial to locate propellers directly in the trailing vortex field to take advantage of the rotary flow.

The above examples illustrate the relative importance of different aspects of the wake for dfferent types of craft, In any case, all of the effects should be investigated for a given design.

5. Design Data and Procedure

Existing design data on the wake of hydrofoils is limited to that produced in two exploratory tests. Breslin[5] conducted wave measurements on a foil of aspect ratio 20, the wave contours o.f which are presented in Figure 6.5. E.T.T.[6,7,8] conducted a series of tandem foil tests from which the average upwash angle along the span of the after foil have been calculated, as shown in Figures 6.9 and 6.10.

All the above tests were conducted at a submergence of 1 chord, with foils of large aspect ratio at relatively low Froude numbers. There is a need for additional data, particularly for small foils at large Froude numbers, in order to make reasonable estfmates of the effect of the wake for a greater variety of designs.

The existing data given in the figures can be used for such configurations where interpolations or extrapolations are reasonable, Methods for calculating the wake effect are given, as follows:

(a) Use of Wave Contour Data

From the contour map of the wave produced by a foil of given aspect ratfo at a given Froude number, the flow can be determined for any point in the wake. Determining the surface flow angle, ε_o , from the contour map, the flow angle at a given depth can be established by use of the methods described in Section 3 above.

The determined flow angles along the span of a foil in the wake can be simply average over the span for a reasonable approximation,

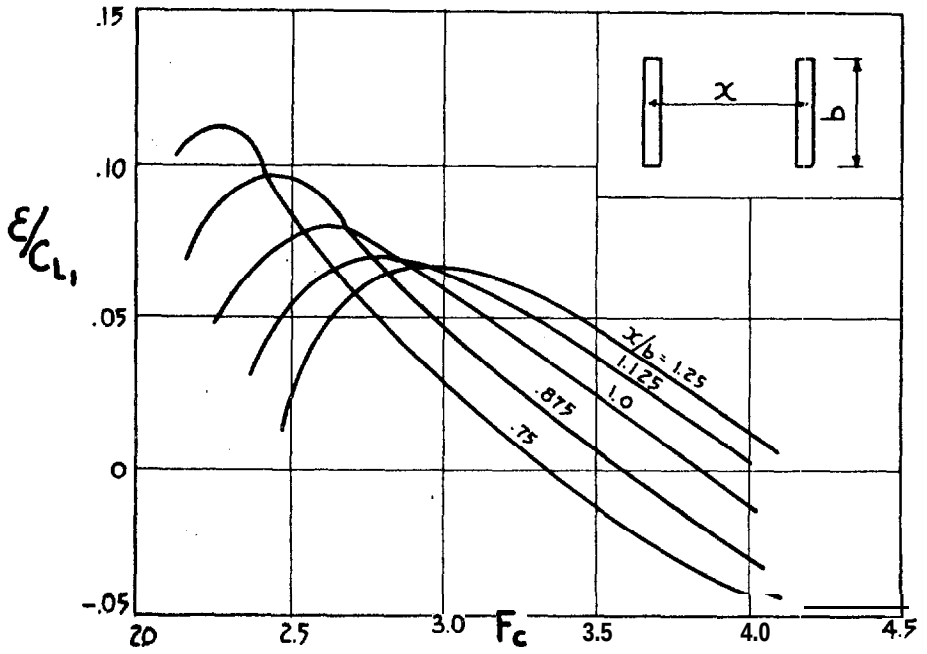

UPWASH ANGLE ON AFT FOIL FOR A= 20 EQUAL. FOILS; h/c=1.0

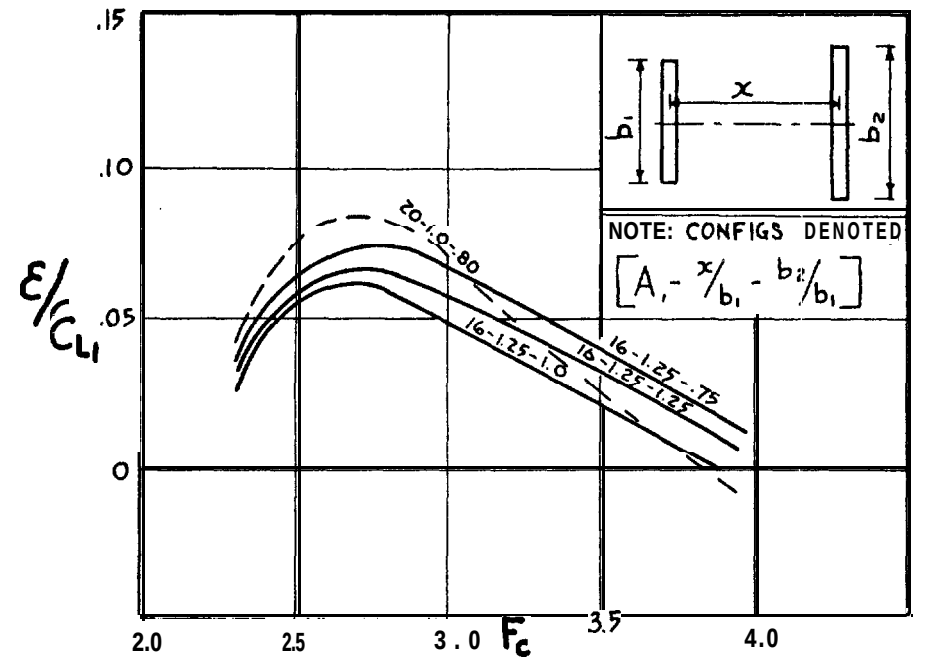

UPWASH ANGLE ON AFT FOIL FOR VARIOUS COMBINATIONS OF LARGE ASPECT RATIO; h/c = 1.0

FIGURE 6.9

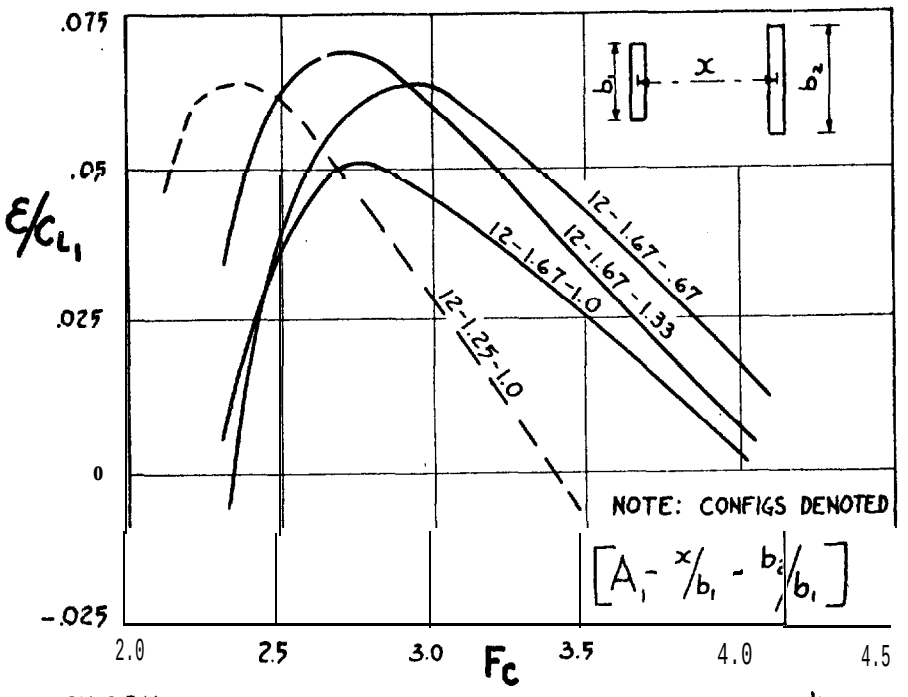

UPWASH ANGLE ON FOILS AFT OF A= 12 FOIL. h/c = 1.0

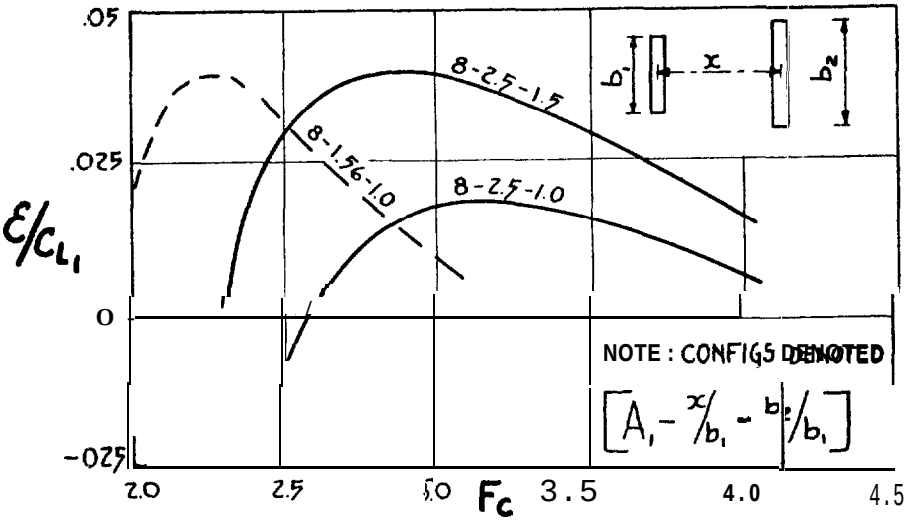

UPWASH ANGLE ON FOILS , AFT OF A = 8 FOIL h/c . 1.0

FIGURE 6.10

(b) Use of Tandem Foil Data

The average upwash data can be interpolated for similar configurations to those tested, and is more direct than the contour data when determining the average upwash on the aft foil, as long as the submergence is the same as that given in the data, When the submergence (of the aft foil) differs from that tested, the data must be corrected by use of the methods of Section 3 above.

(c) Location of Lateral Cusps and Roaches

Where wave contour data is applicable, the location of cusps and "roaches" can be readily observed, and the surface and sub-surface effects readily calculated. (The interference between converging lateral crests, behind the foil midspan, causes a large upsurge of water, commonly called a roach,) Where data is not available for the conditions to be investigated, the approximate locations of crest and troughs can be determined from the theoretical values given in Figure 6.1 for the wave produced by a point disturbance, The waves are assumed to be generated at the foil. tips, The theoretical location of roaches directly behind the midspan of a foil (or midway between the tips of port and starboard foils) can be determined from Figure 6.11. Generally, only the first few waves are of consequence and these only near the cusps and roaches where the amplitudes are large,, Where more than one foil is considered (such as with small foils, P/S), the effects are combined, Since the exact amplitudes of such waves cannot readily be determined, care must be taken in evaluating the importance of different cusps and roaches, particularly when a combination of foils are under study,

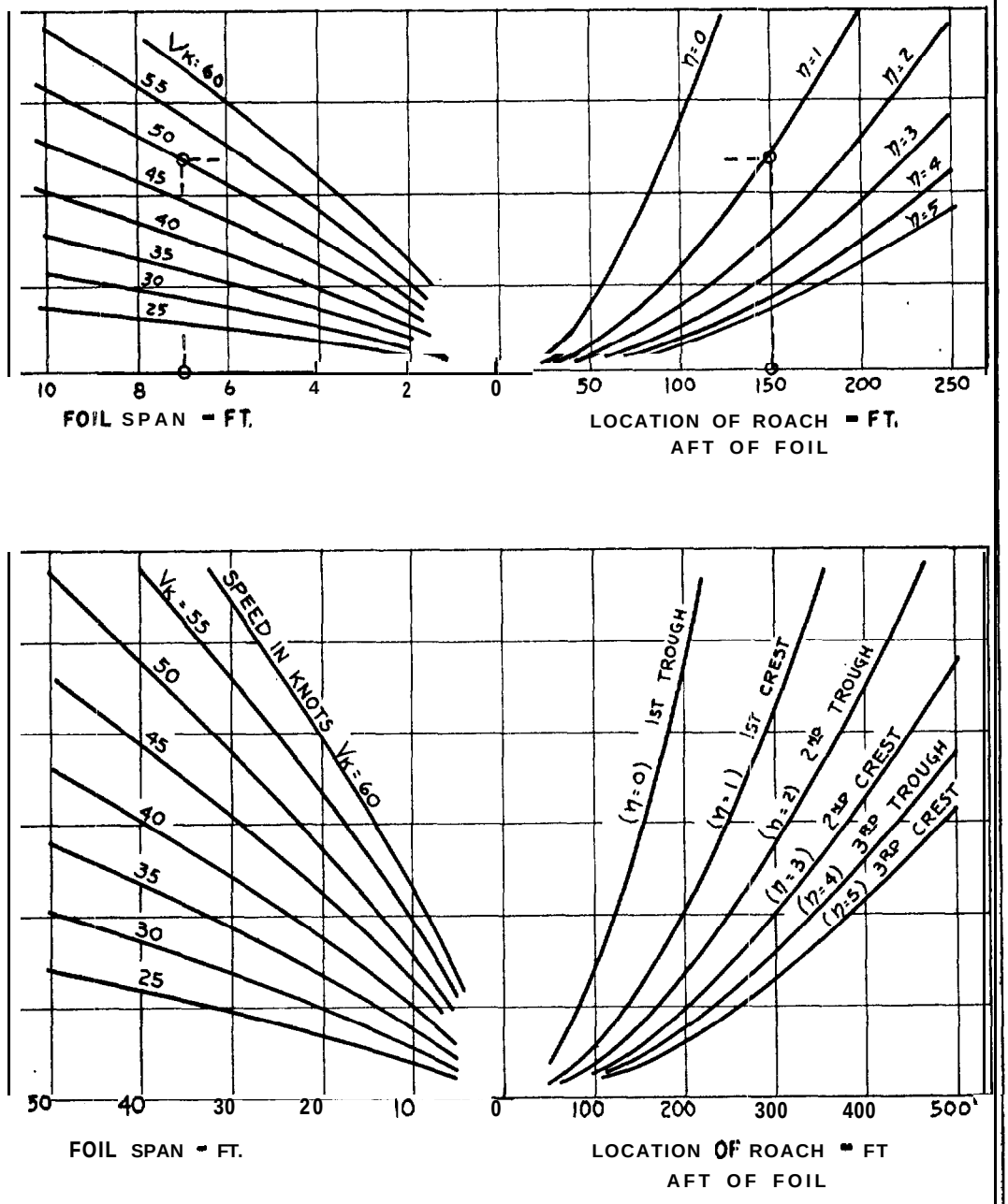

THEORETICAL LOCATION OF ROACHES BEHIND A FOIL

FIGURE 6.11

References

1. Havelock — "The Propagation of Groups of Waves in Despersive Media, With Application to Waves on Water Produced by a Travellfng Disturbance", Proc. of Royal Society, 1908.

2. Lunde — "On the Linearized Theory of Wave Resistance for Displacement Ships in Steady and Accelerated Motion", Society of Naval Architects and Marfne Engineers, 1951.

3. Meyer — "'Surface Waves Produced by Hydrofoils" Hydrofofl Corp, Confidential Technical Memo HM-00, 1950.

4. Durand — "Aerodynamic Theory", Volume II, California Institute of Technology, 1943.

5. Breslin — "An Investigation of the Characteristics of the Waves Produced by a Hydrofoil", BIW Corp. by G&C Inc. Confidential Technical Report No, 13, 19.53.

6. Sutherland — "Extension of Single and Tandem Foil Tests of 2-1/2" Chord Aspect Ratio 20 Hydrofoil", ETT Ltr. Rpt. 410, April 1951.

7. Kaplan — "Extension of Single and Tandem Foil Tests of 2-1/2" Chord Aspect Ratio 20 Hydrofoil and 5" Chord Aspect Ratio 6 Hydrofoil", ETT Ltr. Rpt. No, 428, 1951.

8. Kaplan and Dingee — "Tests of a 5" Chord, Aspect Ratio 6 Hydrofoil Used as a Strut and Tests of 2-1/2" Chord Hydrofoil for Various Aspect Ratios in Single and Tandem Configurations", ETT Ltr. Rpt. No. 429, 1951.

CHAPTER 7. STRUT CHARACTERISTICS

1. Drag Characteristics at Zero Yaw
2. Characteristics in Yaw Prior to Ventilation
3. Characteristics in Yaw When Ventilated
4. Height of Spray

The drag and side force characteristics are given for surface-piercing struts. Spray drag and ventilated characteristics are seen to be functions of section shape, while side force characteristics are shown to be similar to hydrofoil lift characteristics. The hydrodynamic results given include experimental data on spray height,

1. Drag Characteristics at Zero Yaw

Drag Components

The drag of a surface-piercing strut at zero yaw consists of three components: the section drag of the wetted strut and the localized drag at its two ends. The drag at the upper end where the strut pierces the water surface is called "spray drag", being associated with the production of spray at that poiht. At the-lower end, the drag is either "tip drag" for a free-ended strut, or "interference drag" when the strut is connected to a foil or other body.

A wave drag also exists at low Froude numbersl, but becomes negligible above $V/\sqrt{gc} = 3$. Therefore, at the relatively high speeds associated with hydrofoil craft, the wave drag may be ignored.

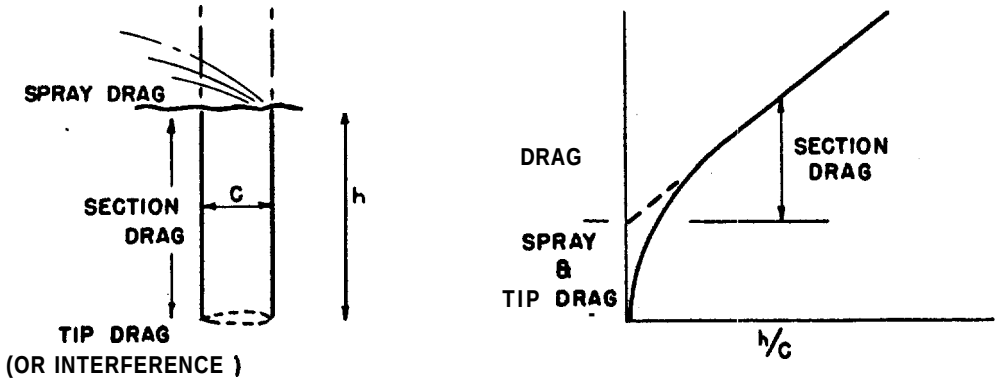

COMPONENTS OF STRUT DRAG

, FIGURE 7.1

Section Drag

The section drag of a strut can be treated in the same manner as for a foil, including all considerations of turbulence, roughness, etc. This material is given in Chapter 4, "Foil Parasite Drag". From equation (4.9), the section drag of the strut can be given:

$$C_{D_{S_b}} = 2 C_f \left[1 + 10 (t/c)_s^2 \right] \qquad (7.1)$$

where $C_{D_{S_b}}$ is the basic section drag coefficient based on the side area of the strut

$(t/c)_s$ is the strut thickness ratio

C_f is the flat plate friction coefficient based on total wetted surface.

The value of C_f can be determined as outlined in Chapter 4, for smooth turbulent, transitional, or standard rough conditions as may be required.*

Spray Drag

The drag arising at the point where the strut pierces the surface is manifested in the development of spray along the forebody of the

* Tank test results on laminar-profile strut sections indicate that the section drag coefficient is in the low drag "bucket" region at test Reynolds numbers as high as 6×10^6. However, foils of comparable profile at lower Reynolds numbers showed fully turbulent section drag coefficients, probably due to a higher level of turbulence in the tank generated by the foil. It is considered that in open waters, the turbulence level is high and the section drag is essentially that in turbulent flow,

strut. This spray drag is a function of the magnitude and distribution of pressure along the forebody, and thus a function of fineness or thickness ratio, t/c, and the sharpness of the leading edge.

At the relatively high speeds associated with hydrofoil craft operation, the spray drag coefficient apparently does not vary with Froude number, according to test results.

Correlated, systematic test results of surface-piercing struts are few in number, and the lack of sufficient data prevents the establishment of a universal function to take into account the fineness and leading edge sharpness. Figure 7.2 shows the spray drag coefficient (based on the area, tc) for several strut sections tested[2,3].

SECTION		$C_{D_{ct}} = \frac{D_{SPRAY}}{stc}$	REFERENCE
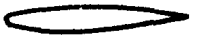	NACA 66-012	0.031	2
	NACA 66-021	0.023	
	BICONVEX $t/c = 0.15$	0.015 - 0.025	3
	DIAMOND $t/c = 0.15$	0.01s	

SPRAY DRAG COEFFICIENTS FOR SEVERAL STRUT SECTIONS

FIGURE 7.2

Generally, it is indicated from these tests that the spray drag coefficient decreases with increasing thickness ratio (but the absolute drag increases, as should be expected), and that the coefficient is less for sharp leading edges than for rounded leading edges such as employed in airfoil sections.

Tip Drag or Interference

The -tip drag of a free-ended strut (i.e. not attached to a foil or other body at its lower end) can be evaluated from airfoil data. Hoerner[4] indicates that for well-rounded tips, there is no tip drag, while for square tips the drag of one tfp is expressed as

$$C_{D_t} = \frac{D_{tip}}{q t^2} = 0.085 \qquad \text{(for square tip)} \qquad (7.2)$$

When attached to a foil, the strut experiences an interference drag at the junction as it similarly imposes an interference drag on the foil, However, the total interference drag at such a junction experienced in tests has been ascribed to the foil for convenience (see Chapter 4), and need not be further considered here.

Effect of Foil Lift

For struts attached to the upper surface of a foil, there is an increase in fluid velocity past the strut due to the circulation around the foil, and therefore an increase in section drag. (There

is no increase in fluid velocity at the water surface and thus no increase in spray drag.) This effect is small (being less than 10% for most applications) and can be approximated by multiplying the strut section drag, equation (7.1), by the following factor

$$\left(1 + J \frac{C_L}{A}\right)^2$$

where J depends on the spanwise location of the strut, a/b, and the submergence-span ratio of the foil, h/b. Values are given in Figure 7.3.

C_L = foil lift coefficient

A = foil aspect ratio

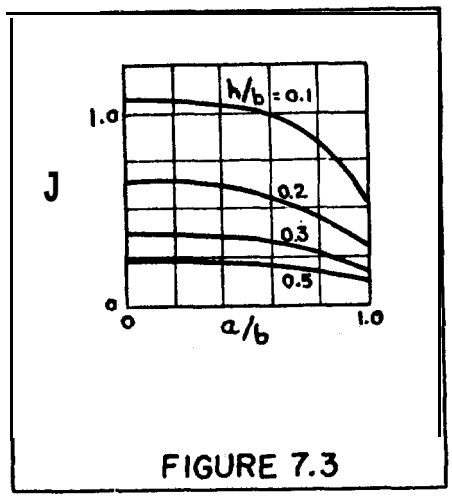

FIGURE 7.3

Effect of Rake

Raking a strut either forward or aft will reduce the section drag from that value produced when the strut is vertical. This is obviously due to the reduction in strut thickness ratio in the direction of fluid flow, and thus the thickness ratio to be employed in equation (7.1) is

$$(t/c)_s / \cos\gamma$$

where $(t/c)_s$ is the nominal section thickness ratio

γ is the angle of rake.

It is not fully evident from existing test data whether there is any real benefit in rake insofar as spray drag is concerned. Generally, it is felt that there is some advantage, but significant gains have not been experienced[2].

Ventilation of Struts

Ventilation is characterized by an air-pocket that is formed at the after-body of a strut, which air-pocket is open to the atmosphere and extends downward along the strut a distance depending on speed and configuration characteristics. (Ventilation should not be confused with cavitation, which is a condition not directly related to the water surface,)

The air-pocket is formed only in the presence of some sharp discontinuity in the flow. The discontinuity produces a vortex which allows the air to penetrate the water surface of constant pressure, after which the full cavity can be formed. Discontinuities arise due to abrupt changes in strut section, local protuberances, momentary yaw angles, etc.

The effect of ventilation is to reduce the section drag of the strut, since air of atmospheric pressure replaces water of sub-atmsopheric pressure at the afterbody, resulting in a forward force component. Quantitative results of this drag reduction are meager and at present fairly inapplicable for the following reasons:

(a) Streamlined free-ended strut sections tested at zero yaw show no tendency to ventilate at moderate and high speeds [2,3]. Whether this condition would prevail in practice where transient yaw angles would be experienced or where local roughness elements might develop sufficiently to "trigger" ventilation is not known., If such were the case, there is no data available on such a condition,

(b) Wedge-shaped strut sections which ventilate throughout the speed range have such a high section drag initially that the reduction in drag due to ventilation does not appear to result in a net gain, as far as existing data indicates [3].

(c) The effect of foil lift on strut ventilation is *not* known. Depending on the foil submergence, the low-pressure region above the foil may "trigger" ventilation (which in turn will lower the lift produced by the foil).

Further experience with actual craft or testing of various configurations under simulated operating conditions is necessary to produce accurate design information regarding ventilation. At present, it is recommended that for streamlined strut sections, the effects of ventilation can be ignored in normal operations at zero yaw.

2. Characteristics in Yaw Prior to Ventilation

The vertical strut having an angle of yaw, ψ, produces a side force and a resultant induced drag. For a fully submerged strut, this is equivalent to the characteristics of an airfoil with a horizontal lift force. For the surface-piercing strut, necessary corrections must be made to account for the boundary effect and for spray-producing drag.

Surface-Piercing Strut

The effect of the surface on the side force characteristics of a strut is a function of Froude number, similar in nature to the effect on the foil discussed in Chapter 2. At low Froude numbers, there is a wave effect and a "rigid wall" effect, the first decreasing the strut efficiency and the latter increasing it.

At high Froude numbers, the surface effect is similar to the "biplane" effect on a foil; hydrodynamically, the strut is then equivalent to one-half of an anti-symmetrically twisted wing.

There are no theoretical analyses presently known that give the force characteristics as a function of Froude number. However, as is indicated in Chapter 2 for foils and in reference 1 for strut wave drag, the region in which wave and rigid wall effects are important is at Froude numbers lower than considered practical for most applications, Therefore, the "biplane" effect is considered to prevail.

On this basis, the aide force characteristics of a surface-piercing strut are approximately as follows:

$$\frac{d\psi}{dC_s} = \frac{E}{2\pi} + \frac{2}{\pi A_s} \tag{7.3}$$

$$\frac{dC_{D_s}}{d(C_s)^2} = \frac{2}{\pi A_s} \tag{7.4}$$

where C_s is the side force coefficient based on the submerged strut area (one side)

C_{D_s} is the strut drag coefficient, based on strut area

A_s is the strut aspect ratio, h^2/S_s

ψ is the angle of yaw

E is the lifting surface correction (see Chapter 2)

Effect of Foil

For the typical case of a strut attached to a foil, the foil exerts an end-plate effect on the yawed strut. This single end plate has a "height" equal to the foil span. Equations (7.3) and (7.4) are thereby modified to the expressions:

$$\frac{d\psi}{dC_s} = \frac{E}{2\pi} + \frac{2}{\pi A_s}\frac{(1+b/h)}{(1+2b/h)} \tag{7.5}$$

$$\frac{dC_{D_s}}{d(C_s)^2} = \frac{2}{\pi A_s}\frac{(1+b/h)}{(1+2b/h)} \tag{7.6}$$

where $\frac{(1+b/h)}{(1+2b/h)}$ is the approximate induced factor for a single end plate

b is the foil span

h is the strut length (foil submergence)

Equations **(7.5)** and **(7.6)** can also be used for a free strut that has an end plate at its lower tip, with the actual end-plate **"height"** being substituted for the foil span, b .

Low Aspect Ratio Correction

Strut aspect ratios are generally low for most hydrofoil applications, and the E factor becomes important, as indicated in Chapter 2. The non-linear effects, which are based on flow across the tips (as shown in Chapter 2), are not expected to be present on a **surface-**piercing strut supporting a foil, since there is no flow across the tips in this case, and equations **(7.5)** and (7.6) still apply. For a free-ended surface-piercing strut, there is flow across the lower tip, and in the absence of specific test data, it is assumed that the non-linear effect is 1/2 that for a submerged foil with both tips free.

Thus,, rewriting equations (7.2) and (7.3) in different form and adding the non-linear terms, we get for free-ended struts:

$$C_S = \frac{\sin\psi}{\frac{E}{2\pi} + \frac{2}{\pi A_s}} + \sin^2\psi\cos\psi \qquad (7.7)$$

$$C_{D_S} = C_{D_{S_o}} + \frac{2}{\pi A_S}\left(\frac{\sin\psi}{\frac{E}{2\pi}+\frac{2}{\pi A_S}}\right)^2 + \sin^3\psi \qquad (7.8)$$

where $C_{D_{S_o}}$ is the parasite drag coefficient of the strut (including spray drag) which is also a function of yaw angle, ψ .

Correlation with Test Data

Tests have been conducted on yawed struts at E.T.T.[5], and results for free-ended struts are shown in Figure 7.4. In the non-ventilated region, equation (7.7) is seen to agree closely with the experimental results for side force.

For the drag, $C_{D_{S_o}}$ was estimated to be 0.012 including spray, for the section at the tested speed. Equation (7.8) was then evaluated (for A = 1/2 and 1, which are identical. A = 2 gives slightly lower drag). The agreement is good.

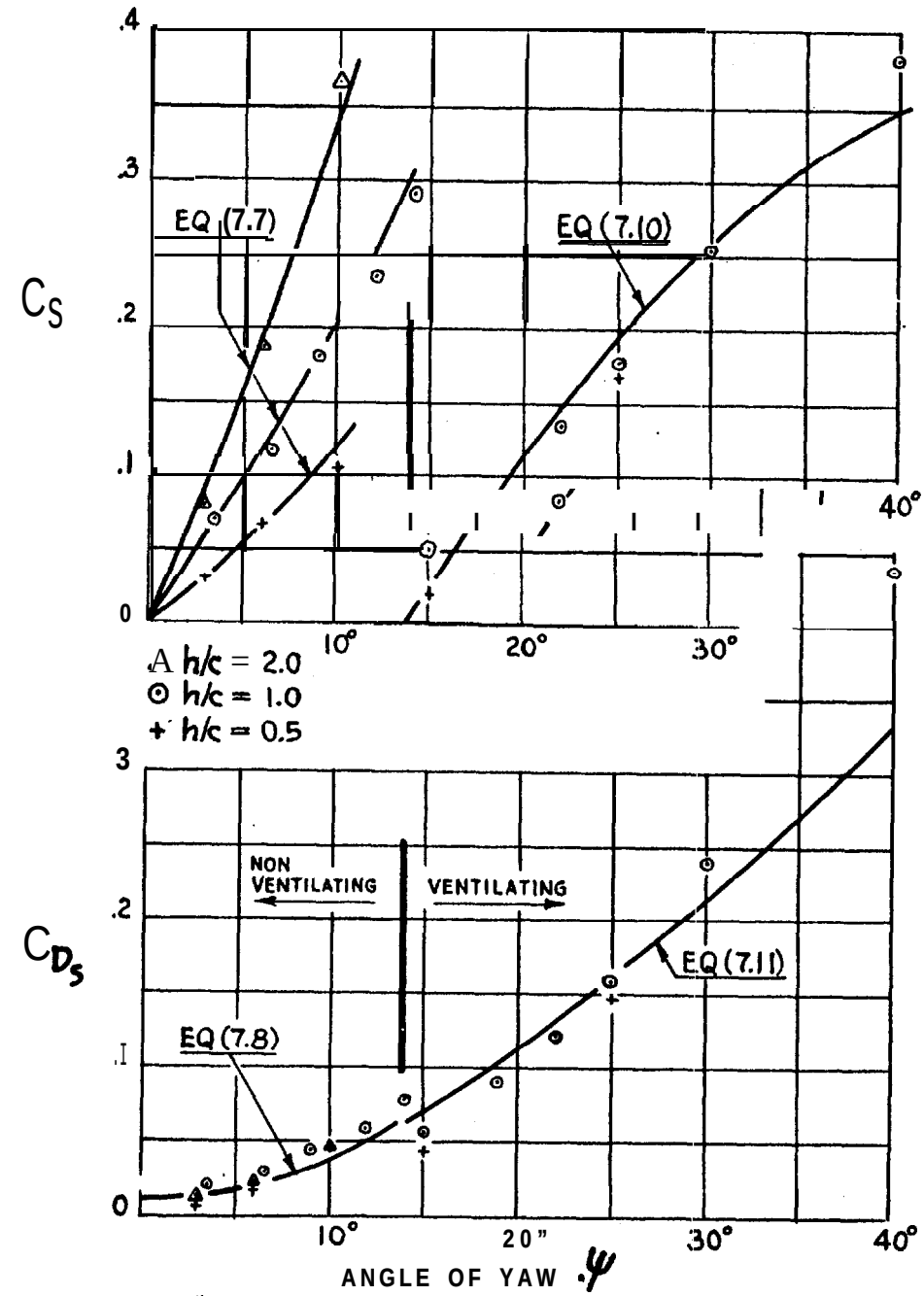

2-1/2" X 12% DOUBLE ARC STRUT
TEST SPEED 25 FPS

SIDE FORCE AND DRAG CHARACTERISTICS OF A SURFACE-PIERCING STRUT

FIGURE 7.4

DESIGN EXAMPLE NO. 7.1

SH 1 OF 2

DETERMINE THE DRAG & SIDE FORCE CHARACTERISTICS OF A SURFACE-PIERCING STRUT, PRIOR TO VENTILATION

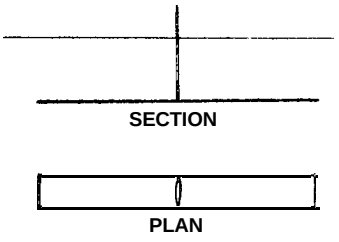

A SINGLE STRUT OF CONSTANT SECTION SUPPORTS A RECTANGULAR FOIL AT MIDSPAN. THE STRUT IS VERTICAL WITH A 12" CHORD AND 10% THICKNESS, THE FOIL IS 6'SPANX 12" CHORD, WITH A SUBMERGENCE OF 2', AND SUPPORTS A LIFT OF 6500 Lb. AT 35 KNOTS

REQUIRED PARTICULARS

$q = \rho/2\ V^2 = \frac{1.99}{2} \times (35 \times 1.69)^2 = 3480$

Foil Lift Coefficient, $C_L = \frac{6500}{3480 \times 6} = 0.31$

Foil Aspect Ratio, $A = 6$

Foil submergence/span ratio, $h/b = 1/3$

Strut Aspect Ratio, $A_S = 2$

Reynolds number (59° sea water) $= \frac{35 \times 1.69 \times 10^5}{1.28} = 4.6 \times 10^6$

STRUT PARASITE DRAG

Section Drag (From Chapter 4)

At $R = 4.6 \times 10^6$, $C_{D_f}(\text{std}) = 0.0041$

and $(C_{D_o})\ \text{std} = 2 \times 0.0041\,[1+10(0.10)^2][1+C_S^2]$

$= 0.0090(1+C_S^2)$

From page 7.6 and Figure 7.3, the factor of additional dynamic pressure is

$(1+0.35 \times 0.31/6)^2 = 1.036$

Then,

$C_{D_o} = 1.036 \times 0.0090\,(1+C_S^2)$

$= 0.0093\,(1+C_S^2)$

DESIGN EXAMPLE NO. 7.1

STRUT PARASITE DRAG (CONT'D)

Spray Drag

From Figure 7.2, take the average value

$C_{D_{ct}} = a.020$ for a biconvex section

Then, assuming frontal thickness varies directly as the yaw angle

$t = 0.10c + \psi c = c(0.10 + \psi)$

and referring the spray drag to the strut area

$$C_{D_{ct}} = \frac{D_{spray}}{q_{ct}} = \frac{D_{spray}}{q_{ch}} \times \frac{h}{t} = A\, C_{D_o} \times h/t$$

Then

$$\Delta C_{D_o} = \frac{c}{h}(0.10 + \psi) \times 0.020 = 0.001 + 0.01\,\psi$$

SIDE FORCE & INDUCED DRAG

From Equation (7.5)

$$\frac{d\psi}{dC_s} = \frac{1.5}{2\pi} + \frac{2}{2\pi}\frac{(1+3)}{(1+6)} = 0.421$$

$$\frac{dC_s}{d\psi} = 2.375$$

From Equation (7.6)

$$\frac{dC_{D_s}}{dC_s^2} = \frac{2}{2\pi}\frac{(1+3)}{(1+6)} = 0.182$$

TOTAL CHARACTERISTICS

Side Force

$C_s = 2.375\,\psi$

Drag

$$C_D = 0.093 + 0.001 + 0.093\,(2.375\,\psi)^2 + 0.01\,\psi + 0.182\,(2.375\,\psi)^2$$

$$= 0.094 + 0.01\,\psi + 1.55\,\psi^2$$

3. Characteristics in Yaw When Ventilated

Inception of Ventilation

As indicated in Section 1 above, ventilation is due to some discontinuity in the fluid flow at the water surface. In the case of the yawed strut, it apparently occurs when the angle of yaw, ψ, exceeds the entrance angle, @ , of the strut section at the surface, as indicated by the test data of Figure 7.4. As has been stated in Chapter 3, the angle, β , is readily determined for a section with sharp leading edge, but has no exact definition for an airfoil section. It appears reasonable to use the angle formed by a circular arc tangent to the section at the point of maximum thickness and passing through the leading edge, as shown in Figure 7.5.

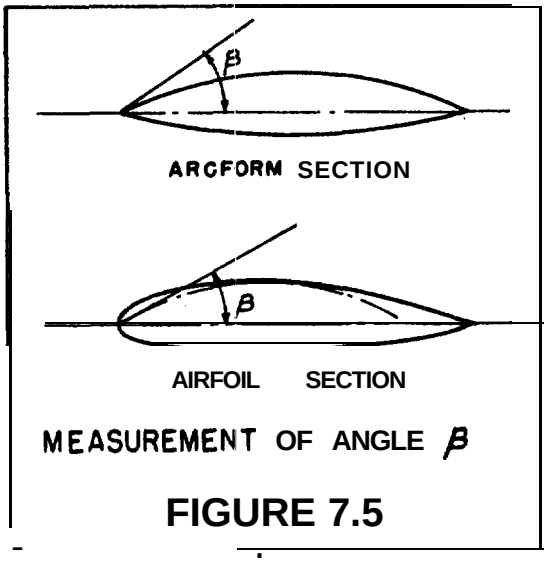

FIGURE 7.5

Lift and Drag

The characteristics of a fully ventilated strut are similar to those of ventilated foils, as treated in Chapter 3, Thus for a flat

plate strut with no flow across the tips, the normal force is

$$C_N = \frac{2\pi \sin\psi}{4 + \pi \sin\psi} \tag{7.9}$$

For a surface-piercing strut with foil attached at the lower tip, there is no cross flow at the tips and equation (7.9) should apply. For a free-ended strut, there is cross flow at the free tip and the resultant normal force is somewhat reduced.

In practical applications, strut sections are not flat on the pressure side. The angle ψ in equation (7.9) must therefore be measured from the angle of zero side force, which is indicated in Chapter 3 for ventilated foils to be the angle at which the trailing edge on the pressure side is in line with the fluid flow. For symmetrical struts, this is the angle of run (the angle β for the trailing edge). Thus, the equation for side force in ventilated condition is

$$C_{S_V} = k_v \frac{\sin\psi' \cos\psi'}{4 + \pi \sin\psi'} \tag{7.10}$$

where k_v is a factor depending on the conditions at the strut tips (1.0 for no cross flow)

ψ' is the yaw angle measured from the angle of zero side force (in ventilated condition).

The drag is not similarly reduced, however, being mainly dependent on the frontal area of the strut exposed to the stream flow. Thus, it is primarily a function of the actual yaw angle, modified to some presently unknown degree by section shape. Tentatively, it is considered

that the drag component of the basic flat plate normal force be applied (modified as required for free tips). Thus:

$$(C_{D_S})_v = C_{D_{S_o}} + k_v \frac{2\pi \sin^2\psi}{4 + \pi \sin\psi} \qquad (7.11)$$

where ψ is the actual yaw angle

$C_{D_{S_o}}$ is the parasite drag coefficient of the strut (including spray). The friction drag in this case is 1/2 that in regular flow since only one side of the strut is wetted.

Comparison with Test Data

For the 12% double arc struts used in the E.T.T.[5] tests, the entrance angle is $\beta = 13.9°$ (for leading and trailing edges). The data of Figure 7.4 indicates the inception of ventilation to occur between 14° and 15°.

The lift data in ventilated condition shows a reasonable fit with equation (7.10), using a factor $k_v = 3/4$ and measuring from the angle of 13.9".

For the drag in ventilated condition, $C_{D_{S_o}}$ was taken as 0.006 (1/2 of that for the non-ventilated case). Using the factor $k_v = 3/4$ derived above, equation (7.11) is shown in the figure, and appears to be a reasonable estimate of the drag.

As previously stated, more test data on a variety of struts under various conditions is required before more reliable design formulas can be advanced and reliable factors established.

4. Height of Spray

The spray produced by a strut is primarily a function of the frontal area of the strut (projected area normal to the fluid flow) in association with the speed of advance. Hoerner[1] has analyzed available data on spray height, for struts at various angles of yaw. His results can be summarized in the following formula.

$$\frac{h_x}{c_s} = 0.86\, F_x \left(\frac{t}{c}\right)_s + 0.026\, F_{c_s}\, \psi \qquad (7.12)$$

where h_x is the maximum height of spray

c_s is the strut chord

F_x is the Froude number based on forebody length

F_{c_s} is the Froude number based on strut chord

$\left(\frac{t}{c}\right)_s$ is the strut thickness ratio

ψ is the angle of yaw.

Equation (7.12) must be considered preliminary, being based on a minimum of data. In particular, the latter terms which include. yaw is based on tests run at low Reynolds number ($R \approx 10^5$) and Froude number ($F_{c_s} = 2.9$), and may not represent conditions at usual operating speeds.

References

1. Hoerner — "Some Characteristics of Spray and Ventilation", BIW Corp. by Gibbs & Cox, Inc. Technical Report No. 15, Contract No. Nonr-507(00), 1953.

2. Coffee and McCann — "Hydrodynamic Drag of 12- and 21-Percent Thick Surface-Piercing Struts', NACA Technical Note 3092, 1953.

3. Kaplan — "Tests of Surface-Piercing Struts" E.T.T. Letter Rpt. No. 488, 1953.

4. Hoerner — "Aerodynamic Drag" Published by Author, 1951.

5. Dingee — "Characteristics of Four Skids and a Surface-Piercing Strut", ETT Letter Rpt. No. 472, 1952.

CHAPTER 8. RUDDER CHARACTERISTICS

The types of rudders likely to be employed on hydrofoil craft are discussed and categorized. It is shown that rudder characteristics can be derived from pertinent foil and strut properties presented in previous chapters.

1. Description of Types

Rudders on hydrofoil craft may be considered in two broad categories: first, as applied to the foil configuration when in flying attitude; second, as applied to the hull, prior to take-off.

For some simpler configurations, one rudder or system of rudders is used for both purposes, whereas in others independent rudders are used for each type of operation. The choice lies in the selection of the configuration to be employed and is a matter of overall design. However, the pertinent hydrodynamic characteristics of the rudder depend on its relative location and intended function.

Thus, rudders that are essentially part of the foil configuration and are used in foilborne operations can be treated in accordance with the foil principles set forth in previous chapters. For rudders that are essentially part of the hull configuration (being used primarily for hull borne operations), the various influences of the adjacent hull must be taken into account.

There are two main types of rudders to be considered: first, the all-movable rudder which is also referred to as a balanced rudder (since the pivot point can be located at the center of pressure), and secondly, the flap rudder which is located behind a streamlined post and is essentially a flap pivoting behind a fixed strut (similar to

a flap on a foil). The characteristics of each type also depend on whether the rudder if fully submerged or surface&piercing.

There are variations which combine both types to some degree, the characteristics of which can be reasonably determined from those of the basic types.

ALL MOVABLE

FLAP

BASIC RUDDER TYPES

FIGURE 8.1

2. Characteristics of All-Movable Rudders

Fully-Submerged Rudders

Rudders that are fully submerged are essentially considered to have the same hydrodynamic characteristics as a foil and thus the lift or side force, drag and moment of the rudder can be readily determined by the principles set forth in Chapters 1 and 2.

Since fully submerged rudders are usually of small aspect ratio, the lifting surface theory should be applied.

Reference should therefore be made to those chapters for the methods and formulas to be used, with the following changes in notation to be employed:

C_S the side force coefficient, instead of C_L

δ_r the rudder deflection angle, instead of α

h_r the "span" of the rudder (height).

Surface-Piercing All-Movable Rudders

All-movable rudders that extend through the water surface are essentially surface-piercing struts, insofar as the hydrodynamic characteristics are concerned. Thus, the material given in Chapter 7 for struts can apply directly to the rudders of the same type, the only distinction being that the rudder is referred tot

δ_R, the rudder deflection angle instead of

ψ, the strut yaw angle.

This applies to ventilated as well as non-ventilated condition, including the end-plate effect of any foil, nacelle, end plate, etc. on the lower tip.

3. Characteristics of Flap Rudders

As illustrated in Figure 8.1, a flap rudder is essentially the after portion of a strut so arranged to pivot (as a flap) behind the fixed forward portion, As such, it is similar to a foil with plain flap and its hydrodynamic characteristics can be determined from the principles of flaps given in Chapter 5.

Side Force of Flap Rudders

Thus, from equation (5.4), with appropriate changes in notation (and noting the angle of zero lift is zero for symmetrical sections, as usually employed on rudders), the side force can be given for submerged or surface-piercing rudders:

$$C_s = \left(\frac{dC_s}{d\psi}\right)(\psi + k_f \alpha_h) \qquad (8.1)$$

where C_s is the side force coefficient, based on total side area of the strut-flap

$\left(\frac{dC_s}{d\psi}\right)$ is the side force curve slope of the unflapped strut, as determined above or in Chapter 7, for the submerged or surface-piercing case, as required.

ψ is the angle of yaw of the fixed strut section

α_h is the flap deflection angle

k_f is an effectiveness factor.

The effectiveness is given in Chapter 5 as

$$k_f = 1.1\sqrt{c_f/c} \qquad (8.2)$$

where c_f/c is the flap chord/total seotion chord ratio. Equation (8.2) is considered valid for flap deflections of less than 15° and flap chords less than 70% of the total chord.

Other Characteristics

Generally, then, all of the flap rudder characteristics can readily be determined from the principles set forth on flaps in Chapter 5 in conjunction with the basic strut charaoterfstios set forth in Chapter 7. Hinge moments, partial-span flaps, drag, etc. oan all be obtained with the same degree of accurao,y as for foil flaps.

Ventilation

The ventilating characteristics of surface-piercing flap rudders are expected to be somewhat different from those of struts and all-movable rudders . It is considered that since the flap rudder gets its Sift due to change in oamber instead of change in angle of attack, the flow across the leading edge of the section is not as great as in the other oases and thus the flap rudder should not ventilate as readily (i.e. it should be capable of higher side foroe prior to rentflation). There is no known data available to support (or disprove) this contention, and therefore tests are required before design formulas can be presented.

4. Rudders on Hulls

Auxiliary rudders are sometimes employed to provide steering when the craft is hull borne, prior to take-off. Such rudders are attached to or in close proximity to the hull and usually rise clear of the water after take-off.

For the type of hull usually employed in hydrofoil craft, these rudders would be located beneath the hull. Thus, no consideration need be given to surface-piercing rudders for the low speed range (low Froude and Reynolds numbers) prior to take-off.

Hull rudders may, therefore, be treated as lifting surfaces in an infinite fluid, and the theory of small aspect ratio foils can be employed to determine their hydrodynamic characteristics, taking into account the influence of the hull.

Theoretically, the influence of the hull is to double the effective aspect ratio of the rudder, when the rudder is attached directly to the hull (zero clearance). As the clearance increases the effectiveness is decreased, so that at about a clearance equal to 1/2 the rudder height the rudder is free of any hull effects. (This can be shown quantitatively, from the treatment of air gap in a wing, given by Durand[1]). To what extent viscous effects influence the rudder effectiveness (boundary layer effects on the clearance and on

the rudder itself) is not known specifically and cannot be generalized due to the variety of possible arrangements on the hull-rudder geometry.

Much information on the characteristics of hull rudders, the effect of various influences and practical approaches to design can be gotten from various marine sources[2,3].

References

1. Durand — "Aerodynamic Theory", Vol. II California Institute of Technology, 1943.

2. Rossell & Chapman — "Principles of Naval Architecture", Vol. II, SNAME, 1941.

3. Mandel — "Some Hydrodynamic Aspect of Appendage Design?,, SNAME Transactions, 1953.

CHAPTER 9. CHARACTERISTICS OF NACELLES AND SMALL APPENDAGES

1. Nacelle Size and Shape
2. Characteristics of Isolated Nacelles
3. Characteristics of Nacelles in a Foil Configuration
4. Drag of Small Appendages

The typical geometry of nacelles used in hydrofoil application is indicated and data on the lift, drag, and pitching moment of isolated nacelles is given. The characteristics of various nacelles in configurations are discussed qualitatively and procedures for determining and using various data are given. The drags of miscellaneous small bodies are tabulated,

1. Nacelle Size and Shape

In hydrofoil applications, nacelles are used primarily for propulsion and transmission machinery. Characteristically, nacelles are streamlined in shape, with cross-sections varying from circular to rectangular (at their largest sections) which generally are faired into rounded noses and conical tails,

The hydrodynamic characteristics of nacelles are commonly expressed in coefficient form, usually based on the wetted surface of the nacelle (in marfne applications).

> The drag of a long slender nacelle (submarine, airship, etc.) with its axis in the direction of flight is primarily due to friction, and thus the wetted surface is the most important reference area in this regard.

However, it is conventient in most cases to refer the nacelle characteristics to the frontal area (maximum cross-section), which is more readily determfned in prelfminary investigations and which is important *in* evaluating the optimum nacelle geometry for a given application.

The ratio of the wetted area to the frontal area is approximately given' for most nacelle shapes as:

$$\frac{S_{wet}}{S_n} = 3\,\ell/d \qquad (9.1)$$

where ℓ is the length of the nacelle

d is the diameter (or equivalent diameter for non-circular shapes) at the maximum cross-section

S_{wet} is wetted surface of nacelle

$S_{\square}$ is frontal area (maximum cross-sectional area).

2. Characteristics of Isolated Nacelles

Parasite Dran with Flow Parallel to Nacelle Axis

The parasite drag of a nacelle in an infinite fluid is composed of friction drag and pressure drag. For a long slender body (hfgh ℓ/d) the friction drag is most important; for a blunt body (low ℓ/d) the pressure drag is predominant, Thus, the total parasite drag is a function of the various shape parameters of the nacelle.

Experimental data on a variety of aircraft bodies (airships, fuselages, etc.) is available in N.A.C.A. reports*. Gertler[2] gives results for streamlined bodies of revolution of high ℓ/d (ℓ/d = 4 to 10). From such sources, the parasite drag can be accurately determined.

From an analysis of such data, Hoerner[1] gives an empirical formula which can be used for preliminary purposes with good accuracy. In terms of the wetted area, this formula is

$$C_{D_{wet}} = C_f \left[1 + \tfrac{1}{2} d/\ell + 6 (d/\ell)^4 \right] \qquad (9.2)$$

and by substituting equation (9.1), the formula in terms of the frontal area is:

---

* See N.A.C.A. "Index of NACA Technical Publications", 1949

$$C_{D_a} = C_f \left[1.5 + 3\, \ell/d + 18 (d/\ell)^3 \right] \qquad (9.3)$$

where C_f is the frictional drag coefficient based on wetted area (see Chapter 4) at the appropriate Reynolds number based on the length of the nacelle.

ℓ/d is the length/diameter ratio, as indicated above.

Figure 9.1 (taken from reference 1) shows the frontal drag coefficient as given in equation (9.3), and as derived from experimental data. The optimum ℓ/d is seen to be close to 2 for such isolated nacelles. (As shown in the following section, the optimum ℓ/d of the nacelle is larger when in conjunction with a foil.)

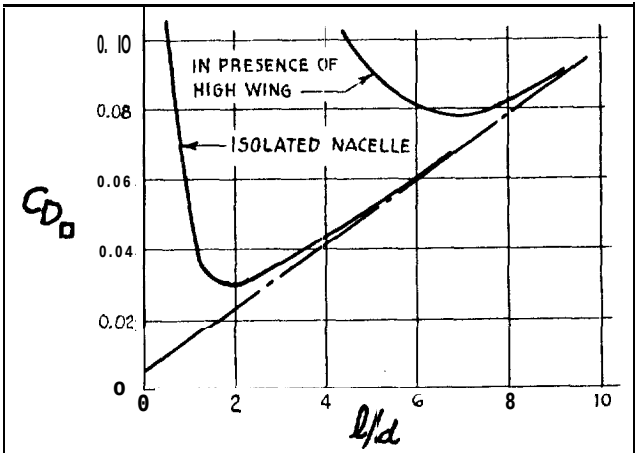

NACELLE FRONTAL DRAG COEFFICIENT

FIGURE 9. I

Wave Drag of Nacelles

In his tests on streamlined bodies of revolution, Gertler[2] also determined the wave drag of bodies with $\ell/d = 7$ at submergences slightly greater than 1 diameter. Prom this data, it is indicated that the wave drag component is appreciable at low Froude numbers (based on the body length) but is negligible above Froude numbers of 1.0 to 1.5. Figure 9.2 shows the results for one of the bodies tested, from which estimates may be made for other cases in the absence of specific test data.

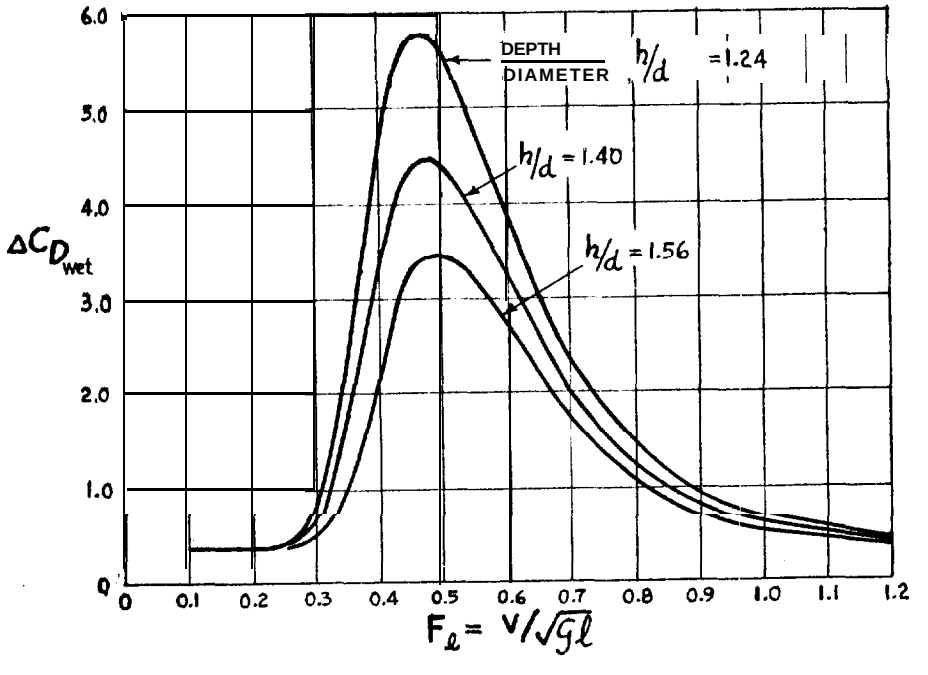

FIGURE 9.2

Characteristics at Angles of Attack

Nacelles may be considered to be foils of small aspect ratio in analyzing the lift, drag and moment character&tics at angle of attack. However, due to the shape of the body, the large "thickness" and different "tip conditions", such analysis would be qualitative only; and reliable values ean only be determined from experimental data, as is available in reports on airship and fuselage characteristics (see NACA Index of Technical Publications). Where the submergence and Froude number are small, tank tests should be run in order to determine the characteristics more exactly as influenced by the water surface.

Figure 9.3 gives some representatfve data, as shown by Hoerner[1], and as given by Jacobs and Ward[3] for several fuselage shapes. The lift and drag coefficients are based on frontal area, The moment coefficient about the quarter length is based on frontal area and fuselage length,

FROM REFERENCE I.

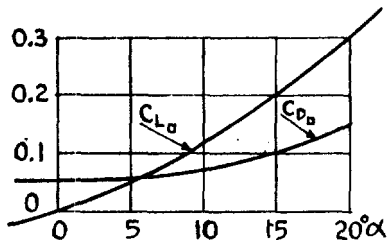

CIRCULAR NACELLE

$\ell/d = 6.7$ $R = 3 \times 10^6$

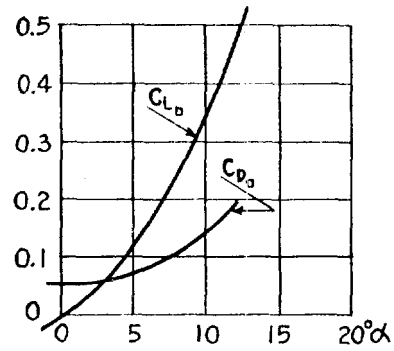

RECTANGULAR NACELLE

$\ell/d = 6.9$ $R = 10^6$

FROM REFERENCE 3.

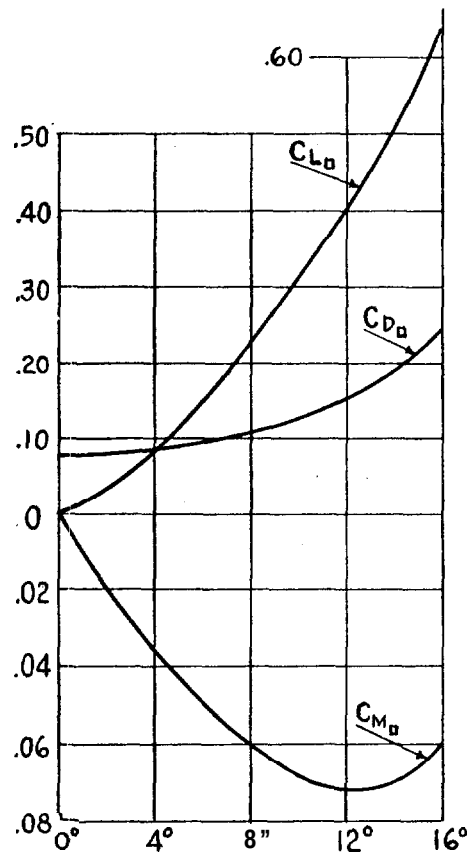

RECTANGULAR NACELLE

$\ell/d = 5.06$

$R = 3.1 \times 10^6$

NOTE : MOMENT COEFFICIENT BASED ON NACELLE LENGTH

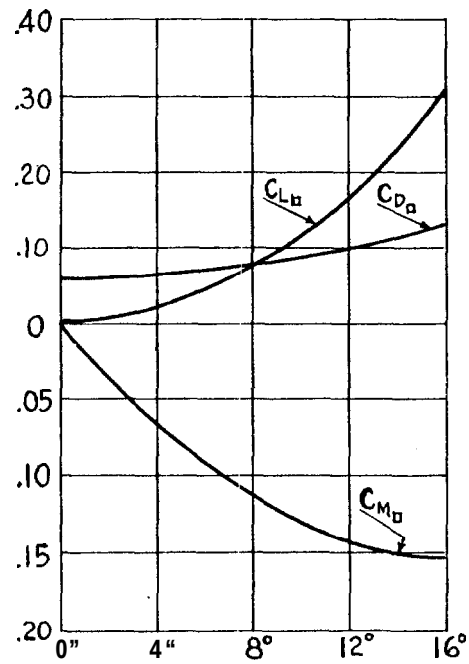

CIRCULAR NACELLE

$\ell/d = 5.86$

CHARACTERISTICS OF NACELLES

FIGURE 9.3

3. Characteristics of Nacelles in a Foil Configuration

General Considerations

When superimposed on a foil configuration, the nacelle exhibits somewhat different characteristics than when isolated, There is a mutual interference effect on both foil and nacelle, which is reflected in different values of lift, drag and moment for the entire configuration.

> In the analysis of such configurations, the standard procedure is *to maintafn* the total foil area, as if the nacelle were not present, The superposition of a nacelle which replaces some of the foil will actually reduce the foil area, resulting in a reduction in foil parasite drag from that basically considered, Therefore, it must be kept in mind that the nacelle characteristics determined from tests, wherein the basic foil drag is deducted from the total configuration drag, consists of several additive components (the basic nacelle drag, the interference drags on both wing and body, and an induced drag Increment due to change in foil lift distribution at the nacelle) and a deductive component (the parasite drag of the foil enclosed by the nacelle),

The total effect of superimposing the nacelle on the foil cannot readily be ascertained for the general case, due to the large number of factors involved, Several factors ares

(a) the characteristics and geometry of the isolated nacelle

(b) the characteristics and geometry of the foil

(c) the angle of attack

(d) the relative size of nacelle and foil

(e) the relative location of nacelle in vertical, horizontal and spanwise directions

(f) the extent of fairing at the fofl-nacelle Junctions.

Qualitative Results of Tests

Examination of data on wind-tunnel tests of various nacelle-foil combinations does indicate certain trends, which are given for a general guide in evaluating configurations,

(a) Typical airplane nacelles mounted on a wfng are of low ℓ/d, with an overall length of the same magnitude as the foil chord. The drag of such nacelles tend to be large[4].

(b) Nacelles and fuselages of higher ℓ/d, and which also have a length appreciably greater than the foil chord, show small increases in nacelle drag depending on the vertical location of the nacelles with respect to the foil. Hoernerl shows the nacelle drag for various "high-wing" arrangements (the results of one analysis are shown in Figure 9.1), which indicates the optimum ℓ/d for the nacelle to be nearly 7.0, and the drag for nacelles of larger ℓ/d to be about 20% higher than when isolated from the foil.

(c) For similar nacelles and fuselages as in (b) above, but with "mid-wing" arrangement, the net nacelle drag is slightly decreased according to tests conducted by Jacobs and Ward[3]. This condition generally holds true for the range of vertical positions, where the drag would be generally as indicated in (b) above, For the complete characteristics of these "mid-wing" configurations, Jacobs and Ward (observe that the simple adding of the independent foil and nacelle characteristics (lift, drag and moment) shows very good agreement with the data (without further consideration of interference, etc.)

(d) The addition of suitable fairings at the foil-nacelle junction tends to reduce the drag appreciably, particularly for high or low wing arrangements.

Recommended Methods

For accurate determination of the characteristics of nacelle-foil configurations, tank tests should be run on the contemplated configuration through the range of speed, attitude, and submergence anticipated in the design. Under certain conditions, data taken from pertinent wind-tunnel tests on similar configurations may be suitable.

However, for preliminary purposes, a simple approximation may be used that ie considered reasonably accurate for hydrofoil applications:

(a) The parasite drag of the configuration is simply that of the isolated nacelle (at zero lift) added to the rest of the configuration.

(b) The lift and moment characteristics are considered those of the foil alone, when the nacelle quarter-length is in line with the foil quarter chord.

This procedure is recommended only when reasonable fairings are employed at the foil-nacelle junction,

4. Drag o.f Small Appendages

In a practical hydrofoil configuration, there is apt to be small protuberances or isolated bodies installed for purposes of control, instrumentation, access, etc. In preliminary considerations these may generally be disregarded, but where careful estimates of drag must be made for performance or structural purposes their characteristics should be noted.

Hoerner[1] gives a comprehensive coverage of the drag of many bodies conceivably to be found in hydrofoil configurations, and reference should be made to that work for the details.

As a general guide, Table 9.1 gfves the drag characteristics of some of the more common shapes.

Where such bodies are isolated from major components of the configuratfon, the given values can be used. However, when attached to a foil or strut, consideration must be given to mutual interference effects, boundary layer effects, etc. in accordance with principles previously set forth.

TABLE 9.1

APPROXIMATE VALUES OF DRAG COEFFICIENT FOR VARIOUS BODY FORMS

Form of Body		L/D	R (based on D)	C_{D_0} based on frontal area
Circular disk	(D = diameter)		$> 10^3$	1.12
Tandem disks	(L = spacing) (D = diameter)	0	$> 10^3$	1.12
		1		0.93
		2		1.04
		3		1.54
Rectangular plate	(I to flow) (L = length) (D = breadth)	1	$> 10^3$	1.16
		5		1.20
		20		1.50
		∞		1.95
Circular cylinder	(axis ∥ to flow) (L = length) (D = diameter)	0	$> 10^3$	1.12
		1		0.91
		2		0.85
		4		0.87
		7		0099
Circular cylinder	(axis ⊥ to flow) (L = length) (D = diameter)	1	10^5	0.63
		5		0.74
		20		0.90
		∞		1.20
		5	$> 5 \times 10^5$	0.35
		∞		0.33
Hemisphere:	Hollow upstream		$> 10^3$	1.33
	Hollow downstream (D = diameter)			0.34
Sphere	(D = diameter)		10^5	0.47
			$> 3 \times 10^5$	0.20
Ellipsoid (1:3, major axis ∥ to flow)	(D = diameter)		$> 2 \times 10^5$	0.06

References

1. Hoerner — "Aerodynamic Drag" Published by Author, 1951.

2. Gertler — "Resistance Experiments on a Systematic Series of Streamlined Bodies of Revolution - For Application to Hfgh Speed Submarine", DTMB Confidential Report C-297, 1950.

3. Jacobs & Ward — "Interference of Wing and Fuselage from Tests of 209 Combinations in the NACA Variable - Density Tunnel", NACA Report No. 540, 1935.

4. Smelt, Smith, Smith & Davison — "The Installation of an Engine Nacelle on a Wing", ARC R&M No. 2406, 1950.

[redacted]

CHAPTER 10. SKID CHARACTERISTICS

1. General Considerations
2. Lfft and Wetted Length
3. Drag and Pitching Moment

The application of skids is discussed, and data on the lift of skfds of various geometry is given. Drag and pitching moment are shown to be obtained from the lift values.

1. General Considerations

Small lifting components that plane on the water surface are used on certain hydrofoil configurations for the purposes of control (sensing the water surface) and for the combined purpose of control and lift (as on the Grunberg type configuration). Such components are essentially flat plates of small aspect ratio and are commonly known as skids. The main feature of skids as compared to foils is their high sensitivity to change in submergence.

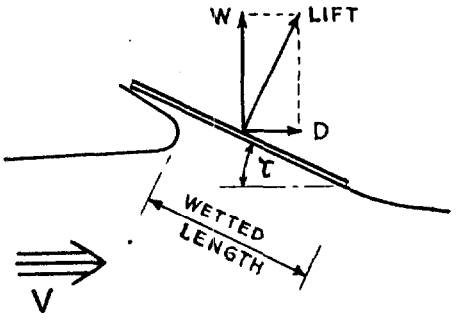

PLANING OF
FLAT PLATE SKID

FIGURE 10.1

As applied to hydrofoil craft, skids are comparatively small in size with consequent high Froude numbers, and operate at large trim angles. Since typical planing hull data (referred to in Chapter 11) is in the range of lower Froude numbers and low trim angles, such hull data is generally not applicable to planing skids. Therefore, specif:Lc flat plate data for the appropriate range of operating conditions must be employed.

The notation used in presenting and analyzing planing data is somewhat different from airfoil notation, although conversion is

readily made. The important planing notation (using NACA "seaplane" coefficients) is as follows:

$C_V = V/\sqrt{gb}$ "speed coefficient"

$C_\Delta = W/wb^3$ "load coefficient"

$C_{L_b} = W/\rho_2 V^2 b^2$ lift coefficient based on the square of the beam ($C_{L_b} = 2\,C_\Delta/C_V^2$)

$\lambda = \ell_m/b$ "wetted length ratio" (the reciprocal of the aspect ratio)

where τ is the angle of trim in degrees

V is speed, ft/sec

ℓ_m is mean wetted length of the plate, ft (see Figure 10.1)

b is breadth of plate (beam, span) = ft.

W is load on plate (lift), lbs.

ρ is the density of the fluid

g is acceleration of gravity

w is the specific weight of the fluid lb/ft^3 ($w = \rho g$)

2. Lift and Wetted Length

At the present time there is no complete three-dimensional planing theory available which correctly predicts the lift, wetted length, etc. over the range met in practice. An empirical equation has been derived by ETT[1] which is good within certain limits of trim, loading, etc. NACA[2] has extended the range of variables for the high speed case (where buoyancy effects are negligible). Both sources also give the Influence of certain variations from the flat plate (deadrfse, chine flare, etc.)

Data based on the NACA tests is presented in Ffgure 10.2, wherein the "lift coefficient" C_{L_b} can be determined as a function of trim angle and λ.

> Generally, since the wetted length is difficult to predetermine, the normal design procedure is to determine C_{L_b} from the trim and balance of the entire craft. Then for various trim angles, the wetted length can be determined,

In addition to the flat plate data, Figure 10.2 shows the lift of skids with various deadrise and local chine conditions as a percentage of the corresponding flat plate lift. Thus, C_{L_b} must be corrected by the factor, k, for the pertfnent case as given in the figure,

> These values of k are average, computed from the NACA data for operating conditions expected to be met by skids, and are considered sufficiently accurate for engineering purposes. For greater accuracy, reference should be made to the original reports[2].

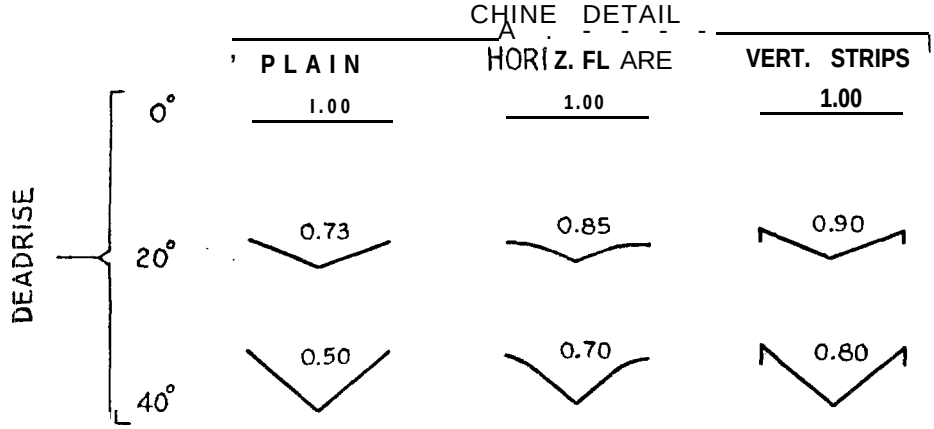

VALUES OF k FOR VARIOUS SKID FORMS

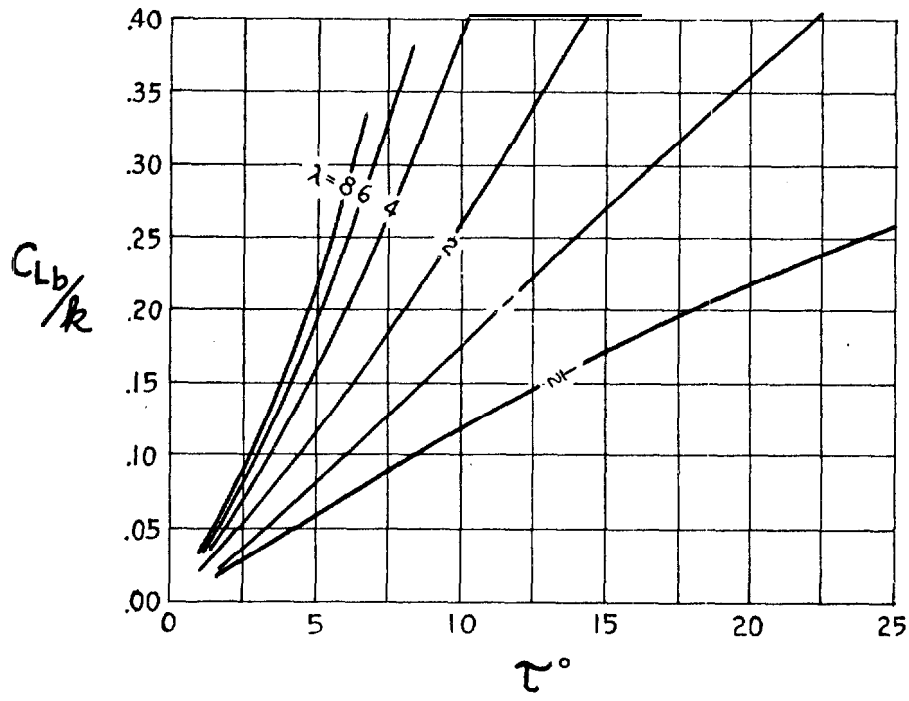

LIFT OF PLANING SKIDS

FIGURE **10.2**

3. Drag and Pitching Moment

The drag of the skid may be found by calculating the induced drag and the frictional drag separately, although the latter is seldom important in a practical ease due to the high trim angles (i.e. the induced drag is predominant.)

The induced drag is simply given by

$$D_i = W \tan \gamma$$

since the dynamic pressures act normal to the plate. The frictional drag is easily determfned (see Chapter 4) once the wetted length is found, as above.

From test data, the center of pressure is found to be about 70% of the mean wetted length forward of the trailing edge, This value may be used for all high speed skids without serious error.

References

1. Savitsky 'Wetted Length and Center of Pressure of Vee-Step Planing Surfaces", E.T.T. - Available as I.A.S.-SMF Paper No. FF-6 - 1951.

2. Series of NACA reports by Kapryan, Weinstein, Chambliss, Boyd and Blanchard describing results of an integrated series of tests in planing surfaces (1952).

NACA Technical Note No.	Deadrise Tested	Type of Chine Detail
2804	20"	Horz. Flare
2842	40°	Horz. Flare
2876	20" and 40°	Plain
2981	0"	Plain
3052	20° and 40°	Vertical Strips

[redacted]

CHARTER 11. HULL DRAG

1. General Considerations
2. Basic Hull Drag
3. Hull Unloading Characteristics
4. Air Drag

Reference is made to standard marine and seaplane data for determining the basic hull drag. Drag through the unloading range can be approximated by a simplified method, as a function of the basic drag, as shown. A formula for the air drag is given, as a function of the hull shape, based on existing data,

[redacted]

1. General Considerations

The drag of the hull is an important component of the total drag at speeds below take-off. At comparatively slow speeds when the foil system provides virtually no lift (or for controllable foils when set at zero lift) the hull supports nearly all of the required weight due to its displacement and/or planing action (if any). Thus, the drag of the hull for this condition must be determined,

Through the take-off range, the hull is gradually "unloaded" by the lift of the foils with consequent raising of the craft and reduction in hull drag. The hull drag in this range is most readily expressed as a percentage of the drag of the fully waterborne hull, as is indicated below.

The air drag of the hull becomes important at the high speeds beyond take-off when the hull is completely clear of the water.

In an important hydrofoil craft design, model test data should be obtained directly for the hull to be employed. However, for preliminary purposes, the methods and formulas proposed herein should be adequate.

2. Basic Hull Drag

Theoretical methods of calculating the resistance of waterborne craft are available[1,2], but the calculations are arduous and the results are not as reliable as those obtained from model tests,

There are several systematic series of model tests available[3,4,5] on various types of hull form along with some collections of results[6,7] on large numbers of specific designs, Table 11.1 lists some of these sources along with a description of the variations' tested and the data reported.

> Since there is a wide variety of hull forms possible for application to hydrofoil craft, and since all of the basic data is readily available in the referenced works, it shall not be produced herein.

The methods of applying the data in each case is given in the sources, and are also described in standard references[8,9]. The main difficulty in utilizing the results usually occurs in the selection of coefficients in the *series to* give a hull form as *similar* as possible to the one in question. In this respect!, a general guide can be given, based on the Froude concept of ship model testing, as follows*

The resistance of the model is assumed to be separable into two components; the "frictional" due to viscous effects and depending on

TABLE 11.1

SOURCES OF EXPERIMENTAL HULL RESISTANCE DATA

Reference	Description	Froude Number Range	Systematic Variations Tested	Results Presented
1	"Taylor's Standard Series" Displacement Ships	$V_k/\sqrt{L}$ 0.30 - 2.00	Fullness, Length-Beam Ratio, Beam-Draft Ratio	"Residual" and "Frictional" resistance
2	Series "50" Planing Hulls	$V_k/\sqrt{L}$ 1.6 - 6.5	Center of Gravity, Beam Draft Ratio, Length-Beam Ratio	Total Resistance, Running Trim, Wetted Area, Stability ("Porpoising")
3	Length-Beam Ratio Series Seaplanes	C_v 0 - 12	Length-Beam Ratio, Loading	Resistance, Trim, Stability
4	Model Resistance Data Sheets-160 Individual Ship and boat model	$V_k/\sqrt{L}$ up to 1.7	None	Resistance
5	Flying Boat Models 100 individual sea-plane models	C_v 0 - 15	None	Resistance, Trim, Stability

the wetted surface and Reynolds number, and the "residual" which influences the wave resistance and "eddy-making" (separation effects) depending on the Froude number, The model is tested at the same Froude number as experienced by the full sized ship, and the model results are corrected by assuming the frictional resistance to be that of a plank of the same area and Reynolds number in each case (ship and model). Test data on planks is available for makfng this correction[10].

The Froude and Reynolds numbers are defined on the basis of speed and length as follows;

$$\text{Froude number} = V/\sqrt{g\ell}$$

$$\text{Reynolds number} = V\ell/\nu$$

where V = speed of advance in ft/sec

a = length in ft.

3 = acceleration of gravity in ft/sec^2

ν = kinematic viscosity in ft^2/sec

The length "ℓ" is usually defined as the wetted length of the ship in the direction of motion with the exception of some data on seaplane models where (for use in the Froude number only) the beam "b" of the model is used, In ship parlance the Froude number is usually abbreviated excluding the constant "g" and using the speed in knots "V_k". Definitions of these quantities are as follows:

Category:	Ships	Seaplanes
Quantitya	"Speed-Length Ratio"	"Speed Coefficient"
Symbol:	$V_k/\sqrt{L}$ *	C_v
Definitfon:	$V_k/\sqrt{L} = 3.36\,V/\sqrt{g}$	$V/\sqrt{gb}$

The general guide, therefore, is to attempt to match the hull form characteristics influencing the wave or residual resistance such as the fullness and Froude number, and to make corrections for differences in frictional resistance (especially wetted surface). A knowledge of the basic mechanism of resistance is indispensable in this respect.

* "L" and "ℓ " have the same meaning

DESIGN EXAMPLE NO. 11.1

SH 1 OF 3

ESTIMATE THE HULL RESISTANCE OF THE FOLLOWING PLANING HULL FORM

LENGTH (B.P.)	62.5'	HULL IS SAME AS THAT GIVEN IN APPENDIX A
BEAM	16.0'	
DISPLACEMENT	50 TONS	
L.C.G.	4.05' AFT ⊗	
SPEED	30 KNOTS —	NO UNLOADING CONSIDERED

SERIES 50 PLANING DATA (REFERENCE 2) IS USED. DATA IS PRESENTED ON RESISTANCE , TRIM, L.C.G. AND WETTED SURFACE FOR A SYSTEMATIC SERIES OF 40" LONG MODELS.

A YYPICAL DATA CHART IS SHOWN BELOW. KNOWING THE HULL CHARACTERISTICS (SPEED ,DISPLACEMENT, LENGTH, ETC.) VALUES ARE READ DIRECTLY FOR THE MODEL AND CONVERTED AS REQUIRED FOR THE FULL SIZE CRAFT.

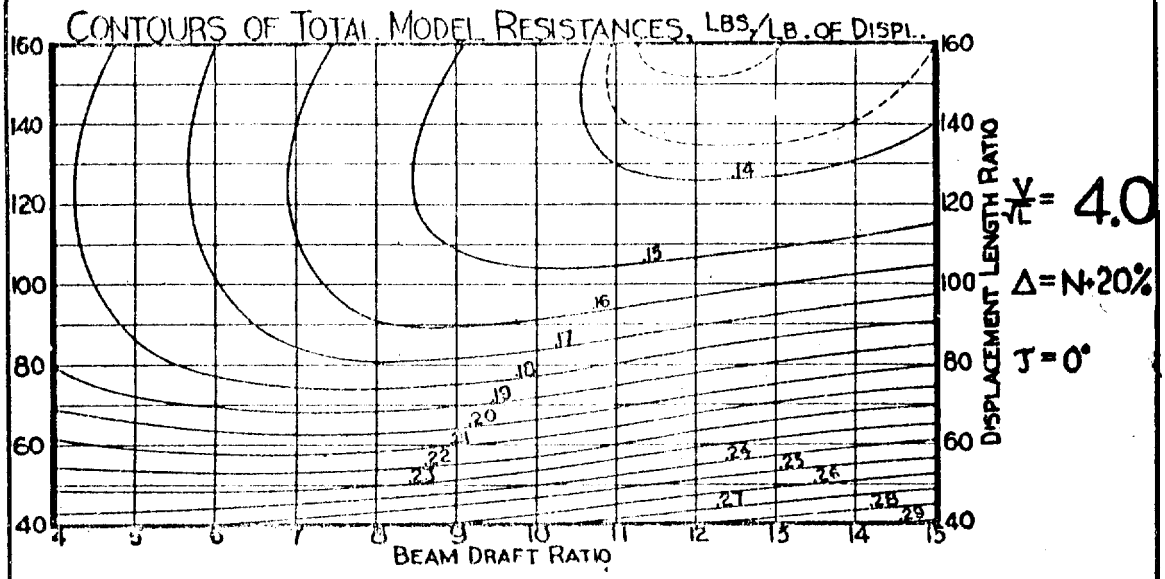

DESIGN EXAMPLE NO, I I .I

FROM THE HULL PARTICULARS, THE LCG IS 56.5 % OF LENGTH AFT OF THE FORD PERPENDICULAR. FROM SERIES 50, THIS CORRESPONDS TO ZERO STATIC TRIM (τ=0 ON THE CHARTS)

THE DISPLACEMENT LENGTH RATIO Of THE HULL IS

$$\frac{\Delta}{(L/100)^3} = 200$$

WHICH IS OUT OF THE MODEL TEST RANGE. HOWEVER, BY CONSIDERING THIS TO BE 20 % OVERLOAD CONDITION, AND THE RATIO TO BE USED IS

$$\frac{\Delta}{(L/100)^3} = 167$$

ON THE CHARTS FOR Δ = N + 20%

THE CORRESPONDING BEAM/DRAFT RATIO IS FOUND (IN THE SERIES 50 TEXT) TO BE

$$B/H = 4.77$$

THE SPEED LENGTH RATIO IS

$$V_K/\sqrt{L} = 3.80$$

THEN, FROM THE CHARTS THE FOLLOWING INFORMATION IS TAKEN:

[τ=0° ; A = N+20% ; $\Delta/(L/100)^3$ = 166]

V_K/L	R/Δ	τ_r°	S_ϕ
3.0			2.47
3.5	0.175	7.2	
4.0	0.180	4.3	2.03
INTERPOLATING			
3.8	0.178	7. 3	2.12

Note : τ_r is "running" trim of the hull

DESIGN EXAMPLE NO. 11.1

SH 3 OF 3

THE MODEL RESISTANCE DATA MUST NOW BE CORRECTED FOR REYNOLDS NO. EFFECT AND A SERVICE ROUGHNESS FACTOR ADDED TO GET THE CORRECT RESISTANCE VALUE FOR THE FULL SIZE CRAFT

MODEL LENGTH **3.33'**
WEIGHT 16.6# [FROM $\Delta/(L/100)^3 = 200$]
SPEED 11.7 f.p.s. [FROM $V_K/\sqrt{L} = 3.87$
REYNOLDS NO. 3.28×10^6 [F.W. @ 69°]
C_f **0.00354** [TURBULENT]

FULL SIZE REYNOLDS NO. 2.23×10^8 [SW. @ 59°]
C_f 0.00186
ROUGHNESS ALLOWANCE **0.00040**
C_f (ROUGH) 0.00226

THUS, THE MODEL RESISTANCE MUST BE REDUCED AN AMOUNT EQUIVALENT TO

$$(\Delta C_f) = 0.00128$$

THIS CORRESPONDS TO

$$(AR) = \Delta C_f \times \rho/2\ V^2\ S\ (\text{model})$$
$$= 0.3\text{-P}$$
$$(\Delta R/W = 0.37/16.6 = 0.022$$

THEN, THE FULL SIZE RESULTS ARE

$$R/\Delta = 0.178 - 0.022$$
$$= 0.156$$

HULL RESISTANCE $= 0.156 \times 112{,}000 = 17{,}500$#

HULL TRIM $= 7.3°$

3. Hull Unloadine Characteristics

The drag of the hull during the "unloading" process prior to take-off is a function of many variables and cannot be readily determined except when the hydrofoil configuration and operating characteristics are specified, Model tests[11,12] have been conducted on several hull models at various specified unloading speeds and angles of trim, but the results are not necessarily applicable to general cases since the trim is difficult to predetermine (except for fully controlled configurations),

Therefore, model tests of the proposed configuration should be conducted for accurate determination of the hull unloading characteristics. For preliminary purposes, hull unloadfng characteristics can be approximated by the method proposed by Ward[13] for both displacement and plating type hulls. Since planing type hulls are generally used in hydrofoil craft application (for moderate size craft, at least), the approximate unloadfng characteristics of the planing hull are proposed for use.

It is assumed that the hull is an essentially flat hull planing at an angle of trim, and that the foil system unloads the hull at the center of gravity, Tt is a characteristic of planing that the center of pressure location relative to the wetted length remains fixed regardless of the trim, and that the lift itself is roughly

proportional to the trim. This causes the craft to pivot, about the forward edge of the wetted area during the process of unloading, as indicated in Figure 11.1.

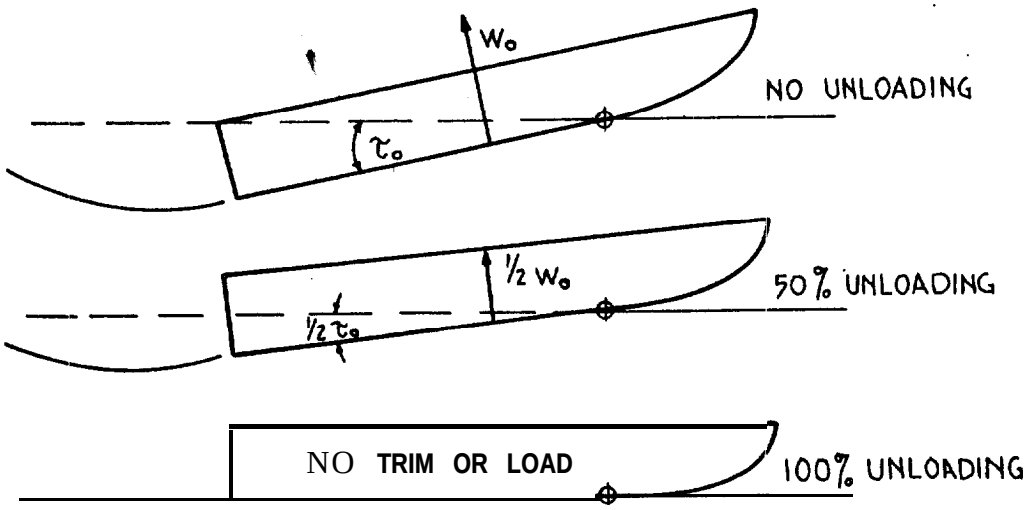

ILLUSTRATING SIMPLIFIED UNLOADING

FIGURE 11.1

It is also evident that the "residual" resistance is equal to the component of dynamic lift in the horizontal plane and therefore proportional to the load on the hull and the angle of trim. The drag (at a fixed speed) may, therefore, be related to the drag at zero unloading as follows;

"Residual"	"Frictional"
$R_r/R_{r_o} = \frac{W}{W_o} \cdot \frac{\tau}{\tau_o}$	$R_f/R_{f_o} = S/S_o$
$\frac{W}{W_o} = \frac{\tau}{\tau_o}$	$S/S_o = 1$
$\frac{R_r}{R_{r_o}} = \left(\frac{W}{W_o}\right)^2$	$R_f/R_{f_o} = 1$

combining:

$$R/R_o = \frac{R_{r_o}}{R_o}\left(\frac{W}{W_o}\right)^2 + \frac{R_{f_o}}{R_o} \qquad (11.1)$$

where R = hull resistance

W = loading on the hull

τ = angle of trim

S = wetted surface

Subscripts:

r = residual

f = frictional

o refers to values of the parameters at zero unloading.

The assumed unloading curve is therefore as given in Figure 11.2. It should be noted that the resistance at zero unloading must be broken down into frictional and residual components which is usually standard procedure in resistance tests on series results, as indicated above for the basic hull drag. The assumption $S/S_o = 1$ naturally does not hold at low values of W/W_o and in fact S/S_o must be equal to zero when the

hull is completely unloaded. The dotted line on the graph (Figure 11.2) represents this transition. The graph is good only for one speed V_K since the ratios R_{V_0}/R_0 and R_{f_0}/R_0 will in general vary with speed.

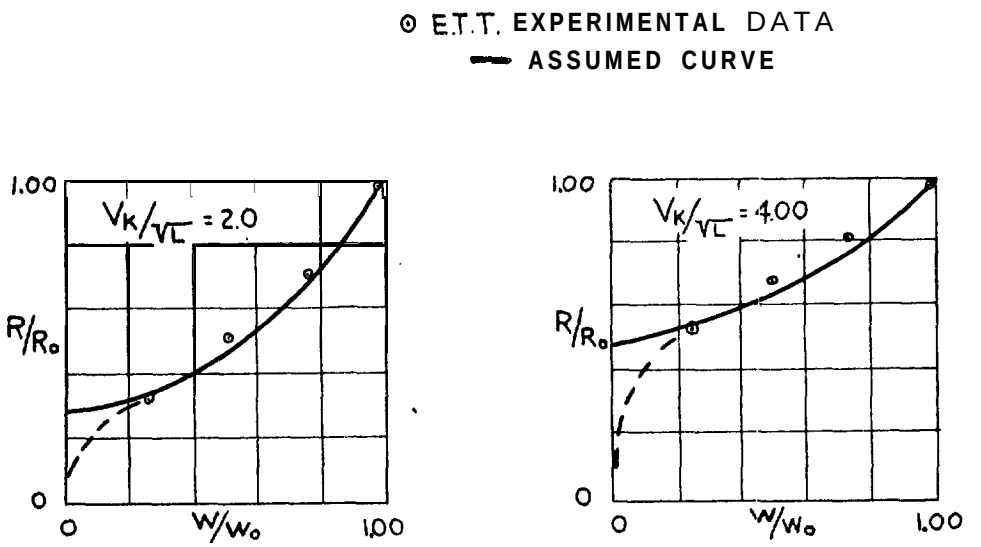

TYPICAL UNLOADING CURVES

FIGURE 11.2

Tests points *are* shown on the graph which were derived from unloading experiments on a series 50 hull[12]. It is seen that the assumed characteristic variation of resistance with unloading is at least approximately correct and sufficient for engineering applications.

4. Air Drag

At the high speeds associated with foil-borne operations of hydrofoil craft, the air drag of the exposed parts of the craft (the hull and superstructure, primarily) must be taken into account. However, while the air drag is important, it is generally a small percentage of the total and may be approximated by a simple expression with reasonable accuracy.

Thus, the air drag may be expressed as:

$$D_{air} = C_D \rho/2 V^2 S \qquad (11.2)$$

where D_{air} is the air drag (in pounds)

ρ is the density of air (0.00238 # sec^2/ft^4, at sea level)

S is the cross-sectional or frontal area of the hull and major superstructure, ft^2

V is the speed in ft/sec

C_D is the drag coefficient based on the area S, and is to be determined,

This may be more conveniently expressed in terms of the speed in knots (V_K), or:

$$D_{air} = K 5 V_K^2 \qquad \text{(where } K = 0.0034 C_D \text{)} \qquad (11.3)$$

Eggert[3] used a drag coefficient of 1.18 for ships based on an assumed cross-sectfonal area of 1/2 B^2 (where **B is** the beam of the ship). However, thfs area is probably less than the actual maximum, including the superstructure, for such cases. Furthermore, there is no attempt at streamlining in the case of large ships as there is in the typical fast craft such as a hydrofoil boat, The effect of streamlining is by far the most important consideration in determining the drag coefficient, It is proposed that a coefficient of 0.60 (which would check with Eggert's formula using B^2 for the area instead of 1/2 B^2) be used for blunt ended hulls and superstructures[14], and 0.30 for well streamlined configurations (seaplanes, with no houses, have coefficients as low as 0.20). The corresponding K values are therefore .002 and .001 respectively.

The recommended formula for the air drag is then

$$D_{air} = (0.001 \text{ to } 0.002)\, S\, V_k^2 \qquad (11.4)$$

where the choice of the factor depends on the amount of streamlining incorporated in the hull and superstructure,

References

1. Lunde — "On the Linearized Theory of Wave Resistance for Displacement Ships in Steady and Accelerated Motion", SNAME Transactions, 1951.

2. Guilloton — "Potential Theory of Wave Resistance of Ships With Tables for Its Calculation", SNAME Transactions, 1951.

3. Taylor — "The Speed and Power of Ships", U.S. Govt. Prfnting Office, Washington, D.C., 1943.

4. — "Tests of Twenty Related Models of V-Bottom Motor Boats", EMB Series 50, D.T.M.B. Rpt. R-47, Mar. 1949 Revised Edition.

5. Davidson & Locke — "General Tank Tests on the Hydrodynamic Characteristics of Four Flying-Boat Hull Models of Differing Length-Beam Ratio", NACA Wartime Rpt. W-105 (originally ARR 4F 15 June 1944).

6. — "Model and Expanded Resistance Data Sheets wfth Explanatory Notes", SNAME Transactions, NOV. 1941, Nos. 1-160.

7. Locke — "A Collection of the Collapsed Results of General Tank Tests of Miscellaneous Flying-Boat-Hull Models", NACA Tech. Note No, 1182, March 1947.

8. Russell & Chapman — "Principles of Naval Architecture", Vol. II, SNAME Transactions, 1941.

9. Murray — "The Hydrodynamics of Planing Hulls", SNAME Transactions, 1950.

10.		"Uniform Procedure for the Calculation of Frictional Resistance and the Expansion of Model Test Data to Full Size", SNAME Bulletin No. 1-2, August 1948.
11.	Sutherland	"Exploratory Model Tests for Engineering Desfgn of a Hydrofoil Vessel", E.T.T. Confidential Rpt. No. 407, 1951.
12,	Kaplan	"Hull Characteristics for Four Basic Hull Types", Confidential ETT Ltr. Rpt. No, 449, 1952.
13.	Hoerner & Ward	"Take-Off Performance of Hydrofoil Craft", Tech, Rpt. No. 6, Contract Nonr-507(00), Bath Iron Works Corp. (Gibbs & Cox, Inc.), 1952.
14.	Foster & Piziali	"Wind-Tunnel Investigation of a 1/16 Scale Model of a Hydrofoil Landing Craft", DTMB Confidential Aero Rpt. 852,1953.

CHAPTER 12. ASPECTS AND INFLUENCE: OF CAVITATION IN THE HYDRODYNAMIC CHARACTERISTICS OF HYDROFOIL BOATS

Notation

1. Physical Mechanism of Cavitation
2. Pnoeption of Cavitation
3. Forces in Cavitating Flow

A preferred field of application for hydrofoil boats is in higher speeds. In fact, realization of speeds above some 40 knots is one reason for the development of these boats. A% such speeds, cavitation is no longer avoidable, both in the propeller and in the hydrofoil system. Consfderation of cavitational effeots upon performance and behavior is, therefore, necessary.

A basic review of cavitation is presented by Ackeret[1], a more recent and more detailed analysis is given by Eisenberg[2], and an extensive bibliography is available in reference 3. Thfs presentation here, reiterates the physical mechanism of cavitation, mentions delay in the onset of cavitation in certain conditions, makes predictions of the critical speed (inception of oavitation) in hydrofoils and presents some force data in cavitating flow.

Notation

d	bubble or body diameter
x	chordwise distance
c	foil chord
t	thickness ,
f	height of camber
b	wing span
h	submergence
A	aspect ratio,
ε	half apex angle of wedges or cones
"α"	air content of water
α	angle of attack
γ	weight density
ρ	mass density
V	speed in ft/sec or knots
q	dynamic pressure, $(0.5\rho V^2)$
p	static pressure
C_p	static pressure coefficient, $\Delta p/q$
σ	cavitation number, $(p_{amb} - p_{vapor})/q$
σ_i	critical cavitation number
D	drag or resistance
C_D	drag coefficient, D/qS
L	lift; also subscript for lift
C_L	lift coefficient, L/qS
R_l	Reynolds number on l, (Vl/ν)

1. Physical Mechanism of Cavftation

The compressibility of water is negligibly small when compared with conditions in air. However, as a function of speed, water flow reaches a critical condition characterized by vaporization and cavitation.

Cavitation Bubbles

Vaporization is the growth of a gas- or vapor bubble. There is an equilibrium in such a bubble between a force (proportional to the projected bubble area $d^2\pi/4$) corresponding to the pressure differential between inside and outside, and a force (proportional to the circumference $d\pi$) due to the surface tension of the bubble (see reference 1). For a given pressure differential, thereforea

$$\frac{\text{Suction}}{\text{Tension}} \sim \text{Diameter} \qquad (12.1)$$

This function means that a critical or minimum diameter is necessary to assure growth of the bubble.

In "clean" water, there are no bubbles or other cavities existing, As a consequence, water which has been distilled does not readily boil at the temperature which is commonly called boiling temperature; and St does not "rupture" or cavitate upon reaching the "vapor pressure" corresponding to temperature.

If certain nuclei (gas bubbles of microscopic or macroscopic size) are available, however, it is to be concluded from equation (12.1) that there is a critical (negative) pressure at which the diameter of the bubbles is just sufficiently large to permit growth. Upon reaching critical conditions, the bubble may suddenly increase its diameter.

In concluding, a certain air bubble content or existence of gas-carrying particles is a necessary prerequisite of cavitation.

Air Content

Water with a "free" surface has the natural characteristic of absorbing afr, There is a maximum amount of air which "saturated" water can retain. Under standard atmospheric conditions, for example, corresponding to 59°F and 760 mm Hg, the saturated air content is in the order of 2% by volume, which is only a ratio of $25/10^6$ by weight. It is the content of bubbles, rather than the dissolved amount of air, which makes cavitation possible[2]. One way of providing such bubbles is locally reducing the static pressure by placing a body in a flow of air-saturated water, In certain preferred places;, the water becomes over-saturated, thus shedding bubbles,

According to basic experiments[4], cavitation starts at pressures close to vapor pressure provided that the air content is close to the saturated condition, In waves and turbulent water, air is entrained

and suspended in the form of bubbles, thus raising the total content above the saturated value. Also, dirt and organic substances seem to carry gas bubbles, Therefore, in practical applications, the nuclei content is always above any critical limits; and ships and hydrofoils are faced with the problem of cavitation.

The air content also has another more direct effect. Existing afr bubbles grow upon entering a low-pressure field, and may combine with each other, The result is a "cavitating" flow pattern without any vapor, which is similar to "real", vapor-type cavitation. Two types of cavitation and two different critical cavitation numbers can, therefore, be consfdereds one indicating the onset of air-bubble formation ("bubble" phase) and the other one definfng incipient ("steady" or "sheet" or "laminar") vapor cavitation. Naturally, air-bubble cavitation usually starts above the vapor pressure.

Erosfon

There have been considerable discussions and arguments about the mechanism of erosion, caused by cavitation, The predominant and accepted effect is the mechanical hammering or impact at spots where vapor-filled bubbles or cavities suddenly collapse upon the surface (see reference 2). In contradfstinctfon, air-bubble cavitation does not lead to erosion because there is no sudden collapse and the introduction of air (ventilation) into a cavitating water turbine has

been found to reduce the noise (of collapsing bubbles) associated with vapor cavitation.

As an example, Figure 12.1 shows lift-coefficient areas indicating inception of cavitation and erosion past a certain hydrofoil section. Impact and damage only take place within the dotted areas, where cavity or bubbles end ahead of the trailing edge. There is

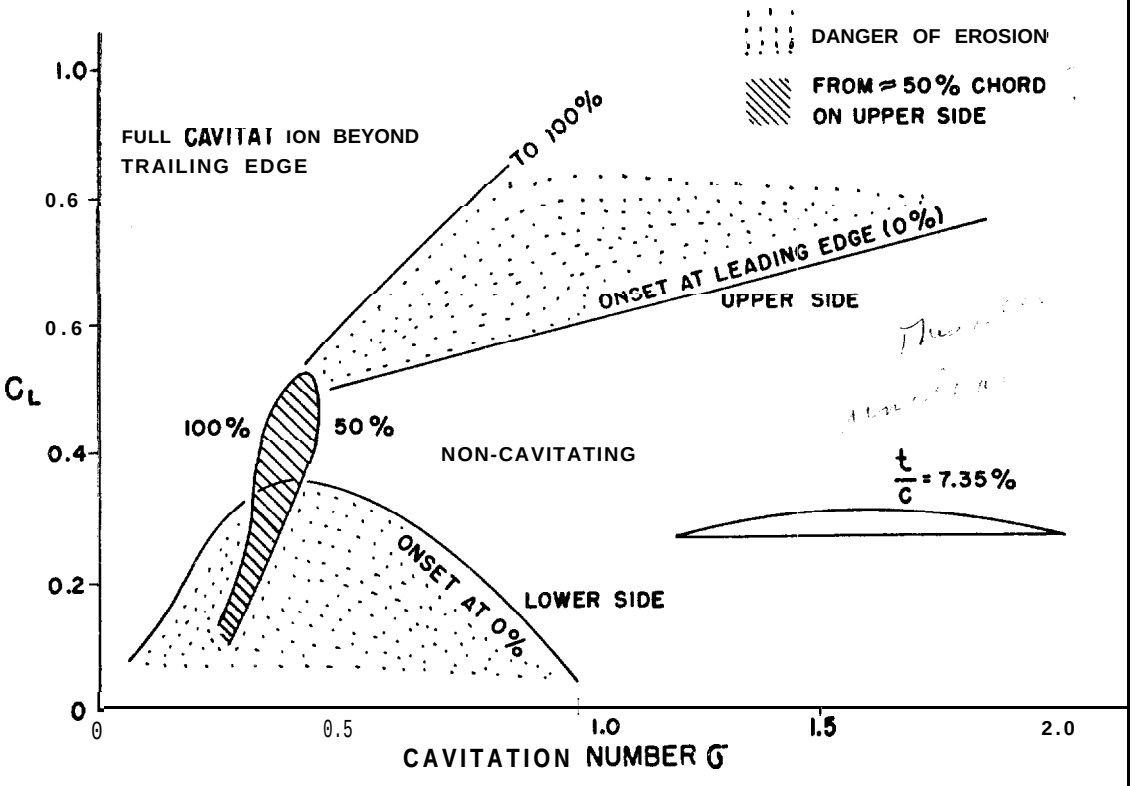

PHASES OF CAVITATION ON CIRCULAR-ARC SECTION (REF. 5)

FIGURE 12 .1

only a restricted'interval of lift coefficient (in the order of $\Delta C_L = \pm 0.1$, at both sides of C_{Lopt}) where cavitation can be avoided at σ in the order of 0.5. After traversing the phase with partial, eroding cavitation, erosion is no longer to be expected within the fully cavitating region.

2. Inception of Cavitation

As a Function of Pressure

Upon increasing the temperature or decreasing the pressure, water is likely to vaporize, boil or cavitate at the vapor-pressure level. At a standard temperature of 59°F (15°C) this pressure, p_{vapor}, is comparatively low (33 lb/ft^2 or 0.55 ft of water, in fresh water); it is less than 2% of the sea-level atmospheric pressure. Therefore, in proximity of the free surface, water is expected to vaporize and to cavitate shortly before reaching p_{min} = zero,

On the basis of the available pressure differential ($p_{ambient} - p_{vapor}$), the cavitation, number is

$$\sigma = \frac{p_{ambient} - p_{vapor}}{q} \qquad (12.2)$$

If disregarding the value of p_{vapor} which is small in many practical applications, the cavitation number simply appears to be the ratio of the undisturbed static to the dynamic pressure of a considered flow of water. The cavitation number is a feature of the flow as such it indicates the "preparedness" of a water flow in respect to cavitation. The smaller σ, the stronger is the tendency of cavitating,

The static pressure in a flow around a body exhibits variations. Tn certain places, the velocity is locally increased, and the static

pressure is consequently decreased. This decrease is indicated by

$$\Delta p_{min} = p_{min} - p_{amb} = q\,(\Delta p/q)_{min} = q\,C_{pmin} \qquad (12.3)$$

where $q \equiv 0.5\rho V^2$ denotes the dynamic pressure of the undisturbed flow, and C_{pmin} indicates a negative static pressure coefficient depending upon shape and attitude of the body involved. The minimum static pressure on the surface of the body

$$p_{min} = p_{amb} + \Delta p_{min} \qquad (12.4)$$

steadily decreases from p_{amb}, approaching zero as the dynamic pressure q increases from zero to the critical value. In other words, at a certain preferred point at the surface of the body, the pressure reduces to the level of the vapor pressure ($p_{min} = p_{vapor}$). The critical cavitation number is, therefore, expected to be

$$\sigma_i \approx -C_{pmin} \qquad (12.5)$$

with the subscript "i" (incipient) indicating the onset of cavitation.

Critical Cavitation Number

The onset of cavitation in experiments can be determined by visual observation, or by a sharp increase in sound level which is associated with the collapse of vapor bubbles, or by the divergence of lift-, drag- or moment coefficients from their undisturbed values. Proper definition of quoted critical cavitation numbers is desirable.

Figure 12.2 presents some experimental results on three-dimensional head shapes, demonstrating the correlation between incipient cavitation number ($\sigma_{i\,vapor}$ taken from reference 7) and the pressure coefficient (taken from reference 6). The graph also indicates the influence of the shape upon the inception of cavitation.

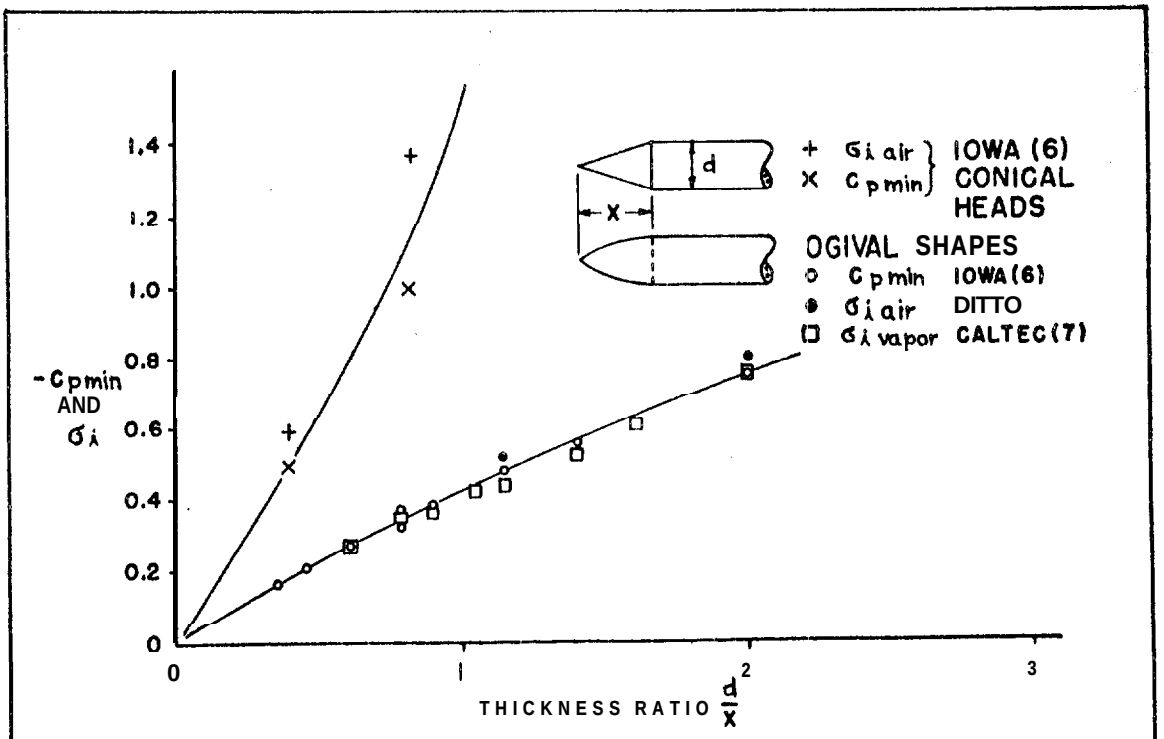

CRITICAL CAVITATION NUMBER OF VARIOUS HEAD SHAPES

FIGURE 12.2

Figure 12.3 presents the pressure characteristics of two-dimensional streamline shapes. For statistical analysis, the fore-body of these sections is considered only, on the basis of the

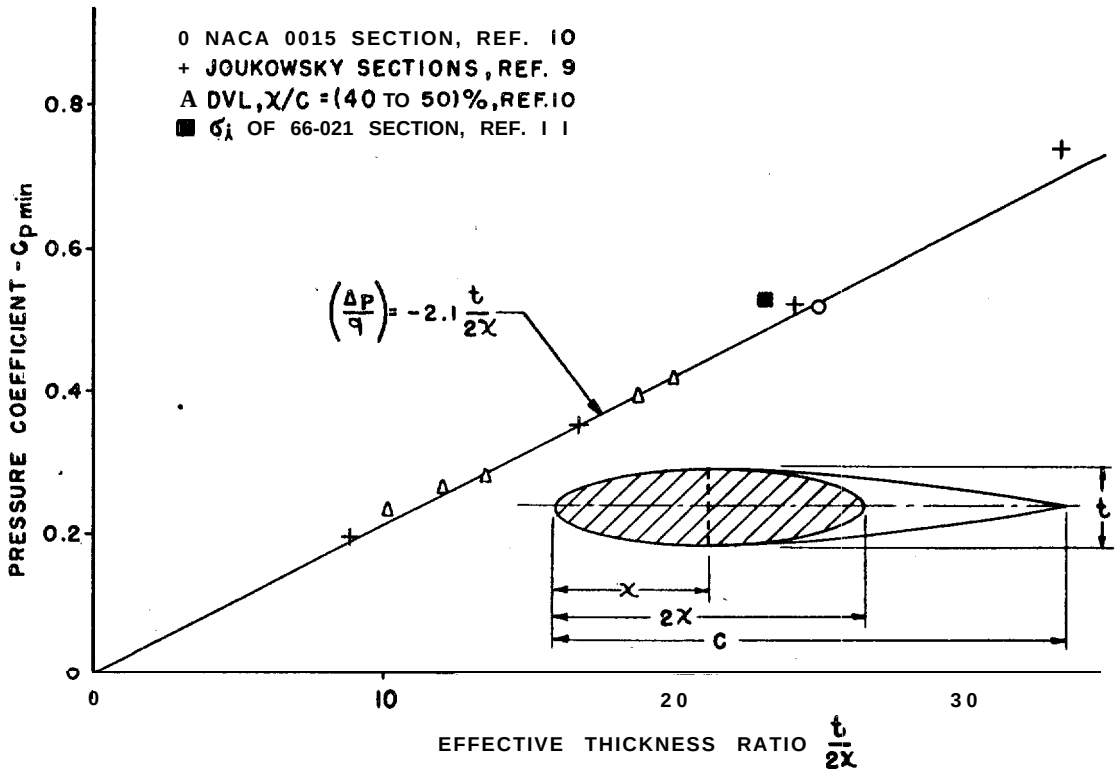

MINIMUM PRESSURE COEFFICIENT AT THE SIDES OF SYMMETRICAL SECTIONS AT ZERO ANGLE OF ATTACK

FIGURE 12.3

length x. It appears that the influence of the afterbody upon the flow pattern past the forebody is of secondary importance. Hence, the minimum pressure coefficient increases in proportion to the thickness ratio of the equivalent, approximately elliptical section. For symmetrical sections at zero lift, the pressure coefficient is approximately

$$C_{p_{min}} \approx 2.1 \frac{t}{2x} \qquad (12.6)$$

with t and x asdefined in Figure 12.3. The constant is nearly equal to the theoretical value of 2.0 for elliptical sections. Unfortunately, there is only one suitable value for σ_i available for Figure 12.3. General experience confirms, however, that in slender shapes $\sigma_i \approx -C_{pmin}$.

The pressure distribution around a lifting foil section is basically composed of a component due to thickness (equation 12.6) and a component corresponding to lift. The average and minimum additional pressure differential at the suction side is simply

$$\Delta C_{pmin} = \left(\frac{\Delta p}{q}\right)_L \approx -0.5\, C_L \qquad (12.7)$$

in the first approximation. The lift, however,, is not uniformly distributed along the chord and the value of the pressure minimum is higher than indicated by the last equation. Distribution and minimum coefficient depend upon the section shape.

Cambered sections have an "optimum" lift coefficient, defined by a flow pattern in which the streamlines meet the section nose without flowing around from one side to the other. This condition may be identified by "smooth" or "symmetrical entrance". As a function of camber ratio f/c, smooth entrance flow is existing at

$$C_{Lopt} \approx (10 \text{ to } 12)\frac{f}{c} \qquad (12.8)$$

With respect to minimum pressure and cavitation, operation in the vicinity of somewhat above C_{Lopt} is expected to provide the highest possible critical speeds for a given foil section at the respective lift coefficient.

Assuming now that the minimum-pressure differential due to lift be simply superimposed on that caused by thickness, it is possible to reduce experimental results to zero thickness, and to isolate approximate values due to lift. Available experimental data presenting the minimum-pressure coefficient at or near the "optimum" lift coefficient,, have been evaluated accordingly, by subtracting a value attributable to thickness as indicated by equation (12.6). The remaining component due to lift is plotted in Figure 12.4 for a number of foil sections. The experimental points are evidently grouped according to thickness location. In each group, cavitation-tunnel results (with σ_i defined by the deviation of drag- and/or lift coefficients from the non-cavitating values) are seen in close agreement with the minimum-pressure measurements. The component due to lift is approximately

$$\Delta\sigma_i \approx -\Delta C_{pmin} \approx k\, c_L \qquad (12.9)$$

where k is a function of thickness location (and probably of other shape parameters as well). Combining the pressure minimum due to lift (which is in the vicinity of 25% of the chord, at C_{Lopt}) with a thickness location at 50%, provides a factor $k \approx 0.7$. An appreciably

higher value results for a location at 30%, where the factor $k \approx 0.85$.

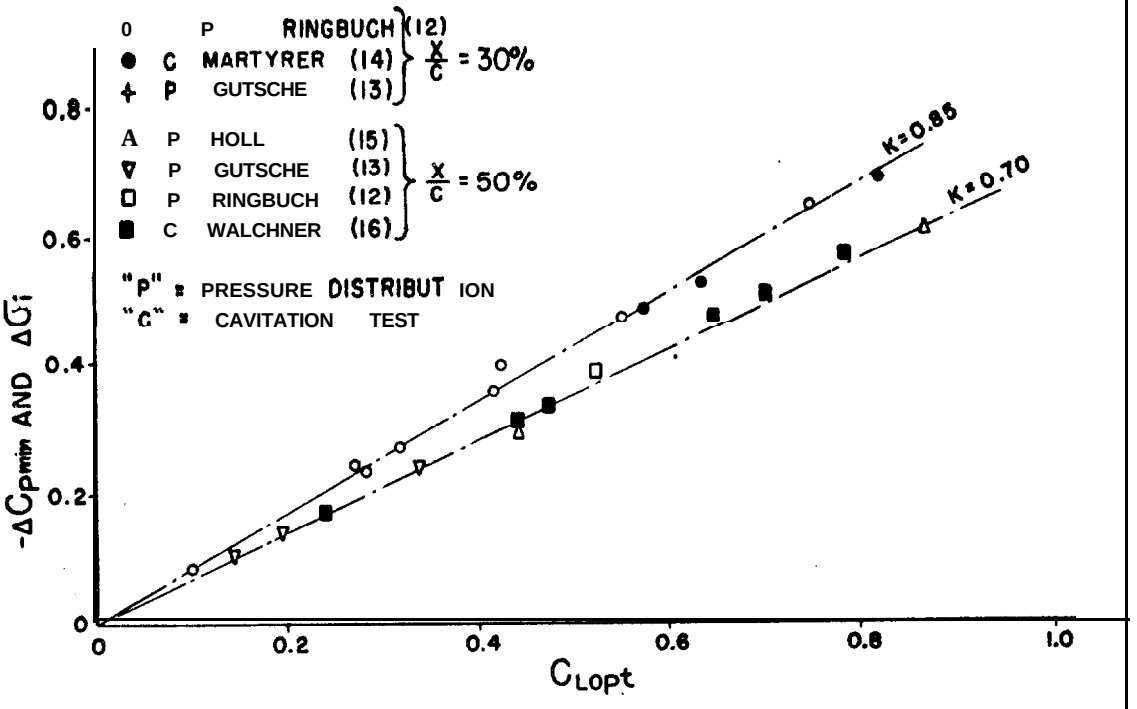

INCREMENT OF THE CRITICAL CAVITATION NUMBER, DUE TO LIFT

FIGURE 12.4

Example

What is the critical cavitation number of a foil section having t/c = 10% (at 0.5 chord) and f/c = 3% ?- According to equation (12.6), the critical cavitation number due to thickness is $\sigma_\lambda = 2.1 \cdot 0.1 = 0.21$. For $C_L = 0.33$, equation (12.9) indicates a $\Delta\sigma_\lambda = 0.7 \cdot 0.33 = 0.23$. Hence, the number indicating incipient cavitation is expected to be $\sigma_i = 0.21 + 0.23 = 0.44$.

Delay of Vapor Cavitation

Even on the basis of a sufficient number of nuclei, cavitation may not exactly start at reaching vapor pressure. Evidently, the growth of air- or vapor-filled bubbles and the transition from liquid to vapor phase require some time. This time element may not be important in many cases where the flow velocity is small and the geometrical size of the low-pressure field is large. In fact, the results in Figures 12.2, 12.3 and 12.4 demonstrate that up to $-C_{pmin} \approx \sigma_i \approx 0.8$, delay in the onset of cavitation is, in general, small. Considering, however, as an example, conditions at the leading edge of a foil, where C_{pmin} may reach values which are ten times as high as those just quoted, and where such values are only existing in narrow peaks (that is, during very short periods of time)- the influence of small size and high speed may be important.

As an example, characteristics are presented in Figure 12.5 of the NACA 64A006 foil section, tested in a wind tunnel[17] and also in a towing tank[18]. The incipient cavitation number σ_i is decisively lower than the value of the corresponding pressure coefficient C_{pmin} for values between $C_L = 0.3$ and 0.5. For example, at $C_L = 0.5$, where $-C_{pmin} = 5$, the incipient cavitation number is only $\sigma_i \approx 2$.

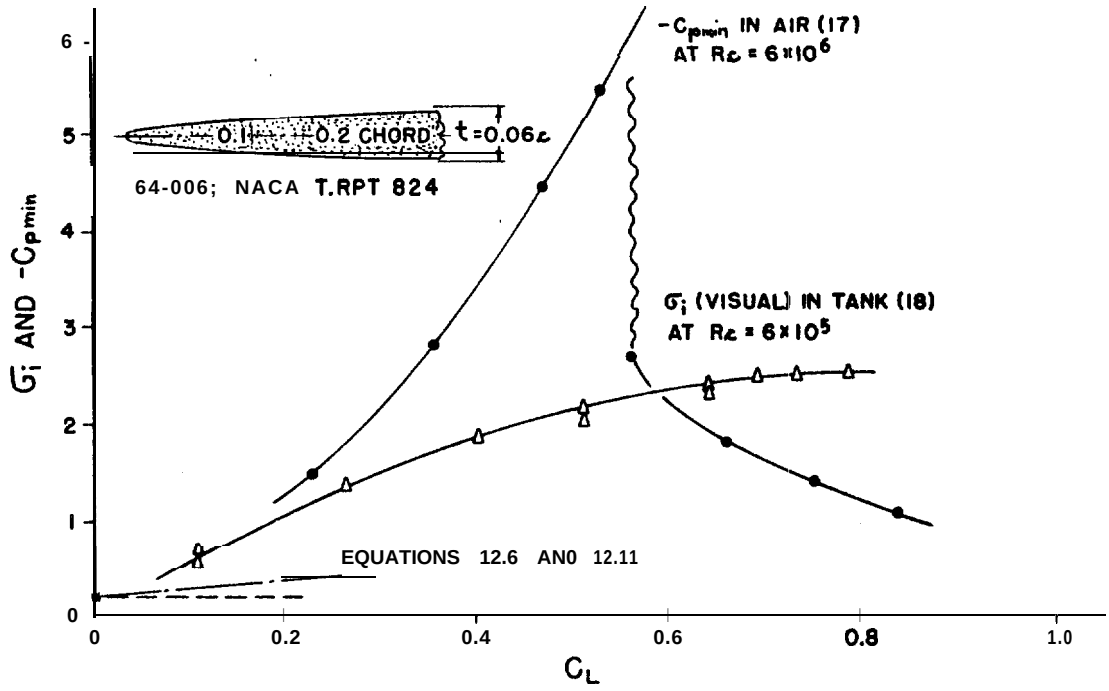

PRESSURE AND CAVITATION COEFFICIENTS OF 64A006 FOIL SECTION

FIGURE 12.5

In the considered foil tests at $C_L = 0.5$, the time during which a particle of water travelling past the point of minimum pressure, is really exposed to pressures below vapor pressure, is only in the order of

$$\text{exposure time} \approx \frac{\text{length}}{V_{local}} \approx \frac{0.002}{2 \times 21} \approx 5/100{,}000 \text{ second} \qquad (12.10)$$

This short interval may be responsible for the discrepancy between $-C_p = 5$ and $\sigma_i = 2$, as observed at $C_L = 0.5$.

Reference 19 presents experfmental results of another foil section, the 4412 section, as tested in a cavitation tunnel. Good agreement between σ_i and $-C_{p_{min}}$ is found at pressure coefficients or cavitation numbers below one[20]. However, at negative as well as at higher positive lift coefficients, where pressure peaks are to be expected at the respective sides of the section, considerable discrepancies of the same magnitude as those in Figure 12.5 are evident.

Cutting off the peak of a really narrow pressure minimum may not mean losing much of the total lift produced in a foil section, The pressure distributions during the cavftatlon-tunnel tests may not have been the same as in the wind-tunnel investigations,, It is suggested as a possfbilitythat in the water tests very small air bubbles (nuclei) may have levelled off the pressure peaks to some extent before visible bubbles could be observed and reported, This levelling-off effect may be combined with the time effect, described above.

Whatever the explanations may be, Figure 12.5 and reference 19 demonstrate that in the case of suction-pressure peaks as may occur on lifting hydrofoil sections, inception of cavitation cannot reliably be predicted from non-cavitating or theoretical pressure distributions. This fact also discourages application of the theoretically correct method (reference 21) of correlating the critical cavitation number with the critical Mach number which is available for many sections and lift coefficients.

The available results on the delay of cavitation (or whatever the effect may be) are assembled in Figure 12.6. It appears that results of slender bodies, or streamline sections in the vicinity of zero lift, having by comparison "no" delay, are compatible with such extreme cases as the lifting section in Figure 12.5. A statistical conclusions is that

$$\Delta\sigma_i \approx -(0.08 \text{ to } 0.12)(C_{p\,min})^2 \qquad (12.11)$$

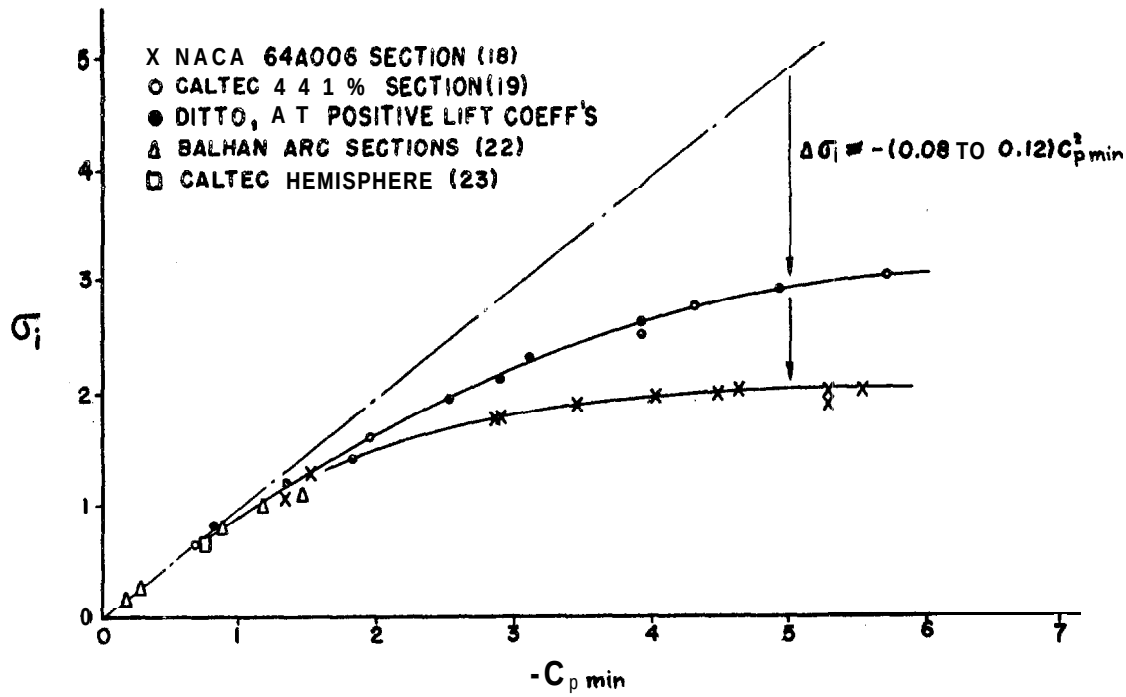

STATISTICAL SURVEY ON THE "DELAY" OF CAVITATION IN PEAKED PRESSURE DISTRIBUTIONS

FIGURE 12.6

Vortex Cavitation

The minimum of the static pressure does not always occur on the surface of an obstacle, Tip vortices, for example, originating from lifting surfaces, have a core with a static pressure on a negative level. According to Prandtl[1], the pressure differential in the core of a wing-tfp vortex is

$$\Delta p/q \approx -1.7\, C_L^2/A^2 \qquad (12.12)$$

where A = aspect ratio of the wing. Cavitation may start accordingly within such cores, as has been observed behind the blade tips of water propellers.

Vortices are also shedding from bodies exhibiting a separated flow pattern, especially in the form of a "vortex street". As an example, cavitation was found starting within the cores of such separation vortices, originating from a blunt, cylindrical head shape (see reference 6) at $\sigma_i = 1.76$, while the minimum pressure coefficient at the surface of thfs body was only $-C_{p\min} = 0.64$. Here again, the pressure distribution would not be a reliable indication for the onset of cavitation; and the deviation would be in the direction opposite to that as found in pressure peaks,

In concluding, equatfon (12.5) only seems to hold for slender bodies (foil and strut sections in Figure 12.3 or three-dimensional

shapes in Figure 12.2) and in "smooth" flow patterns (such as near C_{Lopt} in, Figure 12.4).

Critical Speeds in Hydrofoil Systems

Considering boats with hydrofoils operating beneath the free surface of water, the ambient static pressure is

$$p_{amb} = p_{atm} + \gamma h \tag{12.13}$$

where $\gamma = 62.43$ lb/ft^3 for fresh water and $\gamma = 64$ lb/ft^3 for "Atlantic" sea water. On the basis of a critical cavitation number σ_i (assumed to be known for the system considered), the critical dynamic pressure is then

$$q_{crit} = 0.5 \rho V_{crit}^2 = \frac{p_{atm} - p_{vapor} + \gamma h}{\sigma_i} \tag{12.14}$$

The standard atmospheric pressure is $p_{atm} = 2120$ lb/ft^2, corresponding to a head of 34 ft of fresh water. At a standard temperature of 59°F, the vapor pressure is comparatively low, in the order of 1.6% of the atmospheric pressure; the corresponding head is roughly 0.5 ft of water. Disregarding this small quantity the critical pressure reduces to $q = p_{amb}/\sigma_i$; and in close proximity to the surface (more correctly at $h \approx 0.5$ ft), the critical dynamic pressure is

$$q_{crit} \approx \frac{p_{atm}}{\sigma_i} \approx \frac{2120}{\sigma_i} \quad \left(\frac{lb}{ft^2}\right) \tag{12.15}$$

Using the standard sea-water density ρ = 1.99 (lb sec^2/ft^4), the corresponding "standard" critical speed of hydrofoil systems is found to be

$$V_{crit} \approx \frac{2}{1.99}\frac{2120}{\sigma_i} = \frac{46.2}{\sqrt{\sigma_i}} \quad \left(\frac{ft}{sec}\right) \tag{12.16}$$

In knots, the critical speed is

$$V_{crit} \approx 27/\sqrt{\sigma_i} \tag{12.17}$$

This function is plotted in Figure 12.7.

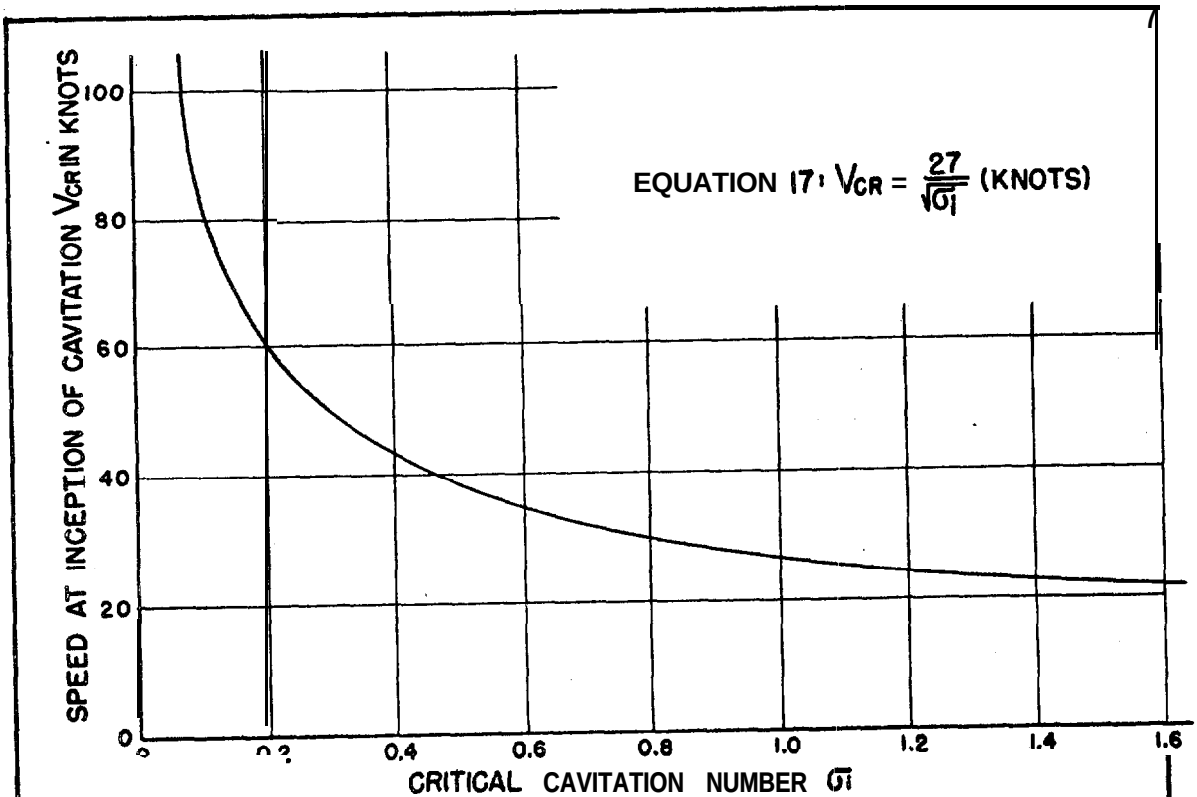

STANDARDIZED RELATION OF SPEED 8 CRITICAL CAVITATION NUMBER

FIGURE 12.7

Example

What is the critical speed of a hydrofoil system operating near the water surface, on the basis of a minimum-pressure coefficient $C_{p_{min}} = -0.44$ (as found in the preceding example)? - Using equation (12.17), $V_{crit} = 27/\sqrt{0.44} = 40$ knots.

Introducing the critical cavitation numbers indicated by equations **(12.6)** and (12.9) into equation (12.17), the standard critical speed of favorably designed hydrofoils can be predicted as a function of section shape and lift coefficient:

$$V_{crit} \approx \frac{27}{\sqrt{2\frac{t}{2x} + 0.7C_L}} \quad \text{(knots)} \tag{12.18}$$

This function is plotted in Figure **12.8.**

Example

What is the maximum permissible lift coefficient of a hydrofoil section having $t/c = 10\%$ (at 0.5 chord) for a speed of 40 knots? - Figure **12.8** indicates $C_L = 0.36$. For comparison, the average lift coefficient in the blades of a destroyer propeller is well below 0.1, to avoid cavitation.

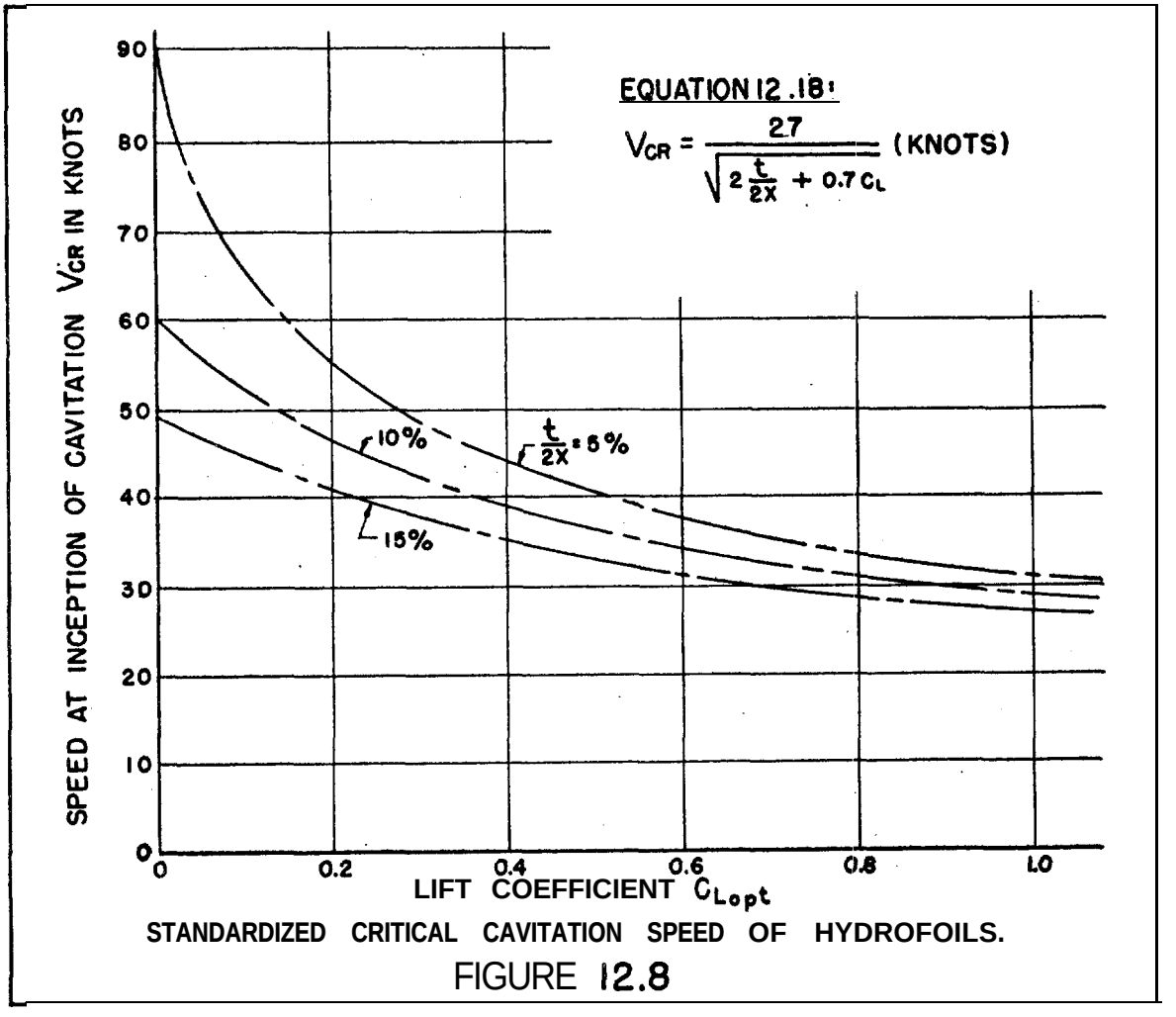

STANDARDIZED CRITICAL CAVITATION SPEED OF HYDROFOILS.

FIGURE 12.8

3. Forces in Cavitating Flow

Transitional Phase

At speeds (or lift coefficients) above the inception of cavitation, lift- and drag coefficients do not immediately change their magnitude, Within the "bubble" phase, they remain essentially at their non-cavitating level; the lift coefficient sometimes increases slightly. Subsequently, as soon as any real, coherent cavity develops, the lift coefficient decreases, the drag coefficient increases. This transition (see Figure 12.11 for illustration) can be rather extended, reaching up to twice the dynamic pressure (1.4 the speed) at which cavitation first sets on. No systematic information can be given on this phase as of this time. Once in fully-cavitating condition, stable flow patterns are prevailing, some of which are presented as follows.

Resistance of Blunt Bodies

In fully cavitating condition, the resistance of an obstacle evidently corresponds to the uniform negative pressure at the rear side (within the cavity) and to the average positive pressure component on the face of the body. For $\sigma = 0$, the latter one has been calculated for wedges[24] and cones[25] as a function of the half apex angle ε.

Upon increasing the cavitation number from zero, the flow pattern past the forebody changes, as explained in reference 26, Accordingly, the drag coefficient is expected to increase as

$$C_D = C_{Do}(1+\sigma) \tag{12.19}$$

where C_{Do} = drag coefficient at $\sigma = 0$. Figure 12.9 presents experimental results of disks, confirming this function very well.

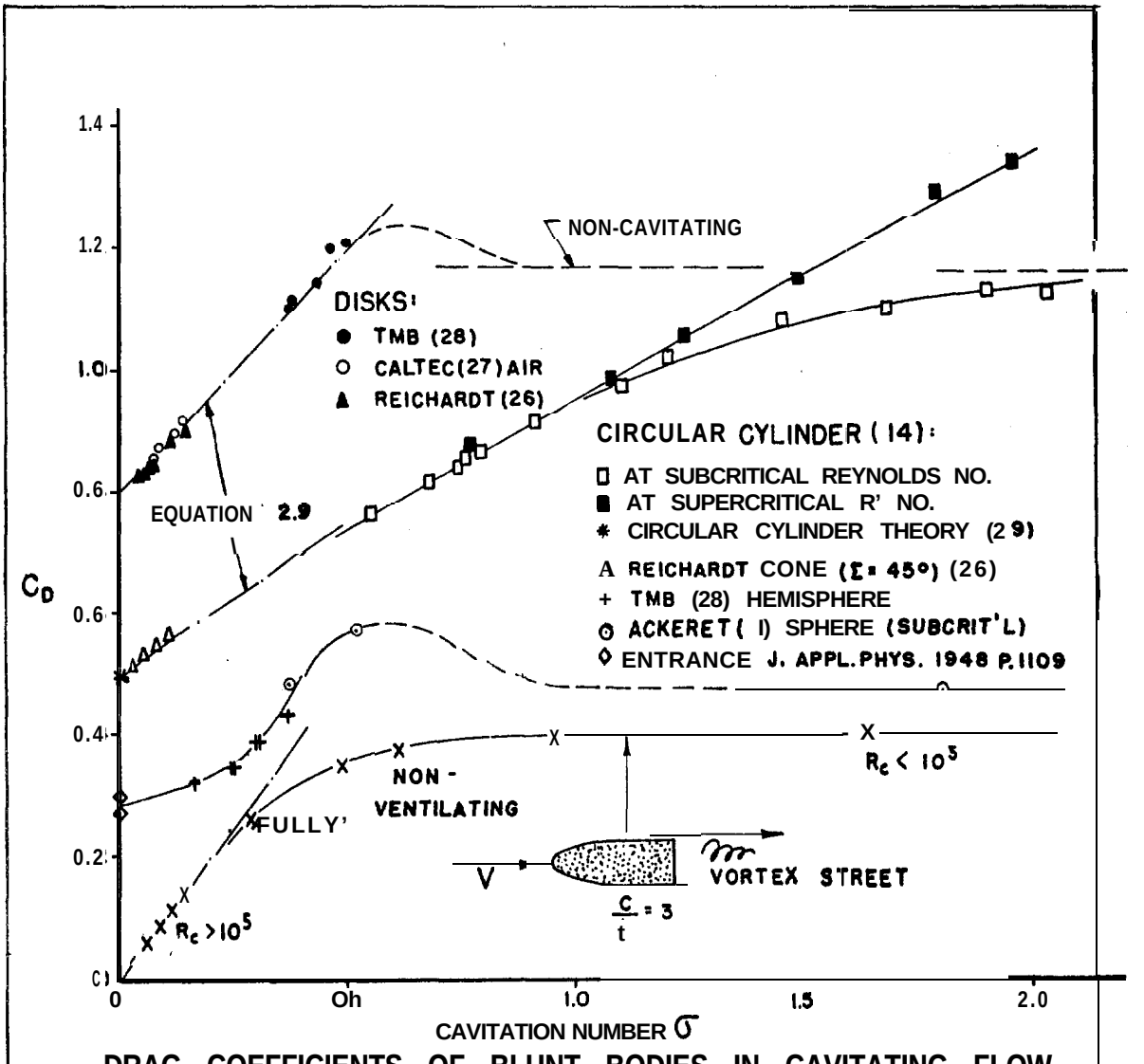

DRAG COEFFICIENTS OF BLUNT BODIES IN CAVITATING FLOW

FIGURE 12.9

In the case of round bodies, the minimum pressure point is located somewhere on the forebody (and not at the trailing edge as in wedges and cones). Cavitation, therefore, starts from that point; and the starting point may move further forward as the cavitation number is decreased, As a consequence, the $C_D(\sigma)$ function is no longer strafght as according to equation (12.19). Such characteristics are demonstrated in Figure 12.9 by results of a hemispherical body[28] and a Sphere'. Results of circular cylinders (in cross flow) also show a divergence from the mechanism according to equation (12.19)

Drag in Ventilating Flow

Insight in the drag mechanism of blunt bodies may be amplified by discussing results of a "streamlined" half section tested in ventilating (rather than cavitating) flow in the Gibbs & Cox towing tank at speeds between 1 and 10 ft/sec. A piece of strut having a chord of 3.1 inches and an aspect ratio of 4 was towed between hollow end plates (connecting the cavity with the atmosphere) at an average submergence $h = 1.5\ c$. The cavitation number is then simply

$$\sigma = \frac{p_{amb} - p_{cavity}}{q} = \gamma h / 0.5 \rho V^2 \qquad (12.20)$$

At higher cavitating numbers (above 0.6), ventilation (or cavitation) does not take place; the drag coefficient is approximately constant and practically equal to the base drag coefficient of such body shape.

Wfthin the range of small cavitation numbers (below 0.3), the coefficient is approximately

$$C_{D_0} = \sigma \qquad (12.21)$$

Flow pattern and drag coefficient would not be the same, however, in cavitating flow. There is evidently a line of minimum pressure somewhere between leading and trailing edge. Cavitation would start from there, rather than from the trailing edge as in ventilating flow; and the drag coefficient would be higher than according to equation (12.21).

Lift in Fully-Cavitating Flow

The force on a flat plate in cavitating flow (at $\sigma = 0$) has been calculated by Kfrchkoff and Rayleigh. Using such a plate as a lifting surface in two-dimensional flow, Betz predicts in reference 30 that the coefficient of the force normal to the plate's surface is

$$C_{normal} = \frac{2\pi \sin\alpha}{4 + \pi \sin\alpha} + \sigma = C_L/\cos\alpha \qquad (12.22)$$

For $\sigma = 0$ and for angles of attack α below some 10°, this function reduces to

$$\frac{dC_L}{d\alpha} = \pi \qquad (12,23)$$

which is only one quarter of the basic lift-curve slope of an airfoil section (which is 2π). Experimental results (see reference 5) of foils tested in a water tunnel (with a geometrical aspect ratio of

one, between the test-section walls), are plotted in Figures 12.10 and 12.11. They evidently confirm the theoretical function - for sufficiently thin sections (up to and including t/c = 7.5%). Thicker sections and sections with rounded noses show lift coefficients, however, which are sometimes higher (because of nose suction), and at small angle of attack lower (cavitation shifting from the upper to the lower section side), than according to the fully cavitating theory.

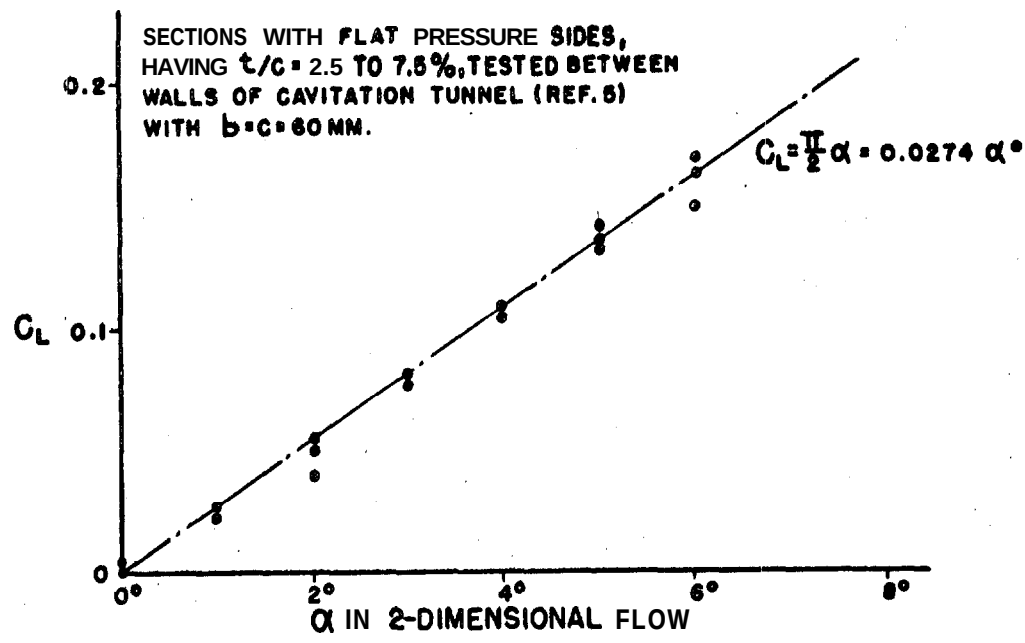

LIFT COEFFICIENT AT $\sigma = 0$

FIGURE 12.10

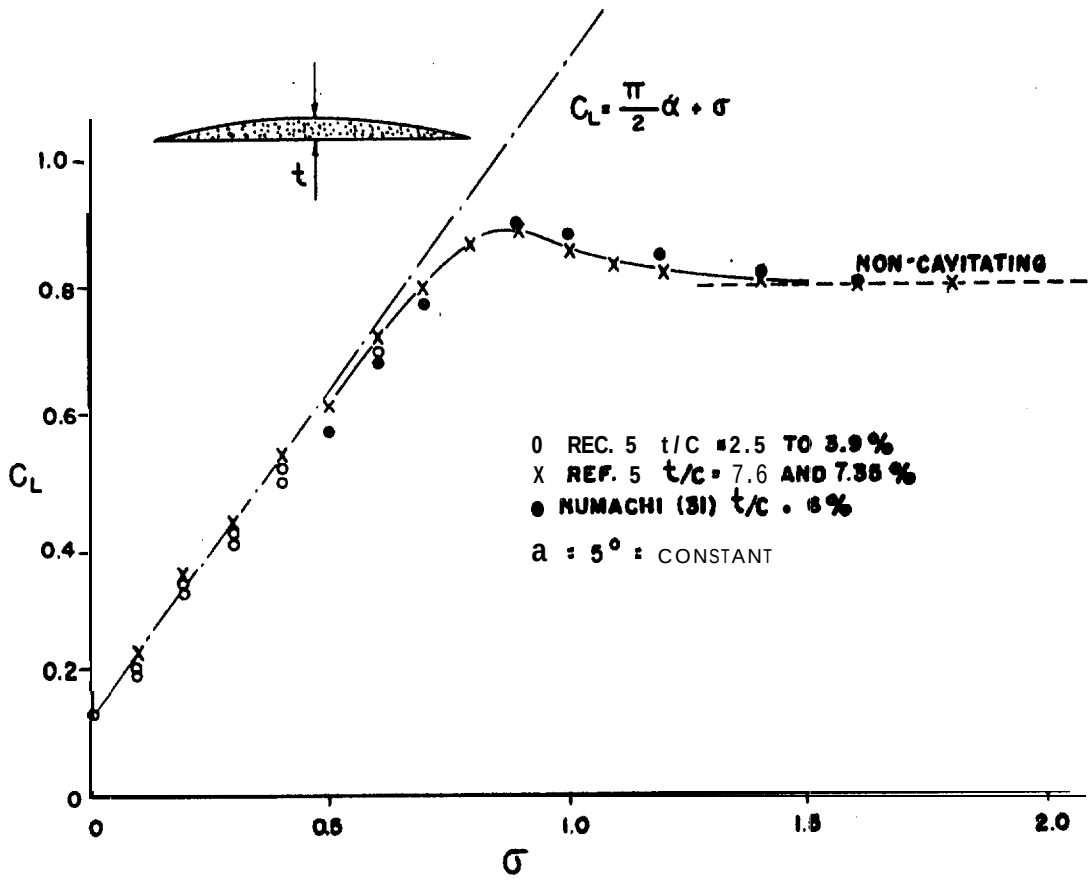

LIFT COEFFICIENT AS A FUNCTION OF CAVITATION NUMBER σ, TESTED BETWEEN TUNNEL WALLS

FIGURE 12.1 I

For a wing of finite span, the induced angle of attack

$$\alpha_i = kC_L/\pi A \qquad (12.24)$$

where k = biplane factor

$A = b^2/S$ = aspect ratio

must be considered; the "α" in equation (12.22) is to be replaced by the effective angle $(\alpha - \alpha_i)$. Consequently

$$C_L = \cos\alpha \left[\sigma + \frac{2\pi \sin(\alpha - \alpha_i)}{4 + \pi \sin(\alpha - \alpha_i)} \right] \qquad (12.25)$$

This equation is compared (in Figure 12.13) with points tested in the Gibbs & Cox Tank on (the flat bottom of) a plate towed in ventilating flow between-hollow end plates. On the basis of a biplane coefficient indicating the effect of the free water surface, $k = 1$, for the tested "box plane" condition at $h/b = 0.25$, magnitude and character of the function according to equation (12.25) seem to be verified.

Resistance of Hydrofoil Sections

Walchner[5,16] is the only source of information available, Indicating resistance of foil sections in truly cavitating condition at or near zero lift. The pressure component of this resistance at $\sigma = 0$, plotted in Figure 12.12 shows some relation to that of wedges, having the same forebody-thickness ratio. Between the values at $\sigma = 0$ and the non-cavitating phase, the drag coefficient decreases considerably (hardly without any first-increasing trend as per Figure 12.9).

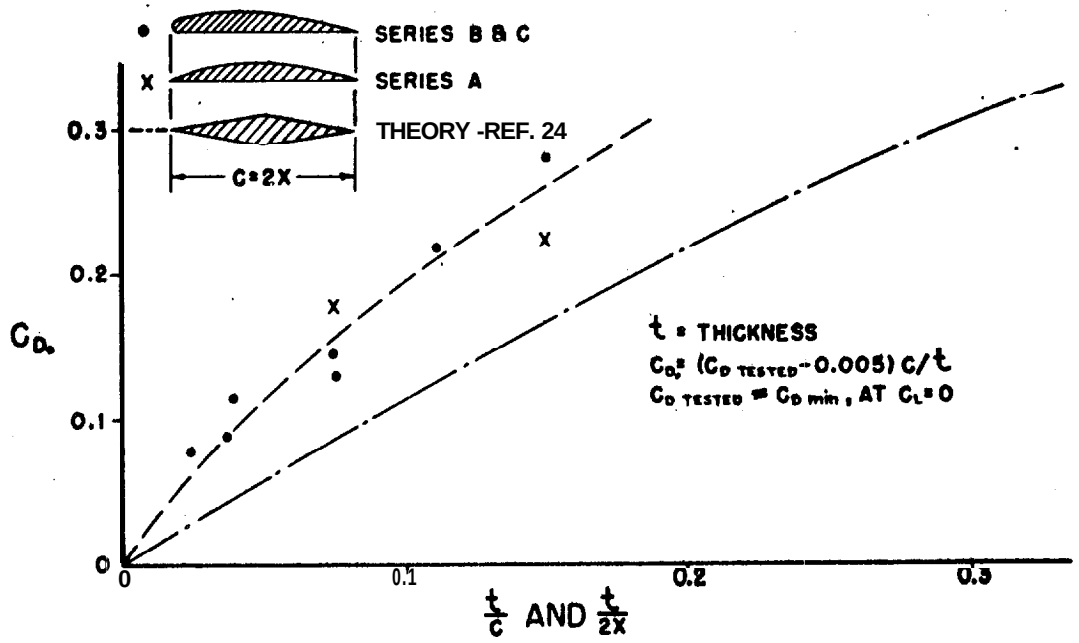

DRAG COEFFICIENT OF SOME FOIL SECTIONS AT $\sigma = 0$, FROM REFS. 5 AND 16

FIGURE 12.12

In lifting foil sections (with fully cavitating upper side, the pressure drag is a geometrical component of the total force. For flat pressure side is

$$C_{D_{pressure}} = C_L \tan \alpha \tag{12.26}$$

where α is indicating the angle of the lower side in two-dimensional flow. Utilizing equation (12.23), this angle is

$$\sin\alpha \approx \frac{\pi}{2}\left(\frac{C_L}{\cos\alpha} - \sigma\right) \tag{12.27}$$

Therefore, the drag due to lift of sections having flat lower sides in two-dimensional, fully cavitating flow is expected to be defined by

$$C_{DL} \approx \frac{2}{\pi}(C_L - \sigma)\, C_L \tag{12.28}$$

For $\sigma = 0$, some experimental evidence can be found in references 5 and 15, confirming the trend of $dC_D / dC_L^2 = 2/\pi$, for circular-ard sections with $t/c < 7.5\%$ and α up to 6°.

For higher angles of attack, as in the case of Ngure 12.13, the complete equation (12.25) has to be employed to find $C_L(\alpha)$ first, and then $C_{D\text{pressure}}$ as a function of C_L and α.

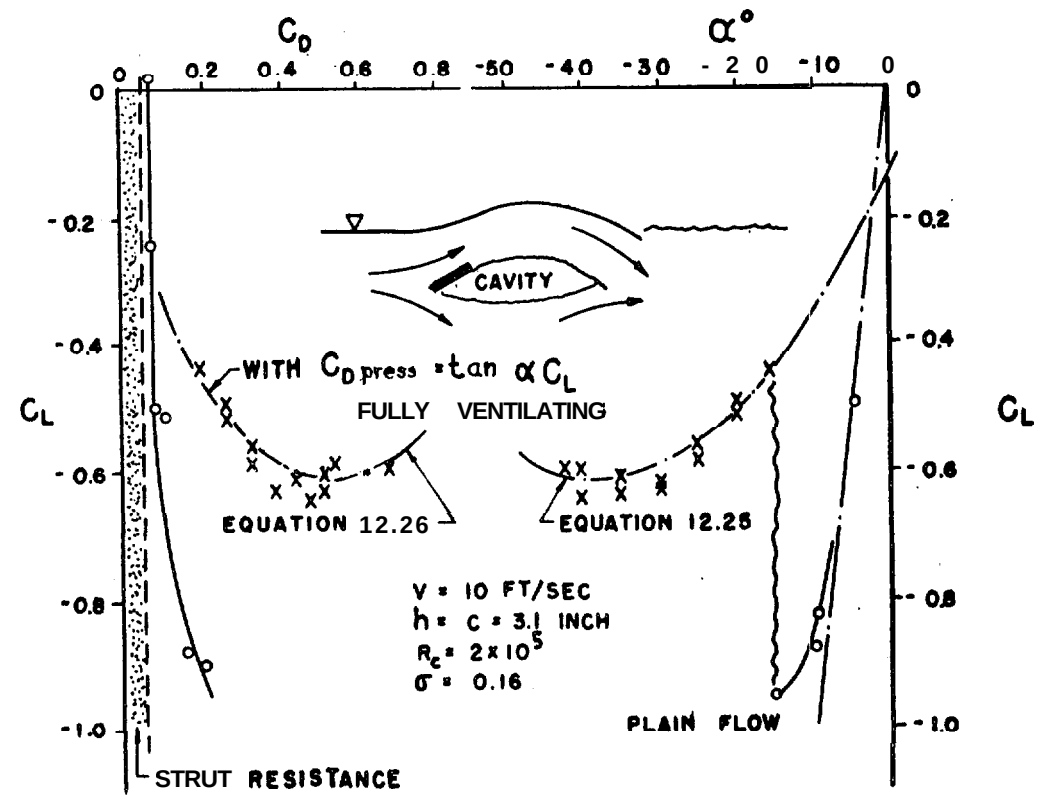

LIFT AND DRAG OF A FLAT PLATE HAVING A=4 BETWEEN END STRUTS, AT NEGATIVE ANGLES OF ATTACK

FIGURE 12.13

Cambered Sections

For a long time, only circular arc sections (with flat pressure sides) have been considered, possibly to be used in cavitating flow conditions. It has been suggested, however, that (cambered pressure

sides should provide higher sectional L/D ratios or lower resistance ratios, respectively - on account of certain forward components of the forces normal to the surface elements of such cambered sections.

Figure 12.14 presents the characteristics of such a section;

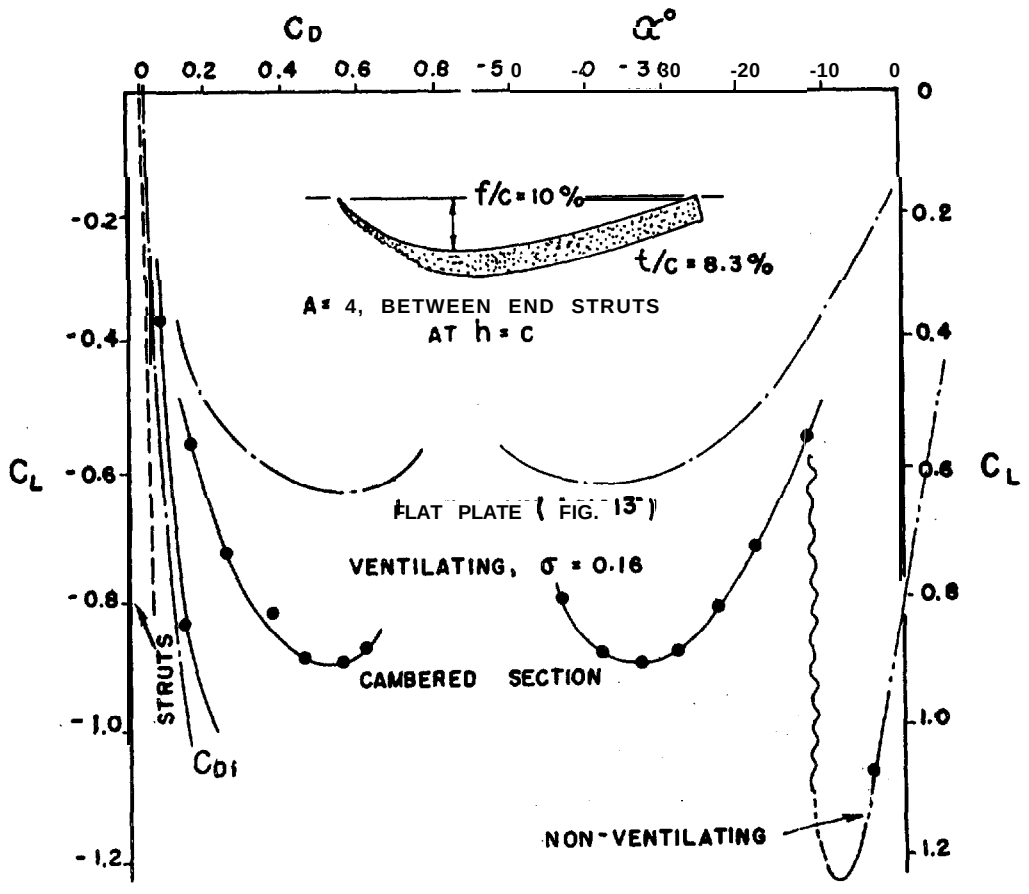

LIFT AND DRAG OF A VENTILATING CAMBERED FOIL SECTION, AS TESTED IN THE GIBBS & COX TANK

FIGURE 12.14

tested in the same manner as the plate in Figure 12.13; that is, in ventilating flow. The transitional phases in these graphs would not be the same in cavitating flow, however: and they should be disregarded if considering vapor cavitation. For the cambered section, the fully ventilating-cavitating phase exhibits considerably higher lift coefficients and appreciably lower resistance ratios than for the flat plate.

The performance of fully-cavitating foil sections, in two-dimensional flow at $\sigma = 0$, has recently been investigated by linearized theoretical methods (see reference 32). The optimum shape is found to be cambered (at the pressure side) according to

$$(f/c)_{opt} \approx 0.2\, C_L\,; \quad C_{Lopt} \approx 5(f/c) \qquad (12.29)$$

Disregarding frictional drag, theory predicts for this camber ratio that the pressure-resistance ratio will only be $\approx 1/6$ of that of the flat plate. The results in Figure 12.14 do not confirm this much of improvement.

References

1. Ackeret — "Experimental and Theoretical Investigatfons of Cavitation", in Tech, Mech. & Thermodynamik - Vol. 1 of Forschung Ingenieurwesen 1930 p. 1; Trans. TMB No. 20.

2. Eisenberg — "Mechanism of Cavitation", TMB Rpt. 792 (1950) and Rpt. 842 (1953).

3. Raven, Feiler & Jespersen — "Annotated Bibliography of Cavitation", TMB Rpt. R-81, 1947.

4. Crump — "Critical Pressure for Inception of Cavitatfon in Fresh and Sea Water as Influenced by Air Content", TMB Rpt. No. 575, 1949.

5. Walchner — "Investigation of Foil Sections in Cavitating Flow", in Hydromechanische Probleme des Schiffsantriebs, HSVA Hamburg, 1932. See NACA Tech. Memo, 1060.

6. Rouse & McNown — "Cavitation and Pressure Distribution, Head Forms", Publication No, 420 Iowa State University (Bulletin No. 32, 1948).

7. Knapp & Doolittle — "Nose Cavitatfon, Ogives and Sphero-gives", Rpt. from Caltec High-Speed water Tunnel, 18 Jan. 1945.

8. Hoerner — "Inception of Cavitation on Hydrofoil Systems", Gibbs & Cox Tech. Rpt. 13431 No, 8, 1952.

9. Fage, Falkner & Walker — "Experiments on a Series of Symmetrical Joukowsky Sections", Brit. ARC RM 1241, 1929.

10. _____ — "Tested Pressure Distributions", Jahrbuch D. Luftfahrtforschung 1941 p.I 101 and German Rpt. ZWB FB 1621 (1943).

11. Coffee & McKann — "Hydrodynamic Drag of 12- and 21-Percent Thick Struts", NACA Tech. Note 3092, 1953.

12. Schrenk — "Pressure Distribution Along the Chord of Wing Sections", Contribution IAll in Ringbuch Luftfahrttechnik, German Ministry for Aeronautics, 1938.

13. Gutsche — "Characteristics of Propeller-Blade Sections" a) Mftteilungen Pr. Versuchsanstalt Wasserbau Schiffbau, Heft 10 (Berlin 1933), b) Yearbook Schfffbautech Gesellschaft 1936 p. 277; 1938 p. 125; and Vol. 41, 1940.

14. Martyrer — "Force Measurements on Cylfnders and Foils at Cavitation", in Hydrodynamische Probleme des Schiffsantriebs, HSVA Hamburg 1932.

15. Holl — "Investigation of Propeller-Blade Sections Having Reduced Cavitation Tendency", Forschung 1932 p. 109.

16. Walchner — "Contribution to the Design of Ship Propellers Without Cavitation", AVA Monograph,, Reports & Translations No. 330, 1947, British Ministry of Aircraft Production.

17. McCullough & Gault — "Boundary Layer and Stalling of NACA 64A006 Airfoil", NACA Tech. Note 1923 (1949), :now Tech, Rpt. 903.

18. King &Land — "Force and Cavitation Characteristics of Aspect-Ratio-4 Hydrofoils", NACA Confidential Rpt. L52J10, 1952.

19. Daily — "Cavitation Characteristics of a Hydrofoil Section", Trans. ASME 1949, p. 269 (Caltec).

20, Pinkerton — '"Pressure Distrfbutfons Over 4412 Airfoil Section", NACA Tech. Rpt. 563, 1936.

21.	Joshua Hendy Corp.	"Hydrofoil Studies and Design Data", Rpt. to ONR, 1950.
22.	Balhan	"Investigation of Some Propeller-Blade Sections in Cavitating Flow", Wageningen Publication No. 99, 1951.
23.	Kermeen	"Observations of Cavitation on Hemispherical Head Models", Caltec Hydrodynamics Laboratory Tech. Rpt. E-354 1952.
24.	Bobyleff	Quoted in paragraph 78 of Lamb's Hydrodynamics
25.	Plesset & Schafer	"Drag in Cavitating Flow", J. Appl. Physics, 994.8, p. 934 and Rev. Mod. Physics, 1948, p. 228.
26.	Reichardt	"Law of Cavitating Bubbles", German Dct, ZWB UM *6628,* Trans. 766 Brit. Min. Aircraft Production.
27.	Brown	"Optimum Slenderness Ratio of Low-Drag Body", Caltec Hydrodynamics Laboratory Memo Rpt. N55, 1949.
28.	Eisenberg & Pond	Water Tunnel Investigation *of* Steady-State: Cavities", TMB Rpt. No, 668, 1948.
29.	Brodetsky	Proc. Roy, Soc. London Ser. A No. 718, 1923.
30.	Beta	"Influence of Cavitation Upon Efficiency of Ship Propellers", Proceedings Third Internat, Congr. Tech. Mechanics, Stockholm *1930,* Vol. I p. 411.
31.	Numachi	"Cavitation Tests on Hydrofoils in Cascade", Trans ASME 1953 p. 1257.
32.	Tulin & Burkat	"Theory About Lifting Foils at Zero Cavitation Number", TMB Confidential Rpt., 1954.

APPENDIX A. CALCULATION OF THE LIFT AND DRAG CHARACTERISTICS OF A PROPOSED 50 TON HYDROFOIL CRAFT

1. General Considerations
2. Characteristics of the Configuration
3. Design Examples

Design examples are given for the drag and required foil settings of a 50 ton "Canard" hydrofoil craft, at two foil-borne speeds.

1. General Considerations

The hydrodynamic characteristics of the components of a hydrofoil craft, as presented in this volume, are used for the purpose of calculating the various performance eharacterfstfcs of a proposed design. Thus, with this information and havfng a knowledge of the methods to be employed, one can calculate the total drag throughout the speed range (including take-off), the turning circle, required foil and rudder angles, etc.

This volume presents only the basic eharacterfstfcs of components, and the methods of utilizing this information is the subject of other volumes. However, for the purpose of illustration, design calculations are included herein. These examples are for the drag and required foil settings of a specific configuration at two foil-borne speeds.

2. Characteristics of the Configuration

The configuration chosen for these examples is that of a 50 ton hydrofoil craft, and is based on the design study reported in reference 1.. Thfs craft is a "Canard" type wfth automatically controlled, fully submerged foils, and wfth the power transmitted through a single nacelle on the main (rear) foil; as shown in Figure A.l. The dimensions of the foil system and other pertinent information are given in Figure A.2.

For the purpose of these calculations, the craft is assumed to be at zero trim and normal submergence under full load condition. Two speeds (30 knot cruising speed and 45 knot maximum speed) were selected.

Reference 1 - Confidential Letter from Bath Iron Works Corp. (by Gibbs & Cox, Inc.) to ONR, file 13531/S1/3(1-1283) of April 3, 1953 - enclosing

"Design Study for 50 Ton Hydrofoil Craft"

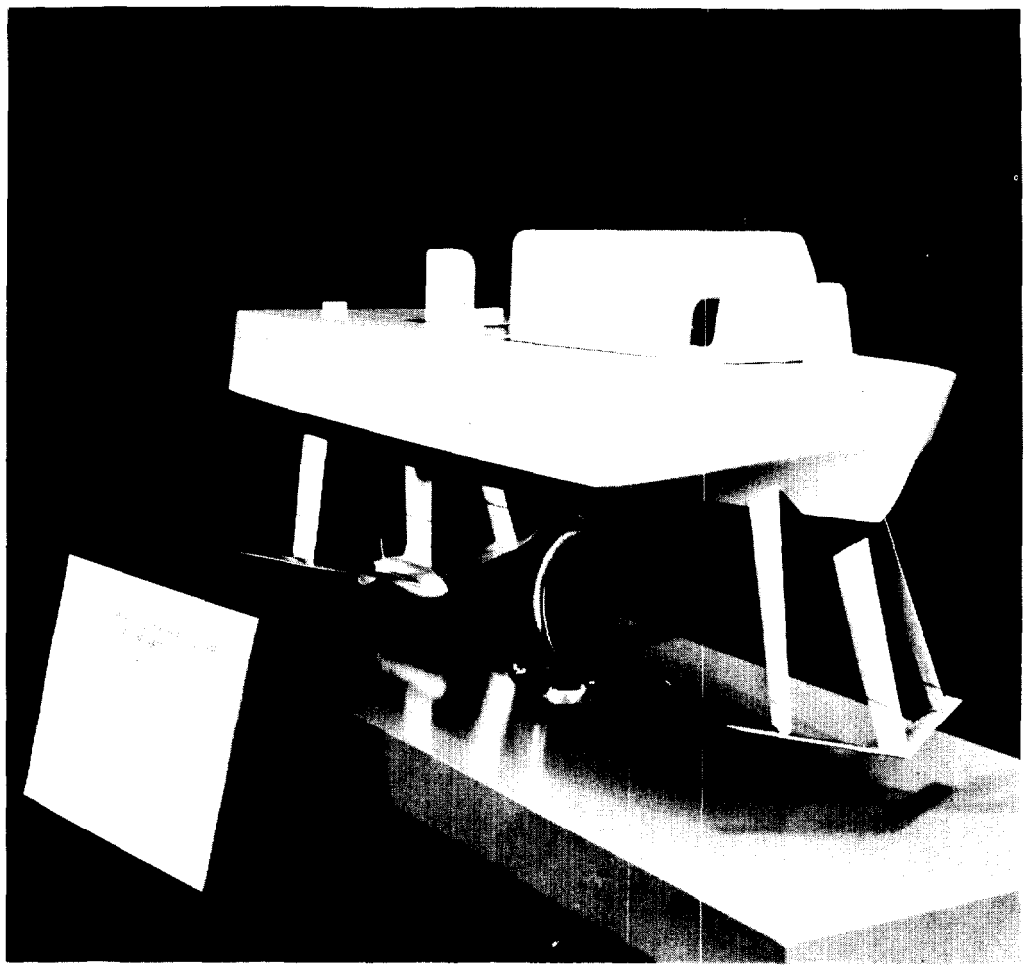

DESIGN STUDY MODEL
OF 50 TON HYDROFOIL CRAFT

FIGURE A.1

3. Design Examples

The overall calculation is broken down into individual design examples, included on the sheets following:

Design Example - A1 Induced Characteristics
A2 Wake Effect
A3 Foil and Flap Settings
A4 Parasite Drag
A5 Summary of Drag and Foil Settings

DESIGN EXAMPLE NO. A.1

SH 1 OF 5

CALCULATE THE INDUCED DRAG & LIFT CHARACTERISTICS FOR THE 50 TON CANARD CONFIGURATION AT 30 AND 45 KNOTS

PRINCIPAL CHARACTERISTICS (1)

QUANTITY	SYMBOL	MAIN FOIL	CANARD FOIL
FOIL SPAN	b	24.00′	14.00′
FOIL AREA	S	67.82 ☐	23.04 ☐
MEAN CHORD	$c = S/b$	2.83′	1.65′
ASPECT RATIO	$A = b^2/S$	8.50	8.50
TOTAL LIFT	—	82,300#	29,700#
BUOYANCY (2)	—	2,390#	270#
DYNAMIC LIFT	L	79,910#	29,430#
FOIL LOADING	L/S	1180#/☐	1280#/☐
CHORD AT TIP	c_t	1.541′	1.167′
CHORD AT CENTER	c_r	3.083′	2.125′
TAPER RATIO	c_t/c_r	0.50	0.55
SUBMERGENCE AT TIP	h_t	1.88′	1.12′
SUBMERGENCE AT CENTER	h_r	4.00′	3.00′
MEAN SUBMERGENCE	h	2.94′	2.06′
DISTANCE OF OUTER STRUTS OFF ℄	$a_s/2$	8.00′	4.92′
SUBMERGENCE OF OUTER STRUTS	h_s	2.59′	1.68′
LIFT COEFFICIENT @ 30 KNOTS (3)	$C_L = L/qS$	0.461	0.500
@ 45 KNOTS	$C_L = L/qS$	0.205	0.222
DIHEDRAL ANGLE	Γ	10.0°	15.0°
ANGLE OF SWEEP	Λ	20.0° (AVG)	28.0°

(1) SEE FIGURES A.1 AND A.2 ; ALSO REFERENCE 1

(2) TOTAL BUOYANCY OF FOIL SYSTEM AND NACELLE

(3) DYNAMIC PRESSURE q = 2560 #/☐ @ 30 KNOTS
= 5750 #/☐ @ 45 KNOTS

DESIGN EXAMPLE NO. A.1

SH 2 OF 5

DETERMINATION OF "K" FACTOR

		MAIN FOIL	CANARD FOIL
1. Biplane Effect	(Equation 2.26)		
h_t/b		0.078	0.080
$(\tan \Gamma)/4$		0.044	0.068
h/b		0.122	0.148
K_b		1.44	1.38
2. Dihedral Effect	(Equation 2.29)		
$\frac{1+h_t/b}{1+h/b}$		0.961	0.941
K_Γ		1.38	1.30
3. Sweep Effect	(Equation 2.28)		
$\cos \Lambda$		0.940	0.883
$K_{\Gamma\Lambda}$		1.47	1.47
4. Strut Effect	(Equation 2.26)		
h_s/b		0.108	0.120
a_s/b		0.667	0.704
$\frac{1}{1+(a_s/b)^3 \cdot h_s/b}$		0.968	0.960
5. Total K Factor			
$K_{\Gamma,\Lambda,s}$		1.42	1.41

Note: Subscripts refer to the K factors after correction for various effects are made

DESIGN EXAMPLE NO. A.1

SH 3 OF 5

AIRFOIL FACTORS

	MAIN FOIL	CANARD FOIL
1. Planform		
Taper ratio, c_t/c_r	0.50	0.55
From Figure 1.9,		
τ (A = 5)	0.046	0.054
τ (A = 10)	0.072	0.084
δ'	0.0027	0.0032
τ (A = 8.5)	0.064	0.075
$\delta = 8.5\,\delta'$	0.023	0.027
2. Induced Effects (Eqs 2.34 & 2.36)		
$1/\pi A$	0.0374	0.0374
K (from Sheet 2)	1.42	1.41
$d\alpha_i/dC_L = (1+\tau)K/\pi A$	0.0566	0.0569
$dC_{D_i}/d(C_L^2) = (1+\delta)K/\pi A$	0.0543	0.0541
3. Section Angle & Lifting Surface Correction (Eq. 2.34)		
h/c	1.04	1.25
u (Figure 2.5)	0.056	0.046
$u/8\,h/c$	0.0067	0.0046
$E = 1 + 2/A^2$	1.028	1.028
$E/2\pi$	0.1637	0.1637
$\left(\frac{d\alpha}{dC_L}\right)_o = \left(E/2\pi + u/8\,h/c\right)/\cos\Lambda\cos\Gamma$	0.1844	0.1971
4. Combined Effects for Angle		
$\left(\frac{d\alpha}{dC_L}\right)_o + \left(\frac{d\alpha_i}{dC_L}\right)$	0.2387	0.2512

DESIGN EXAMPLE NO. A.1

WAVE EFFECTS

Equation (2.34), **deep** water

	MAIN FOIL		CANARD FOIL	
	30 KNOTS	45 KNOTS	30 KNOTS	45 KNOTS
h	2.94'	2.44'	2.06'	2.06'
V (ft/sec)	50.6	76.0	50.6	76.0
$F_h = V/\sqrt{gh}$	5.2 I	7.82	6.22	9.34
h/b	0.123	0.123	0.147	0.147
c/h	0.962	0.962	0.801	0.801
$\left(\frac{e^{-2/F_h^2}}{F_h^2}\right)$ (Figure 2.6)	0.0175	0.0080	0.0125	0.0058
$(K_b - 1)$ (Figure 2.6)	0.43	0.43	0.38	0.38
$\left(\frac{d\alpha}{dC_L}\right)_w = \frac{c}{h}\left(\frac{e^{-2/F_h^2}}{2F_h^2}\right)(K_b - 1)$	0.0012	a. 0033	0.0030	0.0018

TOTAL INDUCED EFFECTS

Values of quantities prior to correction by $(1 + U C_L)$

$\left(\frac{d\alpha}{dC_L}\right)_a$	from sh. 3	0.2387	0.2387	0.2512	0.2512
$\left(\frac{d\alpha}{dC_L}\right)_w$	above	0.0072	0.0033	0.0038	0.0018
$\frac{d\alpha}{dC_L}$	total	0.2459	0.2420	0.2550	0.2530
dC_{Da}	from sh.3	0.0543	0.0543	0.0541	0.0541
$\frac{d\ C_{Dw}}{d(C_L^2)}$	above	0.0072	0.0033	0.0038	0.0018
$\frac{d(C_L^2)}{d(C_L^2)}$	total	0.0615	0.0576	0.0579	0.0559
$(1 + U C_L)$		1.026	1.012	1.028	1.012

[redacted]

DESIGN EXAMPLE NO. A.1

SH 5 OF 5

INDUCED DRAG & FOIL ANGLES

	MAIN FOIL		CANARD FOIL	
	30 KNOTS	45 KNOTS	30 KNOTS	45 KNOTS
$\frac{d\alpha}{dC_L}$ sheet 4	0.2459	0.2420	0.2550	0.2530
C_L	0.461	0.2205	0.5000	0.222
$\frac{d\alpha}{dC_L} \cdot C_L$	0.1134	0.0446	0.1275	0.0562
$(1+UC_L)$	1.026	1.012	1.028	1.012
α (radians)	0.1163	0.0502	0.1311	0.0569
$\frac{dC_D}{d(C_L^2)}$ sheet 4	0.0615	0.0576	0.0579	0.0559
C_L^2	0.212	0.042	0.250	0.049
$[dC_D/d(C_L^2)]\, C_L^2$	0.0130	0.00242	0.0145	0.00273
$(1+UC_L)$	1.026	1.012	1.028	1.012
$C_{D\,(due\ to\ lift)} = C_{D_L}$	0.0133	0.00245	0.0149	0.00276

TOTAL INDUCED DRAG

30 KNOTS $D_L = 0.0133 \times 67.82 \times 2560 = 2309$

$0.0149 \times 23.04 \times 2560 = 879$

3,188 #

45 KNOTS $D_L = 0.00245 \times 67.82 \times 5750 = 955$

$0.00276 \times 23.04 \times 5750 = 366$

1,321 #

DESIGN EXAMPLE NO. A.1

SH 5 OF 5

INDUCED DRAG & FOIL ANGLES

	MAIN FOIL.		CANARD. FOIL	
	30 KNOTS	45 KNOTS	30 KNOTS	45 KNOTS
$\frac{d\alpha}{dC_L}$ sheet 4	0.2459	0.2420	0.2550	0.2530
C_L	0.461	0.205	0.500	0.222
$\frac{d\alpha}{dC_L} \cdot C_L$	0.1134	0.0496	0.1275	0.0562
$(1+uC_L)$	1.026	1.012	1.028	1.012
α (radians)	0.1163	0.0502	0.1311	0.0569
$\frac{dC_D}{d(C_L^2)}$ sheet 4	0.0615	0.0576	0.0579	0.0559
C_L^2	0.212	0.042	0.150	0.049
$[dC_D/d(C_L^2)]\, C_L^2$	0.0130	0.00242	0.0145	0.00273
$(1+uC_L)$	1.026	1.012	1.028	1.012
$C_{D\,(due\ to\ lift)} = C_{D_L}$	0.0133	0.00245	0.0149	0.00276

TOTAL INDUCED DRAG

30 KNOTS $D_L = 0.0133 \times 67.82 \times 2560 = 2304$
$0.0149 \times 23.04 \times 2560 = 879$
$3{,}188\ \#$

45 KNOTS $D_L = 0.00245 \times 67.82 \times 5750 = 955$
$0.00276 \times 23.04 \times 5750 = 366$
$1{,}321\ \#$

DESIGN EXAMPLE NO. A.2

SH 1 OF 1

CALCULATE THE WAKE EFFECT ON THE MAIN FOIL OF THE 50TON CANARD CONFIGURATION AT 30 AND 45 KNOTS

(REFER TO CHAPTER 6)

AERODYNAMIC WAKE

The "aerodynamic" downwash due to the canard foil can be approximated from equation (6.4) and Figure 6.6. The main foil can be considered to lie in the plane of the trailing vortex lines issuing from the canard foil.

Then, the downwash factor j can be determined from Figure 6.6 over the span of 24/14 = 1.71 (times the canard span). By integrating over the span, the average value of j is found to be

$$j = 0.375$$

DOWNWASH AT THE MAIN FOIL

The Froude numbers for the Canard Foil are:

$V/\sqrt{gc}$ = 6.95 at 30 Knots
10.44 at 45 Knots

which are sufficiently high so that the downwash at the main foil is determined from Equation (6.7):

$$\varepsilon = \frac{C_L}{\pi A} j K$$

where C_L, A, and K are for the Canard Foil (See example A.1)

ε = 0.0070 radians at 30 Knots
= 0.0031 radians at 45 Knots

INCREASE OF DRAG ON MAIN FOIL

Drag is LIFT x Downwash D_ε = 79,910 x 0.0070 = 559# @ 30 Knots
= x 0.0031 = 248# @ 45 Knots

DESIGN EXAMPLE NO. A.3

CALCULATE THE FOIL ANGLE SETTINGS AND FLAP DEFLECTIONS FOR THE 50 TON CANARD CONFIGURATION AT 30 AND 45KNdTS

DESIGN CONSIDERATIONS

The main foil is fixed in configuration with 25% full-span flaps on a cambered foil section. The foil is set so that the flap deflection is zero at 45 knots,

The canard foil has no section camber, and pivots about an axis thru its quarter-chord.

The main foil setting is referred to fhe section at mid-span, and is thus the angle derived below, without correction. The msin foil flap and the canard foil angles are referred to planes normal to their axes, and the angles derived must be corrected for sweep and dihedral.

MAIN FOIL

45 KNOTS

The main foil is set at zero angle to the effective fluid flow at 45 knots (the fail section camber is designed to account for the lift at 45 knots).

The induced and downwosh angles are:

$$\alpha_i + \alpha_w = \left[\frac{d\alpha_i}{dC_L} + \frac{d\alpha_w}{dC_L}\right] C_L (1 + \tau C_L)$$

$$= \left[0.0566 + 0.0072\right] \times 0.205 \times 1.012 \text{ (from Example A.1)}$$

$$= 0.0132$$

$$\varepsilon = 0.0031 \text{ (from Example A.2)}$$

Then, foil angle at 45 knots:

$$\alpha_i + \alpha_w + \varepsilon = 0.0163 \text{ radians} = 0.93"$$

[redacted]

DESIGN EXAMPLE NO, A.3

MAIN FOIL (CONT'D)

Requwed foil angle = 0.0502 (Example A.1)
Dewed foil setting = 0.0163
Equivalent angle due to foil camber = 0.0339

NOTE: The foil section must be chosen to have

30 KNOTS $\alpha_{LO} = -0.0339 \frac{\cos 10°}{\cos 20°} = 0.0355 = 2.0°$

Required Foil Angle = 0.1163 (Example A.1)
Downwash Angle + 0.0031 (Example A.2)
Equivalent Setting at 45 knots = 0.0502
Required for flaps = 0.0692

Flap effectiveness (Equation 5.2)

$k_f = 1.1\sqrt{0.25} = 0.55$

Required flap angle equivalent

$0.0692/0.55 = 0.1257$

Actual flap deflection (about own axis)

$\delta = 0.1257 \frac{\cos 10°}{\cos 20°} = 0.1317$ radians

= 7.55"

CANARD FOIL

Required foil angle = 0.1311 @ 30 Knots, 0.0569 @ 45 Knots (Example A.1)

Required angles about own axis

$\alpha = 0.1311 \times \frac{\cos 15°}{\cos 28°} = 0.1434$ radians = 8.22° @ 30 KNOTS

$\alpha = 0.0569 \frac{\cos 15°}{\cos 28°} = 0.0622$ radians = 3.56° @ 45 KNOTS

DESIGN EXAMPLE NO. A.4

SH 1 OF 4

CALCULATE THE PARASITE DRAG OF THE 50 TON CONFIGURATION AT 30 AND 45 KNOTS

FOIL PARASITE DRAG

(From Chapter 4)

	MAIN FOIL		CANARD FOIL	
	30 KNOTS	45 KNOTS	30 KNOTS	45 KNOTS
Mean Chord	2.83'	2.83'	1.65'	1.65'
Reynolds No (S.W. at 59°F)	1.12×10^7	1.68×10^7	6.51×10^6	9.76×10^6
$C_{f(std)}$ · Equation (4.12)	0.00368	0.00350	0.00393	0.00374
$[1 + 10(t/c)^2]$ $(t/c = 10\%)$	1.10	1.10	1.10	1.10
$2 C_{f(std)} [1 + 10(t/c)^2]$	0.00810	0.00770	0.00865	0.00822
ΔC_L	≈ 0	= 0	0.500	0.222
$C_{D_{o(std)}}$ Eq (4.13)	0.00810	0.00770	0.01081	0.00863
$\rho/2\ V^2 S = qS$	174,000#	390,008	59,000	137,500#
D	1,410'	3,000 #	638#	1,143 #

TOTAL FOIL PARASITE DRAG

AT 30 KNOTS **2048** #

AT 45 KNOTS 4143 #

DESIGN EXAMPLE NO. A.4

STRUT DRAG

AREAS

Item	Length	Chord	Area	No.	Total Area
Main Foil - ℄ Strut	2.58'	3.08'	7.95 ☐	1	7.95
" " - P/S "	2.63'	3.08'	8.10 ☐	2	16.203
					24.154
Canard Foil - ℄ Strut	3.00'	2.12'	6.3169	1	6.36
" " P/S "	9.744'	1.775'	3.04 ☐	2	6.00

DRAG

	30 KNOTS			45 KNOTS		
	MAIN P/S & ℄	CANARD ℄	CANARD P/S	MAIN P/S & ℄	CANARD ℄	CANARD P/S
Reynolds No	1.22×10^7	8.37×10^6	6.91×10^6	1.83×10^7	1.26×10^7	1.04×10^7
C_f (std) Eq (4.12)	0.00362	0.00380	0.00390	0.00345	0.00361	0.00370
C_{D_0} (std) Eq (4.13)	0.00796	0.00835	0.00858	0.00760	0.00794	0.00814
Drag Area ($C_{D_0}\times S$) sq ft	0.192	0.053	0.052	0.183	0.051	0.050
C_D spray (Assumed-Figure 7.2)	0.012	0.012	0.012	0.012	0.012	0012
t×c (sq ft)	0.924	0.212	0.350	0.924	0.212	0.350
Spray Drag Area	0.011	0.003	0.004	0.011	0.003	0.004
Total Drag Area	0.203	0.056	0.056	0.194	0.054	0.054
Total Strut Drag Area		0.315			0.302	
$\rho/2\ V^2$		2560			5750	
TOTAL STRUT DRAG		806#			1,737#	

DESIGN EXAMPLE NO. A.4

NACELLE DRAG

(Chapter 3)

Nacelle 2'-5" dia. x 9'-0" long

ℓ/d = 3.72

Frontal Area = $\pi/4\,(2.42)^2$ = 4.60 ft²

Drag	30 KNOTS	45 KNOTS
Reynolds No.	3.56×10^7	5.35×10^7
C_f (std)	0.00318	0.00302
C_{D_a} (Equation 9.3)	0.0413	0.0392
Drag Area $[C_{D_a} \times 4.60]$	0.190	0.180
$\rho/2\ V^2$	2560	5750
Drag	486#	1035#

AIR DRAG (HULL)

(Chapter II)

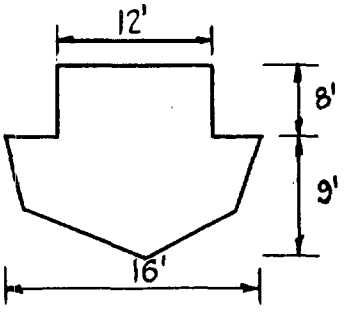

Cross-Sectional Area of the Hull & Main Superstructure:

S= 12 x 8 + 16 x 9 x 0.8 = 211 ft²

From equation 11.4, use a coefficient of 0.0015, (for a fair bow and square stern).

Then,

Dir a y D_{air} = 0.0015 x 211 x 30^2 = 284# (30 KNOTS)

= 0.0015 x 211 x 45^2 = 640# (45 KNOTS)

DESIGN EXAMPLE NO. A.4

SH 4 OF 4

SUMMARY OF PARASITE DRAG

ITEM	30 KNOTS	45 KNOTS
FOILS	2048#	4143#
STRUTS	806#	1737#
NACELLE	486#	1035#
AIR DRAG	284#	640#
TOTAL PARASITE DRAG	3,624#	7,555#

DESIGN EXAMPLE NO, A.5

SH 1 OF 1

SUMMARY OF DRAG AND FOIL SETTINGS FOR 50 TON CANARD CONFIGURATION AT . 30 AND 45 KNOTS

FOIL SETTINGS	30 KNOTS	45 KNOTS
MAIN FOIL ANGLE	0.93°	0.93°
MAIN FOIL FLAP DEFLECTION *	7.55°	——
CANARD FOIL ANGLE *	8.22°	3.56°

* ABOUT OWN AXIS

DRAG		
INDUCED DRAG	3188	1321
WAKE EFFECT	559	248
PARASITE DRAG	3624	7555
TOTAL	7,371#	9,124#
L/D RATIO	15.2	12.3

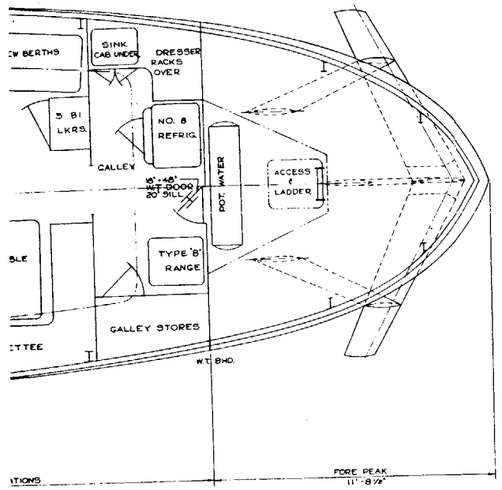

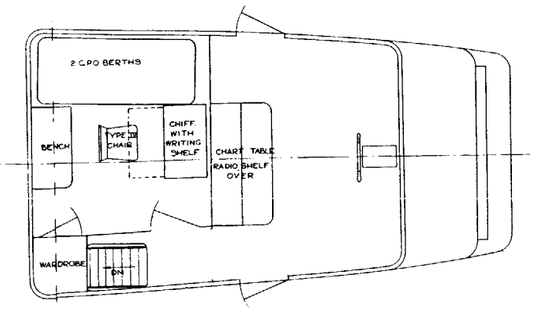

DECK HOUSE ARRG'T.

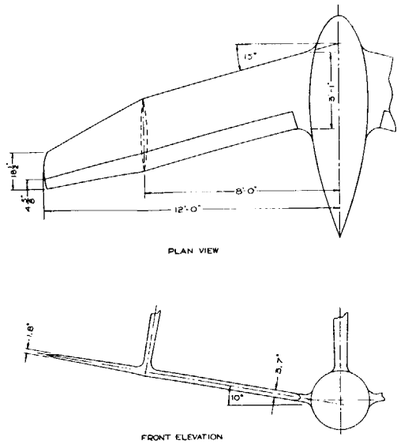

MAIN FOIL

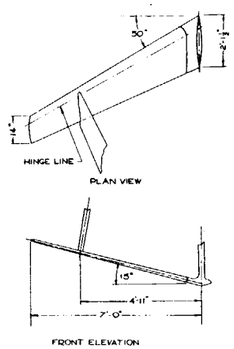

AUX. (FWD) FOIL

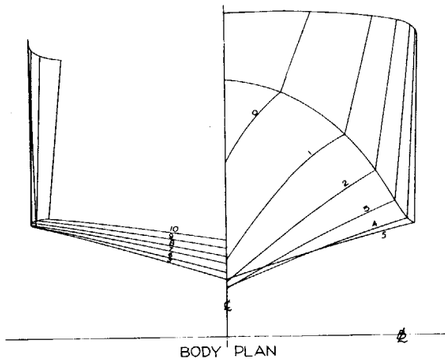

BODY PLAN

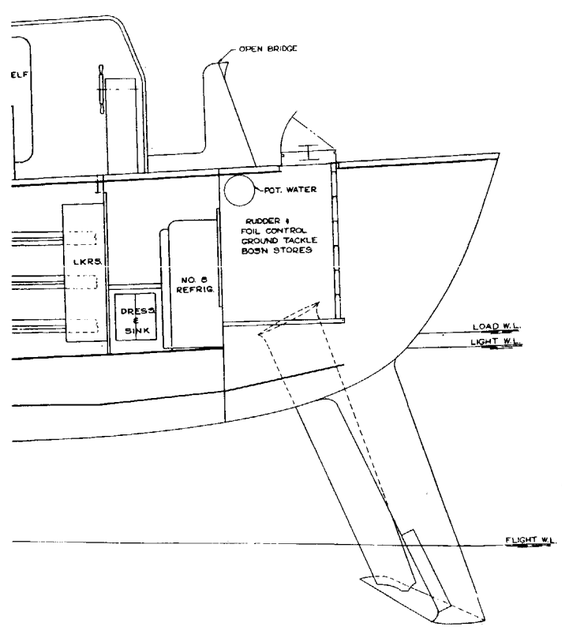

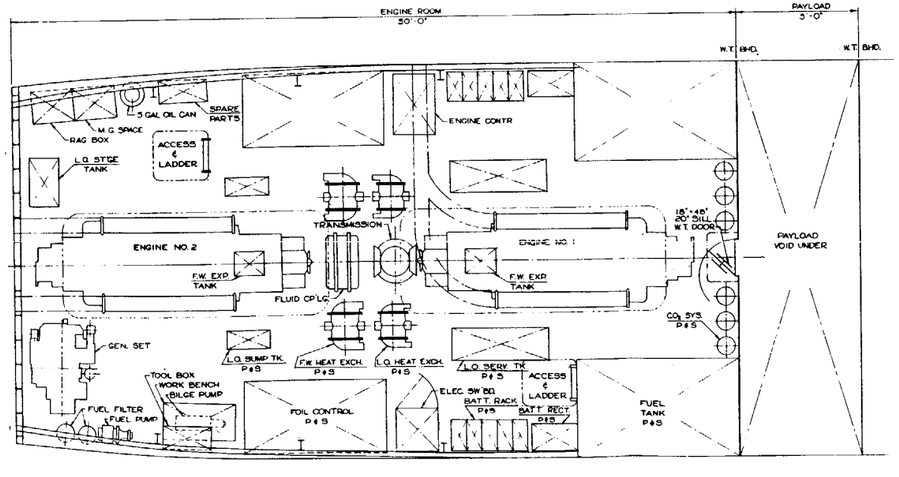

ALTERNATE ENGINE ROOM ARRG'T.

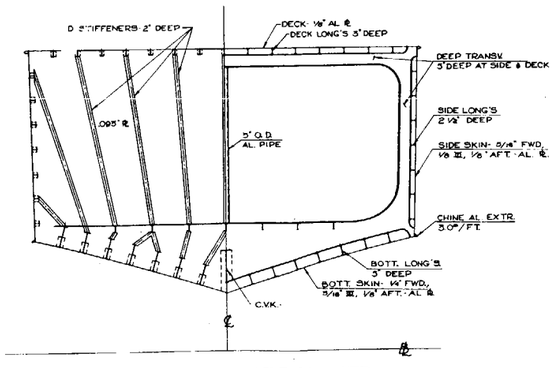

TYPICAL BHD. TYPICAL WEB

PRINCIPAL DIMENSIONS

LENGTH OVER ALL	65'-2½"
LOAD WATER LINE LENGTH	61'-8"
BEAM (MAX.)	16'-0"
DRAFT - HULL DISPLACEMENT CONDITION	4'-0"
DRAFT - MAX. DISPLACEMENT CONDITION	12'-11"
DEPTH	10' AT ⊠
L.C.B. (AFT. OF ⊠)	4.05'
CHANGE IN TRIM - - - - DISP. TO FLYING	2"
DISPLACEMENT	50T

FOIL DIMENSIONS

MAIN FOIL	
MEAN CHORD	54"
SPAN	24'-0"
ASPECT RATIO	8.5
SECTION	10% CAMB.
AREA	68.90 FT.
DIHEDRAL	10°
SWEEPBACK	29° AT TIPS 15° ELSEWH'R
LOCATION OF CENTER OF LIFT (AFT OF ⊠)	16'-6"
AUX. FOIL	
MEAN CHORD	19⅜"
SPAN	14'-0"
ASPECT RATIO	8.5
SECTION	10% SYM.
AREA	23 SQ FT.
DIHEDRAL	15°
SWEEPBACK	30°
LOCATION OF CENTER OF LIFT (FWD OF ⊠)	30'-6"

WEIGHTS

HULL	22,830#
MACHINERY	20,085
FWD. FOIL & STRUTS	2,825
MAIN FOIL & STRUTS	4,500
FUEL OIL	22,400
FITTINGS	7,990
EQUIP & OUTFIT	2,610
CREW & EFFECTS	1,790
POT. WATER	400
STORES	450
PAYLOAD	23,120
MARGIN	3,000
TOTAL	112,000 LBS.

GENERAL NOTES

ITEM	NAPIER-NAC'LE.	PACK. DIR. (NOT SHOWN)
DESIGN SPEED	45 K	45 K
RANGE (NAUT. MI.)	1,000	650
MAX. CONT. SPEED	30 K	45 K
RANGE (NAUT. MI.)	850	650
CRUISING SPEED	30K	30 K
RANGE (NAUT. MI.)	1,440	900
TAKE-OFF SPEED	20-25K	20-25 K
H.P. (CONT. - 2 ENG.)	3,500	2,800
H.P. (MAX. - 2 ENG.)	6,090 (ABT. 3 MIN)	3,000 (15 MIN)
PROP. DIAM.	3'6"	2'-0" EA.

GIBBS & COX, INC.
DESIGN STUDY FOR 50 TON HYDROFOIL CRAFT

FIGURE A.2

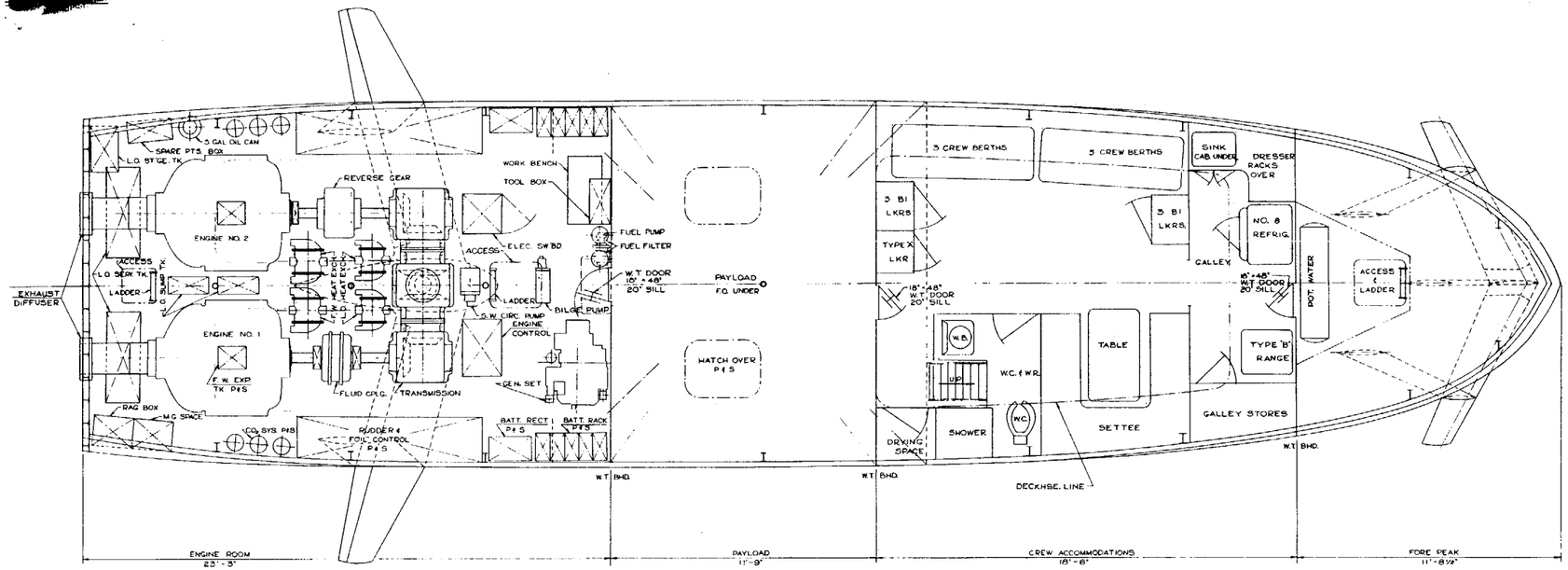

GENERAL ARRG'T

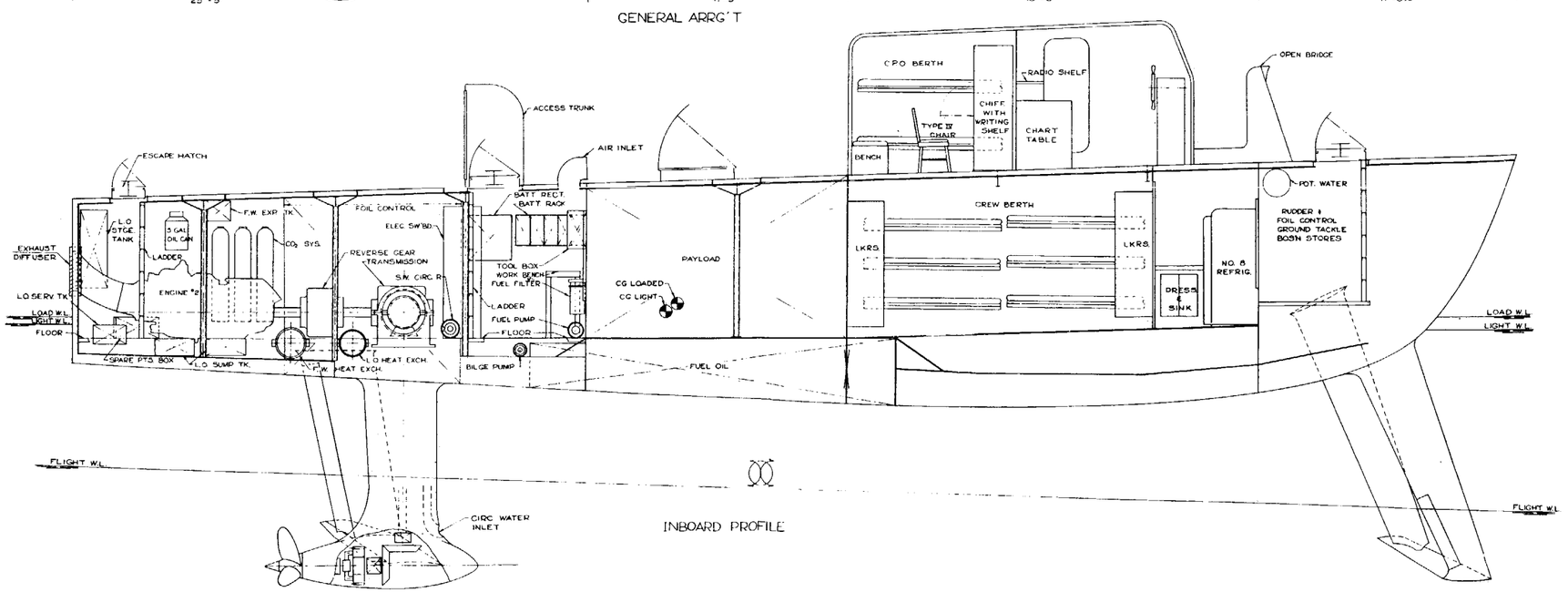

INBOARD PROFILE

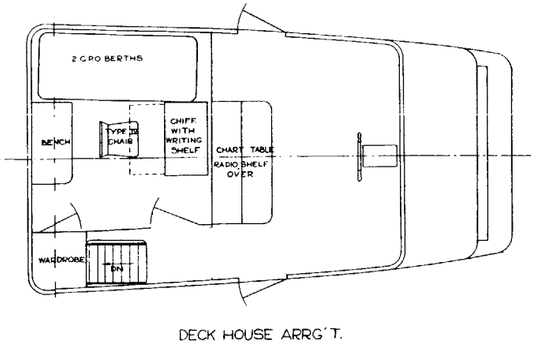

DECK HOUSE ARRG'T.

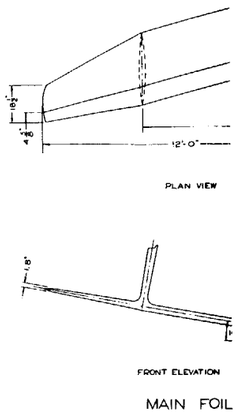

MAIN FOIL

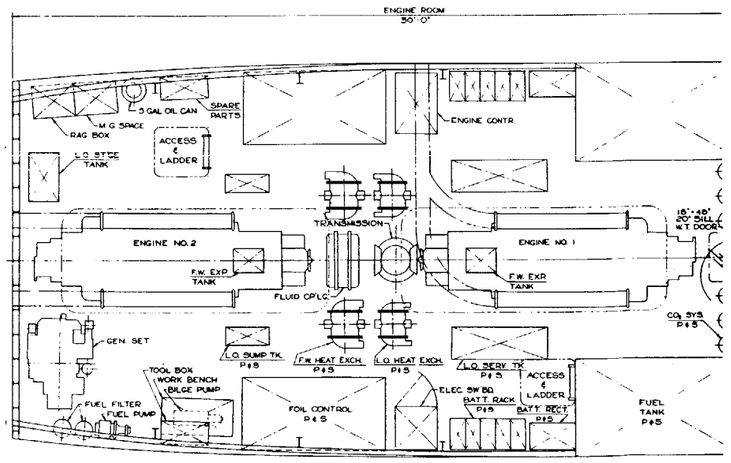

ALTERNATE ENGINE ROOM ARRG'T.